MAX-PLANCK-INSTITUT FÜR POLYMERFORSCHUNG IN MAINZ

From Cyclic Oligopolyphenylenes to Graphenes

Dissertation zur Erlangung des Grades

"Doktor der Naturwissenschaften"

im Fachbereich Chemie, Pharmazie und Geowissenschaften der Johannes Gutenberg-Universität Mainz und in Kooperation mit dem Max-Planck-Institute für Polymerforschung Mainz

Vorgelegt von

Yi Liu

Geboren in Hubei Province / P. R. China

Mainz 2017

Dekan:

1. Berichterstatter:

2. Berichterstatter:

3. Berichterstatter:

Tag der mündlichen Prüfung: 8th June, 2017

Die vorliegende Arbeit wurde in der Zeit von Juni 2012 bis Juni 2016 im Max-Planck-Institut für Polymerforschung in Mainz unter der Anleitung von ausgeführt.

Ich danke für seine wissenschaftliche und persönliche Unterstützung sowie für seine ständige Diskussionsbereitschaft.

My family, and wife

Table of Contents

Index of Abbreviations

1D	one dimensional
2D	two dimensional
3D	three dimensional
B3LYP	BECKE, three-parameter, LEE-YANG-PARR (DFT hybrid functional)
BuLi	butyl lithium
br	broad signal (NMR)
CNT	carbon nanotube
COSY	correlation spectroscopy
CV	cyclic voltammetry
CVD	chemical vapor deposition
calcd	calculated
EEG	electrochemically exfoliated graphene
d	doublet (NMR)
d	days
DCM	dichloromethane
dd	doublet of doublets (NMR)
DFT	density functional theory
DMF	*N*,*N*-dimethylformamide
ε	extinction coefficient
EtOAc	ethyl acetate
Et2O	diethylether
EtOH	ethanol
FD MS	field desorption mass spectrometry
FL	fluorescent spectrometry
GNR	graphene nanoribbon
GPC	gel permeation chromatography

h	hours
HBC	hexa-peri-hexabenzocoronene
HOMO	highest occupied molecular orbital
HPB	hexaphenylbenzene
HR-MS	high resolution mass spectrometry
LUMO	lowest unoccupied molecular orbital
m	multiplet (NMR)
MALDI-TOF	matrix-assistsed laser desorption/ionization time-of-flight
Me	methyl
MeOH	methanol
min	minutes
MS	mass spectrometry
MWCNT	multi-walled carbon nanotube
NG	nanographene
NMR	nuclear magnetic resonance
NOE	nuclear Overhauser effect
NOESY	nuclear Overhauser enhancement spectroscopy
OFET	organic field-effect transistor
OLED	organic light emitting diode
OMe	methoxy
PAH	polycyclic aromatic hydrocarbon
Ph	phenyl
PL	photoluminescence
ppm	parts per million
q	quartet (NMR)
rGO	reduced graphene oxide
RT	room temperature
SAM	self-assembling monolayer

s	singlet (NMR)
sec	seconds
STM	scanning tunneling microscopy
SWCNT	single-walled carbon nanotube
t	triplet (NMR)
TBAF	tetra-iso-butyl ammonium fluoride
tBu	tert-butyl
THF	tetrahydrofuran
TMS	trimethylsilyl
TTC	trisbenzothieno[1,2:7,8:13,14]hexa-peri-hexabenzocoronene
TTOC	trisbenzothieno-*S*,*S*-dioxide[1,2:7,8:13,14]hexa-*peri*-hexabenzocoronene
UPGRADE	bottom-UP blueprinting GRAphene baseD Electronics
UV-Vis	ultraviolet-visible absorption spectroscopy
WAXS	Wide-angle X-ray scattering

1. Introduction

Carbon, featured as the fourth most abound element in the universe by mass and the second most abundant element in the human body,[1] is one of the most significant elements due to its unique bonding diversity and its capability to form at most four covalent bonds. This unusual ability of carbons paves the chemical basement for the construction of arbitrarily long complex molecules and polymers which are the essential components of life, and also made it possible for carbons to exist in considerable distinctive forms, termed allotropes of carbons. The structural diversity of these allotropes renders these molecules or materials a diverse range of distinguishing chemical and physical properties.

In nature, two naturally occurring carbon allotropes are found, namely diamond and graphite, which are composed of extended 3D networks of sp^3- and sp^2-hybridized carbon atoms, respectively, and both exhibit exciting physical properties like hardness and thermal or electronic conductivity. And all these remarkable distinctions between these allotropes are determined by the composition of these atoms with diverse hybridization. (Figure 1-1) As we know, there are three different hybridization types for elemental carbon, namely tetrahedral sp^3-, triangular sp^2-, and linear *sp*-hybridized orbitals with completely different bonding properties and increasing energy. Therefore, conceptually speaking, there exist numerous approaches to construct diverse carbon allotropes by modulating periodical binding networks as well as the composition of sp^3-, sp^2- and *sp*-hybridized carbon atoms in the backbone.[2,3,4,5]

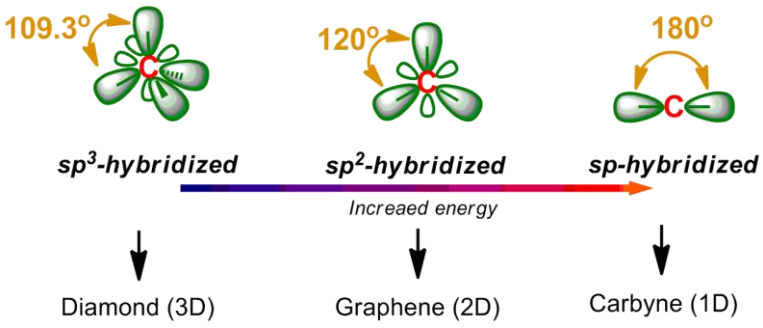

Figure 1-1. Carbon atoms with diverse hybridizations and distinctive bonding models.

1.1 Synthetic sp^2-carbon materials and its substructures

The atoms of carbon are capable of forming allotropes such as crystalline diamond composed of sp^3 tetrahedral frameworks, graphite with layered sp^2-carbon atoms, and amorphous carbon. However, with the advent of fullerene C60 in 1985,[6] the synthetic carbon allotropes and carbon-rich π-systems have attracted the attentions of chemistry more than any other kind of compounds. Meanwhile, the first preparation of microtubules of graphitic carbon [7] in 1991 and successful structural validation of the single-walled carbon nanotubes (SW-CNTs) accomplished independently by two research groups [8,9] in 1993, further sparked the development of new synthetic carbon allotropes.

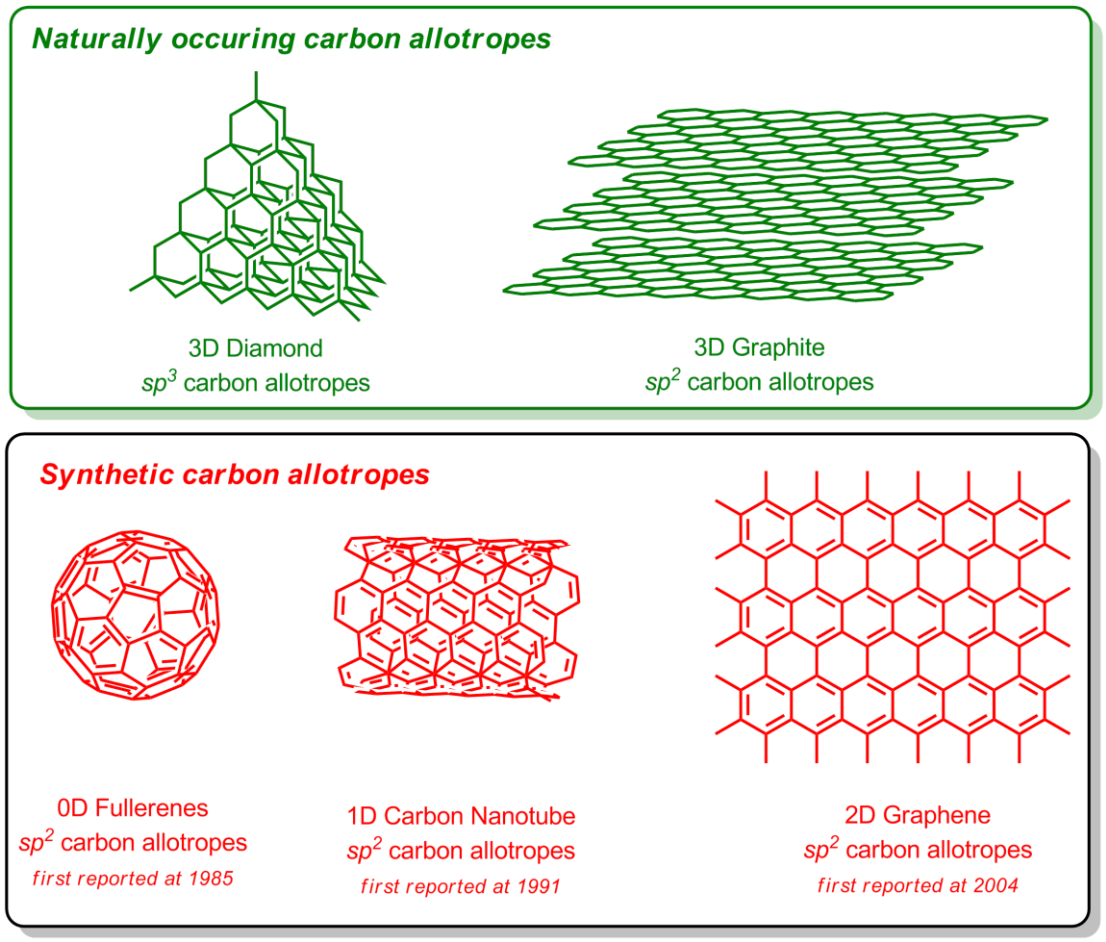

Figure 1-2. Development of carbon allotropes from naturally occurring allotropes (Diamond, and Graphite) to synthetic allotropes (Fullerene, Carbon Nanotube, and Graphene)

1.1.1 One-dimensional carbon nanotubes and its synthetic substructures

Since the first discovery of CNTs by Iijima in 1991[6], the desire to synthesize CNTs with uniform structure has ignited the attention of scientists and engineers. Currently, the synthetic approaches toward CNTS, like arc discharge and chemical vapor deposition, can only produce CNTs as mixtures of diverse structures, which are nearly impossible to be purified toward structurally uniform CNTs. This bottleneck in the field of CNT materials directly limited both the fundamental research and edge-cutting applications of CNTs. Therefore, a much more controllable approach toward uniform CNTs was required, and the bottom-up synthesis of [*n*,*n*]CNTs through templated stepwise growth from a seed compound of CNT , such as [*n*]cycloparaphenylene, was envisioned in the field of synthetic chemistry. In the past decade, a series of [*n*]CPPs (*n* from 5 to 13) have been conceivably synthesized via different approaches with various strain-buffering units [10, 11], for example *cis*-1,4-dimethoxy-2,5-cyclohexadiene-1,4-diyl[12], tetranuclear Pt complexes[13], and *cis*-1,4-dihydroxy-cyclohexane-1,4-diyl[14], which can significantly reduce strain energy during the macrocyclization.

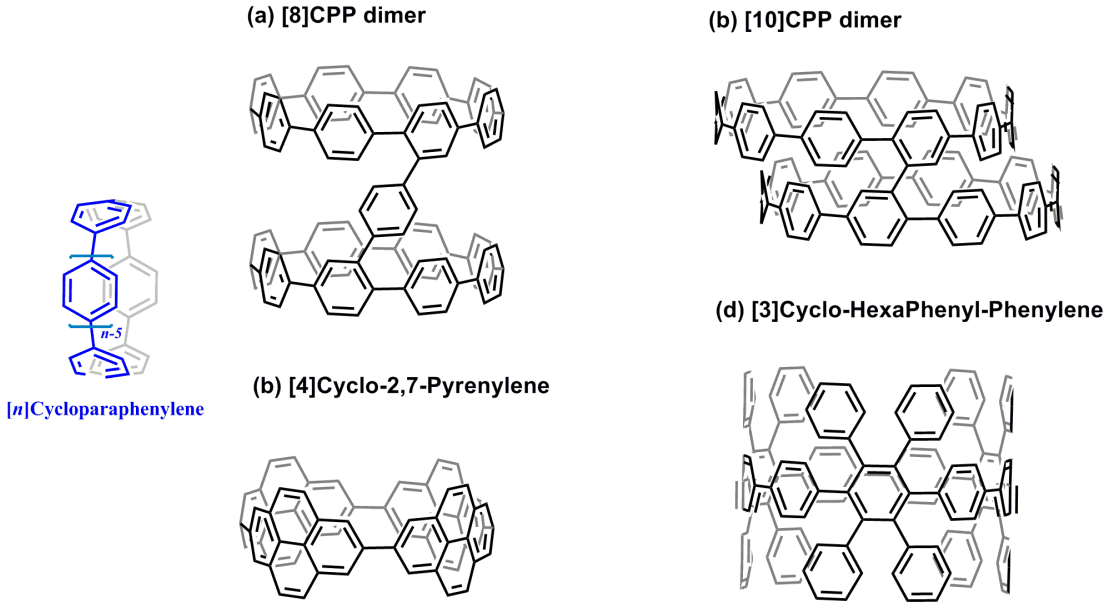

Figure 1-3. Bottom-up synthesis of cycloparaphenylene derivatives with extended belt height toward carbon nanotubes: a) [8]CPP dimer;[15] b) [10]CPP dimer; [16] c) [4]Cyclo-2,7-Pyrenylene;

[17] d) [3]Cyclo-Hexaphenyl-Phenylene. [18]

Represented as the shortest fragment of [*n*,*n*]armchair carbon nanotube (CNT), [*n*]CPPs can be regarded as monomeric precursors or seeds toward the bottom-up construction of uniform [*n*,*n*]armchair CNTs. In the work of the Itami group[19], structurally uniform CNTs can be synthesized by using a cycloparaphenylene ring as the template and ethanol as the carbon source in a chamber at high temperature via "growth-from-template" mechanism. This bottom-up method conceivably paves a promising approach toward the synthesis of uniform CNTs with programmable structural parameters, like radius and edge structure.

Meanwhile, the connection or polymerization between the CPP units can also be applied to realize the longitudinal extension of CPPs in order to accomplish the access to wider polyaromatic hydrocarbon belts and ultimately CNTs,. To fulfill this goal toward CPP units with extended height, the dimers of CPPS, [8]cycloparaphenylene dimer[9] and [10]cycloparaphenylene dimer[10], were synthesized based on the coupling of corresponding halide-functionalized CPP derivatives by the groups of *Jasti* and *Itami*, respectively. Additionally, the *Yamago* group and group had also synthesized the [4]cyclo-2,7-pyrenylene[11], and [3]cyclo-hexaphenyl-phenylene[12] to achieve the π-system extension in the CPP. However, for these extended cycloparaphenylene rings, the annulation of extremely congested phenylene units into the π-conjugated sidewall structure of CNTs remains unsuccessful until now due to the high strain, which also still require a lot of efforts toward the bottom-up building of CNTs.

1.1.2 Two-dimensional graphene and its synthetic substructures

The serendipitous discoveries of fullerene and CNTs have landmarked the beginning of the era of carbon allotropes in the field of chemistry and materials science. Additionally, the distinguishing electronic properties of fullerene and CNTs have also spurred the further development of sp^2-carbon-rich semiconducting materials for optoelectronic devices because of their remarkable electronic properties. In 2004, this

concept toward new carbon allotropes has been realized and awarded again by the rediscovery and successful synthesis of single-layered graphite, graphene[20].

Currently, the fabrication and production of graphene sheets usually include methods like exfoliation of graphite, and chemical vapor deposition. However, their intriguing electronic properties and perfect 2D structure also stimulate new synthetic methods toward graphene subunits [21,22], which are also structurally featured as nanographenes, or extended polycyclic aromatic hydrocarbons (PAHs). Through these molecular models, the synthesis of these nanographenes can be rationalized as a model to study their unique properties, spawn the development of functional carbon materials with remarkable properties, and further pave a promising approach toward bottom-up synthesis of structurally uniform carbon allotropes.

New laboratory methods for the chemical syntheses of PAHs were pioneered by the *Scholl* group [23,24,25] and *Clar* group[26,27,28], and further developed throughout the entire 20th century. The typical strategy toward extended PAHs is based on the intramolecular dehydrogenation for conversion of the corresponding 3D dendritic or hyperbranched oligophenylenes into quasi-zero-dimensional nanographenes. Following this synthetic strategy, a series of PAHs (from **1-3** to **1-16** in Figure 1-2, C_n, n = 42[29], 48[30], 52[31], 60[32,33], 70[34], 72[35], 78[36], 80[37], 96[38], 114[30], 132[39], 150[40], and 222[41]) comprising an inconceving number *n* of sp^2-hybridized carbons has been rationally build up, and characterized with the advanced analytical techniques (Figure 1-5). Starting from the most basic units of graphene, namely benzene rings (C6), the frontier of the synthetic nanographene derivatives has been gradually pushed forward to hexa-*peri*-hexabenzocoronene (**1-3**, C_{42}), tetrabenzo[8]circulene (**1-4**, C_{48}), and ultimately to a disk-shaped nanographene consisting of 222 sp^2-carbon atoms with the approximate diameter of 3.0 nm, which all show size-dependent optical energy gaps.

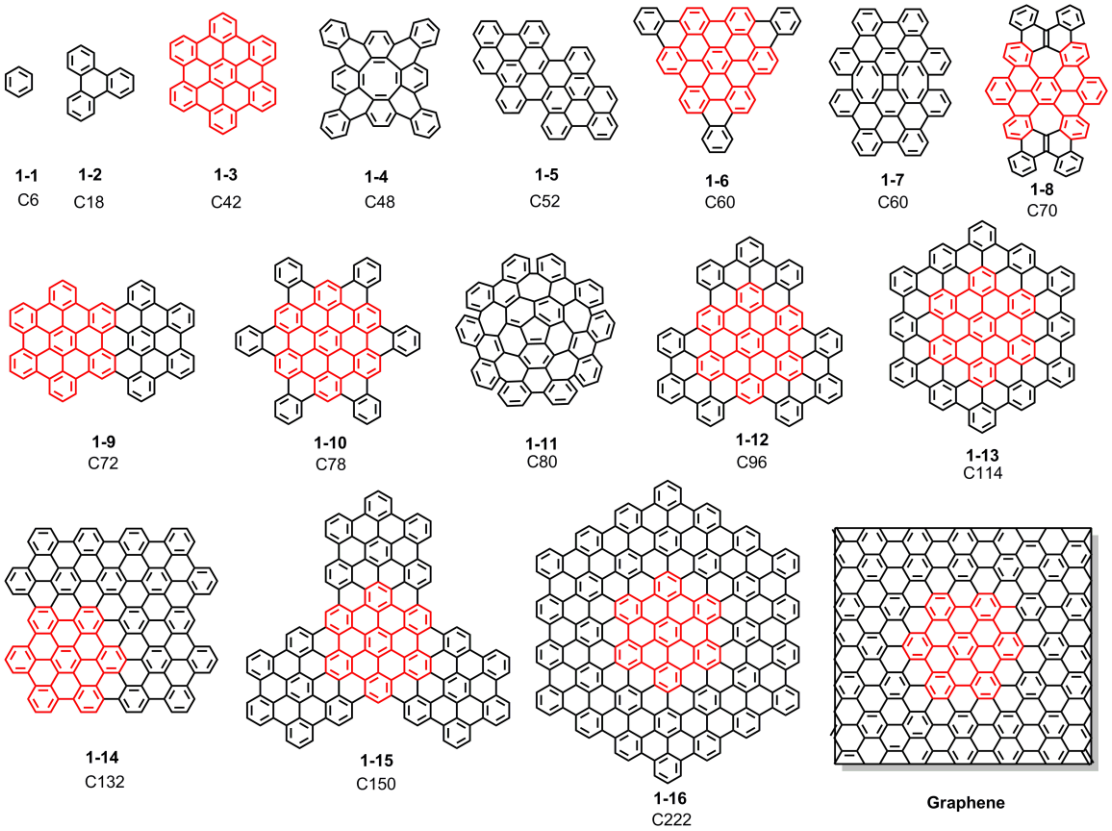

Figure 1-4. Structural evolution from benzene (**1-1**, C_6), triphenylene (**1-2**, C_{18}), to nanographene (from **1-3** to **1-16**, C_n, n = 42, 48, 52, 60, 70, 72, 78, 80, 96, 114, 132, 150, and 222), and ultimately to 2D infinite sheets of sp^2 carbon (Graphene, $\mathbf{C}_\infty$)

For these extended PAHs, no matter if planar or curved, they all are structurally featured as confined nanosized segments of graphene. As a consequence of the strong π-stacking between each molecule, the derivatives of these PAH have the tendency to form highly ordered columnar structures in the solid state, and the overlapped π-orbital area of the PAHs in the column qualify them as active semiconductors in organic field effect transistors and photovoltaic devices.[42] However, the further exploration of the frontiers of synthetic nanographenes has halted at the construction of PAH **1-16**, which was attributed to the complicated arrangement of benzene rings and incomplete dehydrogenation reaction in the last annulations process toward PAHs. Furthermore, the current characterization techniques also failed to analyze the insoluble PAHs with high molecular weight and melting temperature. Therefore, the bottom-up synthesis of graphene still requires a lot of efforts and the cooperation between different fields.

1.2 Elusive one-dimensional *sp*-carbon allotropes and its synthetic substructures

As a consequence of the remarkable physical properties of the sp^2-carbon allotropes (such as fullerene, carbon nanotube, and graphene) discovered until now, it has been quite appealing to develop new synthetic carbon allotropes. Contrasted with the naturally occurring diamond composed entirely of sp^3-carbons and graphite purely consisting of sp^2-carbons, the carbon allotropes which are completely constructed from *sp*-hybridized carbons remain quite rare both in the real world and scientific community. Spurred by the discovery of the synthetic sp^2-carbon allotropes, the synthesis of *sp*-carbon allotropes began to attracte considerable interest from the field of chemistry and material science

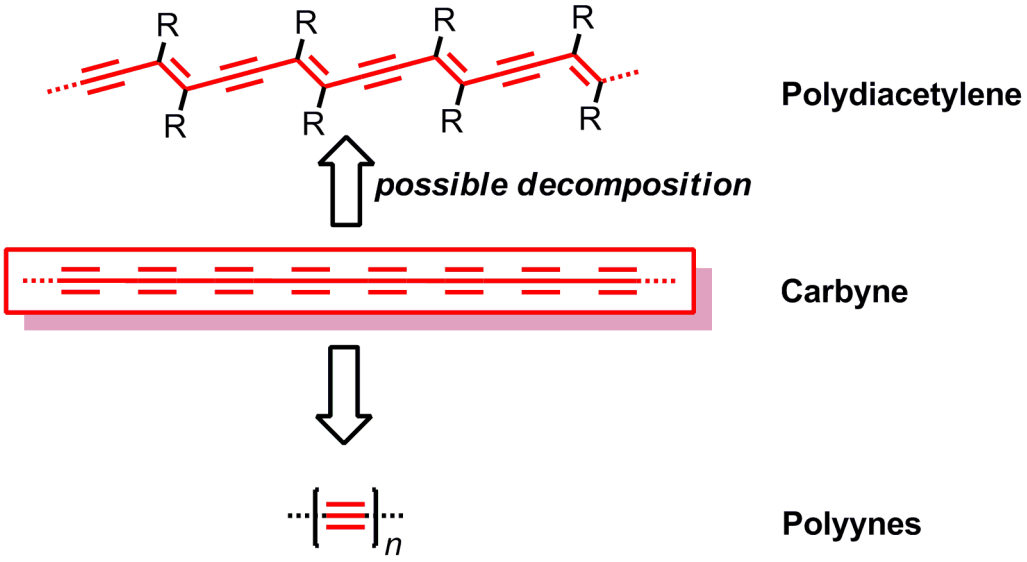

Figure 1-5. Structural scheme of 1D allotrope of *sp*-carbons and its possible decomposition approach, as well as the polyyne analogues.

As the simplest synthetic allotrope, carbyne is a 1D *sp*-carbon allotrope composed of chains of *sp*-hybridized carbon atoms with alternating single and triple bonds. Parallel with the discovery [43,44] and development [45,46] of this fascinating allotrope since 1960s, the structural identification has remained controversial for a long time due to a lack of the crystalline form of carbyne with defined structure and sufficient length.

Furthermore, the existence of the such an allotrope under ambient conditions has been discussed for a long time because of its instability which probably originates from the interchain exothermal crosslinking of the linear carbons,[47] like the 1,4-addition polymerization toward polydiacetylene (Figure 1-7)[48].

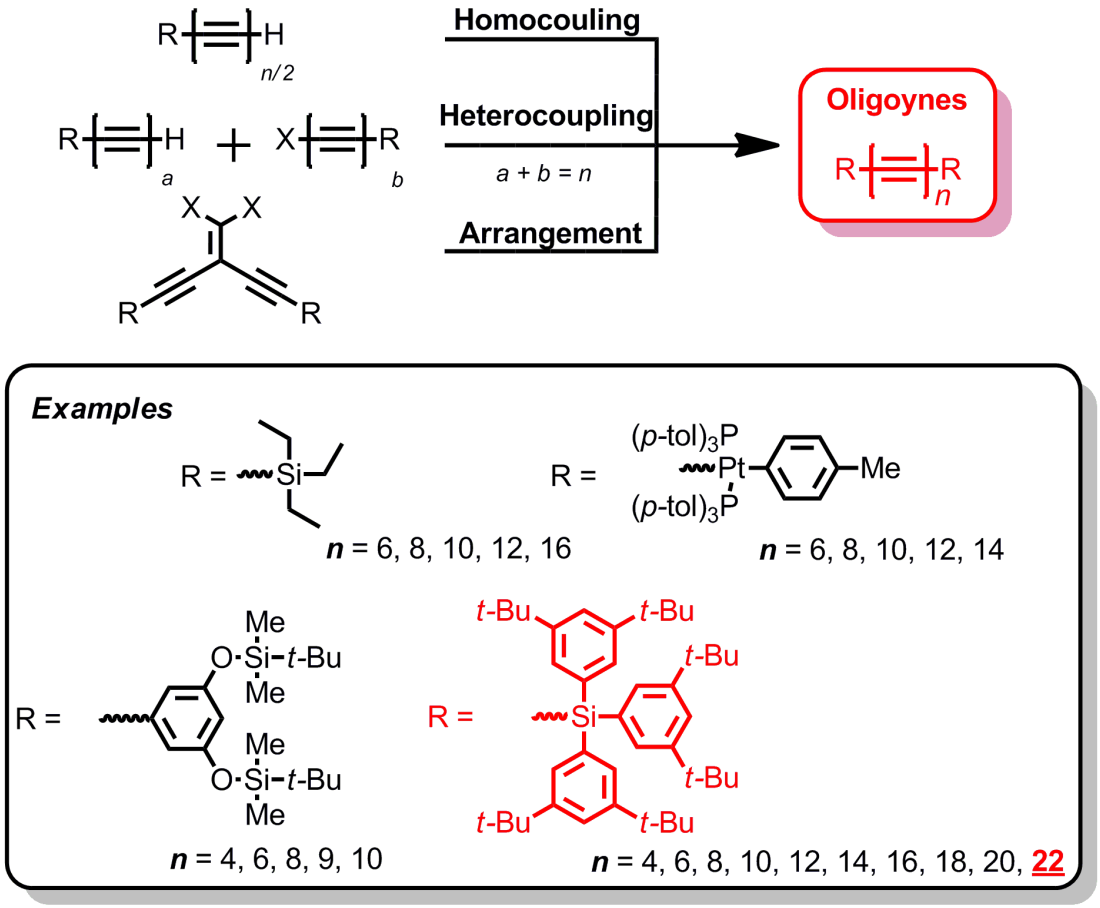

Figure 1-6. Synthetic approaches toward oligoynes with various sterically bulky end-capping units and number (*n*) of acetylene repeating units.

However, intrigued by the possible extraordinary properties, such as high strength and high modulus comparable with diamond, this mysterious allotrope still attracted a lot of interest. These continuing efforts have ultimately furnished the synthesis of short oligomer subunits of carbyne, namely the polyyne derivatives composed of acetylene segments with defined length.[49,50] A series of oligoynes with diverse number of acetylene repeating units have been successfully obtained by the oxidative homocoupling[51] or heterocoupling[52,53] of acetylene precursors[54,55], or the eliminative arrangement reaction (such as the Fritsch-Buttenberg-Wiechell

rearrangement of carbene/carbenoid intermediates[56]) of corresponding precursors in the last step toward oligoynes[57,58,]. In order to obtain uncontestable oligoyne samples which are stable at ambient condition, various sterically-demanding end-capping groups[59] were introduced as protective moieties into the oligoyne chains to stabilize the targeted long carbyne-like oligoacetylene chains. Among these are triethylsilyl [60], 3,5-di(*tert*-butyldimethylsiloxyl)-phenyl[61], and *p*-tolyl-substituted platinum units abbreviated as {Pt(*p*-tol)[P(*p*-tol)$_3$]$_2$}[62]. Numerous investigations have also unambiguously revealed the dependence of the number (*n*) of acetylene repeating units in stable oligoyne samples on the structure of the end-capping groups (Figure 1-8).

Based on these oligoyne derivatives with well-defined structure and various lengths, the expected physical properties of the ultimate carbyne allotrope with infinite length can be evaluated by the convergence of the physical properties of these oligomers with their length approaching a constant value.[63] Until now, the longest stable oligoyne sample obtained consists of 44 contiguous acetylenic carbons and end protected with the extremely bulky tris(3,5-di-t-butylphenyl)methyl moiety.[64] Taking into account the convergence behavior of the rigid π-conjugated oligo- and polymers, a solution bandgap of 2.56 eV (λ_{max} = 485 nm) could be estimated for the 1D infinite *sp*-carbon allotrope carbyne [65].

However, there still seems to be a limit of the repeating unit number (*n*) of stable oligoynes approached by the conventional synthetic strategies, and these synthetic efforts have also spontaneously resurged the interest to construct this intriguing and hypothetical linear form of carbon *via* other methods. In an attempt to synthesize this very long linear and unstable *sp*-carbon allotrope, trapping the chains of carbynes in a confined space or matrix to overcome the instability issue appears to be the most promising method to obtain well-defined or indisputable sample of this allotrope.[66] Following this strategy, an exceptionally long and stable carbyne chain with more than 6,000 *sp*-carbon atoms was produced with protection in a double-walled CNTs.[67]

Considering the expected amazing electronic and mechanic properties of carbynes, both the bulk production of carbyne and solution-based synthesis of end-capped polyyne would definitely further push forward the investigation and application of this theoretical carbon allotrope in the future.

1.3 Elusive two-dimensional *sp*-sp^2-hybridized-carbon materials and its synthetic substructures

In the past decade, the extraordinary electronic properties of the 2D graphene sheet of sp^2 carbons have vigorously stimulated the exploration of 2D carbon allotropes. Furthermore, the infinite combinations of *sp*, sp^2, and sp^3-hybridized carbon atoms in the carbon frameworks have rendered numerous possibilities for constructing new 2D carbon allotropes.

1.3.1 Graphyne and its synthetic substructures

Graphyne, structurally featured as a diverse family of carbon allotropes consisting of 2D planar sheets containing only *sp* and sp^2-carbon atoms, was firstly proposed by a visionary group of theoreticians led by A. T. Balaban as a 2D non-natural carbon allotropes at 1968[68]. By modulating the arrangement of the *sp* and sp^2 carbons in the periodical carbon networks, a diversity of graphynes with minimized steric hindrance and strain within the 2D plane can be hypothesized, such as α-graphyne, β-graphyne, and γ-graphyne demonstrated in Figure 1-9. [69], Reliable predictions of the physical properties of these new allotropes based on theoretical calculations have convincingly revealed the existence of versatile Dirac cones in these novel 2D carbon materials, which suggests comparable or even better electronic properties than that of the well-known graphene[70,71]. Although these allotropes are thermodynamically unstable when compared with graphite, these phases are predicted to exhibit kinetic stability and hence be resistant to the graphitization. [72]

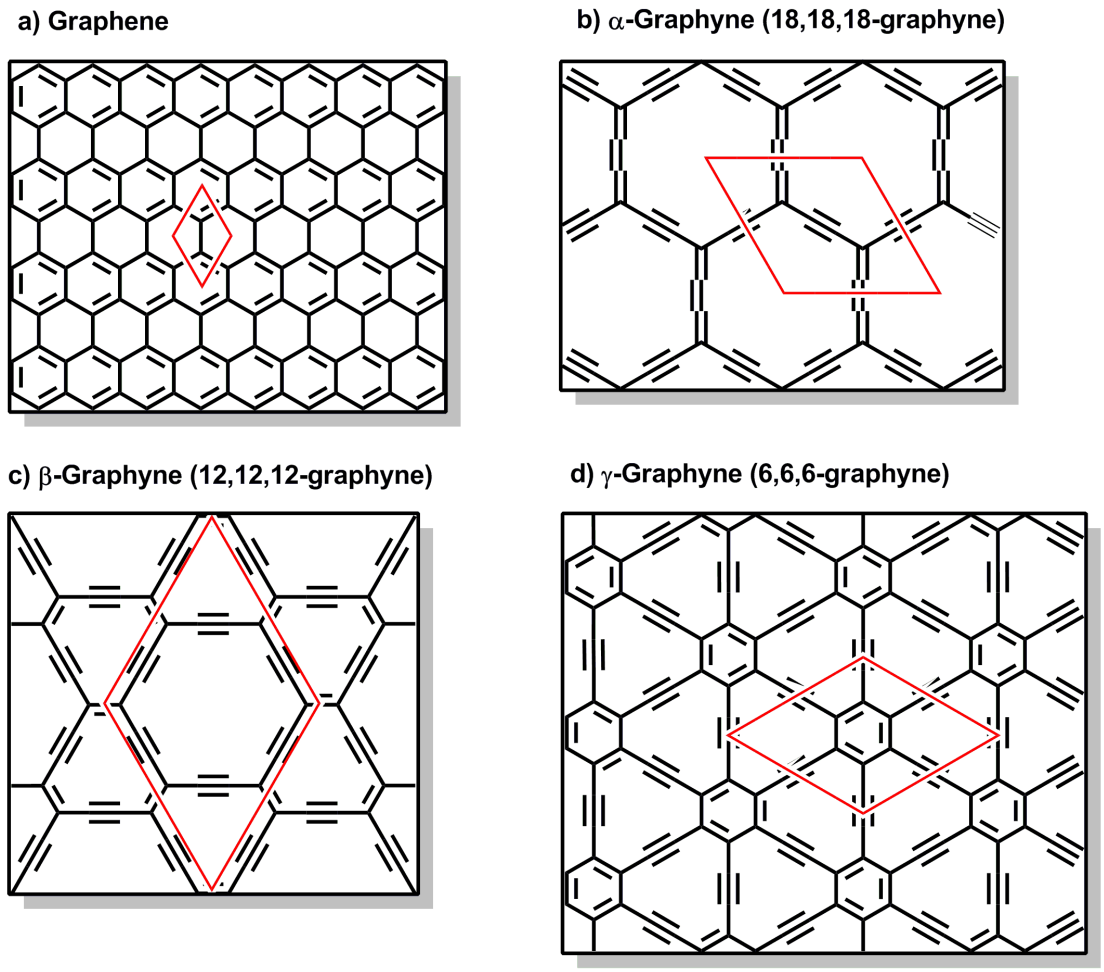

Figure 1-7. Schematic illustration of (a) graphene, and other three possible graphynes: b) α-graphyne, c) β-graphyne, d) γ-graphyne. Red quadrangle indicates the unit cell.

Although the synthesis of graphynes still remains elusive, kind of small substructures of these infinite 2D carbon allotropes composed of *sp* and sp^2-hybridized carbons have been initially identified by the synthetic chemistry of dehydrobenzoannulenes (DBA), and then extensively developed in the past decades. Hexadehydrotribenzo[12]annulene ([12]DBA, **1-17**), envisioned structurally as the smallest macrocyclic subunit of γ-graphyne, has been synthesized firstly with low yield 40 year ago[73,74], and numerous improvement have been accomplished for the synthesis to increase the yield of this macrocyclic subunit over the past four decades[75].

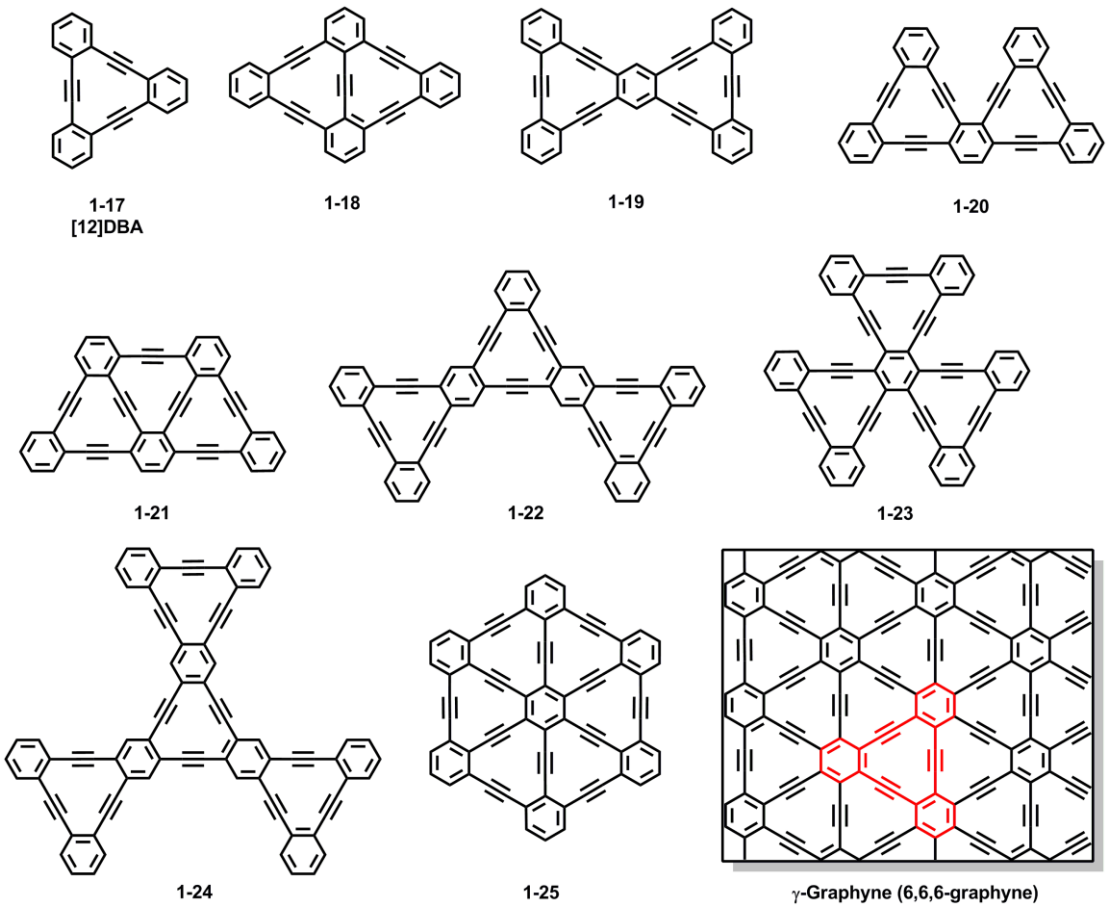

Figure 1-8. Synthetic subunits of γ-graphyne based on the dehydrobenzo[12]annulene.

Additionally, a variety of multiply fused [12]DBAs derivatives has been synthesized as the nanosized substructures of γ-graphyne[76,77], such as the "rhombic-shaped" bis[12]DBA **1-18**,[78,79] "bowtie-shaped" bis[12]DBA **1-19**[80,81], "boomerang-shaped" bis[12]DBA **1-20**[82], "trapezoid-shaped" tris[12]DBA **1-21**, "linear-shaped" tris[12]DBA **1-22**[83], "trefoil-shaped" tris[12]DBA **1-23**[84], and "star-shaped" tetrakis[12]DBA **1-24**[85]. (Figure 1-11) However, the ultimate "wheel-shaped" hexakis[12]DBA **1-25**, a substructural motif of γ-graphyne, has not been successfully synthesized yet until now. Meanwhile, the thermo-stability of these [12]DBA derivatives under high temperature, which possess melting points within the range of 250-300 ℃, also further confirm the stability of the robust graphyne allotrope.

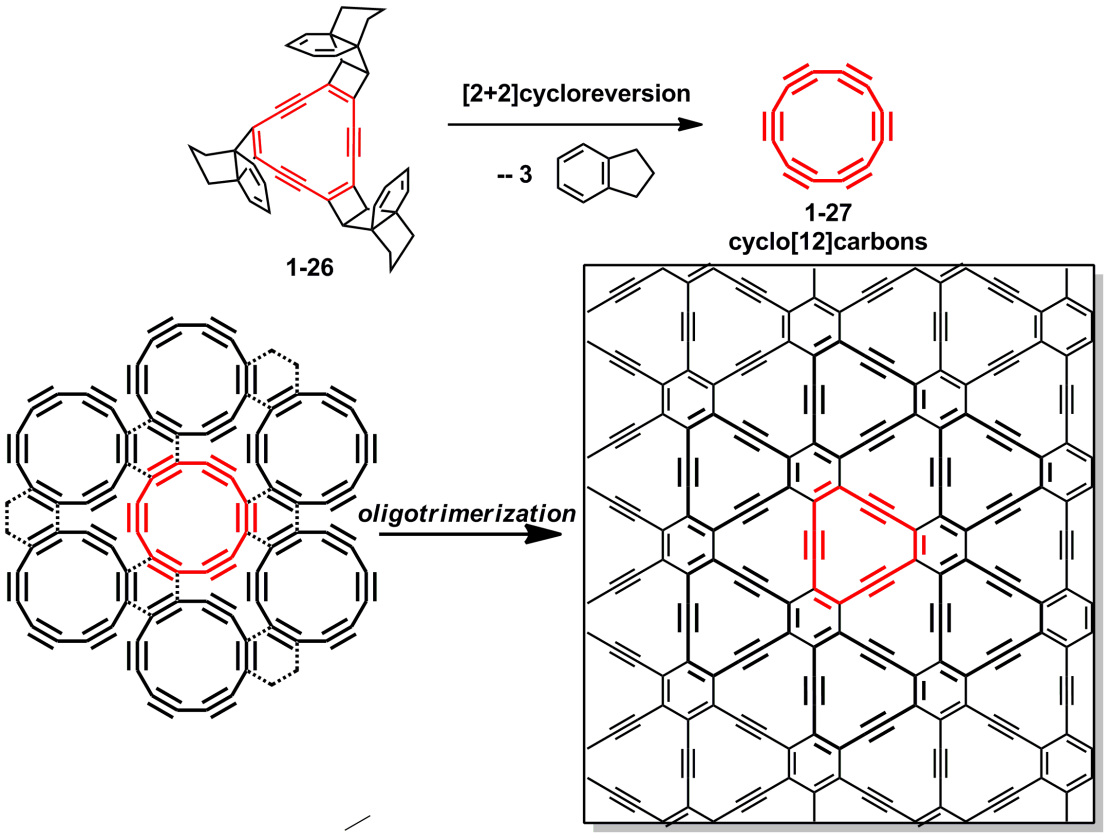

Figure 1-9. Structural illustration of elusive 2Dcarbon allotropes composed of *sp*- and sp^2-carbons, γ-graphyne, which can be synthesized by the oligotrimerization of Cyclo-C_{12} **1-27.**

Although numerous macrocyclic segments have been conceivably prepared as the network mimics of γ-graphyne, this infinite 2D carbon allotrope still remains elusive. In the pioneering works of F. Diederich at 1994[86], one synthetic route toward the 2D γ-graphyne has been proposed by the controlled cyclotrimerization of the cyclo[12]carbons (**1-27** in Figure 1-12). Although the strategy toward 2D carbon networks of firstly spatially aligning the molecular components into layered structures, and then initiating the reaction between adjacent components to transform the supramolecularly associated layer into extended 2D networks has already been proved in the recent works focusing on the organic synthesis of 2D polymers[87,88], the synthesis and separation of basic component cyclo[12]carbons still remains outside the realm of synthetic endeavors now. [89] Due to the instability of the antiaromatic [*4n*] electron system in cyclo[12]carbons, the targeted building block cyclo[12]carbons can only be experimentally observed in the mass spectrum

measurement. However, the recent development of metal surface catalyzed synthesis of graphene-related materials, such as graphene nanoribbons with defined edge structure and width, [90.91] have shed some light on the future fabrication of bulk graphyne materials.

1.3.2 Graphdiyne and its synthetic substructures

Replacing the acetylene linkages of γ-graphyne with diacetylene segments generates another theoretical *sp*-*sp*^{2} carbon allotrope called graphdiyne, which is theoretically predicted to be to date the most stable non-natural carbon allotrope involving diacetylene motif. Structurally similar to γ-graphyne, the other DBA derivative, namely hexadehydrotribenzo[18]annulene ([18]DBA, **1-28**), can be envisaged as the model substructure for this fantastic allotrope. Compared with the substructures of graphyne (from **1-17** to **1-25**), the synthesis of multiply fused [18]DBA derivatives was much easier due to the ready Cu(I) or Cu(II)-catalyzed homocoupling of terminal acetylene units.[92,93,94] A series of graphdiyne substructures consisted of various number of [18]DBA units and distinctive geometric topologies were synthesized by the group of *M. M. Haley*, such as allotrope subunits containing two[95,96] (from **1-29** to **1-31**), three[97] (from **1-32** to **1-34**), four[98] (from **1-35** to **1-37**) [18]DBA motifs. However, the synthesis of the "full-wheel" shaped hexakis[18]DBA **1-38** was not realized due to the size of the targeted multiply-fused [18]DBA backbone and the number of simultaneous intramolecular homocouplings required for "full-wheel" formation. According to the literature, these new substructures will be unstable and decompose above 200 ℃, which also sheds some light on the stability of this diacetylenic allotrope. [99]

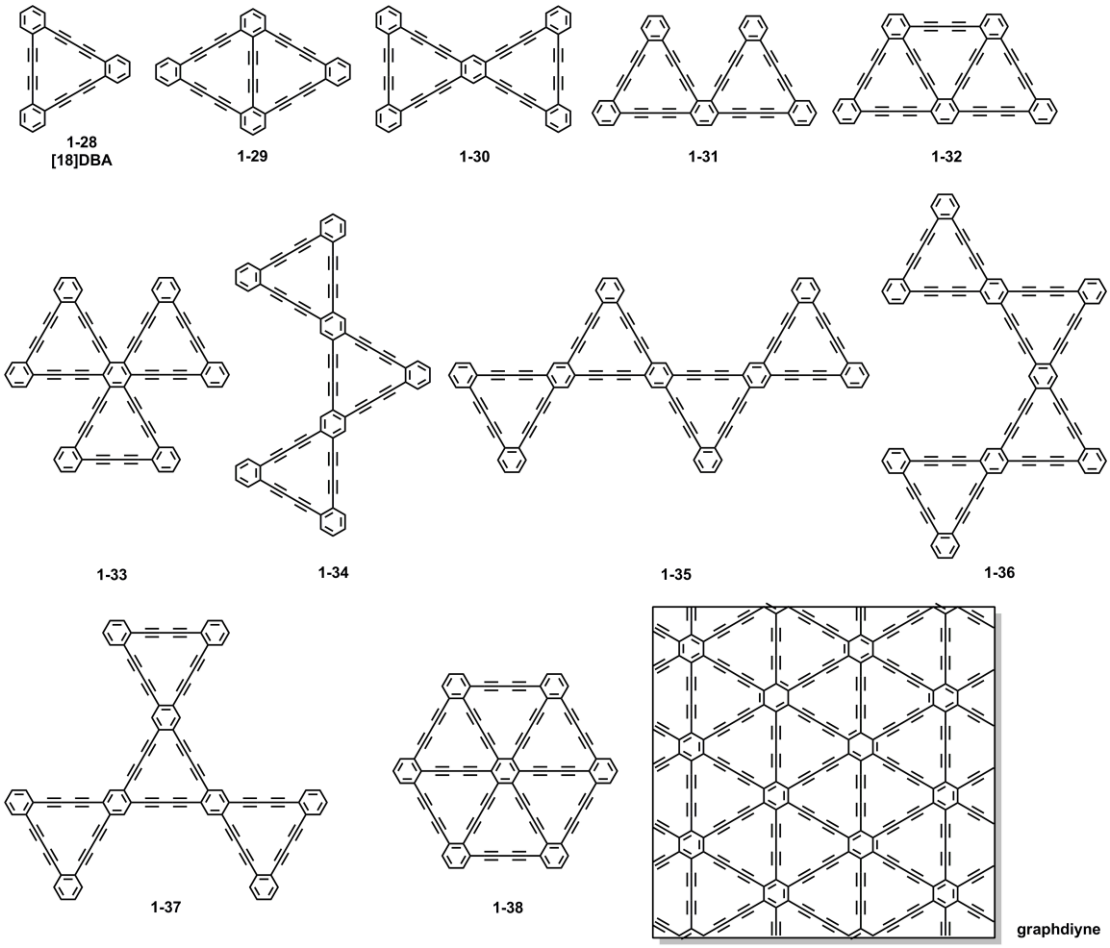

Figure 1-10. Synthetic substructures of graphdiyne based on the dehydrobenzo[18]annulene with different repeating units and topologies.

In attempts to establish feasible methods for the production of graphdiyne., the controlled oligotrimerization[100] of cyclo[18]carbons **1-39**[101] appears to furnish the targeted 2D carbon scaffolding directly, however, the difficulty of isolating large quantities of cyclo[18]carbons sample obviously became the bottleneck for the generation of the bulk graphdiyne materials. Therefore, the fabrication of graphdiyne from hexaethynylbenzene **1-40**[102] *via* the oxidative coupling of terminal acetylene, which have already been proven as a powerful approach for constructing carbon scaffolds and networks.[103]

In 2010, a graphdiyne film with area of 3.61 cm^2 and thickness of about 1 μm has been successfully fabricated on the surface of copper foil by the *in-situ* Glaser coupling reaction of monomer **1-40**, in which the copper ot only function as the substrate for graphdiyne film growth but also as the catalyst in the cross coupling

process.[104] Since then, two following works from the same group have produced graphdiyne nanotubes and nanowires by employing the same synthetic methodology with a template-assisted method[105] and a vapor-liquid-solid growth process[106], respectively. Recently, a group in Peking University has reported a feasible synthetic route toward graphdiyne nanowalls via a modified Glaser-Hay coupling reaction with hexaethynylbenzene **1-40** as the presurcor, in which the fine lattice structure of graphdiyne was confirmed in some areas with high crystallinity. [107] Employing this graphdiyne nanowall materials as the photocathode in photoelectrochemical cells has also convincingly indicated that graphdiyne is a promising metal-free hole-transporting material to fabricate a device for water splitting by solar energy.[108]

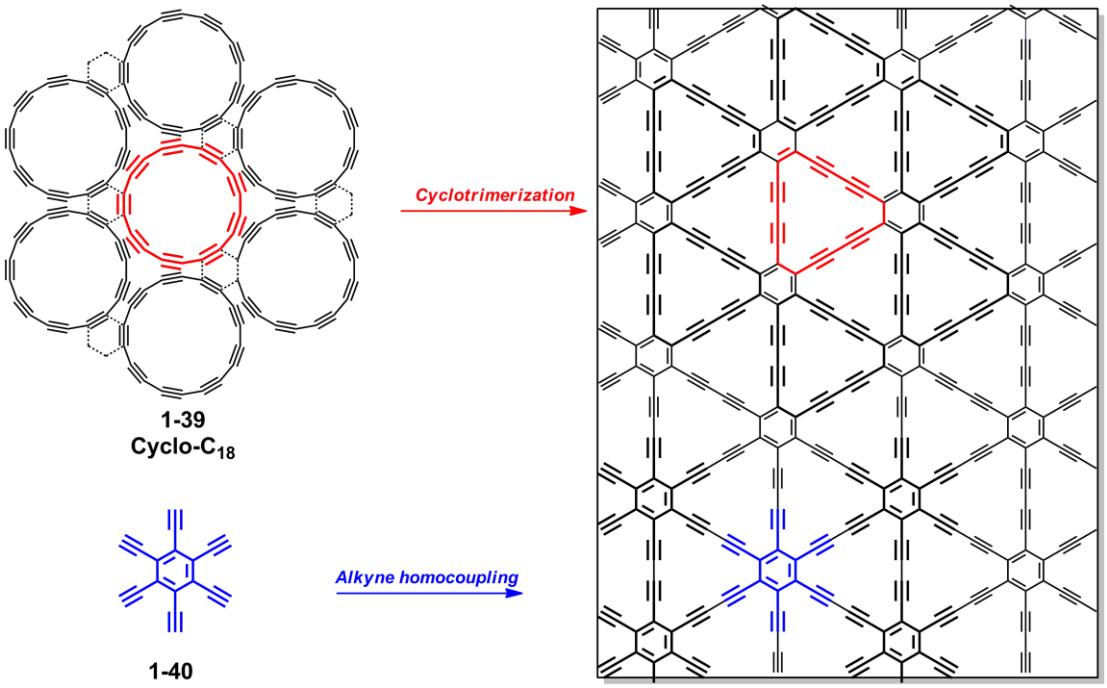

Figure 1-11. Structural illustration of elusive 2D carbon allotrope consisted of *sp*-*sp*^{2}-carbons, namely graphdiyne, which can be synthesized by the cyclotrimerization of Cyclo[18]carbons **1-39** or oxidative homocoupling of hexaethynylbenzene **1-40**.

Structurally featured as a rigid 2D carbon network[109] with delocalized π-system, highly conjugated structures, and uniformly distributed pores, graphdiyne is predicted to be a semiconductor with a band gap of 0.46 eV with a theoretical electron mobility reaching $2*10^5$ $cm^2/(V\ s)$ at room temperature and hole mobility reaching the order of 10^4 $cm^2/(V\ s)$,[110] which is similar to silicon. Owing to these attributes, the

graphdiyne material is forecasted to be promising for various applications[111,112,113] in gas separation,[114,115] lithium-ion storage,[116] electrode materials[117,118] and so on. Therefore, fabricating 2D graphdiyne materials with controlled structures beyond nanosized substructures still remains a challenge and of great significance to the development of synthetic carbon allotropes.

1.3.3 From 2D carbon allotropes to carbon-rich macrocycles

In the past two decades, tremendous efforts have been made toward the construction of monomeric model compounds (mainly [12]DBA, and [18]DBA) and more complicated macrocyclic substructures of non-naturally occurring 2D graphyne and graphdiyne carbon allotropes based on the rebirth of annulene chemistry. A vast majority of these synthetic accomplishments can be attributed to the discovery of efficient synthetic reactions, most notably the Pd-catalyzed cross coupling between *sp* and sp^2 carbons.[119] Owing to these synthetic improvements, the previously laborious macrocycle synthesis now becomes more quick and efficient with the combination of various metal-catalyzed cross-coupling reactions, and template-directed strategies[120].

Parallel to the synthesis of the graphyne and graphdiyne segments[121], the revival of acetylene chemistry also stimulates the development of shape-persistent macrocycles[122,123] with phenylethynyl, phenylbutadiynyl, or both moieties.[124,125] For all these macrocycles with phenylene-ethynylene backbones, the substructures of graphyne and graphdiyne are fully conjugated *ortho*-fused phenylene-ethynylene macrocycles. Through modulating the fusion patterns and linkage moieties,[126] a large variety of *meta*-fused phenylene-ethynylene macrocycles (**1-41**[127], **1-42**[128], and **1-43**[129] in Figure 1-11) and mixed-fused phenylene-ethynylene macrocycles (**1-44**[130], and **1-46**[131,132] in Figure 1-11) have been prepared via the intermolecular oxidative coupling of corresponding dimer units or intramolecular cyclization of defined open-chain oligomers. Due to the stiffness of the acetylene linkage and benzene rings, these phenylene-ehtynylene macrocycles are all endowed with a shape-persistent conformation.

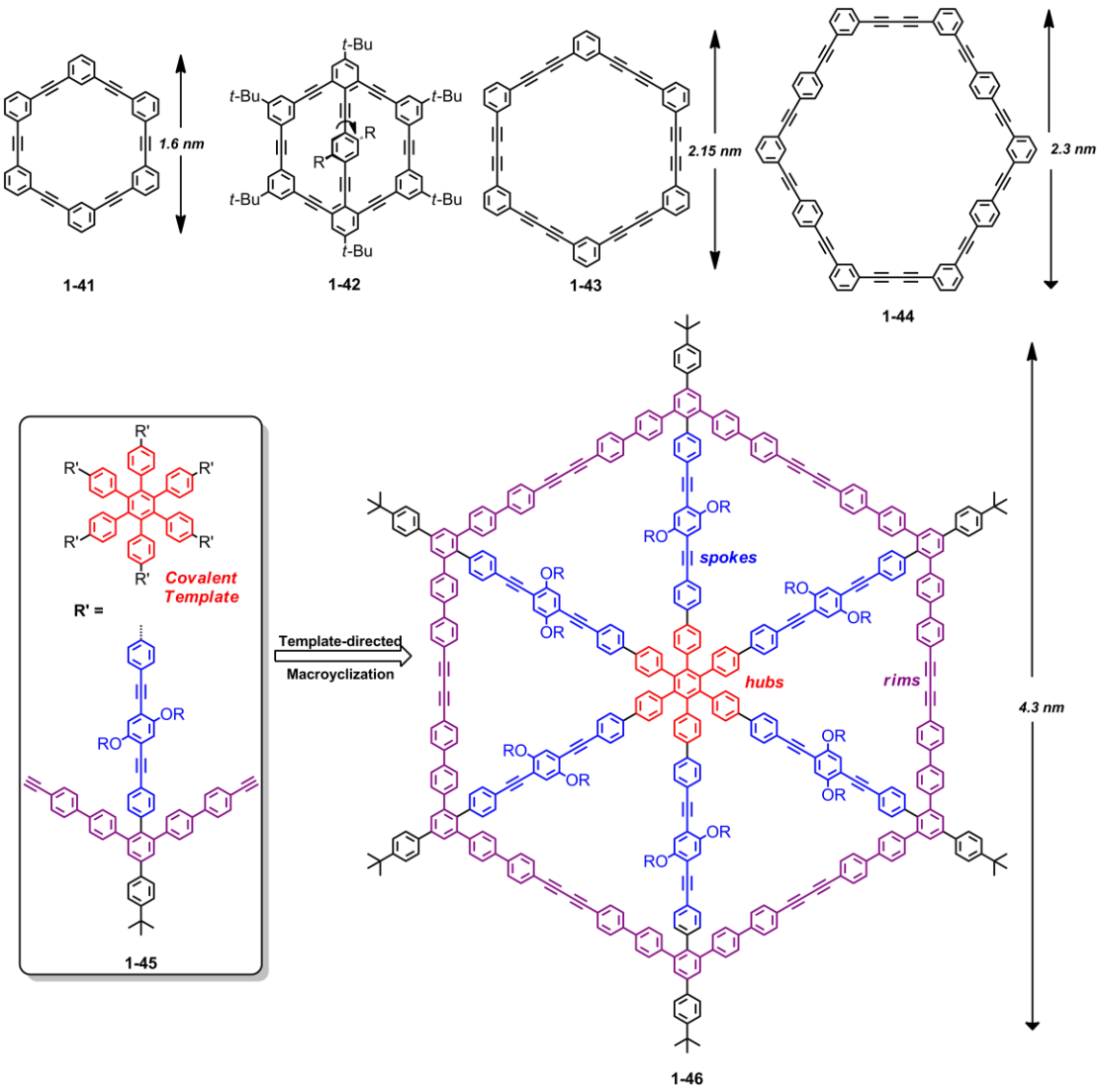

Figure 1-12. Structural illustration for the m*eta*-fused and mix-fused phenylene-ethynylene macrocycles, especially a giant "wheel-like" macrocycle **1-46** with the diameter around 4.3 nm prepared via covalent-template directed appraoches.

Especially with the assistance of a covalent template (such as hexaphenylbenzene unit in precursor **1-45**), the efficiency of intramolecular cyclizations via homocoupling of acetylene groups has been greatly enhanced, which can also guarantee the successful size expansion of the prepared shape-persistent macrocycles. In 2014, the largest shape-persistent macrocycle (**1-47** in Figure 1-12) to data composed of phenylene-acetylene backbones was constructed via covalent template directed cyclization, in which the diameter of the giant molecular has reached approximately12 nm.[133] Despites all these synthetic advances, there still remains a long way for the chemists to go for fabricating 2D carbon allotropes or carbon-rich networks.

And great efforts are still required to resolve the issues concerning the strategy for 2D network expansion and characterization of the usually insoluble resultant.

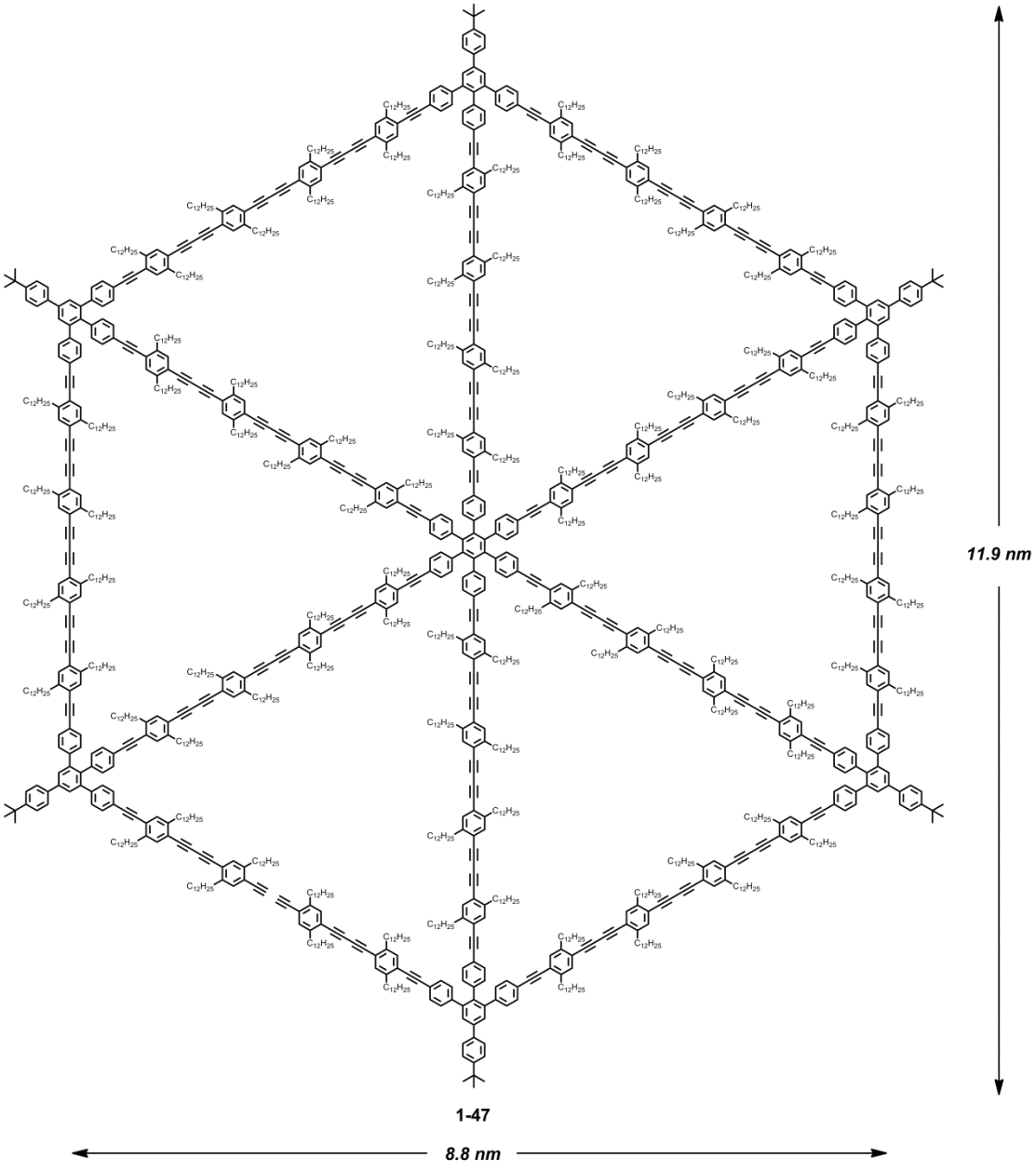

Figure 1-13. Chemical structure of a giant shape-persistent phenylene-ehtynylene macroccyle **1-47** (molecular formular: $C_{1878}H_{2682}$) with a corner-corner diameter of 11.9 nm and a rim-rim diameter of 8.8 nm.

1.4 Elusive three-dimensional sp^2-carbon materials "Cubic Graphite" and its synthetic substructures

1.4.1 Geometric elucidation of "cubic graphite"

Although the allotropes entirely composed of sp^2-hybridized carbons are the most well-investigated class of carbon allotropes, including 0D fullerene, 1D carbon nanotube, 2D graphene, and 3D graphite, the search for new sp^2 carbon allotropes with novel structures are still of great importance when considering the remarkable electronic properties of sp^2 carbon atoms. Motivated by the curved structure of sp^2 carbon networks in fullerene, numerous possible 3D networks of all sp^2-carbon atoms have been proposed at the theoretical level.[134,135,136]

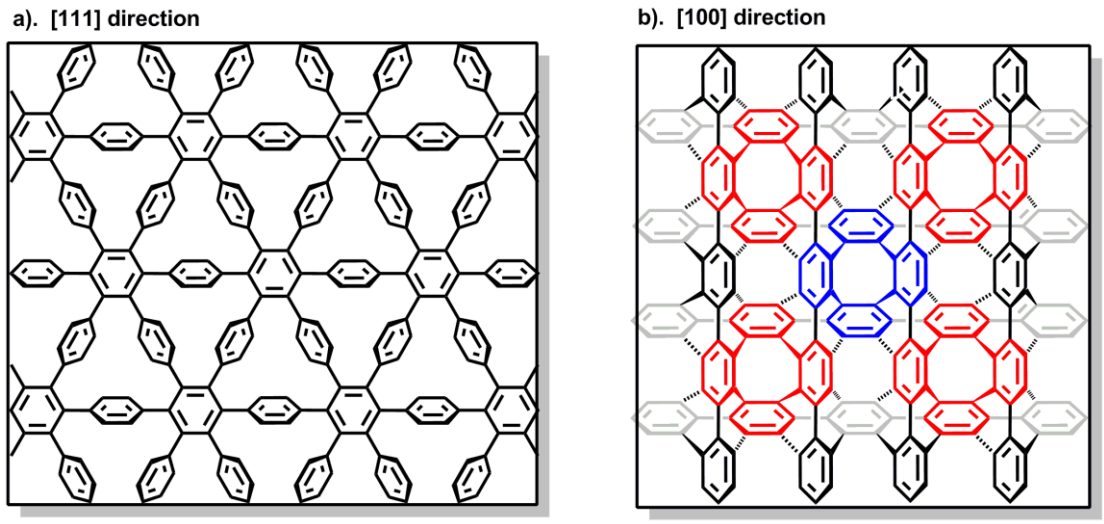

Figure 1-14. (a) Schematic illustration of the heuristic relationship between a graphite sheet and the structure of cubic graphite viewed down the [111] direction. (b) schematic illustration of the relationship between the structure of *o*-tetraphenylene and cubic graphite and the structure of cubic graphite envisaged along the [100] projection.

Among these intriguing structures, only a 3D sp^2-carbon allotrope called "cubic graphite", which has been proposed as early as 1946 by Gibson, Holohan, and Riley,[137,138] appears to be more stable than the well-known synthetic allotrope C60. The specific term "cubic graphite" originated from the cubic symmetry of this 3D

carbon phase (space group Pn-3m) and the relationship between its solid-state structure and that of conventional graphite. This hypothetic carbon phase is composed entirely of benzene rings, with each benzene ring attached to six other neighboring rings via sp^2-sp^2 C-C single bond, and thus this carbon allotrope was also called "polybenzenes" in the theoretical research of O'Keeffe at 1992.[139] additionally, this carbon phase is also forecasted to be an indirect semiconductor with band gap of 2.89 eV.[140]

Viewing the cubic graphite from the [111] direction of the hypothetic crystal structure, the entire carbon phase is envisaged to be composed of infinite 2D polyphenylene networks as shown in Figure 1-14(a) with a model substructure **1-48**, which is constructed by breaking one-sixth of the carbon-carbon bonds in a monolayer graphite sheet. Two-third of the benzene rings of the 2D polyphenylene layer are tilted out of the plane with a degree of 70.5 °, which permits the interlayer covalent bond formation to form 3D cubic graphite. These intersheet covalent bond between those tilted phenylene rings and identical rings in the adjacent layer **1-48** (as shown in the Figure 1-15) led to the formation of 3D sp^2-carbon allotrope, in which all the carbon atoms are equivalent. The resulting structure is also free of strain due to the absence of any distortions of C-C-C bond angles from 120 °, which also makes this allotrope far more stable than C60.

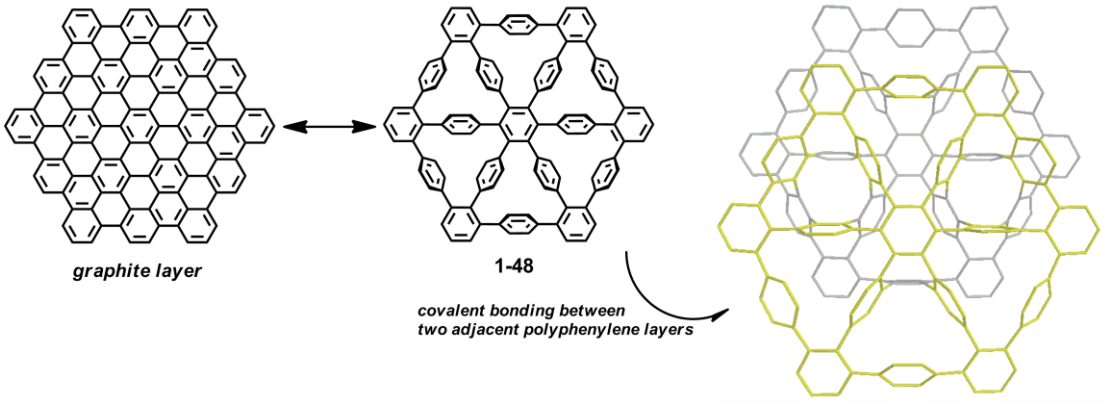

Figure 1-15. Schematic illustration between the 2D graphite sheet, 2D polyphenylene network (**1-48**), and 3D cubic graphite.

The theoretical C-C bond lengths in cubic graphite are predicted to be 1.396 Å in the

benzene rings and 1.474 Å between the benzene rings, which are quite close to the average length in the crystal structure of hexaphenylbenzene, 1.397 Å and 1.499 Å respectively.[141] This geometric consistence also further confirms the close structural relationship between cubic graphite and the 2D polyphenylene networks with the substructure **1-48**, which is composed of densely connected hexaphenylbenzene units.

The images obtained from the [100] projection of cubic graphite structure also implied that the complete connection and annelation of *o*-tetraphenylenes will also give the 3D sp^2-carbon network with the space group Pn-3m.[142] For example, the multiply fused *o*-tetraphenylene derivative **1-49** composed of five annelated *o*-tetraphenylene moieties could be directly observed in the cubic graphite from the [100] direction (Figure 1-16). The formation of the o-tetraphenylene moiety can also be envisioned in the covalent bond formation between the tilted benzene rings of adjacent 2D polyphenylene sheets.

Therefore, both the hexaphenylbenzene and *o*-tetraphenylene can be imaged as the model compound of the fantastic 3D sp^2-carbon allotrope from the viewpoint of chemists. Although the strain inside the allotrope is quite small, the prospect for fabricating such a complicated carbon allotrope is still vague due to both thermodynamic and kinetic considerations. Firstly, this carbon phase is not a thermodynamically preferred form of carbon when compared with graphite, and is predicted to be about 5.5 kcal/mol higher in energy for each carbon atom than graphite.[143] The synthesis is also kinetically disfavored due to the inadequate space in the carbon lattice to accommodate the reagents required for the new C-C bonds. However, there are still some substructures of cubic graphite been successfully synthesized, which can help shed some light on the geometry and channel structure inside the allotrope.

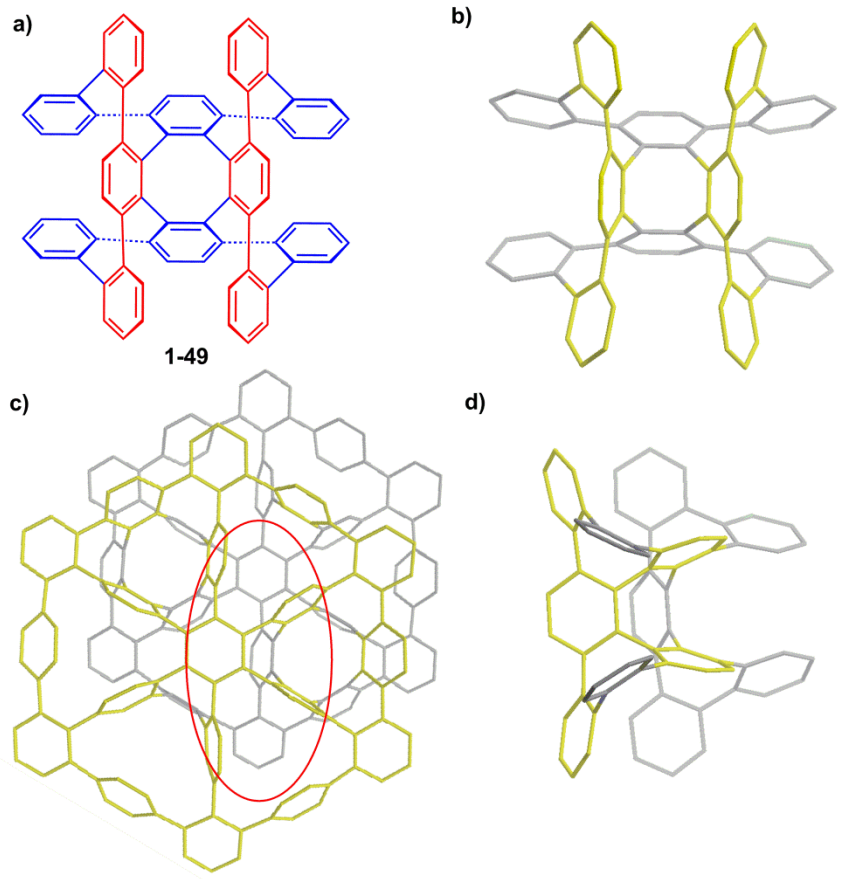

Figure 1-16. a) Structural illustration of the multiple fused *o*-tetraphenylene unit **1-49** in the cubic graphite; b) simulated geometry of **1-49**; c) bilayer structure of the cross-inked 2D polyphenylene networks **1-48**; d) illustration of the relationship between the multiple fused *o*-tetraphenylene unit **1-49** and the cross-linked 2D polyphenylene networks.

1.4.2 Synthetic substructures of "cubic graphite" based on hexaphenylbenzene

Taking into account the *o*-tetraphenylene and *hexa*-phenyl-benzene topology in the carbon lattice of cubic graphite, several polyphenylene nanostructures[144,145] with similar topology have been synthesized by the group of Robert A. Pascal, Jr. To alleviate the crowding effect of those benzene rings in cubic graphite, the benzene moieties in *o*-tetraphenylene and *hexa*-phenyl-benzene topology are replaced by a much larger oligophenylene unit, *hexa*-phenyl-benzene unit, which will be linked in the same fashion as the benzene rings in cubic graphite.

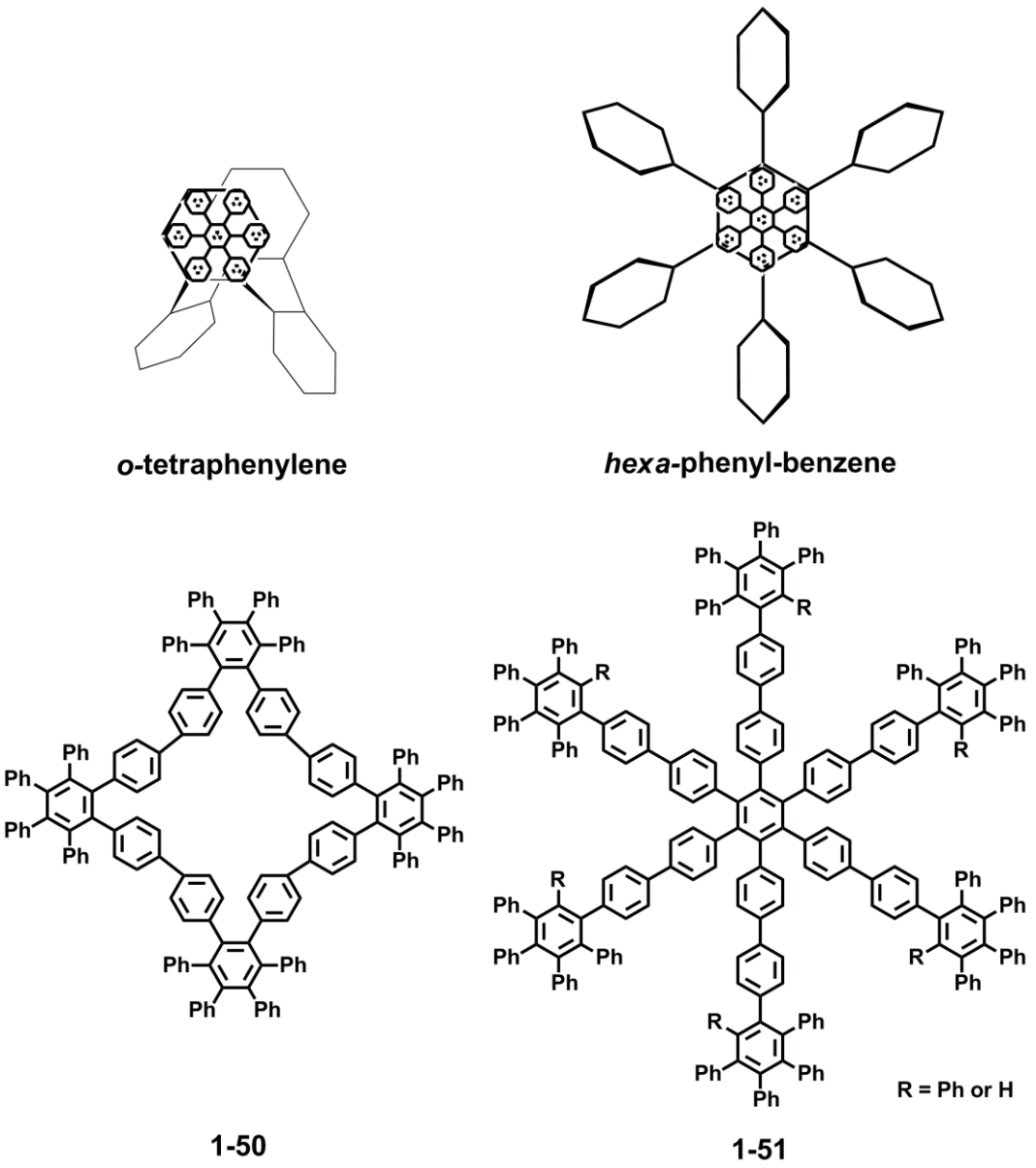

Figure 1-17. Polyphenylene nanostructures **1-50** and **1-51** with the topology similar to *o*-tetraphenylene and *hexa*-phenyl-benzene as the phenylogous substructures of cubic graphite.

The oligophenylene macrocycle **1-50**[146,147] with the molecular topology identical to *o*-tetraphenylene has been prepared via various approaches. The single crystal structure of this compound has confirmed the existence of a large central cavity in the crystal, which is occupied by the solvent molecules. In addition, the molecules of **1-50** are packed in a manner that forms large and infinite channels in the crystal, which is also a structural feature in the cubic graphite. The "propeller shaped" polyphenylene dendrimer **1-51**[148] related to the "cubic graphite" was also synthesized, in which all

the six peripheral *hexa*phenylbenzene rings rotate out of the plane for minimizing the steric strains.

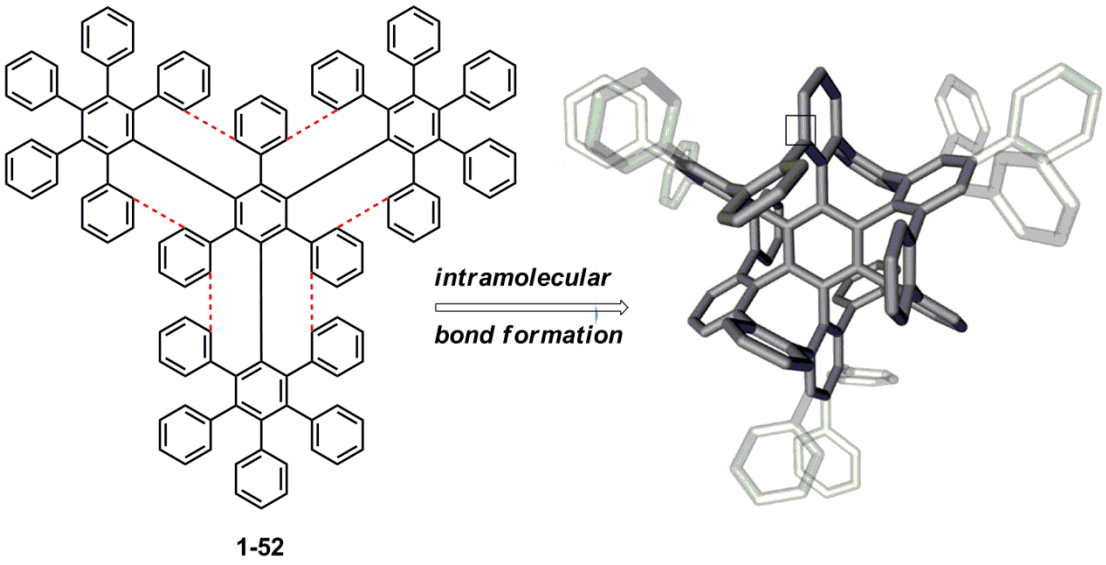

Figure 1-18. Necessary bond formations from crowded oligophenylene **1-52** (red dotted lines) towards a cage-containing subunit of cubic graphite.

An extremely crowded oligophenylene **1-52** based on hexaphenyl-benzene moiety was constructed via the Diels–Alder cycloaddition reaction in the group of K. Müllen.[149] The densely packed benzene rings render the possibility for this molecular to construct the cage-containing substructure of cubic graphite via six intramolecular bond formation as shown in Figure 1-14. Although the crowded environment would strongly attenuate the access of catalyst and thus prohibit the generation of intermediates, the efforts to search for more efficient synthetic approaches and create suitable precursors toward this challenging carbon allotrope is still worthwhile for developing novel and intriguing carbon phases.

1.4.3 Synthetic substructures of "cubic graphite" based on *o*-tetraphenylene

As implied by the structure projected from the [100] direction of cubic graphite, this 3D carbon network can also be conceived as completely connected *o*-tetraphenylene networks. A 1D double helical polyphenylene molecular **1-55** with sequentially annelated *o*-tetraphenylene units can be derived from this carbon phase. [150] The

group of A**.** Rajca has reported the successful synthesis of the double helical octaphenylene **1-54** by direct oxidative coupling of corresponding *o*-tetraphenylene monomer **1-53**. However, the synthesis of higher homologoues of **1-54**, especially the double helical polymer **1-55**, still remains a synthetic challenge until now due to the low yield of *o*-tetraphenylene formation and enantioselective coupling between homochiral building blocks.

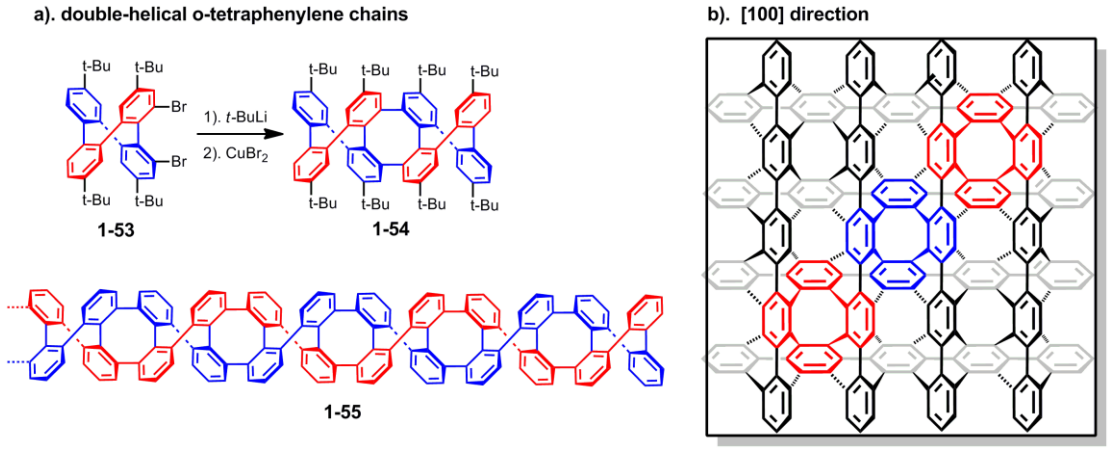

Figure 1-19. a) Synthetic routes toward the double helical octaphenylene **1-54**, and its utilmate double helical polyphenylene molecule **1-55** which can be derived from cubic graphite; b) schematic illustration of the existence of double helical *o*-tetraphenylene chains **1-55** in cubic graphite.

In the attempts to construct such fascinating double helical structure, which is common in the geometry of DNA structures, the recent development of helicenes,[151,152,153] which also belong to a big family of polyaromatic molecules and twisted and distorded π-systems, would definitely shed some light on the construction of helical oligophenylene backbones.

In summary, the chemistry of carbon has definitely dominated current organic chemistry, which can be directly verified from the classical organic chemistry textbook that are categorized according to different carbon-based functional groups. The emerging carbon materials with outstanding material properties are also attracting the efftorts from the community of material science and engineering, represented by the existing graphene and carbon nanotubes. At this age when the silicon-based

matreials and technology are approaching their fundamental bottlenecks, the exploration of synthetic carbon materials and carbon-rich systems targeting the fabrication of electronic devices is highly promissing. Therefore, synthetic carbon materials and networks with aesthetically appealing architectures and promising materials properties define a research area worthwhile of increased efforts and attentions. However, to fully investigate the possible structure combinations for carbons materials and realize their application in diverse areas like nanoelectronics, considerable fundamental research to construct different carbon networks with novel structures and binding patterns still remains necessary.

Reference

[1] A. M. Mannion, Carbon and its Domestication (Springer, **2006**).

[2] H. R. Karfunkel, T. Dressler, *J. Am. Chem. Soc.* 1992, *114*, 2285.

[3] F. Diederich, Y. Rubin, *Angew. Chem. Int. Ed.* **1992**, *31*, 1101.

[4] F. Diederich, M. Kivala, *Adv. Mat.* **2010**, *22*, 803.

[5] H. Andreas, *Nat. Mat.*, **2010**, *9*, 868.

[6] H. W. Kroto, J. R. Heath, S. C. O'Brien, R. F. Curl, R. E. Smalley, *Nature*, **1985**, *318*, 162.

[7] S. Iijima, *Nature*, **1991**, *354*, 56.

[8] S. Iijima, T. Ichihashi, *Nature*, **1993**, *363*, 603.

[9] D. S. Bethune, C. H. Kiang, M. S. De Vries, G. Gorman, R. Savoy, J. Vazquez, R. Beyers, *Nature*, **1993**, *363*, 605.

[10] H. Omachi, Y. Segawa, K. Itami, *Acc. Chem. Res.* **2012**, *45*, 1378

[11] S.E. Lewis, *Chem. Soc. Rev.*, 2015, **44**, 2221.

[12] R. Jasti, J. Bhattacharjee, J. B. Neaton, C. R. Bertozzi, *J. Am.Chem. Soc.* **2008**, *130*, 17646.

[13] S. Yamago, Y. Watanabe, T. Iwamoto, *Angew. Chem., Int. Ed.* **2010**, *49*, 757.

[14] H. Takaba, H. Omachi, Y. Yamamoto, J. Bouffard, K. Itami, *Angew. Chemie Int. Ed.* **2009**, *48*, 6112.

[15] J. Xia, M. R. Golder, M. E. Foster, B. M. Wong, R. Jasti, *J. Am. Chem. Soc.* **2012**, *134*, 19709.

[16] Y. Ishii, S. Matsuura, Y. Segawa, K. Itami, *Org. Lett.* **2014**, *16*, 2174.

[17] T. Iwamoto, E. Kayahara, N. Yasuda, T. Suzuki, S. Yamago, *Angew. Chemie Int. Ed.* **2014**, *53*, 6430.

[18] T. Nishiuchi, X. Feng, V. Enkelmann, M. Wagner, K. Müllen, *Chemistry* **2012**, *18*, 16621.

[19] H. Omachi, T. Nakayama, E. Takahashi, Y. Segawa, K. Itami, *Nature Chem.* **2013**, *5*, 572.

[20] K. S. Novoselov, A. K. Geim, S. V. Morozov, D. Jiang, Y. Zhang, S. V. Dubonos, I. V. Grigorieva, A. A. Firsov, *Science*, **2004,** *306***,** 666.

[21] A. Narita, X. Y. Wang, X. L. Feng, K. Müllen, K, *Chem. Soc. Rev.* **2015**, *44*, 6616.

[22] L. Chen, Y. Hernandez, X. L. Feng, K. Müllen, *Angew. Chem., Int. Ed.*, **2012**, *51*, 7640.

[23] R. Scholl, C. Seer, *Liebigs Ann. Chem.*, **1912**, *394*, 111.

[24] R. Scholl, C. Seer, *Chem. Ber.*, **1922**, *55*, 330.

[25] R. Scholl, C. Seer, R. Weitzenböck, *Chem. Ber.*, **1910**, *43*, 2202.

[26] E. Clar, J. F. Stephen, *Tetrahedron*, **1965**, *21*, 467.

[27] E. Clar, W. Schmidt, *Tetrahedron*, **1979**, *35*, 2673.

[28] E. Clar, D. G. Stewart, *J. Am. Chem. Soc.*, **1953**, *75*, 2667

[29] A. Stabel, P. Herwig, K. Müllen, J. P. Rabe. *Angew. Chem. Int. Ed.* **1995**, *34*, 1609.

[30] Y. Sakamoto, T. Suzuki, *J. Am. Chem. Soc.*, **2013**, 135, 14074.

[31] T.-A. Chen, R.-S. Liu, *Chem. – Eur. J.*, **2011**, *17*, 8023.

[32] X. L. Feng, J. S. Wu, M. Ai, W. Pisula, L. J. Zhi, J. P. Rabe, K. Müllen. *Angew. Chem. Int. Ed.* **2007**, *46*, 3033.

[33] F. Schlütter, T. Nishiuchi, V. Enkelmann, K. Müllen, *Angew. Chem., Int. Ed.*, **2014**, *53*, 1538.

[34] K. Y. Cheung, X. Xu, Q. Miao, *J. Am. Chem. Soc.*, **2015**, *137*, 3910.

[35] M. Müller, V. S. Iyer, C. Kübel, V. Enkelmann, K. Müllen, *Angew. Chem. Int. Ed.* **1997**,

36, 1607.

[36] F. Dötz, J. D. Brand, S. Ito, L. Gherghel, K. Müllen. *J. Am. Chem. Soc.* **2000**, *122*, 7707.

[37] K. Kawasumi, Q. Zhang, Y. Segawa, L. T. Scott, K. Itami, *Nat. Chem.*, **2013**, *5*, 739.

[38] V. S. Iyer, M. Wehmeier, J. D. Brand, M. A. Keegstra, K. Müllen *Angew. Chem. Int. Ed.* **1997**, *36*, 1603.

[39] Simpson, C. D. Ph.D. Thesis, University of Mainz, 2003.

[40] J. Wu, Ž. Tomović, V. Enkelmann, K. Müllen, K. *J. Org. Chem.* 2004, *69*, 5179.

[41] C. D. Simpson, J. D. Brand, A. J. Berresheim, L. Przybilla, H. J. Rader, K. Müllen. *Chem. Eur. J.* **2002**, 8, 1424.

[42] J. Wu, W. Pisula, K. Müllen, *Chem. Rev.* **2007**, *107*, 718.

[43] V. I. Kasatochkin, A. M. Sladkov, Y. P. Kudryavtsev, N. M. Popov, V. V. *Korshak, Dokl. Akad. Nauk SSSR*, **1967**, *177***,** 358.

[44] A. Sladkov, Y. P. Kudryavtsev, *Priroda*, **1969**, *5***,** 37.

[45] P. P. K. Smith, P. R. Buseck, *Science*, **1982**, *216*, 984.

[46] R. J. Lagow, J. J. Kampa, H. C. Wei, S. L. Battle, J. W. Genge, D. A. Laude, C. J. Harper, R. Bau, R. C. Stevens, J. F. Haw, E. Munson, *Science* **1995**, *267*, 362.

[47] R. H. Baughman, *Science*, **2006**, *312*, 1009.

[48] A. Sun, J. W. Lauher, N. S. Goroff, *Science*, **2006**, *312*, 1030.

[49] S. Szafert, J. A. Gladysz, *Chem. Rev*. **2003**, *103*, 4175.

[50] S. Szafert, J. A. Gladysz, Chem. Rev. **2006**, *106*, PR1.

[51] A. S. Hay, *J. Org. Chem.* **1962**, *27*, 3320.

[52] Y. Nishihara, K. Ikegashira, K. Hirabayashi, J.-i. Ando, A. Mori, T. Hiyama, *J. Org. Chem*. **2000**, *65*, 1780.

[53] S. Kim, S. Kim, T. Lee, H. Ko, D. Kim, *Org. Lett*. **2004**, *6*, 3601.

[54] P. Siemsen, R. C. Livingston, F. Diederich, *Angew. Chem. Int. Ed.*, **2000**, *39*, 2632.

[55] Shi, W.; Lei, A. *Tetrahedron Lett.* **2014**, *55*, 2763.

[56] E. Jahnke, R. R. Tykwinski, *Chem. Commun*. **2010**, *46*, 3235.

[57] W. Kirmse, *Angew. Chem. Int. Ed.* **1997**, *36*, 1164.

[58] R. Knorr, *Chem. Rev.* **2004**, *104*, 3795.

[59] W. A. Chalifoux, R. R. Tykwinski, R. R, *C. R. Chim*. **2009**, *12*, 341.

[60] R. Eastmond, T. R. Johnson, D. R. M. Walton, *Tetrahedron*, **1972**, *28*, 4601.

[61] T. Gibtner, F. Hampel, J. P. Gisselbrecht, A. Hirsch, *Chem. Eur. J.*, **2002**, *8,* 408.

[62] Q. Zheng, J. C. Bohling, T. B. Peters, A. C. Frisch, F. Hampel, J. A. Gadysz, *Chem. Eur. J*. **2006**, *12*, 6486.

[63] S. Eisler, A. D. Slepkov, E. Elliott, T. Luu, R. McDonald, F. A. Hegmann, R. R. Tykwinski, *J. Am. Chem. Soc.*, 2005, **127,** 2666.

[64] W. A. Chalifoux, R. R. Tykwinski, *Nature Chem.*, **2010**, *2***,** 967.

[65] H. Meier, U. Stalmach, H. Kolshorn, *Acta Polym*. **1997**, *48*, 379.

[66] X. Zhao, Y. Ando, Y. Liu, M. Jinno, T. Suzuki, *Phys. Rev. Lett., 2003*, 90, 187401.

[67] L. Shi, P. Rohringer, K. Suenaga, Y. Niimi, J. Kotakoski, J. C. Meyer, H. Peterlik, M. Wanko, S. Cahangirov, A. Rubio, Z. J. Lapin, L. Novotny, P. Ayala, T. Pichler, *Nature Mat.*, **2016**, *15*, 634.

[68] A. T. Balaban, C. C. Rentia, E. Ciupitu, *Rev. Roum. Chim.* **1968,** *13*, 231.

[69] D. Malko, C. Neiss, F. Vines, A. Gorling, *Phys. Rev. Lett*. **2012**, *108*, 086804.

[70] B. G. Kim, H. J. Choi, *Phys. Rev. B*, **2012**, *86*, 115435.

[71] A. N. Enyashin, A. L. Ivanovskii, *Phys. Status Solidi B*, **2011**, *248*, 1879.

[72] R. H. Baughman, H. Eckhardt, M. Kertesz, *J. Chem. Phys.* **1987**, *87*, 6687.

[73] I. D. Campbell, G. Eglinton, W. Henderson, R. A. Raphael. *J. Chem. Soc., Chem. Commun.* **1966**, 87.

[74] H. A. Staab, F. Graf. *Tetrahedron Lett. 1966*, 751.

[75] U. H. F. Bunz, Y. Rubin, Y. Tobe, *Chem. Soc. Rev.* **1999**, *28*, 107-119.

[76] M. M. Haley, *Pure Appl. Chem.*, **2008**, *80*, 519.

[77] J. A. Marsden, G. J. Palmer, M. M. Haley, *Eur. J. Org. Chem.* **2003**, 2355.

[78] J. M. Kehoe, J. H. Kiley, J. J. English, C. A. Johnson, R. C. Petersen, M. M. Haley. *Org.*

Lett. **2000**, *2*, 969.

[79] M. Sonoda, Y. Sakai, T. Yoshimura, Y. Tobe, K. Kamada. *Chem. Lett.* **2004**, *33*, 972.

[80] O. S. Miljanic, K. P. C. Vollhardt, G. D. Whitener. *Synlett 2003*, 29.

[81] M. Iyoda, S. Sirinintasak, Y. Nishiyama, A. Vorasingha, F. Sultana, K. Nakao, Y. Kuwatani, H. Matsuyama, M. Yoshida, Y. Miyake. *Synthesis* **2004**, *9*, 1527

[82] K. Tahara, T. Yoshimura, M. Ohno, M. Sonoda, Y. Tobe, *Chem. Lett.* **2007**, *36*, 838.

[83] C. A. Johnson II, Y. Lu, M. M. Haley. *Org. Lett.* **2007**, *9*, 3725.

[84] T. Yoshimura, A. Inaba, M. Sonoda, K. Tahara, Y. Tobe, R. V. Williams. *Org. Lett.* **2006**, *8*, 2933.

[85] H. Kozuma, Y. Arikuma, Y. Yamamoto, K. Tahara, Y. Tobe, "*Synthesis of Star-Shaped Tetrakis(dehydrobenzo[12]annulene)*" 19th Symposium on Fundamental Organic Chemistry, **2009**.

[86] F. Diederich. *Nature* **1994**, *369*, 199.

[87] P. Kissel, R. Erni, W. B. Schweizer, M. D. Rossell, B. T. King, T. Bauer, S. Gotzinger, A. D. Schluter, J. Sakamoto1, *Nature Chem.*, **2012**, *4***,** 287.

[88] P. Kissel, D. J. Murray, W.J. Wulftange, V. J. Catalano, B. T. King, *Nature Chem.*, **2014**, 6**,** 774.

[89] Y. Tobe, H. Matsumoto, K. Naemura, Y. Achiba, T. Wakabayashi. *Angew. Chem., Int. Ed. Engl.***1996**, *35*, 1800.

[90] L. Talirz, P. Ruffieux, R. Fasel, *Adv. Mater.*, **2016**, DOI: 10.1002/adma.201505738

[91] P. Ruffieux1, S. Wang, B. Yang, C. Sánchez-Sánchez, J. Liu, T. Dienel, L. Talirz, P. Shinde, C. A. Pignedoli, D. Passerone, T. Dumslaff, X. Feng, K. Müllen, R. Fasel, *Nature*, **2016**, *531*, 489.

[92] C. Glaser, *Ber. Dstch. Chem. Ges.*, **1869**, *2*, 422.

[93] G. Eglinton and A. R. Galbraith, *Chem. Ind.*, **1956**, 737.

[94] A.S. Hay, *J. Org. Chem.*, **1960,** *25*, 1275.

[95] M. M. Haley, S. C. Brand, J. J. Pak, *Angew. Chem., Int. Ed. Engl.* **1997**, *36*, 836.

[96] W. B. Wan, S. C. Brand, J. J. Pak, M. M. Haley, *Chem. Eur. J.* **2000**, *6*, 2044.

[97]W. B. Wan, M. M. Haley, *J. Org. Chem*. **2001**, *66*, 3893.

[98] J. A. Marsden, M. M. Haley, *J. Org. Chem*. **2005**, *70*, 10213.

[99] E. L. Spitler, C. A. Johnson II, M. M. Haley, *Chem. Rev*. **2006**, 106, 5344

[100] K. P. C. Vollhardt, *Angew. Chem., Int. Ed. Engl.* **1984**, *23*, 539.

[101] F. Diederich, Y. Rubin, C. B. Knobler, R. L. Whetten, K. E. Schriver, K. N. Houk, Y. Li, *Science* **1989**, *245*, 1088.

[102] R. Diercks, J. C. Armstrong, R. Boese, K. P. C. Vollhardt, *Angew. Chem., Int. Ed. Engl.* **1986**, *25*, 268.

[103] Y. Q. Zhang, N. Kepčija, M. Kleinschrodt, K. Diller, S. Fischer, A. C. Papageorgiou, F. Allegretti, J. Bjork, S. Klyatskaya, F. Klappenberger, M. Ruben, J. V. Barth, *Nat. Commun.* **2012**, *3*, 1286.

[104] G.X. Li, Y. L. Li, H. B. Liu, Y. B. Guo, Y. J. Li, D. B. Zhu, *Chem. Commun.* **2010**, *46*, 3256.

[105] G.X. Li, Y. L. Li, X. M. Qian, H. B. Liu, H. W. Lin, N. Chen, Y. J. Li, *J. Phys. Chem. C,* **2011**, *115*, 2611.

[106] X. M. Qian, Z. Y. Ning, Y. L. Li, H. B. Liu, C. B. Ouyang, Q. Chen, Y. J. Li, *Dalton Trans.* **2012**, *41*, 730.

[107] J. Zhou, X. Gao, R. Liu, Z. Xie, J. Yang, S. Zhang, G. Zhang, H. Liu, Y. Li, J. Zhang, Z. Liu, *J. Am. Chem. Soc.*, **2015**, *137*, 7596.

[108] J. Li, X. Gao, B. Liu, Q. L. Feng, X. B. Li, M. Y. Huang, Z. F. Liu, J. Zhang, C. H. Tung, L. Z. Wu, *J. Am. Chem. Soc.*, **2016**, *138*, 3954.

[109] N. Narita, S. Nagai, S. Suzuki, K. Nakao, *Phys. Rev. B: Condens. Matter Mater. Phys*. **1998**, *58*, 11009−11014.

[110] M. Long, L. Tang, D. Wang, Y. Li, Z. Shuai, *ACS Nano* **2011**, *5*, 2593.

[111] A. L. Ivanovskii, *Prog. Solid State Chem*. **2013**, *41*, 1.

[112] Y. Li, L. Xu, H. Liu, Y. Li, *Chem. Soc. Rev.* **2014**, *43*, 2572

[113] J. Zhang, M. Terrones, C. R. Park, R. Mukherjee, M. Monthioux, N. Koratkar, Y. S. Kim, R. Hurt, E. Frackowiak, T. Enoki, Y. Chen, Y. Chen, A. Bianco, *Carbon*, **2016**, *98*, 708.

[114] M. Bartolomei, E. C. Novillo, M. I. Hernández, J. C. Martínez, F. Pirani, G. Giorgi, *J. Phys. Chem. C*, 2014, *118*, 29966.

[115] M. I. Hernández, M. Bartolomei, J. C. Martínez, *J. Phys. Chem. A*, **2015**, *119*, 10743.

[116] S. Zhang, H. Du, J. He, C. Huang, H. Liu, G. Cui, Y Li, *ACS Appl. Mater. Interface*, 2016, *8*, 8467.

[117] K. Krishnamoorthy, S. Thangavel, J. C. Veetil, N. Raju, G. Venugopal, S. J. Kim, *Inter. J. Hydrogen Energy*, **2016**, *41*, 1672.

[118] H. Ren, H.Shao, L. Zhang, D. Guo, Q. Jin, R. Yu, L. Wang, Y. Li, Y. Wang, H. Zhao, D. Wang, *Adv. Energy Mater*. **2015**, *5*, 1500296

[119] J.A. Marsden, M. M. Haley, "In Metal-Catalyzed Cross-Coupling Reactions 2nd ed." Edited byA. de Meijere, F. Diederich, *Wiley-VCH: Weinheim*, **2004**, 317.

[120] Sigurd Höger *Beilstein J. Org. Chem.* **2014,** *10,* 1670–1671.

[121] M. M. Haley, J. J. Pak, S. C. Brand, *Top. Curr. Chem.* **1999**, *201*, 81.

[122] J. S. Moore. *Acc. Chem. Res.* **1997**, *30*, 402.

[123] C. Grave, A. D. Schlüter. *Eur. J. Org. Chem.* **2002**, 3075.

[124] S. Höger. *Angew. Chem., Int. Ed.* **2005**, *44*, 3806.

[125] W. Zhang, J. S. Moore. *Angew.Chem., Int. Ed.* **2006**, *45*, 4416.

[126] M. Iyoda, J. Yamakawa, M. J. Rahman, *Angew. Chem. Int. Ed.* **2011**, *50*, 10522.

[127] O. Y. Mindyuk, M. R. Stetzer, P. A. Heiney, J. C. Nelson, J. S. Moore, *Adv. Mater*. **1998**, *10*, 1363;

[128] T. C. Bedard, J. S. Moore, *J. Am. Chem. Soc.* **1995**, *117*, 10662.

[129] Y. Tobe, N. Utsumi, A. Nagano, K. Naemura, *Angew. Chem. Int. Ed.* **1998**, *37*, 1285.

[130] S. Höger, *Pure Appl. Chem.* **2010**, *82*, 821.

[131] D. Mössinger, J. Hornung, S. Lei, S. De Feyter, S. Höger, *Angew. Chem. Int. Ed*. **2007**, *46*, 6802.

[132] D. Mössinger, D. Chaudhuri, T. Kudernac, S. Lei, S. De Feyter, L. M. Lupton, S. Höger, *J. Am. Chem. Soc*. **2010**, *132*, 1410.

[133] R. May, S. S. Jester, S. Höger, *J. Am. Chem. Soc.*, **2014**, *136*, 16732.

[134] R. Hoffmann, T. Hughbanks, M. Kertesz, P. H. Bird, *J. Am. Chem. Soc*, **1983**, *105*, 4831.

[135] M. Itoh, M. Kotani, H. Naito, T. Sunada, Y. Kawazoe, T. Adschiri, *Phys. Rev. Lett,* **2009**, *102*, 055703.

[136] Y. Yao, J. S. Tse, J. Sun, D. D. Klug, R. Martoňak, T. Iitaka, *Phys. Rev. Lett*, **2009**, *102*, 229601.

[137] J. Gibson, M. Holohan, H. L. Riley, *J. Chem. Soc.* **1946**, 456.

[138] H. L. Riley, *J. Chem. Phys. Phys. Chim. Biol.* **1950**, *47*, 565.

[139] M. O'Keeffe, G. B. Adams, O. F. Sankey, *Phys. Rev. Lett*, **1992**, *68*, 2325.

[140] C. Y. He, L. Z. Sun, C. X. Zhang, J. X. Zhong, *Phys. Chem. Chem. Phys.*, **2013**, *15*, 680.

[141] E. M. Larson, R. B. Von Dreele, P. Hanson, J. D. Gust, *Acta Crys.*, **1990**, *C46*, 784.

[142] A. Rajca, S. Rajca, M. Pink, M. Miyasakaa, *SYNLETT*, **2007**, *12*, 1799.

[143] R. H. Baughman, C. Cui, *Synth. Met.* **1993**, *55*, 315.

[144] A. J. Berresheim, M. Müller, K. Müllen, *Chem. Rev.* **1999**, *99*,1747.

[145] M. D. Watson, A. Fechtenkötter, K. Müllen, *Chem. Rev.* **2001**, 101,1267.

[146] X. Shen, D. M. Ho, R. A. Pascal, Jr., *Org. Lett*. **2003**, *5*, 369.

[147] Q. L. Song, C. W. Lebeis, X. F. Shen, D. M. Ho, R. A. Pascal, *J. Am. Chem. Soc.* **2005**, *127*, 13732.

[148] X. Shen, D. M. Ho, R. A. Pascal , *J. Am. Chem. Soc.*, **2004**, *126*, 5798.

[149] D. Wasserfallen, G. Mattersteig, V. Enkelmann, K. Müllen, *Tetrahedron* **2006**, *62*, 5417.

[150] A. Rajca, A. Safronov, S. Rajca, R. Shoemaker, *Angew. Chem. Int. Ed. Engl.* **1997**, *36*. 488.

[151] M. Gingras, *Chem. Soc. Rev*. **2013**, *42*, 968.

[152] M. Gingras, Guy Félix, R. Peresutti, *Chem. Soc. Rev*. **2013**, *42*, 1007.

[153] M. Gingras, *Chem. Soc. Rev*. **2013**, *42*, 1051.

2. Motivation and objectives

As a 2D carbon material composed of densely packed sp^2-hybridized carbon atoms, graphene has obtained wide interest from the academic and industrial communities as a result of its intriguing properties and promising applications. However, due to the limitation of the zero band-gap structure of pristine graphene, efforts are still required to open up the original band gap of the graphene-based material. Therefore, considerable academic research has been focused on the development of new graphene-based materials or new carbon materials which are structurally similar to graphene. In the chapters 3 and 4, the design and synthesis of new carbon networks with novel structure were covered.

As the principal focus of current research on functional carbon materials, graphene is a 2D hexagonal network of sp^2 carbon atoms linked by strong triangular σ bonds. To overcome the limitation of the zero band gap electronic structure of graphene, some 2D carbon allotropes (like graphyne, and graphdiyne) with similar structure have been proposed and investigated at a theoretical level. Experiments toward these carbon allotropes proved the bottom-up synthesis of these 2D carbon allotropes with perfect hexagonal networks to be quite difficult. Therefore, by confining these infinite 2D carbon sheets into nanosized fragments with defined sizes and shapes, several subunits of these 2D allotropes had been successfully synthesized, for example macrocycles with phenylene-acetylene or phenylene-diacetylene backbones with shape-persistent structure (molecule **2-1** in Figure 2-1).

However, the sp-hybridization of carbon atoms involved in the graphynes and graphdiynes is energetically disadvantageous compared with that of sp^2- and sp^3-carbon atoms. And the presence of sp-carbons is not a necessary precondition for extraordinary electronic properties. Therefore, new types of 2D carbon networks composed of all sp^2 carbons, were proposed by replacing the acetylene linkage of graphyne and graphdiyne with phenylene units.

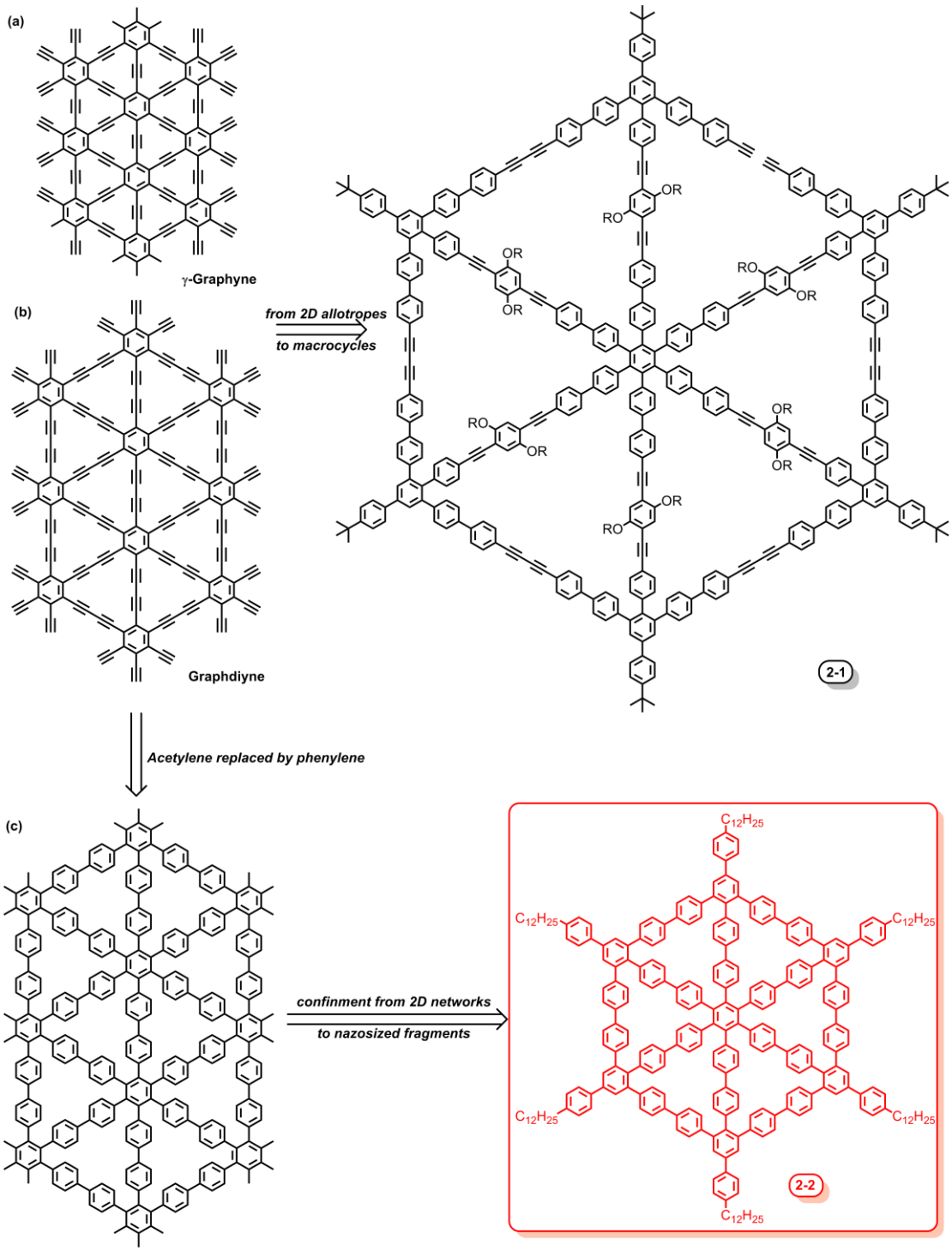

Figure 2-1. Schematic illustration of the development from 2D carbon allotropes to nanosized shape-persistent macrocycles.

The synthesis of the macrocyclic subunits (molecule **2-2** in Figure 2-1) of these novel sp^2 carbon networks will be introduced in detail in the chapters 3.2.1 and 3.2.2. By applying the covalent template-directed approach, the star-shaped oligophenylene precursors with the hexaphenybenzene moiety as the template will be first synthesized.

The final cyclization reaction is accomplished by *Yamamoto* coupling under microwave conditions in a one-step procedure to yield corresponding star-shaped oligophenylene macrocycles.

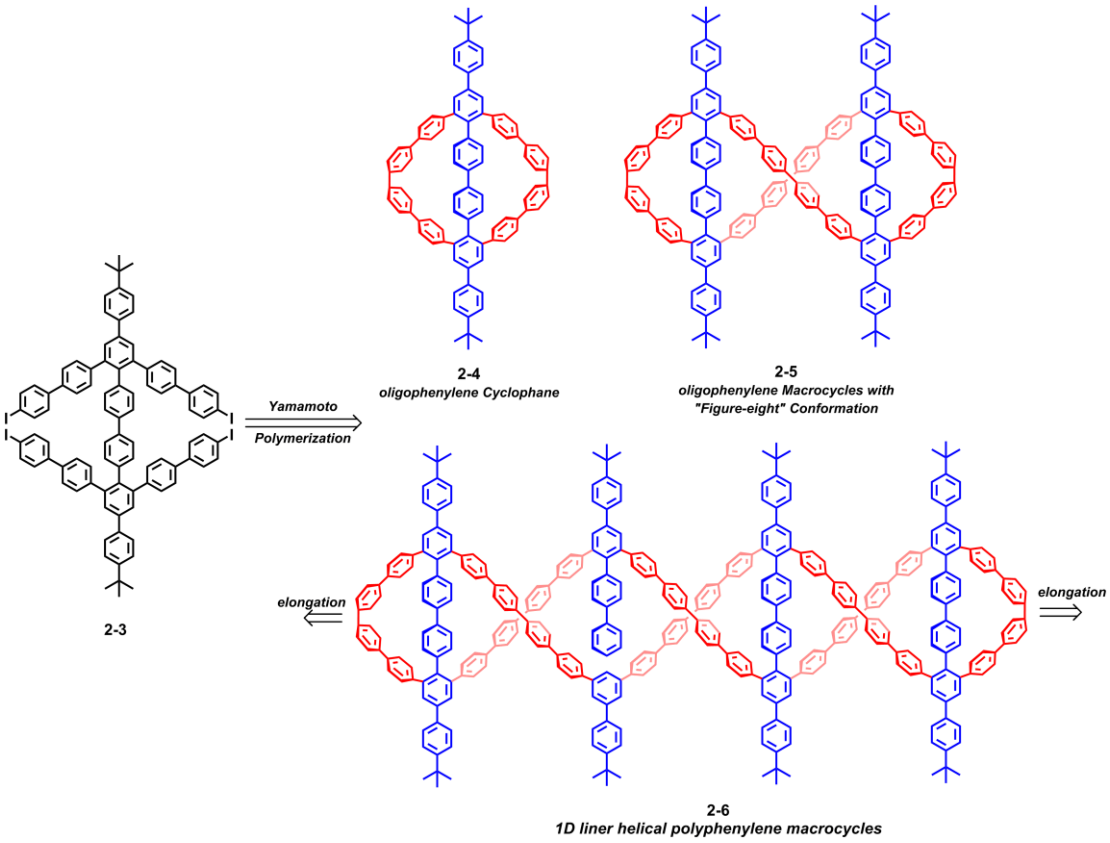

Figure 2-2. Schematic illustration of 1D sp2 carbon allotropes with helical nanostructure (**2-6**), related oligophenylene cyclophane (**2-4**), and "figure-eight" macrocycles (**2-5**).

Completely distinct from the 2D planar networks of sp^2 carbons described above (Figure 2-1), another type of 1D carbon framework **2-6** with helical conformation and extremely congested structure (Figure 2-2), was targeted in chapter 4. In contrast to the CNTs as 1D sp^2 carbon allotrope of cylindrical nanostructures and GNRs with strip-like nanostructures, the double-helical polymer **2-6** is another 1D sp^2 carbon network with "figure-eight" conformation in each repeating unit, and is structurally related to the double helical substructures **1-55** in "cubic graphite". After the *Yamamoto* coupling of the oligophenylene monomer (**2-3** in Figure 2-2), the intramoleculatr closure will yield the intriguing cyclic oligophenylenes (**2-4**), with extremely congested structure, while intermolecular coupling would lead to the cyclic

oligophenylene **2-5** and 1D linear helical polyphenylene **2-6** with "figure eight" conformation.

These two chapters will cover all the synthetic procedures toward carbon rich systems with novel geometry related to "cubic graphite", as well as their structural proof which is supported by NMR spectroscopy, MS spectroscopy and STM imaging. These results will open a new approach to develop polyphenylene macrocycles with intriguing structure, like single-sided *Möbius*-strip geometries, and shape-persistent frameworks. Furthermore, these efforts will guide the constructions of carbon materials with different dimension and structure, no matter whether 2D planar and extremely curved.

In terms of the development of functional carbon materials, the design and synthesis of novel carbon rich systems related to "cubic graphite" is presented in chapters 3 and 4. However, a lot of modifications have also been successfully accomplished on the pristine graphene to break the sub-lattice symmetry and perturb the band structure around the Dirac point for fabricating graphene materials with better electronic performance. In contrast to these chemical or physical functionalizations of pristine graphene, the bottom-up synthesis of graphene subunits has proven to be significant from the viewpoint of organic synthesis. By confining 2D infinite graphene into nanosized graphene segments (NGs) and 1D graphene nanoribbons with nanosized width (GNRs), the electronic properties of these materials can be effectively tuned via in-depth structural modulation. In chapters 5 and 6, chemical modification of the nanographene segments and pristine graphene will be investigated to tune the electronic properties of these graphene materials.

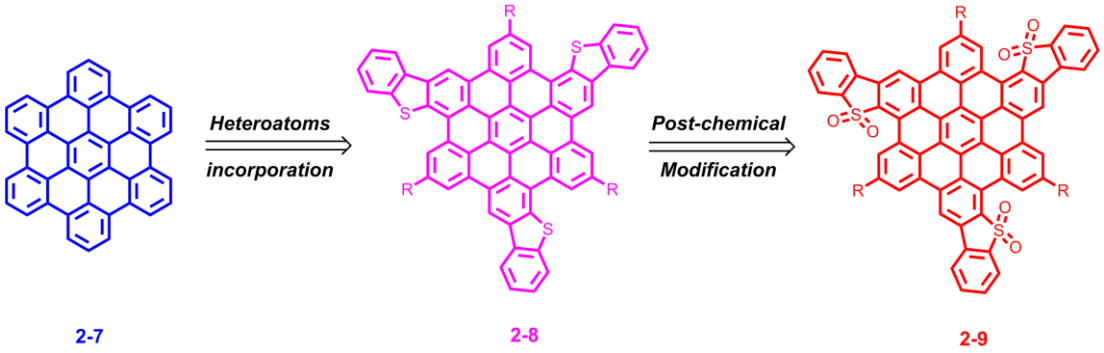

Figure 2-3. Energy level modulation of nanosegments of graphene via heteroatoms incorporation and further chemical modification.

Taking into account the development of semiconducting polymers with heteroatoms, we had extended the development of NGs by incorporating sulfur atoms at the edge of hexabenzo[*bc,ef,hi,kl,no,qr*]coronene (HBC, **2-7** in Figure 2-3). Through the *Scholl* dehydrogenation of the corresponding oligophenylene precursor, a series of benzothiophene-fused HBCs was synthesized, which can be further transformed into the respective NGs modified by sulfonyl groups. This post-modification method paves a new way for the development of new functional NGs, especially with n-type semiconducting properties.

This chapter will cover the synthetic details. A systematic investigation of the impact of *sulfur* incorporation and oxidation on the electronic properties of NGs will also be presented, as well as their influence on the supramolecular organization behavior in the solid state.

In chapter 6, a work focusing on molecular building blocks will be presented, which are capable of self-assembley and grafting onto graphene surfaces. Although much research on the chemical modification of graphene had been reported in the past decade, the spatial control of the entire modification process still remains elusive. To realize the well-ordered grafting on the basal plane of graphene surfaces, we combine the covalent chemistry of graphene with the supramolecular chemistry of small molecules on solution/HOPG interfaces (Figure 2-1). Therefore, a series of molecules composed of long linear alkyl tails and reactive functional heads (like diazirine,

diazonium, and azide) was synthesized. After forming the submolecular self-assembling monolayer on the graphene surface, the chemical grafting process and sp^3-defect generation could be trigged by the exterior stimulus, like light irradiation, electrochemical signals, and heating.

This chapter will cover all the details of the synthesis process of those molecular building blocks, as well as their wet chemistry with graphene materials. Meanwhile, the STM imaging will also be utilized to investigate the SAM formation for confirming the organization of reactive groups.

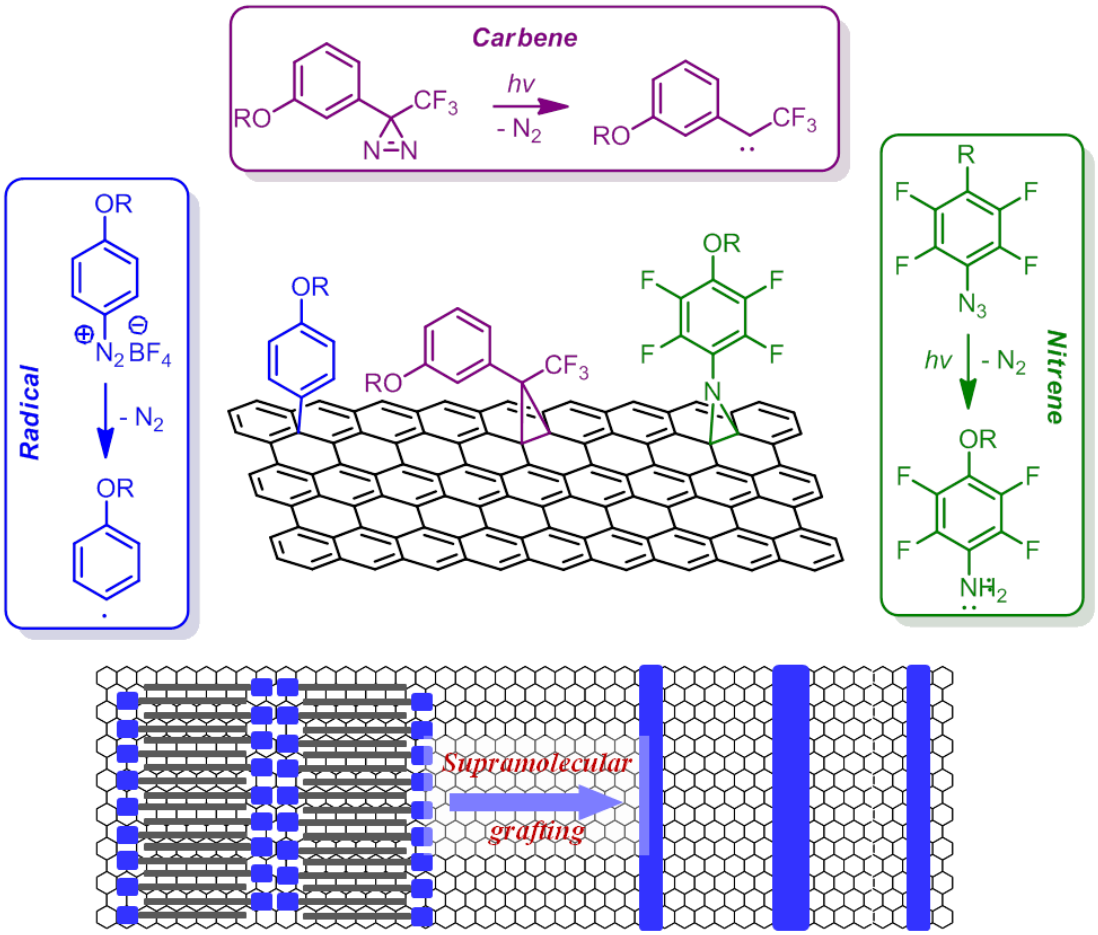

Figure 2-4. Generation of graphene nanoribbons via supramolecular assembling directed covalent grafting on pristine graphene.

3. A shape-persistent π-conjugated polyphenyle--ne macrocycle with all sp^2 carbons

3.1 Introduction

Based on the structural analysis of the γ-graphyne and graphdiyne, we propose two new purely sp^2-hybridized carbon networks herein, named **graphenylene-1** and **graphenylene-2**, by replacing the acetylene units of γ-graphyne and graphdiyne with 1,4-phenylene rings, respectively (Figure 3-1). Compared with the graphyne and graphdiyne, these two carbon networks are thermodynamically more stable due to the absence of the sp-hybridized carbon atoms. From a topological viewpoint, these two 2D polyphenylene networks resemble graphene with specific sub-nanometer pores and atomic periodicity. As a consequence, they can be seen as porous graphene, which may show electronic properties and potential industrial applications distinct from the pristine graphene. Furthermore, the 2D polyphenylene network **graphenylene-1** can be conceived as a model of the cubic graphite [1,2] when envisaged from the [111] direction. The synthetic efforts toward the carbon network **graphenylene-1** will also shed some light on the construction of the hypothetic cubic graphite.

Currently, the synthetic chemistry of 2D polymers with periodic structures is in its infancy, [3,4] although some successful examples have emerged recently via different approaches, such as molecular framework, surface science, and crystal engineering. Therefore, the synthesis toward the two proposed carbon networks would be more realistic when confining the infinite 2D carbon sheets into nanosized substructure with defined size and shape. In this chapter, two nanosized macrocyclic subunits (**3-1** in scheme 3-1, and **3-2** in scheme 3-2) of the **graphenylene-1** and **graphenylene-2** are introduced. Completely different from the widely-studied macrocycles with phenylene-ethynylene backbones, [5,6] these two unique macrocyclic molecules are shape-persistent polyphenylene macrocycles composed of all sp^2 carbons.

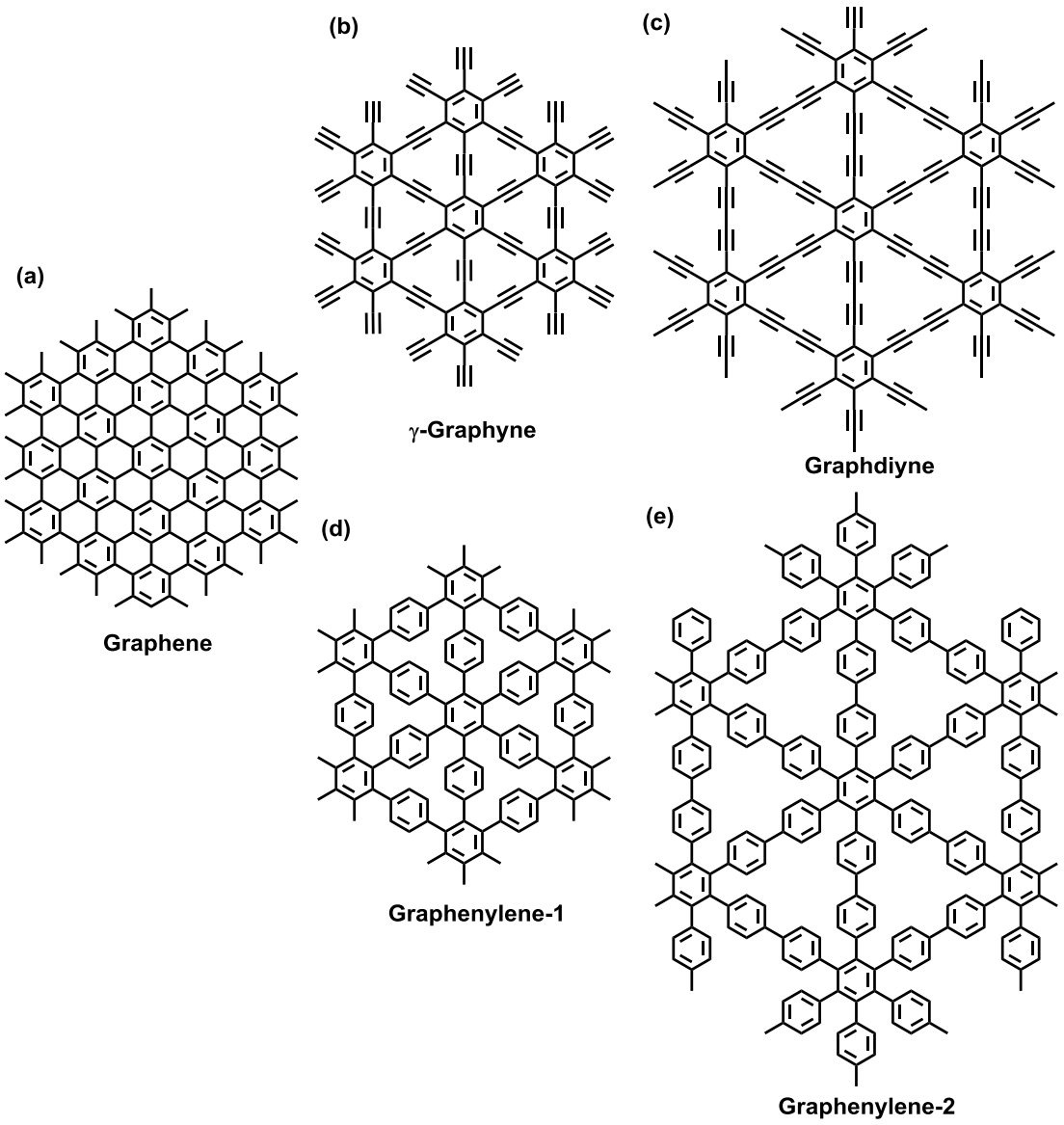

Figure 3-1. Structural representations of 2D carbon materials: (a) graphene, (b) γ-graphyne, (c) graphdiyne, and two newly proposed, purely sp^2-hybridized structures (d) graphenylene-1 and (e) graphenylene-2.

In general, the usage of appropriate templates is almost the most dominating key in building up the shape-persistent macrocycles. The template-directed synthesis can enhance the intermolecular ring closure reaction and attenuate the intramolecular undesired reaction, no matter whether a covalently bonded template or a non-covalent bonded one is introduced. Herein, a star-shaped precursor molecule with 12 terminal bromide atoms at the ideal geometrical position and hexaphenylbenzene as the covalent template, is convergently synthesized for homocoupling the adjacent

aromatic halides and forming six defined rigid biphenyl bridges as the rim of the macrocycles (Figure 3-3). In contrast to the commonly utilized Glaser coupling in constructing macrocycles with phenylene-ethynylene backbones, Nickle catalyzed homocoupling of phenyl halides (Yamamoto coupling) would be more favorable for the formation of macrocycles with all sp^2-hybridized carbon atoms in this chapter.

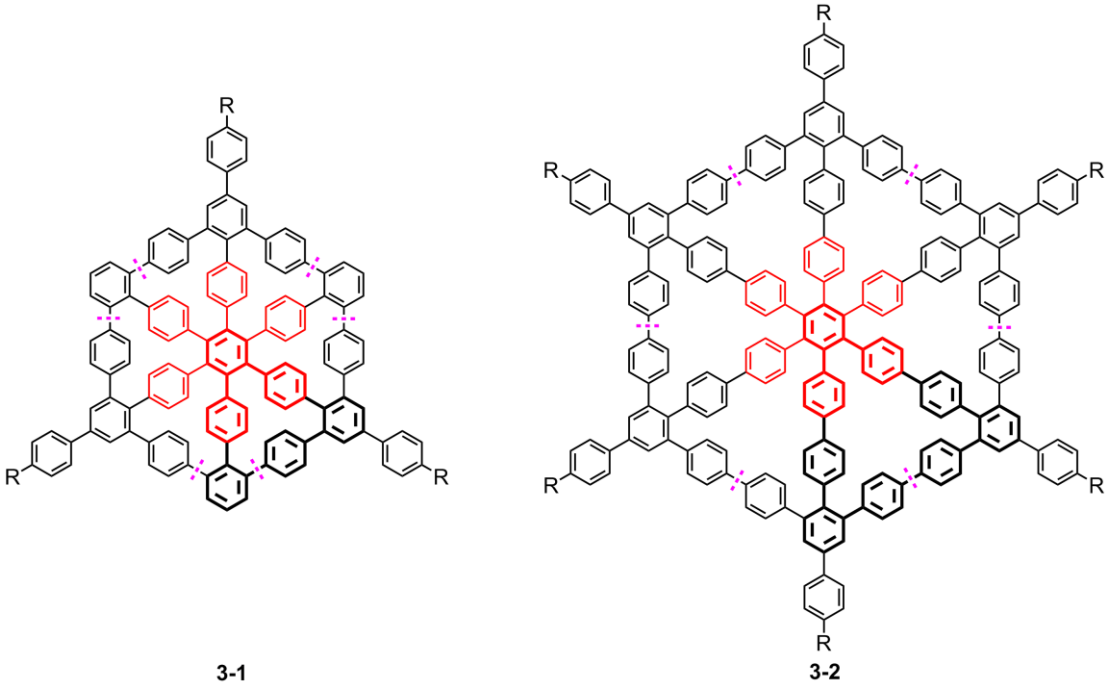

Figure 3-2. Structural representations of nanosized polyphenylene segments of the two proposed purely sp^2-hybridized networks. Bolded triangle parts indicate the unit cells. Red colored parts indicate the cyclization template, pink dash lines suggest the targeted cyclization linkage in the retrosynthesis.

3.2 Results and Discussion

3.2.1 Synthesis of 3-1

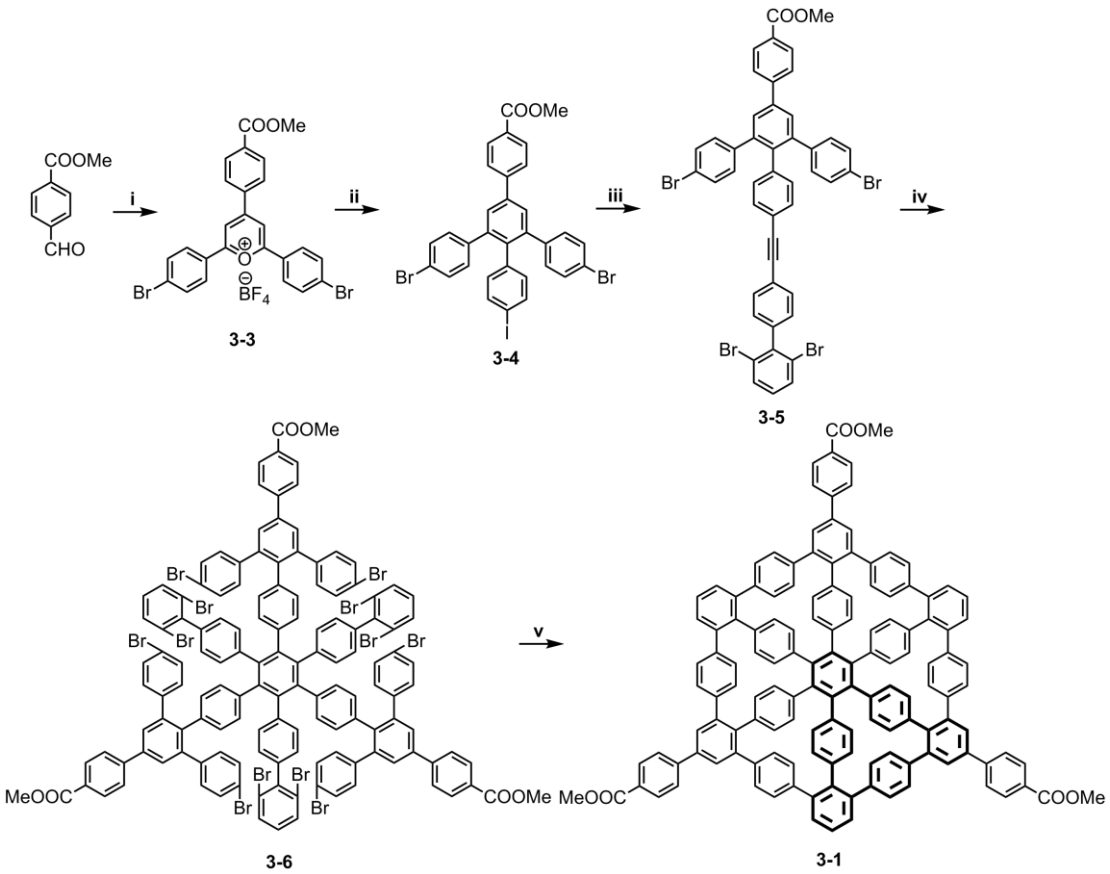

Scheme 3-1. Synthetic routes toward the subunit **3-1**of graphenylene 1. Bolded triangle parts indicate the unit cells of graphenylene-1. Conditions: (i) 4-bromoacetophenone, BF_3-Et_2O, 100 ℃, 12h, 40%; (ii) 4-iodophenacetic sodium, Ac_2O, 150 ℃, 12h, 45%; (iii) $Pd(PPh_3)_2Cl_2$, Et_3N, THF, 12 h, rt, 90%; (iv) $Co_2(CO)_8$, Toluene, 110 ℃, 23%; (v) $Ni(COD)_2$, COD, Bipyridine, THF, 120 ℃, microwave reactor, 0%.

Firstly, in the attempt to construct the polyphenylene macrocycle **3-1**, a subunit of **graphenylene-1**, a dendritic polyphenylene precursor **3-6** with defined C_3 symmetry was synthesized within four steps (Scheme 3-1). To obtain the desired oligophenylene precursor **3-6** with C_3 symmetry from its constitutional isomer with distinctive symmetry, strongly polar benzoate groups were attached to the peripheral benzene rings to seperate two possible isomeric products after alkyne trimerization of **3-5**.

The synthetic route toward the star-shaped precursor **3-6** consisted of the Lewis acid catalyzed condensation of methyl 4-formylbenzoate with 4-bromoacetophenone[7,8] and the condensation reaction of sodium 4-iodophenacetate and triphenylpyrylium salts **3-3** in refluxing acetic anhydride.[9,10] Finally, after a *Sonagashira* coupling of compound **3-4** with the synthesized 2,6-dibromo-4'-ethynyl-1,1'-biphenyl, the asymmetric acetylene compound **3-5** was obtained by the dicobalt octacarbonyl catalyzed alkyne cyclotrimerization of in refluxing toluene in approximate 23% yield. [11] (scheme 3-1)

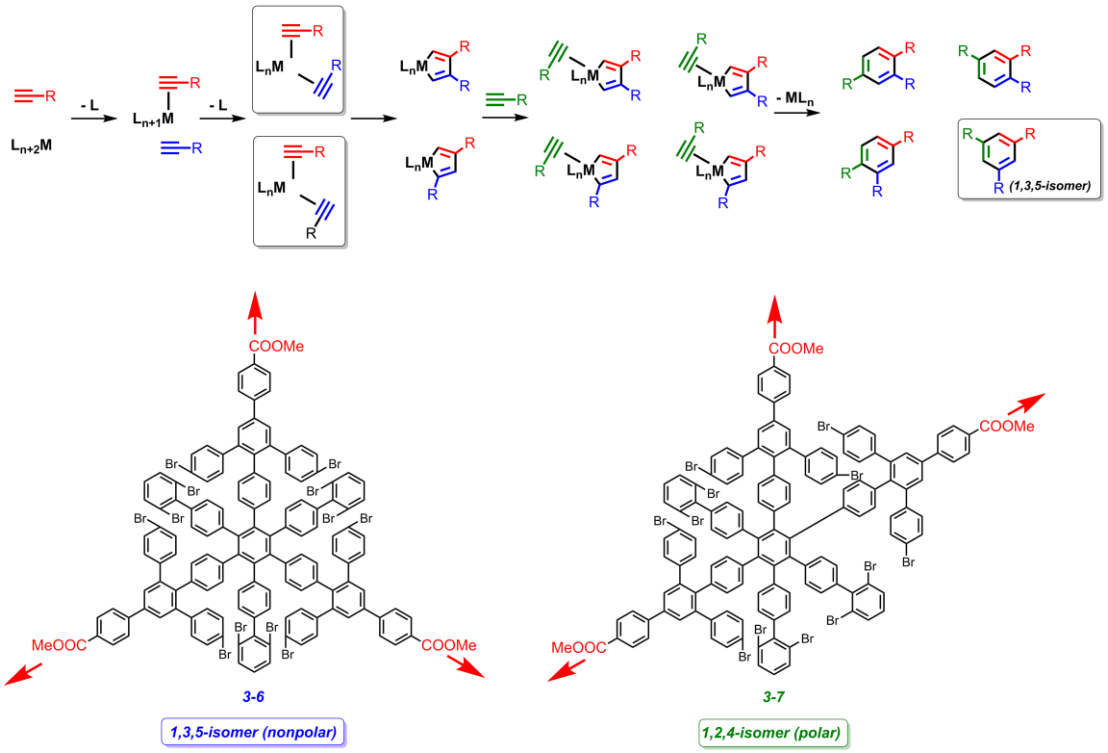

Figure 3-3. Mechanism of cyclotrimerization of the asymmetric acetylene compound leading to two possible regioisomers, and structural analysis of **3-6** (*1,3,5-arrangement*) with its regioisomer **3-7** (*1,2,4-arrangement*).

Due to the formation of two possible metallocyclopentadiene complexes and two pathways for the final alkyne insertion in the cyclotrimzation of the asymmetric acetylene,[12] two possible products may be formed (*1,3,5- regioisomer vs 1,2,4-regioisomer* in figure 3-4).[13] Therefore, after the cyclotrimerization of **3-5**, there would be another contaminant **3-7** (*1,2,4-regioisomer*) mixed with our targeted compound **3-6 (***1,3,5- regioisomer***)** in the final product mixture, which have the

identical molecular weight and similar structure. Fortunately, in contrast to the polar molecular **3-7**, our targeted molecule is nonpolar although it still possesses polar ester bonds, because the intermolecular polar bonds are symmetrically distributed in the molecular, the local bond dipoles cancel and thus do not create a molecular dipole. Therefore, we could see two close spots in the TLC analysis of the product mixture, and the targeted molecule **3-6** could be easily separated from its counterpart via careful silica gel column chromatography.

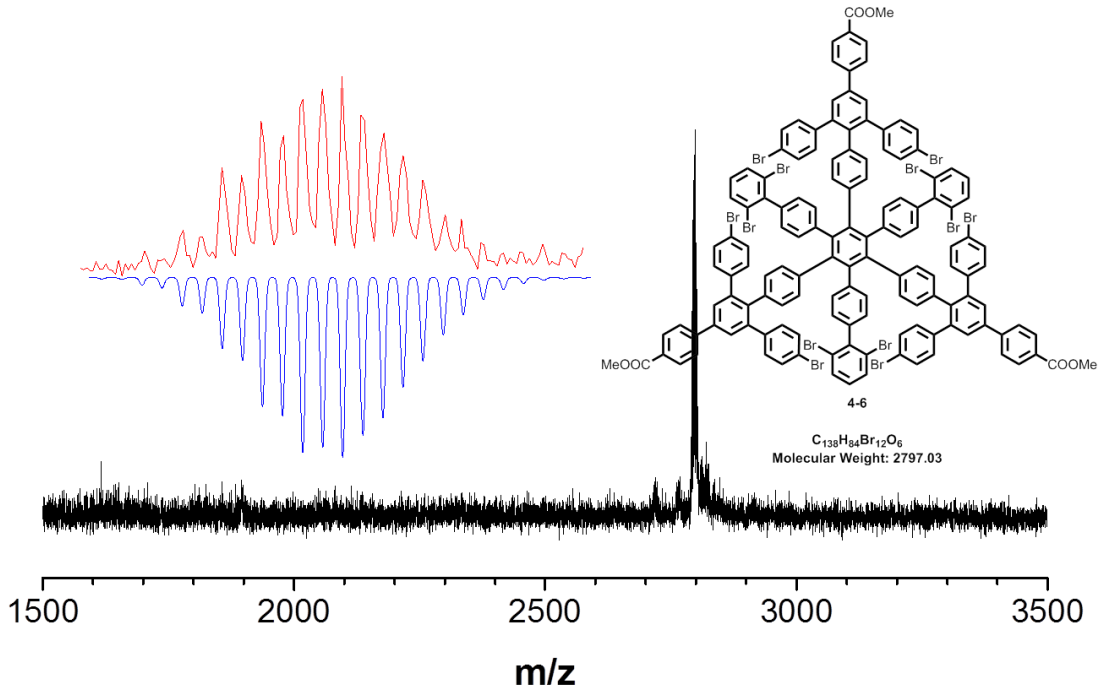

Figure 3-4. MALDI-TOF mass spectrum of the star-shaped oligophenylene precursor **3-6**.

MALDI-TOF mass spectrum (figure 3-4) of compound **3-6** indicated a major species with desired molar mass, and the experimental isotopic distribution is also consistent with the theoretical calculation. Additionally, some unidentified small peaks were also observed, which might originate from impurities or mass spectrum measurement process. To further confirm the structure of the targeted precursor **3-6**, a detailed NMR (figure 3-5) investigation of the molecular was conducted combined with 2D COSY NMR (Figure 3-6) measurements which help to assign each proton peaks in the spectrum of precursor **3-6**.

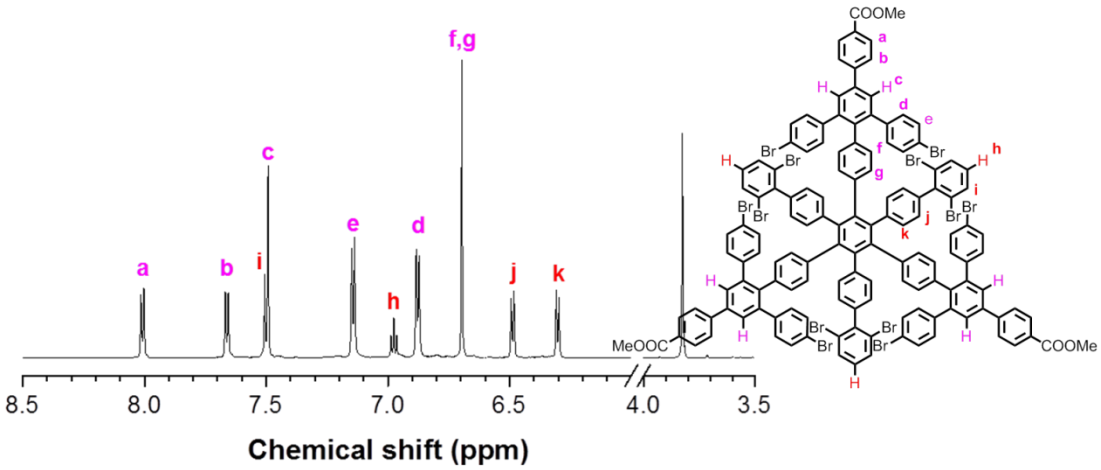

Figure 3-5. ^{1}H NMR spectrum of the star-shaped oligophenylene precursor 3-**6.**

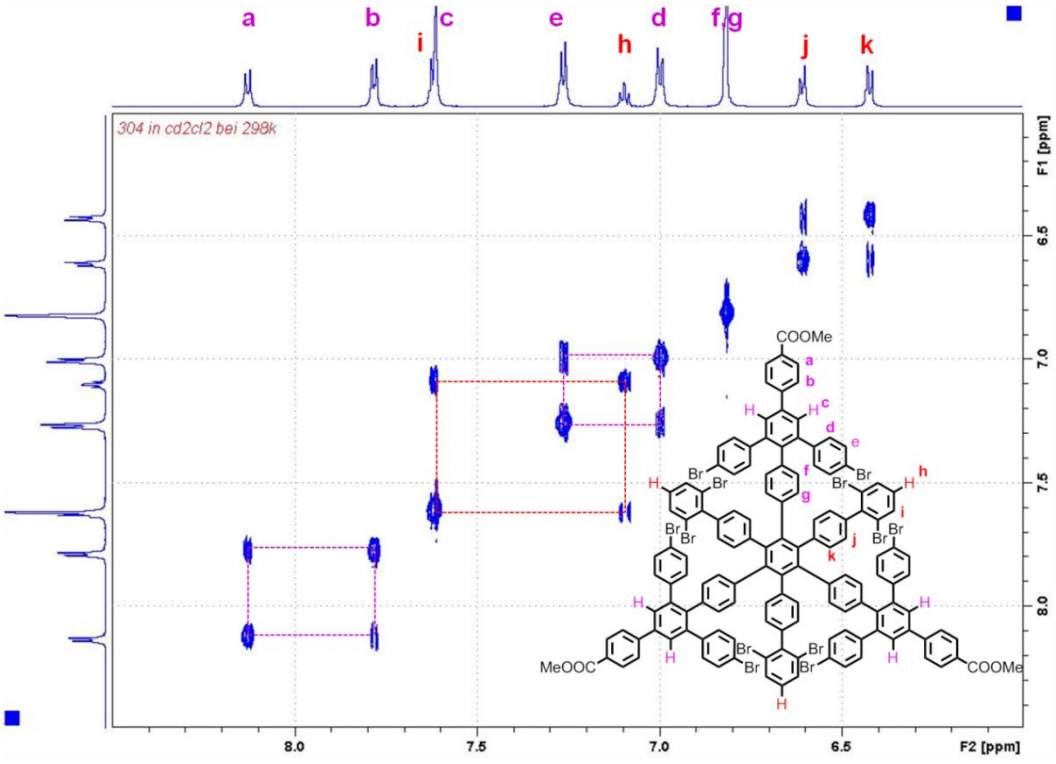

Figure 3-6. 2D ^{1}H-^{1}H COSY NMR spectrum of the star-shaped oligophenylene precursor **3-6.**

At last, the *Yamamoto* coupling of precursor **3-6** toward the proposed polyphenylene macrocycle **3-1** was applied in refluxing THF in common microwave reactor to build up the six exterior biphenyl bridges and finally form the desired shape-persistent macrocycle **3-1**. However, the FD-MS spectrum of the reaction mixture after heating for 12 hours suggested the absence of the targeted macrocycle **3-1** and the failure of

the intramolecular nickle-catalyzed ring closure, which was probably due to the extremely high steric hindrance of the *o*-bromo-biphenyl unit.

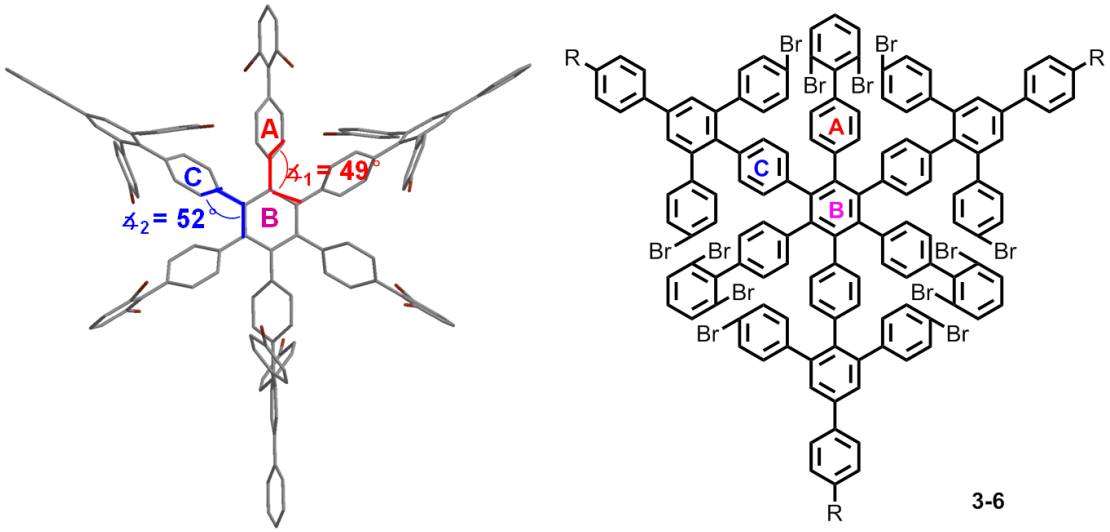

Figure 3-7. Simulated geometry of the highly congested oligophenylene precursor **3-6** via the MM2 method, the angles ∢$_1$ and ∢$_2$, and ∢$_3$, which are measures of π-conjugation extension in the molecular.

Based on the optimized geometry (Figure 3-7) of the dendritic precursor **3-6**, the dihedral angles between the benzene rings (A and C) and the central benzene ring B are approxiamately 50 °. However, the peripheral benzene rings where the reactive Br-atoms are substituted, are nearly perpendicular to the central benzene ring because of the high steric hindrance. The six pairs of reacting sites are too far away from each other, and thus the intermolecular coupling will be more favorable than the desired intramolecular coupling. Additionally, the reactivity of Br- substitutions on the 2,6-dibromo-1,1'-biphenyl unit is very low due to the hindrance from the adjacent benzene ring. Therefore, the Yamamoto coupling of precursor **3-6** fails to give rise to the targrted cyclic oligophenylene **3-1**.

3.2.2 Synthesis and characterization of 3-2

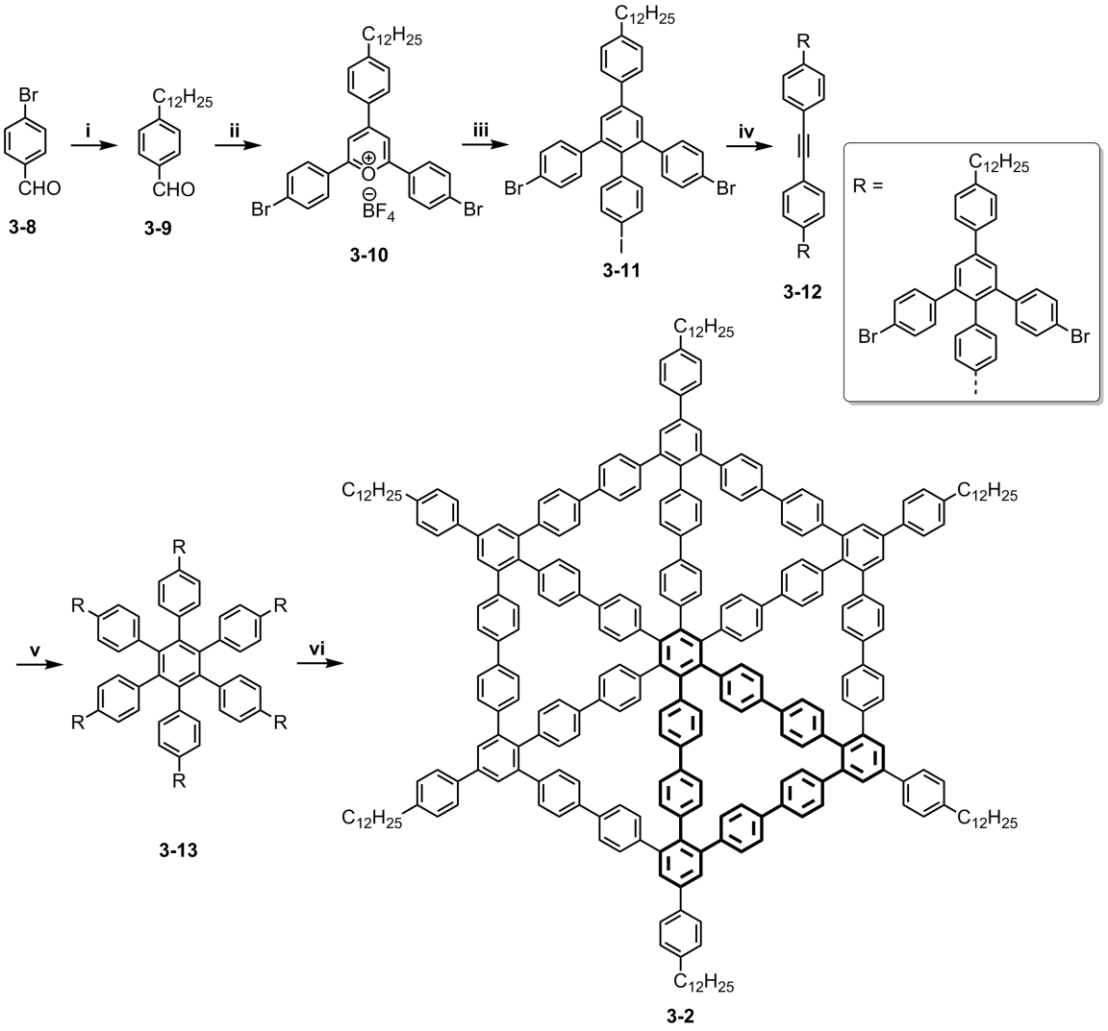

Scheme 3-2. Synthetic routes toward the subunit of gradiphenylene 2. Bolded triangle parts indicate the unit cells of gradiphenylene-2. Conditions: (i) (a) 1-dodecyne, 9-BBN, THF, rt. 2h, (b). $Pd(dppf)Cl_2$, THF, K_2CO_3, 80 ℃, 76%; (ii) 4-bromoacetophenone, BF_3-Et_2O, 100 ℃, 12h, 40%; (iii) 4-iodophenacetic sodium, Ac_2O, 150 ℃, 12h, 45%; (iv) $Pd(PPh_3)_4$, Et_3N, THF, 4,4′-(acetylene-1,2-diyl)bis(phenylboronic acid pinacol ester), Methanol/H_2O, 12 h, rt, 90%; (v) $Co_2(CO)_8$, toluene, 110 ℃, 34%; (vi) $Ni(COD)_2$, COD, Bipyridine, THF, 120 ℃, microwave reactor, 56%.

The synthesis of the polyphenylene macrocycle subunit **3-2** was following a similar strategy as shown in the synthesis of the molecular **3-1**. Firstly,

4-dodecylbenzlaldehyde **3-9** was prepared by the Suzuki coupling of readily synthesized 9-dodecyl-9-borabicyclo(3.3.1)nonane with 4-bromobenzldehyde **3-8**, followed by the Lewis-acid catalyzed condensation of **3-9** with 4-bromoacetophenone to afford the dodecyl chain substituted triphenylpyrylium salt **3-10.** Then, the crude product of **3-10** ,was readily treated with 4-iodophenacetate sodium in refluxing acetic anhydride to yield PAH compound **3-11**, followed by the Suzuki coupling between **3-11** and 1,2-bis(4-(4,4,5,5-tetramethyl-1,3,2-dioxaborolan-2-yl)phenyl)ethyne to yield the symmetric acetylene **3-12**. At last, the star-shaped oligophenylene dendrimer **3-13** was obtained *via* the dicobalt octacarbonyl catalyzed trimerization of **3-12** in refluxing toluene in 34% yield (Scheme 3-2). MALDI-TOF mass spectrometry of the oligophenylene precursor **3-13** indicated a single species with the molar mass and isotopic distribution consistent with the calculation, and the ^{1}H NMR spectrum also confirmed the chemical identity of the precursor **3-13**. In contrast to the complex synthesis toward similar oligophenylene precursor **3-6**, the cyclotrimization of the symmetric acetylene **3-12** leads to one single product, namely the targeted oligophenylene precursor **3-13**.

The cyclization reaction from dendritic precursor **3-13** toward oligophenylene macrocycle **3-2** was realized by nickel-catalyzed intramolecular coupling in a microwave reactor at the scale of 50 mg without catalyst activation. Due to the difficult in purification of the desired macrocycle, the purification of **3-2** was applied by preparative gel permeation chromatography (GPC) with the concentration of 50mg/10mL in chloform. At last, the shape-persistent polyphenylene macrocycle **3-2** could be obtained as a colorless solid with the yield of 56%. MALDI-TOF MS spectrometry of **3-2** (Figure 3-8) indicated a single species with the desired molar mass, and the experimental isotopic distribution was consistent with the theoretical calculation. Therefore, the six-fold intramolecular homocoupling was successfully realized in the construction of shape-persistent oligophenylene macrocycle **3-2**.

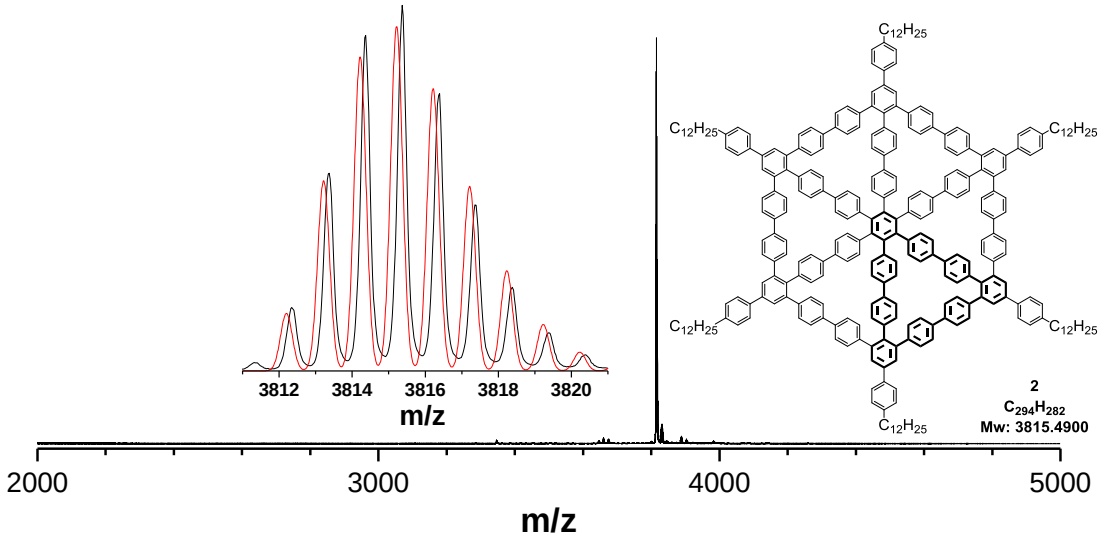

Figure 3-8. MALDI-TOF MS spectrum of the polyphenylene macrocycle subunit **3-2**. Inset: isotopic distribution (black) compared with mass spectrum simulated (red) for $C_{294}H_{282}$.

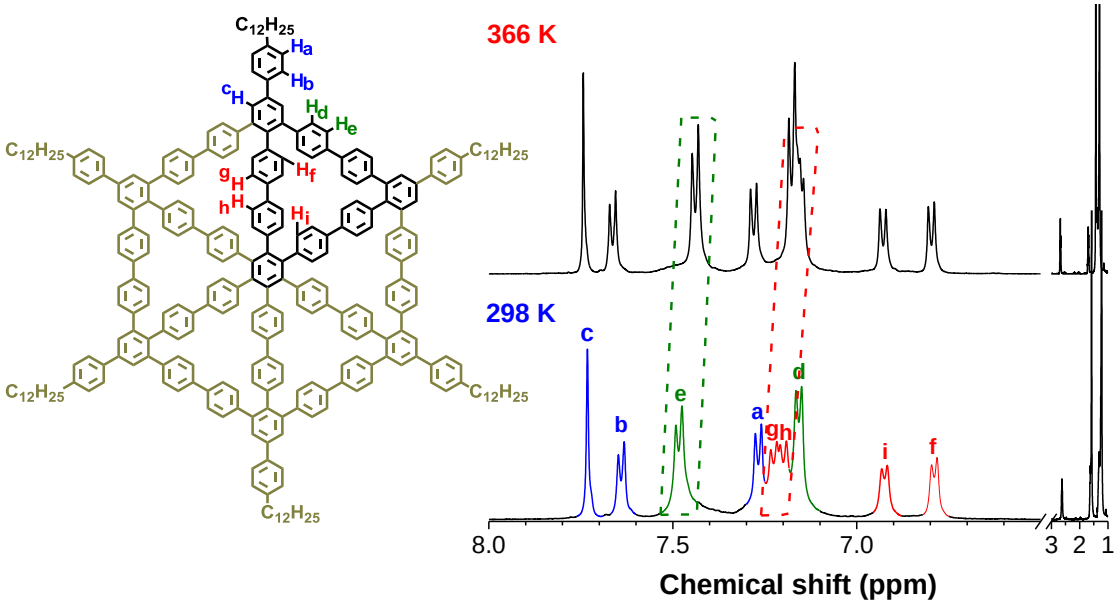

Figure 3-9. ^{1}H NMR spectrum of the polyphenylene macrocycle subunit **4-2** in $C_2D_2Cl_4$ at room temperature with the assignment of aromatic protons.

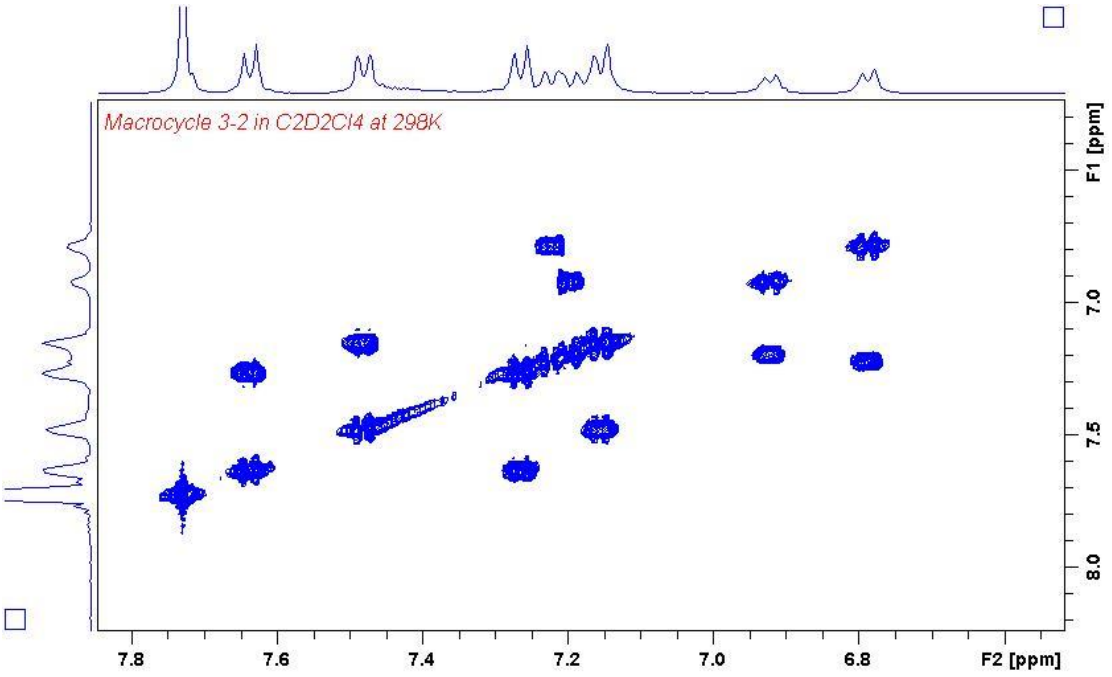

Figure 3-10. 2D ^{1}H-^{1}H COSY NMR spectrum of the polyphenylene macrocycle **3-2** in $C_2D_2Cl_4$ at 298K.

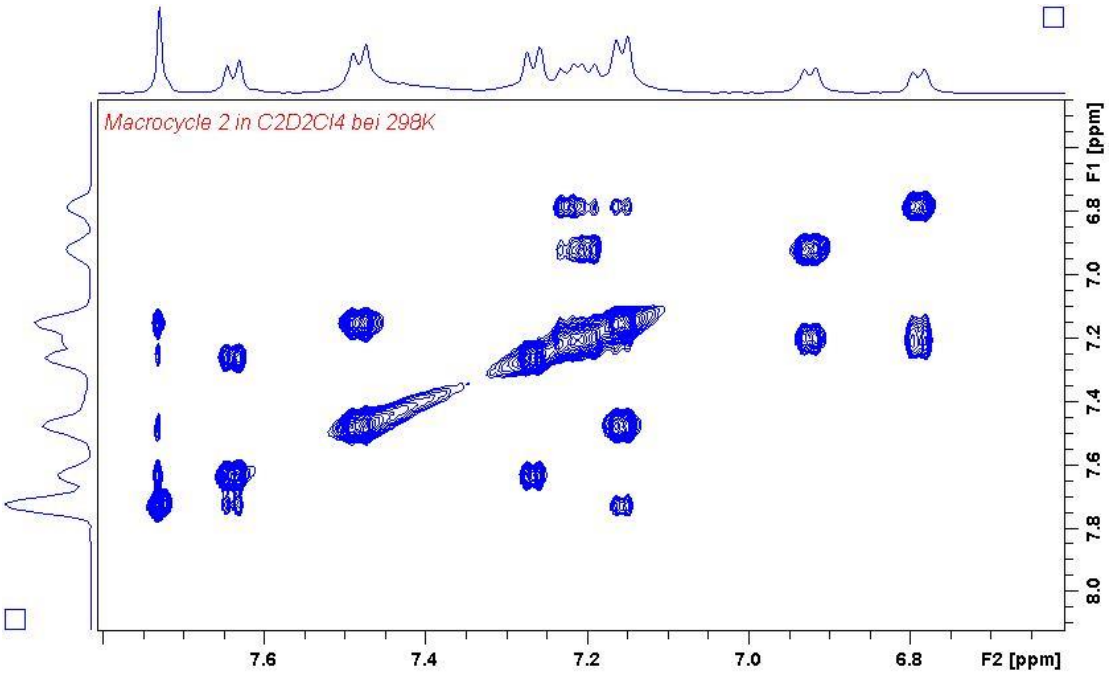

Figure 3-11. 2D ^{1}H-^{1}H NOESY NMR spectrum of the polyphenylene macrocycle **3-2** in $C_2D_2Cl_4$ at 298K

To further confirm the chemical identity of the macrocycle **3-2**, ^{1}H NMR spectrum (Figrue 3-9) with 2D COSY (Figrue 3-10), and NOESY spectra of **3-2** (Figrue 3-11)

were recorded, and every aromatic proton signal could be unambiguously assigned. Notably, the ^{1}H NMR spectrum (Figure 3-9) clearly displayed that only the signals from protons pointing toward the internal cavity, i.e., H_e, H_g, and H_h, were slightly up-field shifted from 7.49, 7.23, and 7.20 ppm to 7.44, 7.15, and 7.14 ppm, respectively, when the temperature was raised from 298 to 366 K. Due to the steric repulsion, the biphenyl segments (where H_e, H_g, and H_h are all in the *ortho* position) in macrocycle **3-2** is rotated out of the plane and confined in the internal cavity. Along with the increasing temperature, the benzene rings in biphenyl segments are capable of rotating more freely, which leads to a reduced deshielding effect from the adjacent benzene rings and thus an upfield shift in the NMR spectra. [14,15]

Table 3-1. Chemical shift of aromatic protons in macrocycle **3-2** at 298 K and 366K.

Temperature	$\delta(H_a)$	$\delta(H_b)$	$\delta(H_c)$	$\delta(H_d)$	$\delta(H_e)$	$\delta(H_f)$	$\delta(H_g)$	$\delta(H_h)$	$\delta(H_i)$
298 K	7.27	7.64	7.73	7.16	7.49	6.79	7.23	7.20	6.92
366 K	7.28	7.66	7.74	7.18	7.44	6.80	7.15	7.14	6.93

The DOSY diffusion NMR spectrum (figure 3-12) of the rigid polyphenylene macrocycle is recorded to determine the size of the molecule **3-2** in solution. In the spectrum, a calculated self-diffusion constant (*D*) of 7.06 × 10^{-11} m^2 s^{-1} for the molecule **3-2** is obtained. According to the Stokes-Eisntein equation, the diameter of the polyphenylene macrocycle **3-2** in tetrachloroethane is calculated to be 3.89 nm based on the measured self-diffusion constant (*D*), where *r* is the van der Waals radius of the molecule in meters, *k* is the Boltzmann constant (1.380 × 10^{-23} J K^{-1}), *T* is the temperature in Kelvin, η is the viscosity of the solution in Pascal seconds (Pa s = 1000 centipoises) and *D* is the self-diffusion constant.

Stokes-Eisntein equation $$r = \frac{kT}{6\pi\eta D}$$

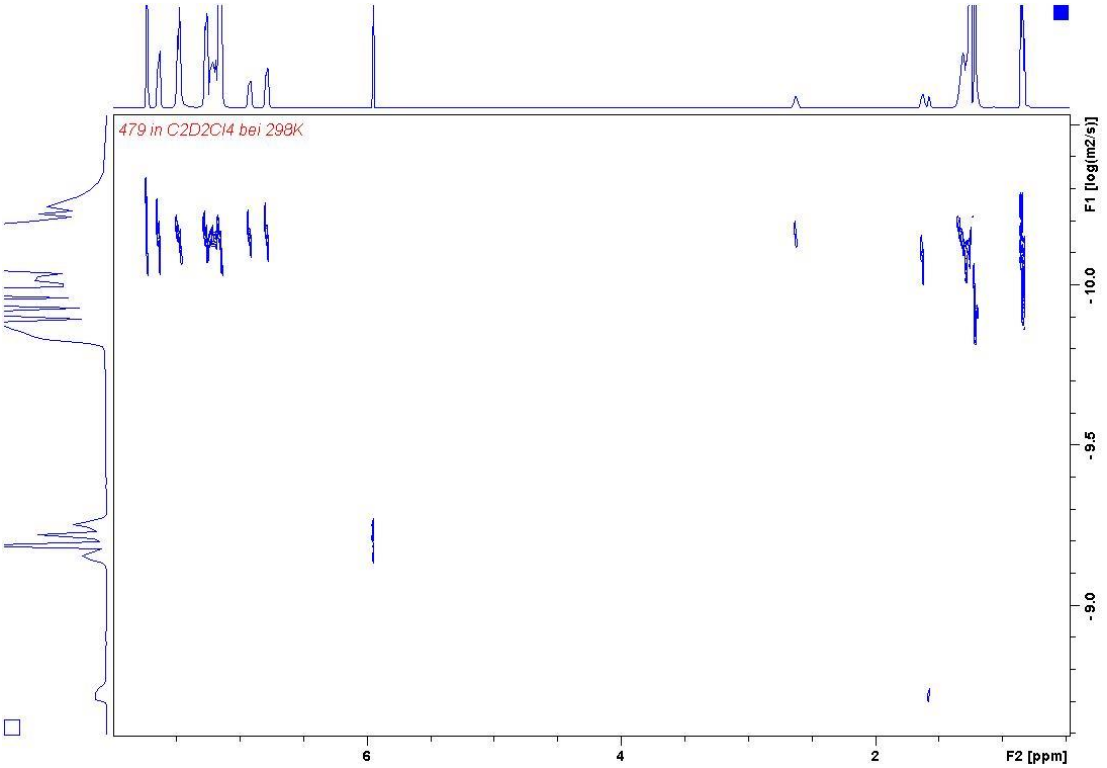

Figure 3-12. DOSY diffusion NMR spectrum of polyphenylene macrocycle subunit **3-2.**

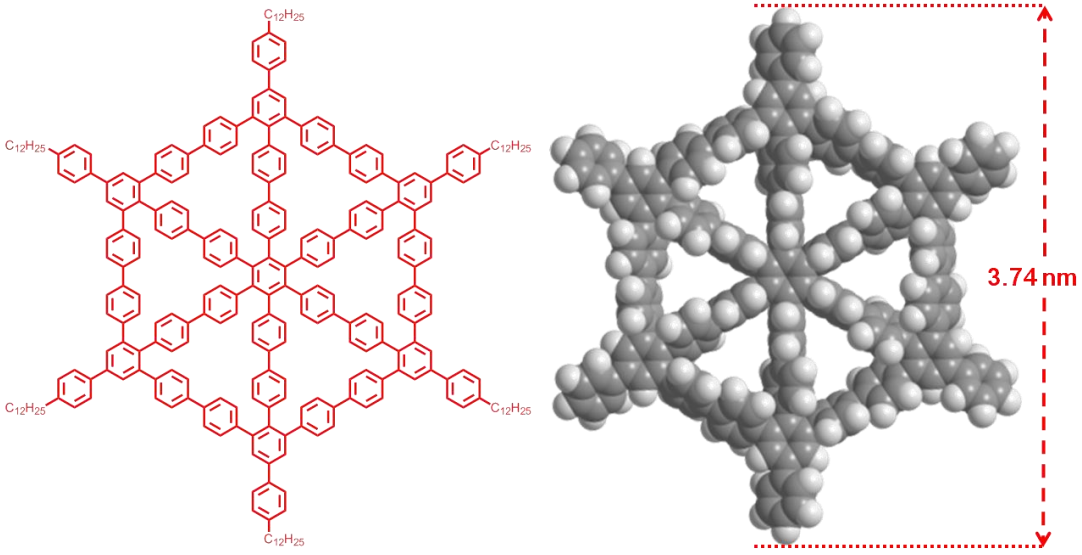

Figure 3-13. Molecular structure of polyphenylene macrocycle **3-2** and its simulated geometry on the basis of B3LYP/6-31G(D) using the Gaussian software. (dodecyl chains are omitted for calculation)

For better comparison, the geometry of the polyphenylene macrocycle **3-2** is also simulated with the Gaussian software on the basis level of B3LYP/6-31G(d)[16] (figure

3-13), while the dodecyl chains were omitted in order to simplify the calculation. And the simulated molecular size of the polyphenylene core of the macrocycle **3-2** is determined to be 3.74 nm. Taking into account the peripheral six *n*-dodecyl chains (around 1.6 nm), the approximate diameter of the macrocycle **3-2** is calculated to be 6.9 nm. Compared with this simulated size, the experimental size (3.89 nm) of the molecule **3-2** in the solution of tetrachloroethane is significantly smaller. The difference could be attributed to the influence of the calculation method. The theoretical simulation is valid for a molecule in the gas state, however, the DOSY diffusion NMR approach investigates the molecule in the solution. When the molecule is dissolved in the organic solvent, the peripheral *n*-dodecyl chains will definitely be crowded around the polyphenylene core. By contrast, these *n*-dodecyl chains are assumed to be fully extended in the theoretical simulation. Therefore, the experimental size will be smaller than the simulated one. Additionally, the molecule is assumed to be a sphere when calculating the diameter *via* the Stokes-Eisntein equation from the diffusion NMR results, however, the macrocyclic molecular **3-2** is a rigid and planar disk-like molecular indicated by the simulation. This difference between the assumed shape in the equation and the real geometry of the molecule will also influence the accuracy of calculated diameter.

To check the influence of cyclization on the structure of the conjugated backbone, the UV-Vis spectrum and cyclic voltammetry are applied including a comparison with its oligophenylene precursor **3-13** (Figure 3-14). Cyclic voltametry shows an obvious decrease of the reduction potential for the macrocycle **3-2** ($E_{red(onset)}$ = -1.03 eV) after the formation of the macrocycle, while the reduction potential of oligophenylene precursor **3-13** is $E_{red(onset)}$ = -0.80 eV. Furthermore, the absorption spectra clearly indicate a blue shift for macrocycle **3-2** (λ_{abs} = 297 nm, ε = 7.10 × 10^4 $M^{-1}cm^{-1}$, and λ_{abs} = 283nm, ε = 7.51 × 10^4 $M^{-1}cm^{-1}$) when compared with its star-shaped precursor **3-13** (λ_{abs} = 286 nm, ε = 9.50 × 10^4 $M^{-1}cm^{-1}$, and λ_{abs} = 310 nm, ε = 1.03 × 10^5 $M^{-1}cm^{-1}$). However, the photoluminescence spectra suggest a red shift for

macrocycle **3-2** (λ_{fl} = 422 nm) when compared with the open-ring precursor **3-13** (λ_{fl} = 393 nm).

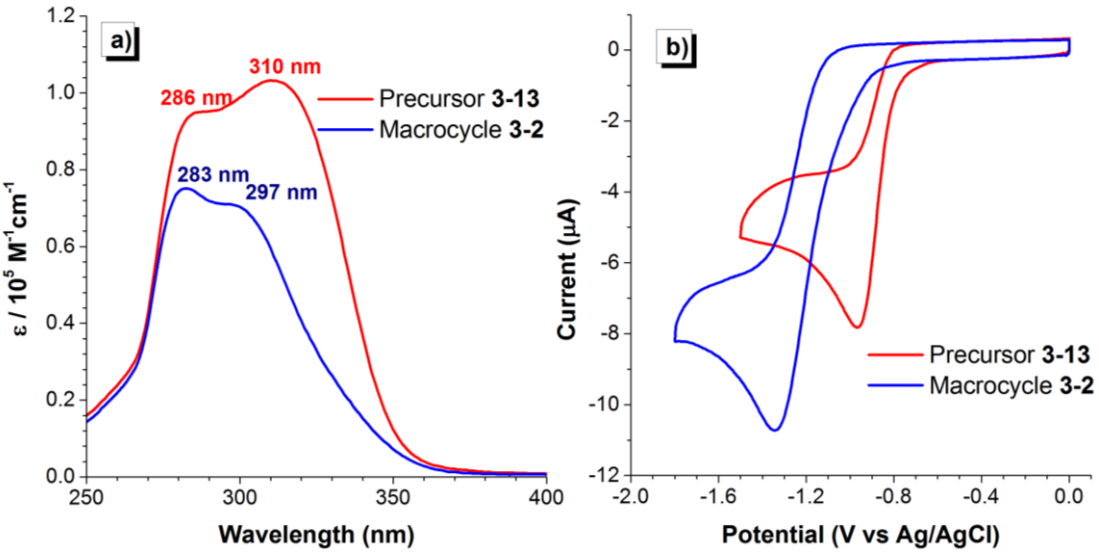

Figure 3-14. a) UV-Vis spectra of oligophenylene precursor **3-13** and macrocycle **3-2** in $CHCl_3$ (with the concentration of 1.0×10^{-5} M). b) Cyclic voltammetry spectra of compound **3-13** and macrocycle **3-2** in CH_2Cl_2 with 0.1 M $[Bu_4N][PF_6]$ as electrolyte.

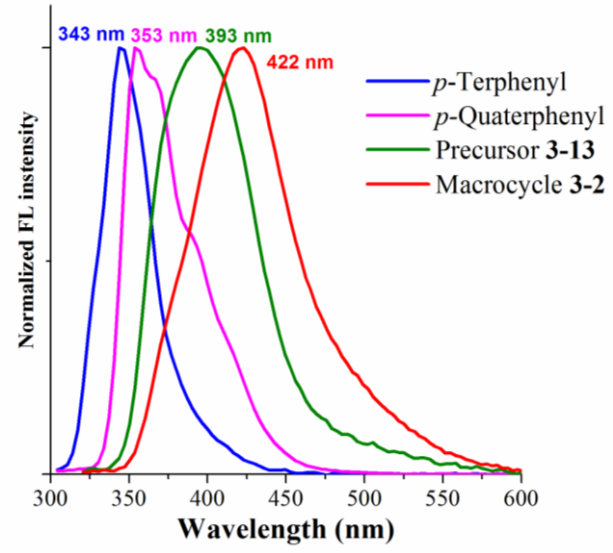

Figure 3-15. FL spectra of *p*-terphenyl, *p*-quaterphenyl, oligophenylene precursor **3-13** and macrocycle **3-2** in $CHCl_3$ (with the concentration of 1.0×10^{-5} M).

Compared with the spoked-wheel shaped macrocycles with phenylene-acetylene backbones developed by Hoger's group (**1-46** in Figure 1-12, and **1-47** in Figure 1-13),

the macrocycles normally show red-shifted absorption and fluorescence peaks after ring closure.[17,18] This difference between the phenylene-acetylene macrocycle and our polyphenylene macrocycle is certainly attributed to the intramolecular strain and π-extension degree in the macrocycle framework. And I will discuss it in detailed according to the simulated structure below.

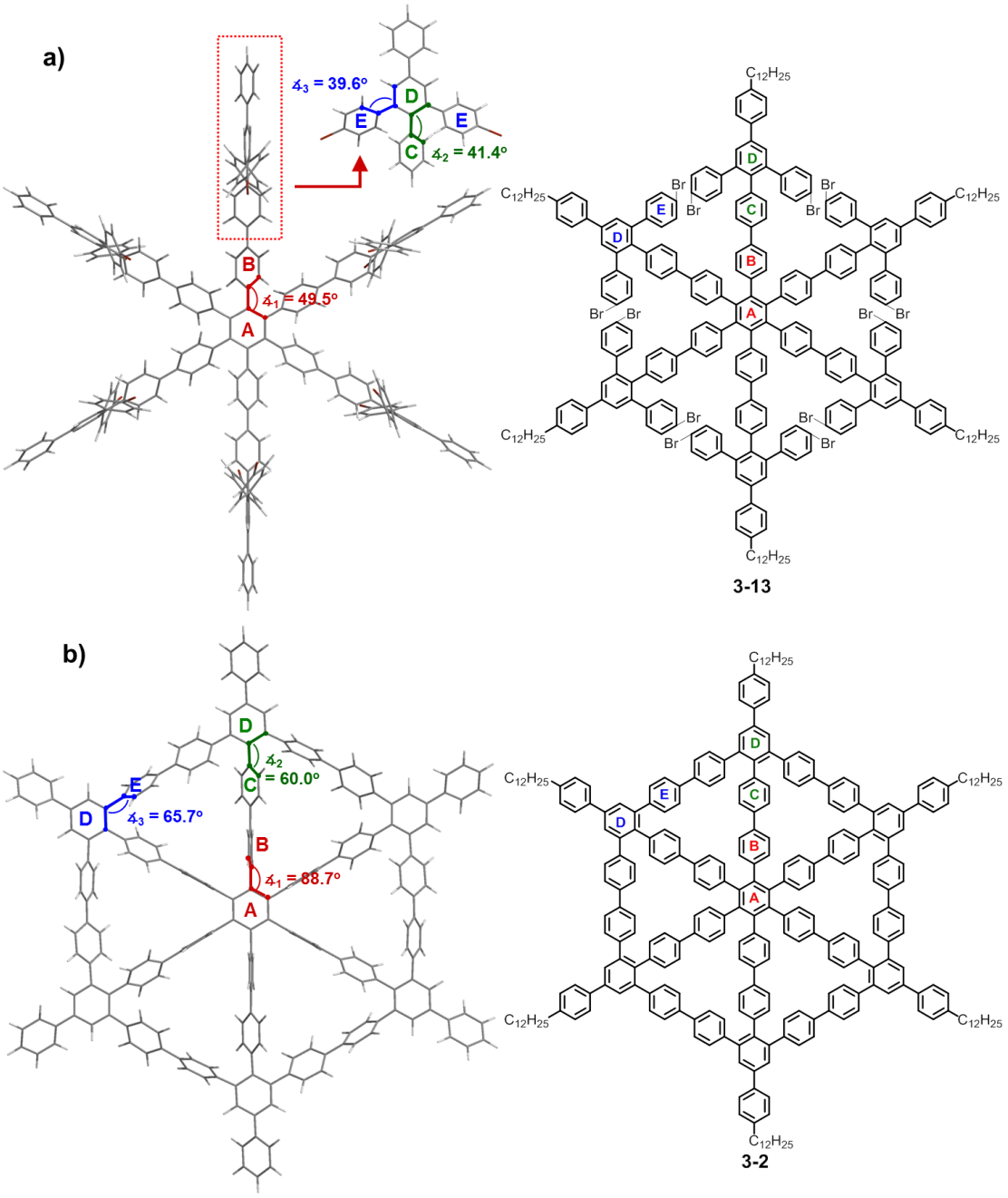

Figure 3-16. Tube models and molecular structures of star-shaped oligophenylene precursor **3-13** (a) and shape-persistent macrocycle **3-2** (b) on the basis of B3LYP/6-31G(d) level with the angles ∢$_1$ and ∢$_2$, and ∢$_3$, which are measures of π-conjugation extension in the molecular.

According to the simulated geometry of the dendritic precursor **3-13** and the macrocycle **3-2** (Figure 3-16), the dihedral angle $\measuredangle_1$ between the *spoke*-like benzene ring B and the central benzene ring A has changed dramatically from 49.5 ° in **3-13** to 88.7 ° in **3-2** after ring closure. Meanwhile, the dihedral angle $\measuredangle_2$ between the bridging *spoke*-like benzene unit C and periphenral benzene ring D, as well as the dihedral angle $\measuredangle_3$ between the *hub*-like phenylene unit E and periphenral benzene ring D, have both increased from 41.4 ° and 39.6 ° in precursor **3-13** to 60.0 ° and 65.7 ° in the resulting macrocycle **3-2**, respectively. These increased dihedral angles have directly interrupted π-conjugated backbones in the planar macrocycle, which led to the blue shift of the absorption peaks compared with the open-ring precursor **3-13**. On the other hand, the fluorescence spectra displayed a red shift and a larger Stokes shift for **3-2** (λ_{fl} = 422 nm, with a shift of 125 nm) compared with those of **3-13** (λ_{fl} = 393 nm, with a shift of 83 nm) (Figure 3-15), which suggested that the excited state of **3-2** had a more planarized structure than that of **3-13**, with extended π conjugation in contrast to their ground-state structures.

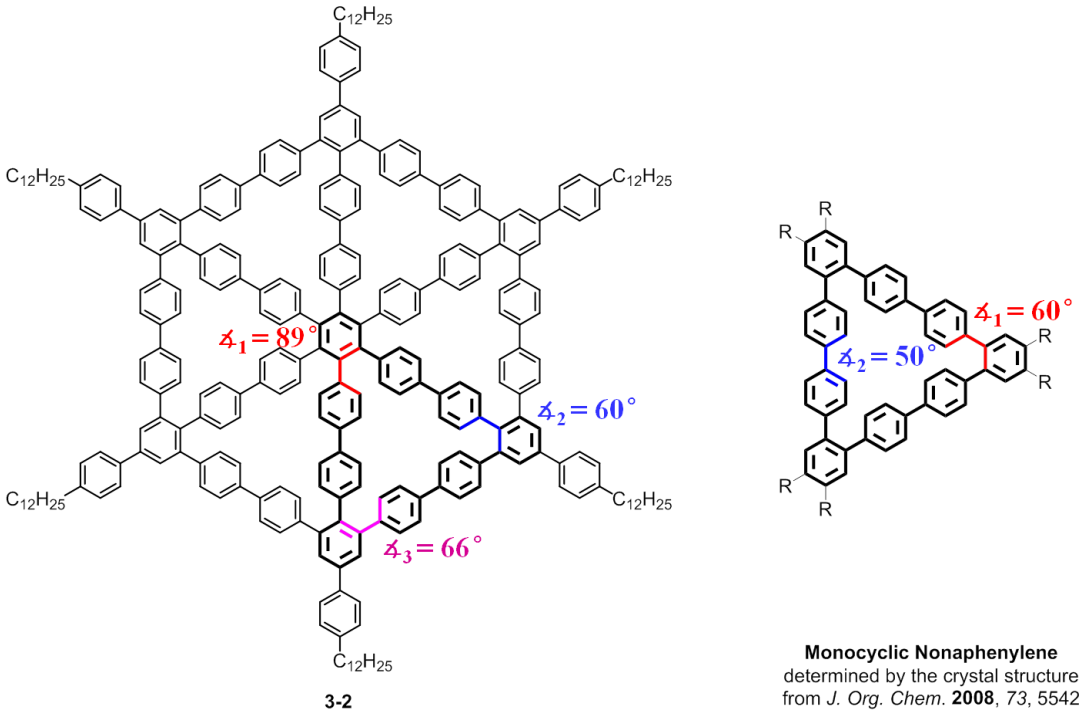

Figure 3-17. Molecular structures of shape-persistent macrocycle **3-2** and monocyclic substructure Nonaphenylene with the dihedral angles $\measuredangle_1$ and $\measuredangle_2$, and $\measuredangle_3$, which are measures

of π-conjugation extension in the molecular.

Relative to the macrocycle with phenylene-acetylene backbones (**1-46** in Figure 1-12), the butadiyne linkage in the *spoke* and *rim* of the wheel have greatly diminished the intramolecular strain and help to maintain the π-extension of the conjugated system. Thus the macrocycle will show a hypsochromic shift in both the UV-Vis and FL spectra in comparison with its open-ring precursor.

Structurally similar to the shape-persistent macrocycle **3-2**, a monocyclic nonaphenylene and its derivatives (Figure 3-17) have been repoted by Kamada and Iyoda,[19] which could be viewed as a substructure of the macrocycle **3-2**. The UV-Vis absorption spectra of an alkyl chain substituted monocyclic nonaphenylene show absorption maxima at 283-289 nm, while the shape-persistent macrocycle **3-2** displays two absorption peaks at 283 nm and 297 nm. Based on the optimized geometry of compound **3-2** and the crystal structure of monocyclic nonaphenylene, we find that the dihedral angles in the macrocycle **3-2** have dramatically increased to approximate 66 ° and 89 ° compared with the monocyclic nonaphenylene with approximate dihedral angle around 60 °. These increased dihedral angles will interrupt the π-conjugation and extension in the macrocycle, and thus the nonaphenylene substructure in the spoke-wheel shaped macrocycle is only partly conjugated with the neighboring cyclic nonaphenylene substructure. Therefore, an absorption maxima (283 nm) similar to that of the monocyclic nanophenylene could be observed, and a red-shifted shoulder peak around 297 nm could also be observed due to the slightly π-extended structure. In addition, the macrocycle **3-2** also exhibits a red shifted emission maxima ($_{fl}$ = 422 nm) in comparison with the monocyclic substructure ($_{fl}$ = 400 nm), which can be ascribed to the π-extended structure.

3.2.3 STM measurements and structural proof of 3-2

Whereas the spectroscopic characterizations such as NMR, and UV-Vis absorption spectroscopy have provided a clear proof for macrocyclic structure of **3-2**, microscopic analyses by scanning tunning microscopy (STM) can directly validate the

shape-persistent macrocycle skeleton of **3-2**. Based on the simulated geometry of **3-2**, the polyphenylene backbones of **3-2** were confined into a 2D planar sheet by the peripheral biphenyl bridge. Following the macroscopic example of spoked wheels, the building blocks of the shape-persistent wheel-like macrocycles can be divided into three different segments, referred to *hubs* (*n*-fold cores), *spokes* (stiffening rods), and *rims* (macrocyclic rings). Combining the simulated geometry and structural analysis, the planar geometry was maintained by the *hub*-like benzene cores and further rigidified by other *rim*-like and *spoke*-like phenylene segments. In contrast to the *hubs* which are parallel with the macrocyclic planar, those *rim*-like and *spoke*-like segments are all tilted out of the plane (figure 3-18). In particular, the dihedral angle $\measuredangle_1$ around 88.7 ° indicated that the six *spoke*-like benzene rings B are nearly perpendicular to the 2D macrocycle surface. And those aromatic hydrogens on *rim*-like and *spoke*-like segments which are pointing outward the macrocyclic planar, provide a possibility for multiply CH-π interaction between the macrocycle and the π-surface of highly oriented pyrolytic graphite (HOPG) and drive the formation of a physisorbed monolayer of macrocycle **3-2** on HOPG. Therefore, the scanning tunneling microscopy measurement is possible for this rigid macrocycle **3-2**, which prove us another approach for structural characterization.

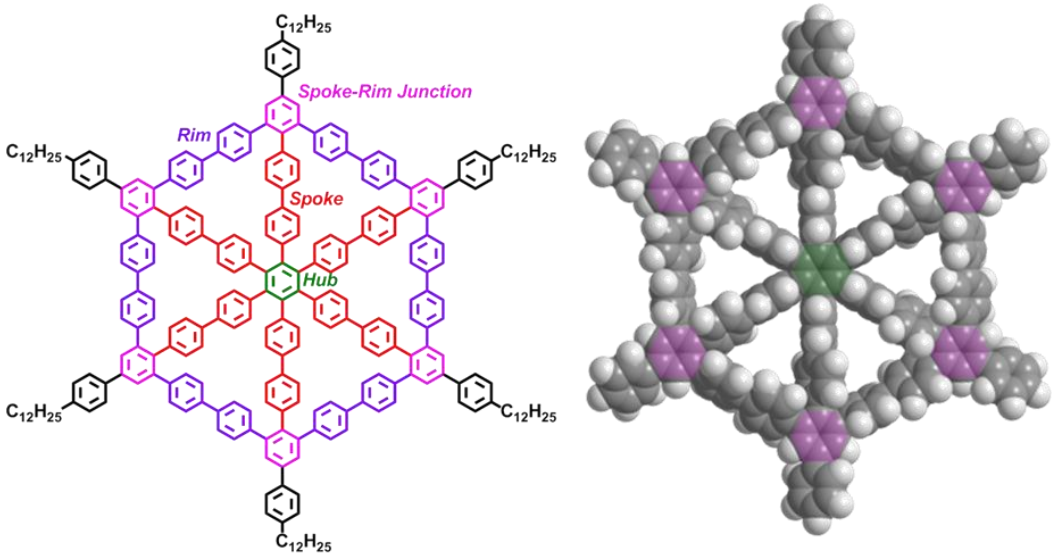

Figure 3-18. Structural analysis of "wheel-like" macrocycle **3-2**, which are composed of the ***hub*** (the center of the wheel), ***spokes*** (radiating rots from the center), and ***rim***

(outer-edge of the rim); and the optimized geometry of the macrocycle **3-2** on the basis level of B3LYP/6-31G(d).

Therefore, to confirm the structure of the macrocycle **3-2**, the STM (figure 3-19) is applied to image a self-assembled monolayer of **3-2** at the solution/solid interface of 1-phenyloctane (PO) and highly oriented pyrolytic graphite (HOPG) at ambient conditions. The STM visualization of the macrocycle **3-2** is carried out by the group of Prof. Steven de Feyter at Katholieke Universiteit Leuven, Belgium. Firstly, the macrocycle **3-2** is dissolved in 1,2,4-Trichlorobenzene (TCB) with the concentration of 10^{-4} M, and then the droplet of the solution is deposited onto the freshly cleaved HOPG surface. After addition of the high boiling point solvent 1-phenyloctane (1-PO) onto the surface, the STM images are collected at the 1-PO/HOPG interface under different sample biass and tunneling current after TCB is evaporated.

At higher voltage (sample bias = -1.7 V) with tunneling current of 25 pA, a submonolayer coverage was observed while the molecular domains also extended over a few tens of nanometers. From the STM images, the macrocycle **3-2** forms a hexagonal 2D pattern on the substrate with the unit cell parameters of $a = b = 4.7 \pm 0.2$ nm and $\alpha = 60 \pm 3°$, while the *n*-dodecyl chains of adjacent molecules interdigitate with each other. Based on the size of the aromatic core (3.75 nm) and the length of *n*-dodecyl chains (1.60 nm), the cell parameter of the hexagonal arrangement should be around 5.3 nm which is comparable with the STM imaging results. Considering the shape and size of the macrocycle **3-2** and the interdigitation of the dodecyl chains between neighboring macrocycle **3-2**, the hexagonal packing model is proposed and perfectly matches with the experimental results.

The molecular model (Figure 3-19b) built using the experimentally obtained lattice parameters reveals that the dodecyl chains possibly interact with each other via van der Waals interactions. The model also shows that the region between the dodecyl chains is largely empty, and thus it is possibly filled by mobile solvent molecules. The dimension of the polyphenylene core obtained from calibrated STM images (as indicated by the dashed line in Figure 3-19d: ~2.4 nm) matches closely with the one

obtained from the theoretically calculated structure (2.2 nm). Furthermore, the STM contrast of the aromatic core matches closely with the anticipated structure of **2**. Each bright feature consists of a hexagonal frame ('*rim*-like' biphenylylenes) filled with a star-shaped feature ('*spoke*-like' biphenylylenes) with a central dark blob. The '*spoke*-like' biphenylylenes give rise to six adjacent pores as expected from the molecular structure (Figure 3-19c and 3-19d). The tilted biphenylylenes have presumably enhanced the self-assembly by multiple "CH-π" interactions with the graphite surface. The peripheral phenyl rings that form a part of the phenyl dodecyl substitution are also visualized (arrows in Figure 3-19a and 3-19b). Thus, the STM analysis not only proved the chemical structure of the targeted compound **3-2**, but also provided direct evidence for its shape-persistent conformation on a solid substrate, which was not accessible via conventional characterization methods.

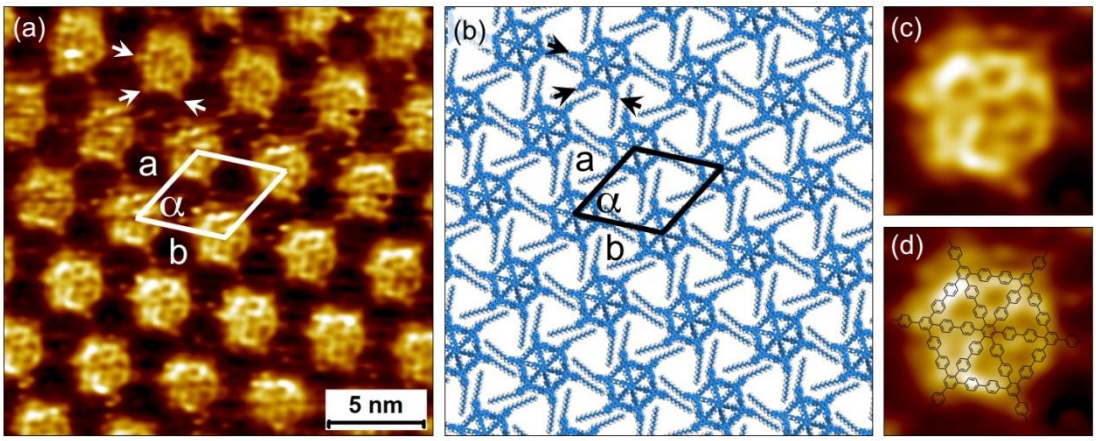

Figure 3-19. (a) High-resolution STM image of a self-assembled monolayer of polyphenylene macrocycle **3-2**. The unit cell parameters are a = b = 4.7 ± 0.2 nm, and α = 60 ± 3.0° (one molecule per unit cell). Tunneling current, I_{set} = 25 pA; Sample bias, V_{bias} = –1.5 V. (b) Molecular model of the self-assembled network of polyphenylene macrocycle **3-2**. (c) Digital zoom (4.1 nm × 4.1 nm) of the STM image provided in panel (a) showing the aromatic core of a single molecule of polyphenylene macrocycle **3-2**. (d) Same image as in (c) but overlapped with the molecular structure of polyphenylene macrocycle **3-2**.

The contrast of the macrocycle **2** is also very dependent on the imaging parameters. At high voltage (–1.5 V), the aromatic core appears as a spoked wheel corresponding to the expected structure of the macrocycle, as shown in the main text. When the sample bias is decreased to -0.7 V and the tunneling current is maintained at 25 pA, the contrast of the STM image is inverted and the center of the molecule appears dark (Figure 3-20). Besides, each molecule seems connected with its neighbors *via* bright lines present in locations that can correspond with the positions of alkyl chains within the network. Those interdigitating dodecyl chains could be roughly observed which also confirmed the packing model proposed above (Figure 3-19b).

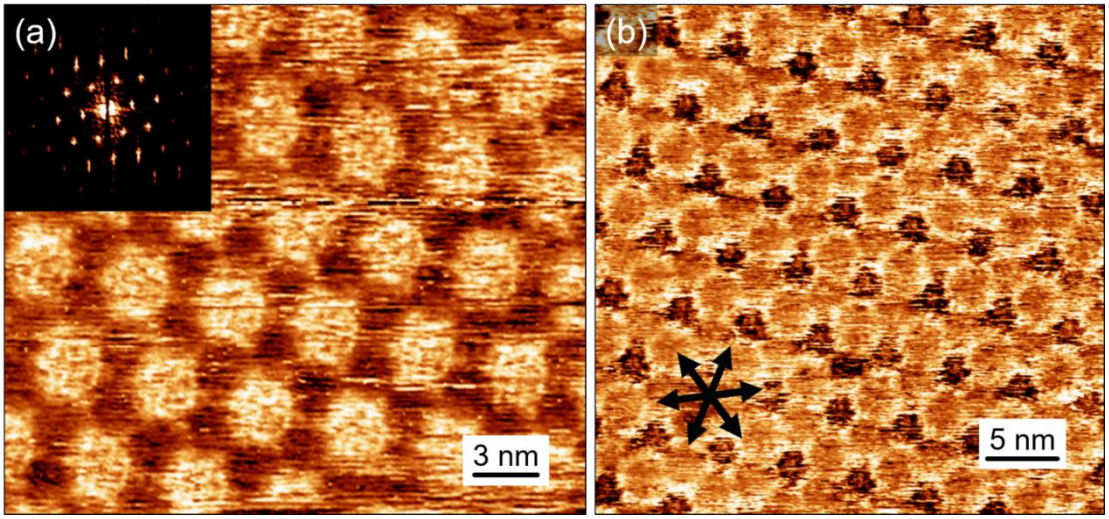

Figure 3-20. High-resolution STM images of the self-assembled monolayer of polyphenylene macrocycle **3-2**. (a) Tunneling current, I_{set} = 25 pA; Sample bias, V_{bias} = –1.5 V. (b) Tunneling current, I_{set} = 25 pA; Sample bias, V_{bias} = –0.7 V. A Fourier transform is inserted in panel (a), and the graphite axes are represented by the arrows on panel (b).

To further investigate the interaction mechniasm between the macrocycle **3-2** and HOPG, a proof of concept NMR investigation on the complexation between the macrocycle **3-2** and a nanographene derivative *t*Bu$_6$-HBC, as a model of HOPG is conducted. (2,5,8,11,14,17-hexa-tert-butylhexabenzo[bc,ef,hi,kl,no,qr]coronene, Figure 3-21)

Compared with the ^{1}H NMR spectra of the pristine *t*Bu$_6$-HBC and macrocycle 3-**2**, we can clearly observe the obvious downfield shift for the signals of those aromatic

protons locating on the *spoke* segments (H_g, H_h, H_f, and H_i) and on the *rims* segments (H_d, and H_e) surrounding the interior pores, while the signals from other protons located on the *hubs* (H_c) and peripheral benzene rings (H_a, and H_b) remain inert after addition of *t*Bu_6-HBC. These NMR signal alternations on the protons neighboring the interior cavities unambiguously support the probable non-covalent interaction between nanographene *t*Bu_6-HBC and the pores of the polyphenylene macrocycle **3-2**.

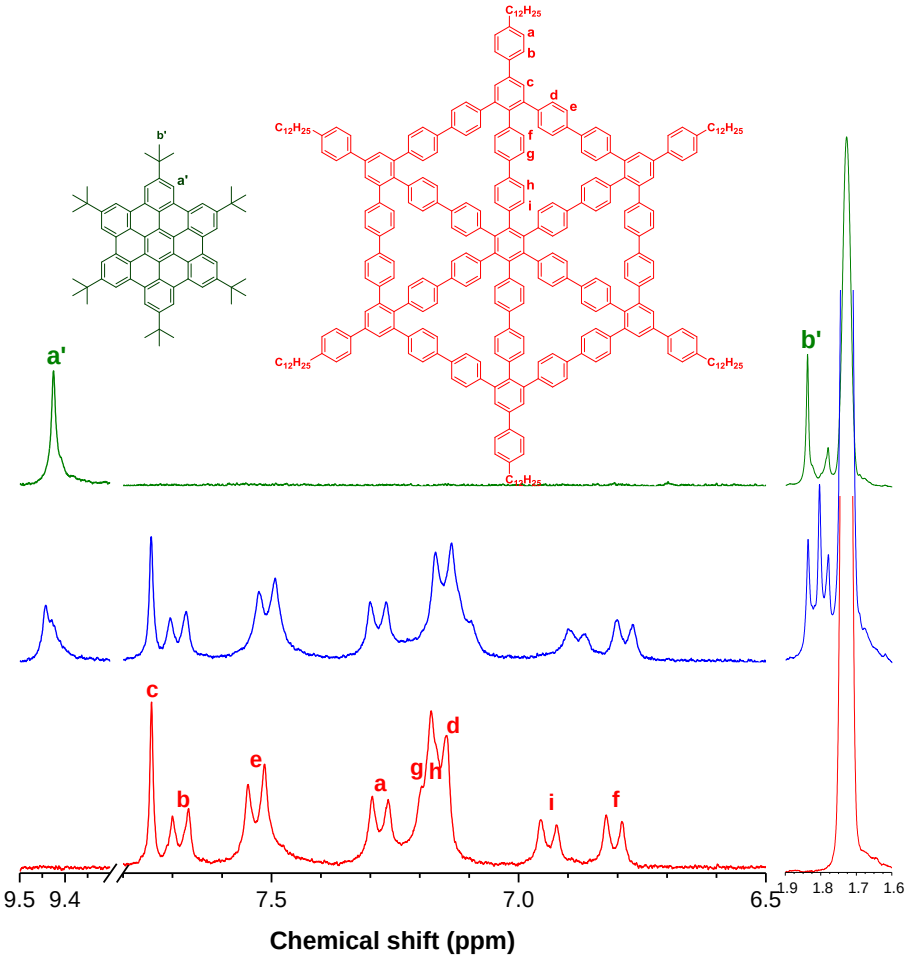

Figure 3-21. ^{1}H NMR spectra of *t*Bu_6-HBC (up), the mixture of *t*Bu_6-HBC with macrocyclic polyphenylene **3-2** (molar ratio: 1.1/1.0, middle), and macrocyclic polyphenyle1**3-2** (bottom).

Therefore, a complexation model between *t*Bu_6-HBC and **3-2** was proposed (Figure 3-22), in which the π-conjugated surface of HBC is interacting with the interior hexaphenylbenzene core based on the multiple "CH-π" interactions, and the *tert*-butyl groups are located in the center of the interior pores.[20] As a result of the interactions between nanographene and macrocycle **3-2**, the signals from hydrogns on the

hexaphenylbenzene core (H_i and H_h) have shown a upfield shift of approximate 0.07 ppm due to the shielding effect from the π-electrons of HBC, and the signals of other protons surrounding the cavity also exhibited an upfield shift of 0.03 ppm.

In addition, the signals of the aromatic protons ($H_{a'}$) on *t*Bu_6-HBC have also broaden and down-field shifted with approximate 0.03 ppm due to the deshielding effect from the π-electrons of the *spoke* segments on macrocycle **3-2**. And a new proton signal appeared at 1.81 ppm adjacent to the original signal from the *tert*-butyl group ($H_{b'}$, δ = 1.85 ppm), which is ascribed to the shielding effect from the π-electrons around the interior pores of macrocycle **3-2**. All these observations have supported the formation of supramolecular complex between the nanographene and macrocycle **3-2** *via* multiple "CH-π" interactions.

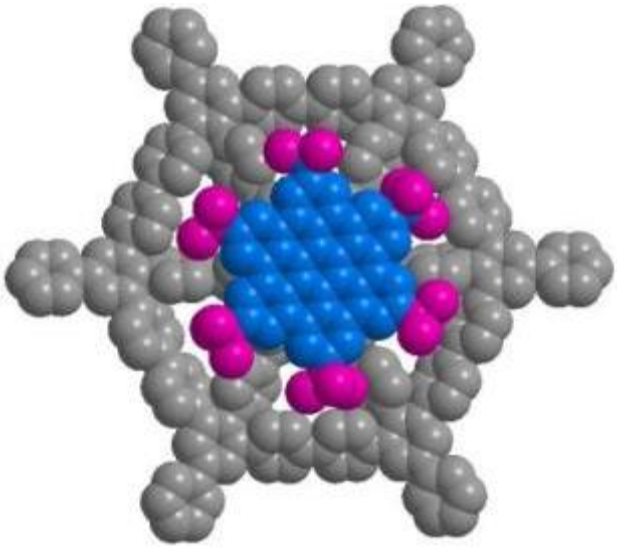

Figure 3-22. Possible complexation model between polyphenylene macrocycle **3-2** with the model compound of HOPG (*t*Bu_6-HBC) *via* multiple "CH-π" interactions.

3.3 Summary

In summary, we have proposed two new 2D carbon networks composed of sp^2-carbons (**graphenylene-1** and **graphenylene-2**) based on the structural analysis of graphene, graphyne, and graphdiyne. In order to investigate the structural details of 2D carbon networks composed of all sp^2-carbon atoms, the synthetic routes toward the shape-persistent macrocyclic substructures (**3-1**, and **3-2**) are proposed.

With the assistance of the hexaphenylbenzene core as the cyclization template, the rigid macrocyclic polyphenylene backbone was proposed to be constructed via six-fold intramolecular Yamamoto coupling with the template-directed synthesis. Therefore, two star-shaped oligophenylene precursors (**3-6**, and **3-13**) were readily synthesized via the cyclotrimerization of the corresponding acetylene derivatives (**3-5**, and **3-12**), and the defined geometry of these two precursors was verified via MALDI-TOF MS and NMR spectra. After Yamamoto coupling at low concentration in a microwave reactor, one targeted macrocycle (**3-2**) was obtained after purification via recycling GPC with the scale of 50 mg.

In order to verify the chemical structure of the spoke-wheel shaped molecule **3-2**, NMR spectroscopy was applied to elucidate the structural details of the shape-persistent polyphenylene macrocycle with the support of a MALDI-TOF mass spectrum. The comparison between the simulated geometry of **3-2** and experimental radius of **3-2** via DOSY NMR also helps to further confirm the chemical identity of the targeted polyphenylene macrocycle **3-2.** The investigation of the optoelectronic properties of the polyphenylene macrocycle **3-2** and its open-ring precursor **3-13**, as well as the comparison with its reported monocyclic substructures, both indicate the hypsochromic shift of the absorption maxima after ring closure. This contrast directly suggests the rigid conformation of the polyphenylene macrocycle and its disturbance on the π-conjugation of the spoked wheel **3-2**.

At last, scanning tunneling microscopy (STM) was applied to directly visualize the molecular structure and shape-persistent conformation of the polyphenylene spoked wheel (the radius of the polyphenylene framework of **3-2** is around 3.8 nm). The STM images clearly show a hexagonal packing pattern with the unit cell parameters of $a = b = 4.7 \pm 0.2$ nm and $\alpha = 60 \pm 3°$, which perfectly matches the size of the macrocycle **3-2**. In addition, the hexagonal shape of the macrocycle **3-2** could be clearly observed in the STM images with higher resolution, while six adjacent voids appearing in each hexagon in the STM images also completely validate the existence of the cavities in the polyphenylene macrocycle **3-2**. The complexation between the shape-persistent macrocycle **3-2** and nanographene segments (tBu$_6$-HBC) was also studied by the proton NMR measreument. The shift of the proton signals implies a complexation model in which the nanographene moiety is incorporated onto the macrocycle via multiple CH-π interactions and the peripheral *tert*-butyl groups are located close to the interior cavities. This result also supports that such a molecular structure with six internal pores (approximately 4Å in diameter as measured on both models and STM images) can be highly interesting for supramolecular interactions with other guest molecules or ions, since they are expected to accommodate ions[21] and small aromatic compounds[22].

In summary, this chapter opens up a new avenue for designing and synthesizing a further variety of unprecedented 2D carbon structures and their subunits. Although the construction of the targeted 2D carbon network with well-defined and defect-free structure still requires a lot of efforts, the recent development in the fileds of 2D polymer synthesis[23], which is mainly approached *via* molecular framework, surface science and crystal engineering methods, will certainly push forward the exploration of 2D carbon materials in the future.

Reference

[1] J. Gibson, M. Holohan, H. L. Riley, *J. Chem. Soc.* **1946**, 456.

[2] R. H. Baughman, C. Cui, *Synth. Met.* **1993**, *55*, 315.

[3] J. W. Colson, W. R. Dichtel, *Nat. Chem.*, **2013**, *5*,453..

[4] P. Payamyar, B. T. King, H. C. Öttingerc, A. D. Schlüter, *Chem. Commun.*, **2016**,*52*, 18.

[5] D. Mössinger, J. Hornung, S. Lei, S. De Feyter, S. Höger, S. *Angew. Chem. Int. Ed.* **2007**, *46*, 6802.

[6] R. May, S. S. Jester, S. Höger, *J. Am. Chem. Soc.* **2014**, *136*, 16732.

[7] S. Klyatskaya, N. Dingenouts, C. Rosenauer, B. Muller, S. Hoger, *J Am Chem Soc* **2006**, *128*, 3150.

[8] G. Ohlendorf, C. W. Mahler, S. S. Jester, G. Schnakenburg, S. Grimme, S. Hoger, *Angew Chem Int Edit* **2013**, *52*, 12086.

[9] T. Zimmermann, *J Prak Chem-Chem Ztg* **1994**, *336*, 303.

[10] T. Zimmermann, G. W. Fischer, *J Prakt Chem* **1987**, *329*, 975.

[11] N. Agenet, O. Buisine, F. Slowinski, V. Gandon, C. Aubert, M. Malacria, *Organic Reactions* **2007**, 68:1:1–302.

[12] J. H. Hardesty, J. B. Koerner, T. A. Albright, G. Y. Lee, *J. Am. Chem. Soc.* **1999**, *121*, 6055.

[13] O. V. Ozerov, Brian O. Patrick, F. T. Ladipo, *J. Am. Chem. Soc.*, **2000**, *122*, 6423.

[14] R. J. Kurland, W. B. Wise, *J. Am.Chem. Soc.*, **1964**, *86*. 1877.

[15] R. E. Mayo, J. H. Goldstein, *Mol. Phys.*, **1965**, *10*, 301.

[16] Gaussian 09, Revision D.01, M. J. Frisch, G. W. Trucks, H. B. Schlegel, G. E. Scuseria, M. A. Robb, J. R. Cheeseman, G. Scalmani, V. Barone, B. Mennucci, G. A. Petersson, H. Nakatsuji, M. Caricato, X. Li, H. P. Hratchian, A. F. Izmaylov, J. Bloino, G. Zheng, J. L. Sonnenberg, M. Hada, M. Ehara, K. Toyota, R. Fukuda, J. Hasegawa, M. Ishida, T. Nakajima, Y. Honda, O. Kitao, H. Nakai, T. Vreven, J. A. Montgomery, Jr., J. E. Peralta, F. Ogliaro, M. Bearpark, J. J. Heyd, E. Brothers, K. N. Kudin, V. N. Staroverov, T. Keith, R. Kobayashi, J. Normand, K. Raghavachari, A. Rendell, J. C. Burant, S. S. Iyengar, J. Tomasi, M. Cossi, N. Rega, J. M. Millam, M. Klene, J. E. Knox, J. B. Cross, V. Bakken, C. Adamo,

J. Jaramillo, R. Gomperts, R. E. Stratmann, O. Yazyev, A. J. Austin, R. Cammi, C. Pomelli, J. W. Ochterski, R. L. Martin, K. Morokuma, V. G. Zakrzewski, G. A. Voth, P. Salvador, J. J. Dannenberg, S. Dapprich, A. D. Daniels, O. Farkas, J. B. Foresman, J. V. Ortiz, J. Cioslowski, and D. J. Fox, Gaussian, Inc., Wallingford CT, 2013.

[17] A. Thiessen, D. Würsch, S. S. Jester, A. V. Aggarwal, A. Idelson, S. Bange, J. Vogelsang, S. Höger, J. M. Lupton, *J. Phys. Chem. B* **2015**, *119*, 9949.

[18] V. Aggarwal1, A. Thiessen, A. Idelson, D. Kalle, D. Würsch, T. Stangl, F. Steiner, S. S. Jester1, J. Vogelsang, S. Höger, J. M. Lupton, *Nat. Chem.*, **2013**, *5*, 964.

[19] M. J. Rahman, J. Yamakawa, A. Matsumoto, H. Enozawa, T. Nishinaga, K. Kamada, M. Iyoda, *J. Org. Chem*., **2008**, *73*, 5542.

[20] G. Ohlendorf, C. W. Mahler, S.-S. Jester, G. Schnakenburg, S. Grimme, S. Höger, *Angew. Chem. Int. Ed*. **2013**, *52*, 12086.

[21] S. J. Emond, P. Debroy, R. Rathore, *Org. Lett.*, **2008**, *10*, 389.

[22] H. C. Kang, A. W. Hanson, B. Eaton, V. Boekelheide, *J. Am. Chem. Soc*., **1985**, *107*, 1979.

J. W. Colson, W. R. Dichtel, *Nat. Chem*., **2013**, *5*, 453

[23] J. W. Colson, W. R. Dichtel, *Nat. Chem*., **2013**, *5*, 453

4. Synthesis of oligophenylene macrocycles with "*figure eight*" conformations

4.1 Introduction

Parallel with the development of 2D carbon allotropes and related planar shape-persistent macrocyclic subunits, the design and synthesis of novel π-conjugated molecules with an unusual nonplanar architecture have also attracted attention due to their intriguing topology and functional properties. At the middle of last century, Riley has proposed an elusive carbon allotrope, namely "cubic graphite",[1,2] in which the 3D carbon backbone can be conceived as composing of double helical π-conjugated polymers **4-1** with sequentially annelated tetra-*o*-phenylene units (Figure 4-1a). Inspired by the beauty of the double-helical structure and possible material properties of these polyphenylenes, numerous research works have been accomplished in the past decade toward the design and construction of double helix systems[3,4], either by straightforward organic synthesis (Figure 4-1b)[5] or complementary hydrogen bonding bridging (Figure 4-1c)[6,7]. In this chapter, a new polyphenylene chain (**4-6**) with a double helical π-conjugated system was designed (Figure 4-1e), and the synthetic routes are based on the Yamamoto polymerization of the specific precursor which is enlightened by the ring closure reaction from open-ring oligophenylene precursor **4-4** to extremely congested phenylene bicyclophane **4-5** (Figure 4-1d)[8].

As the repeating unit of the targeted double-helical chain, oligophenylene macrocycle **4-7** (Figure 4-2b) is featured with the "figure eight" topology. Usually, the twisting and fixation of the macrcyclic compound into a "figure eight" knotted topology is driven by the hydrogen bonding (cyclic terephalaide Figure 4-2a)[9,10], metal-ligand coordination (expanded porphyrins in Figure 4-2a),[11] and constrained molecular structure. However, even through the strong metal-ligand interaction, the "figure eight" conformation in a macrocyclic framework is still flexible enough to undergo conformational exchange.[12] In contrast to the well-studied expanded porphyrins, the

"figure eight" conformation of **4-7** is proposed to be locked by the peripheral phenylene bicyclophane units, and its backbone is entirely composed of π-conjugated phenylene units.

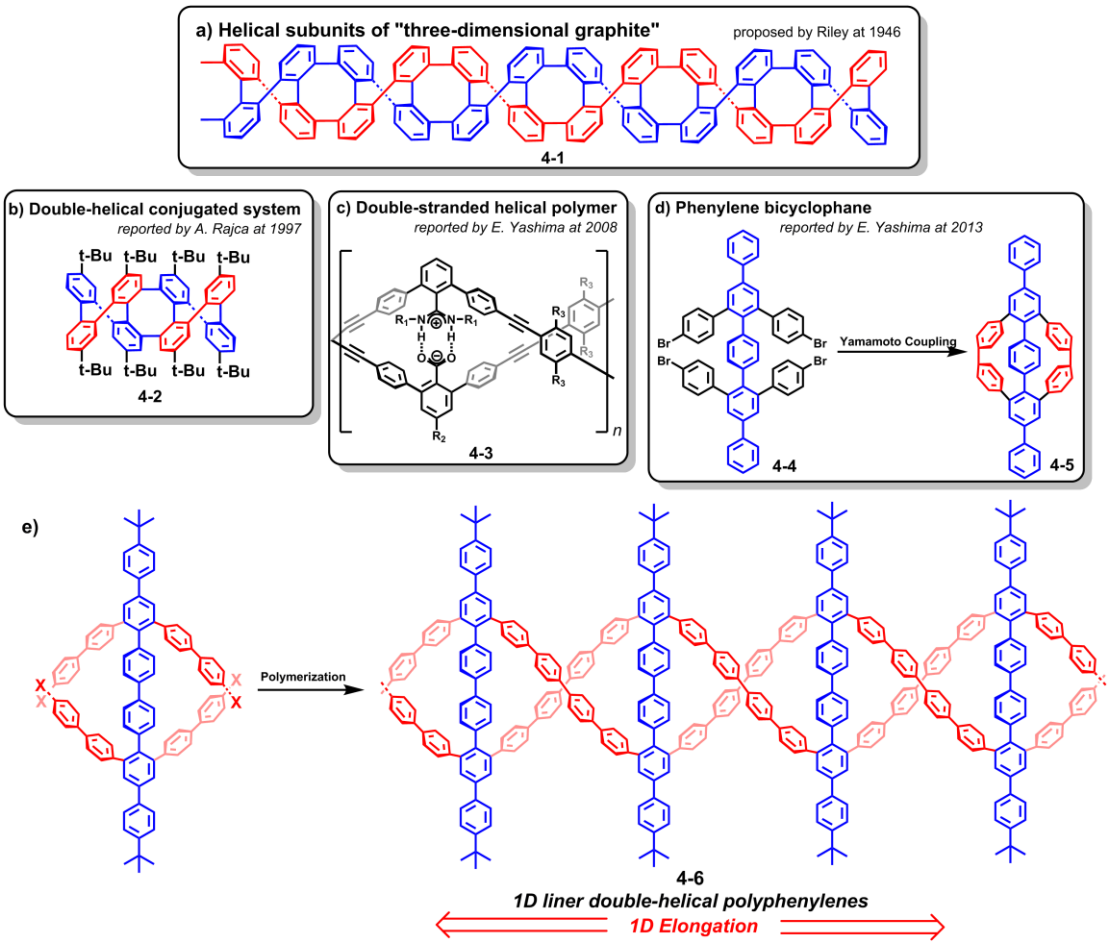

Figure 4-1 Structural illustration of double –helical conjugated polymers as 1D carbon allotrope: a) 1D double helical subunit (**4-1**) derived from the 3D graphite proposed by Riley; b) double helical octaphenylene (**4-2**) synthesized as the repeating units for 4-1; c) double stranded polymer (**4-3**) constructed via complementary hydrogen bonding; d) phenylene bicyclophane (**4-5**) synthesized via *Yamamoto* coupling which can be seen as monomer for a new double helical polymer; e) the targeted 1D double helical polyphenylene (**4-6**) in this chapter.

In addition, several large macrocycle rings adopting twisted "figure eight" structures owing to the inherent molecular flexibility, such as the expanded porphyrins,[13] appear to exhibit Möbius aromaticity and topology.[14,15] Although not all expanded

porphyrins with “figure eight” structure exhibit Möbius topology, its still worth of studing the possible conformer with Möbius geometry in the oligophenylene macrocycle **4-7** with distorted “figure-eight” structure.

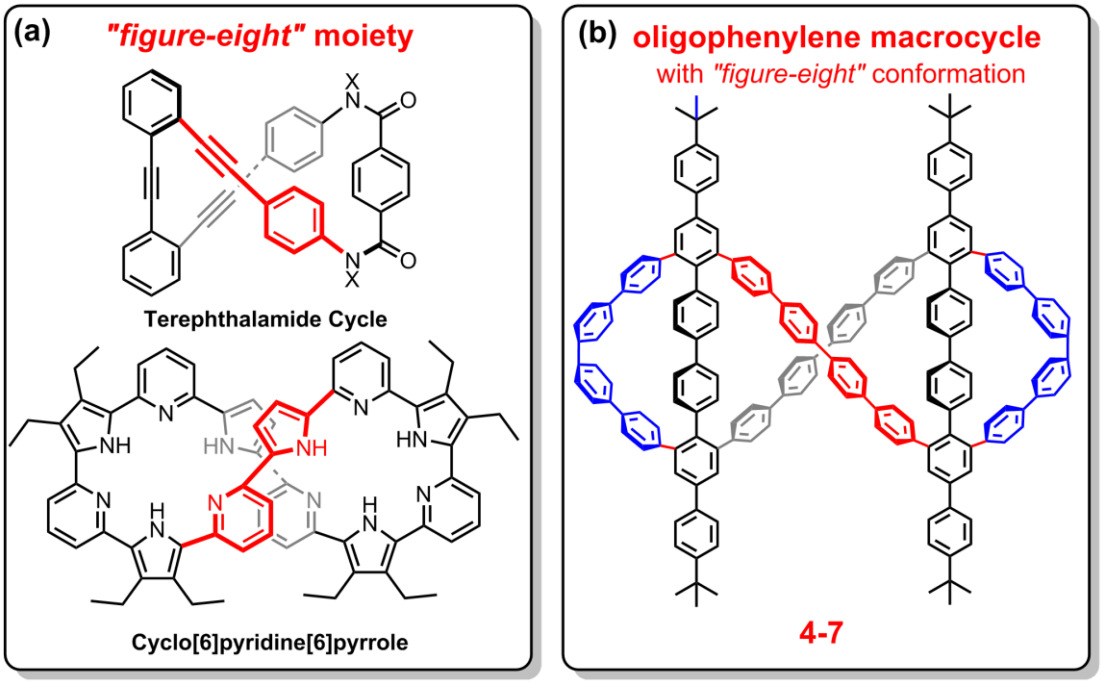

Figure 4-2 Structural illustration of (a) reported “figure-eight” motif with teraphthalamide or expanded porphyrins backbone, and b) targeted oligophenylene macrocycle with locked “figure-eight”conformation (**4-7**) in this chapter.

4.2 Results and discussions

4.2.1 Synthesis of phenylene bicyclophane and “figure-eight” macrocyclic oligophenylenes

The synthesis toward the linear double-helical polyphenylene chain **4-6** and its oligophenylene macrocyclic monomer with locked “figure eight”conformation was based on the Yamamoto coupling from oligophenylene precursor 4-12. (Scheme 4-1) The tetraiodo precusor **4-12** (Scheme 4-2) with oligophenylene backbones and four iodide units at appropriate position was firstly synthesized.

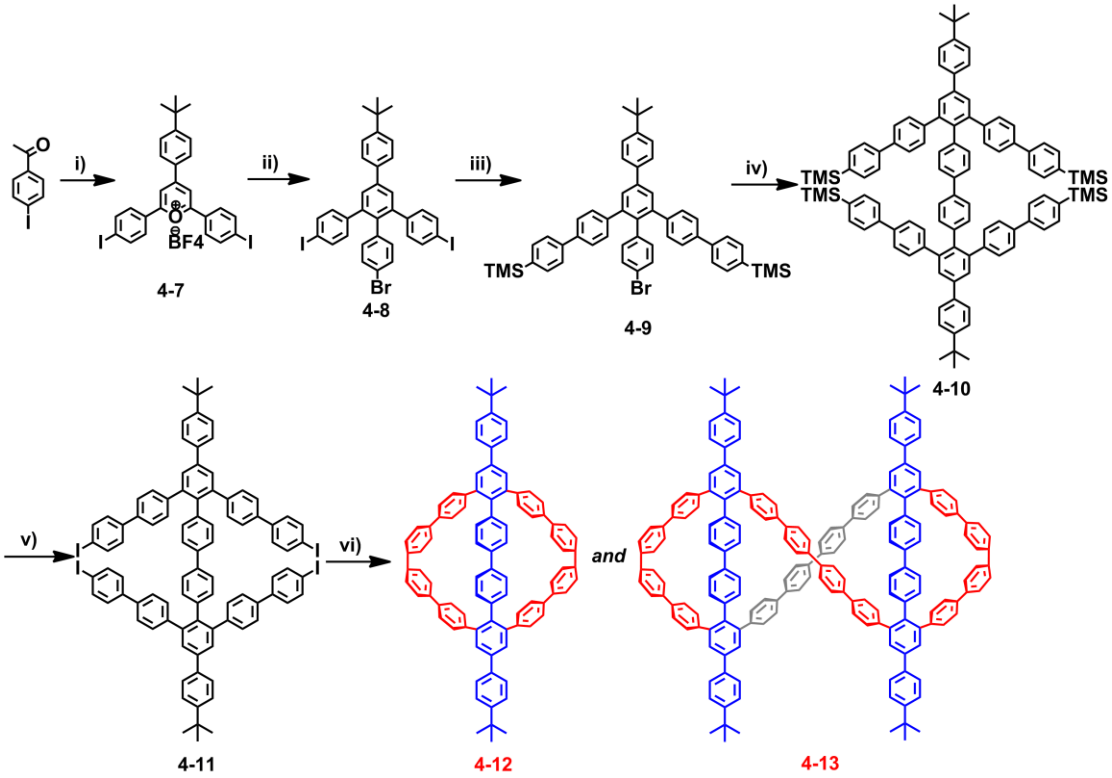

Scheme 4-2. Synthetic routes toward the phenylene bicyclophane **4-13** and "figure eight" oligophenylene macrocycle **4-7**. Conditions: (i) 4-iodooacetophenone, BF_3-Et_2O, 100 ℃, 12h, 39%; (ii) 4-bromophenacetic sodium, Ac_2O, 150 ℃, 12h, 32%; (iii) $Pd(PPh_3)_4$, K_2CO_3, 4-(Trimethylsilyl)phenylboronic acid, THF, 12 h, 60 ℃, 76%; (iv) $Ni(COD)_2$, Bipyridine, COD, Toluene/DMF, 100 ℃, 95%. (v) ICl (1.0 M in DCM), DCM, 0 ℃, 99%; (vi) $Ni(COD)_2$, Bipyridine, COD, THF, 120 ℃, microwave reactor, 48.5% for **4-13**, and 3% for **4-7**.

The synthesis of tetraiodo **4-12** was accomplished over 5steps with the overall yield around 8%. (Scheme 4-2) The triphenylpyrylium salt **4-8** was produced *via* Lewis acid-catalyzed condensation of methyl 4-formylbenzoate with 4-iodoacetophenone, which was subsequently subjected to the condensation reaction with sodium 4-bromophenacetate in refluxing acetic anhydride to yield the oligophenylene derivative **4-9**. Selective Suzuki coupling between compound **4-9** and 4-(trimethylsilyl)phenylboronic acid, and subsequent Yamamoto homocoupling of the oligophenylene **4-10** directly gave rise to the precursor **4-11** which was structurally validated by the MALDI-TOF mass spectrum (Figure 4-3). The conversion of the TMS-protecting group in compound **4-11** into the iodide units in compound **4-12** was

accomplished quantitatively with the treatment of ICl solution. However, due to the low solubility of compound **4-12** in solvents like THF, chloroform, and dichloromethane, the tetraiodo precursor **4-12** used directly in the next step after precipitation without further purification.

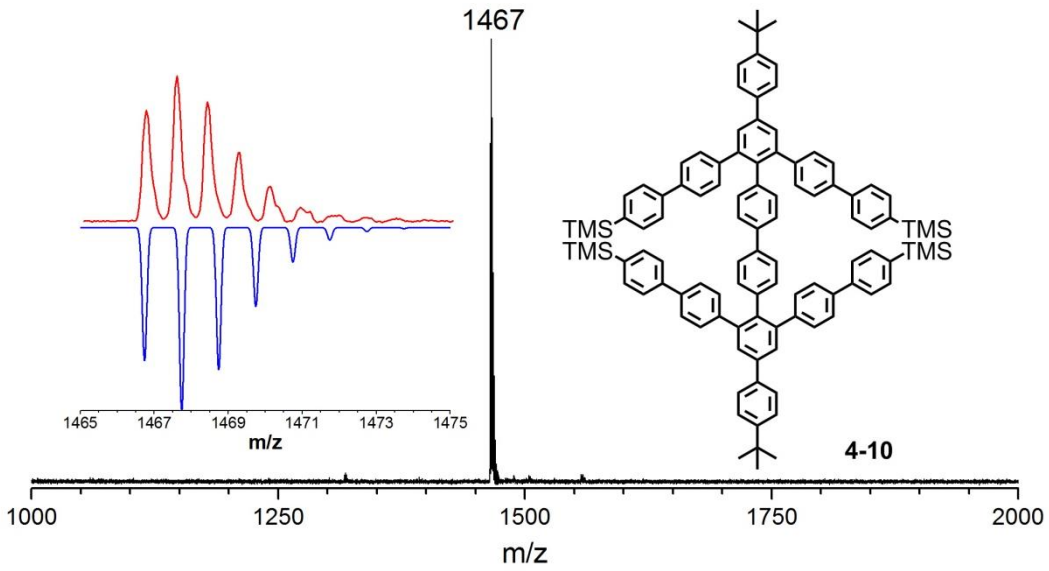

Figure 4-3. MALDI-TOF MS spectrum of oligophenylene **4-11**. Inset: red line indicates the experimental distributions, and blue line is the simulated distribution.

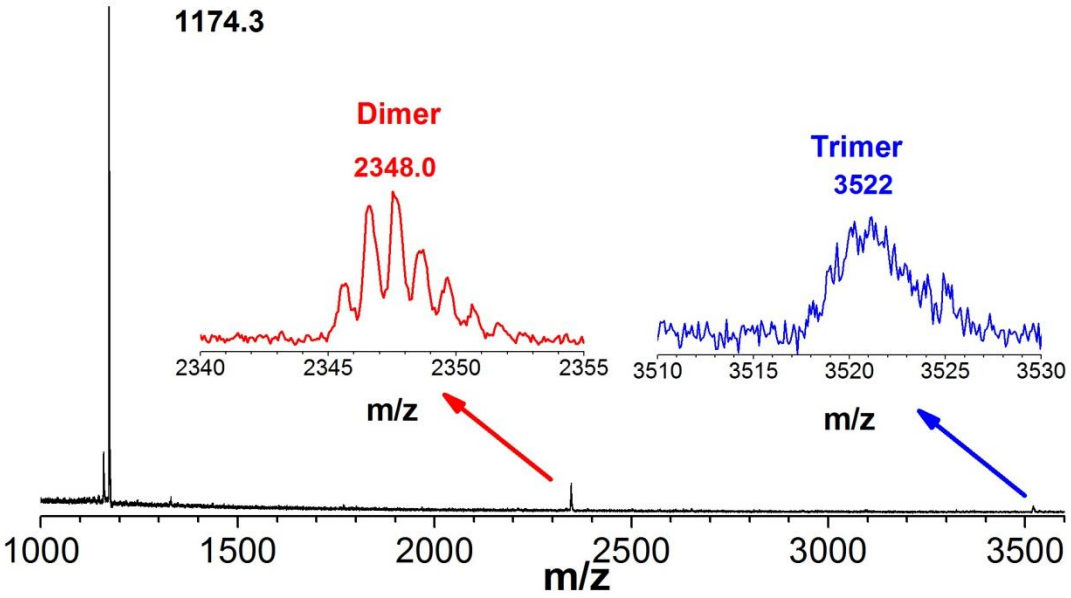

Figure 4-4. MALDI-TOF MS spectrum of crude product after Yamamoto coupling of oligophenylene precursor **4-12** in THF.

Then the tetraiodo precursor **4-12** was treated with bis(1,5-cyclooctadiene)nickel ([Ni(COD)$_2$]) and 2,2'-bipyrdine in a mixture of anhydrous THF and 1,5-cyclooctadiene (COD) in a microwave oven with the concentration of 1.48 mM under the temperature of 120 ℃. The MALDI-TOF MS spectrum (Figure 4-4) of the crude product clearly suggested that the intramolecular coupling toward **4-13** was overwhelming in the reaction indicated by the dominant peak (m/z = 1174.3). Meanwhile, a small peak with m/z = 2348.0 and an almost neglectable peak (m/z = 3522) attributed to the dimer (**4-7**) and trimer can also be observed in the spectrum, while the desired double-helical polyphenylene **4-6** was completely surpressed. The driving force of this astonishing reaction is the preorganization of the phenyl units in the tetraiodo-substitued precursor **4-12**. After insertion of the nickel catalyst into one of the aryl-iodide bonds, the transmetalation with the nearby aryl-iodide bond can readily undergo prior to the competing intermolecular transmetalation.[16,17] Therefore, no polymer was observed even after increasing the concentration of the precursor **4-12** to 6.0 mM

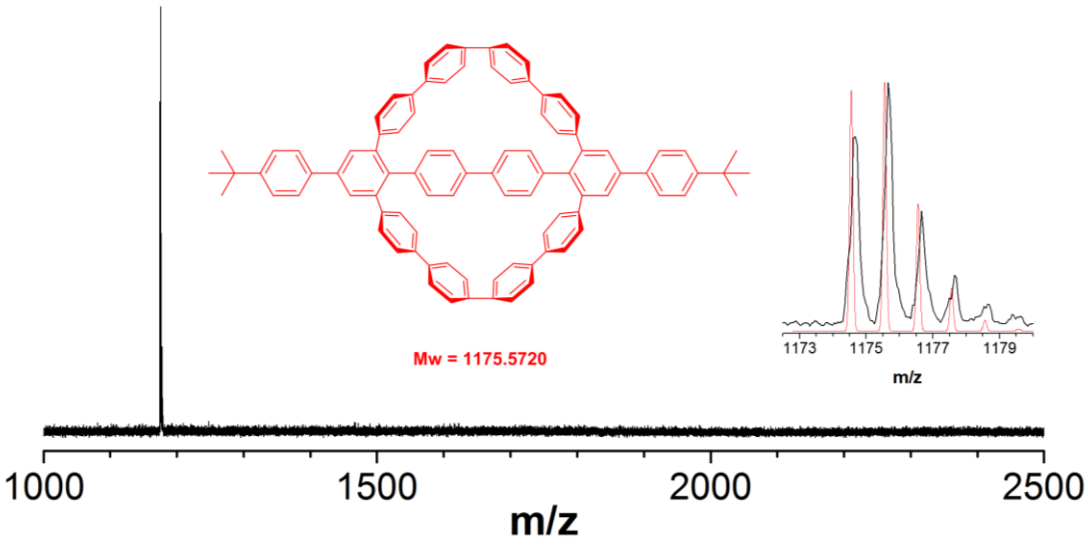

Figure 4-5. MALDI-TOF MS spectrum of phenylene biscyclophane **4-13** in THF.

The crude product was first roughly purified through a flash chromatography with THF as the eluent to remove the catalyst Then, preparative gel permeation chromatography (GPC) with chloroform as eluent allowed for the complete

purification and provided the phenylene bicyclophane **4-13** in 48% yield as a colorless solid (with the elution time of 65 mins). MALDI-TOF MS spectrum (figure 4-5) of **4-13** indicated the presence of a single species with m/z = 1175.7, consistent with the desired molar mass of 1175.6 g/mol, and the experimental isotopic distribution was also in good agreement with the simulated pattern (figure 4-5). In addition, another portion with the elution time of 56 mins on the preparative GPC curve was collected, and finally gave out a colorless solid with the yield of approximate 3%, which could be probably attributed to the oligophenylene **4-7** with "figure eight" conformation, and will be investigated in detail in the next section.

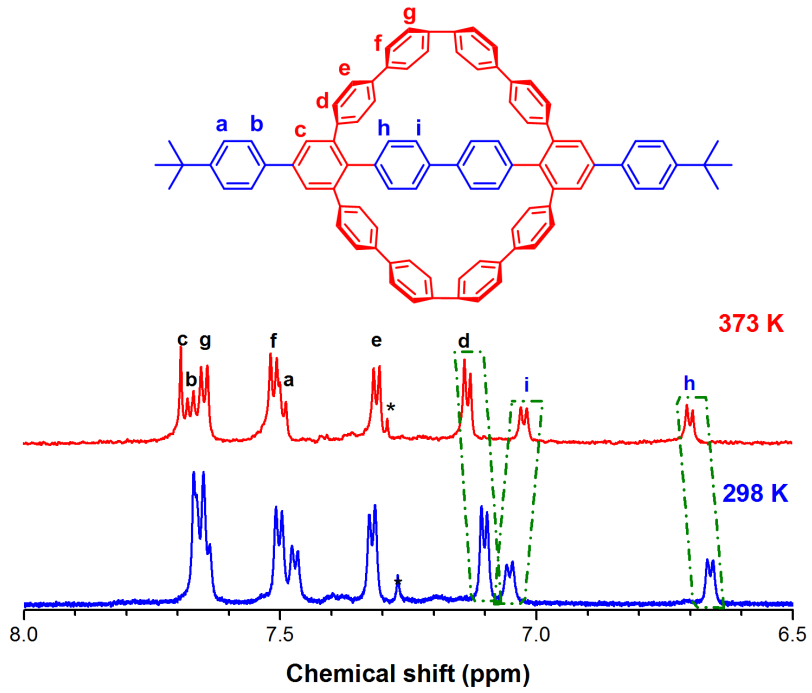

Figure 4-6. ^{1}H NMR spectrum of phenylene biscyclophane **4-13** in $C_2D_2Cl_4$.

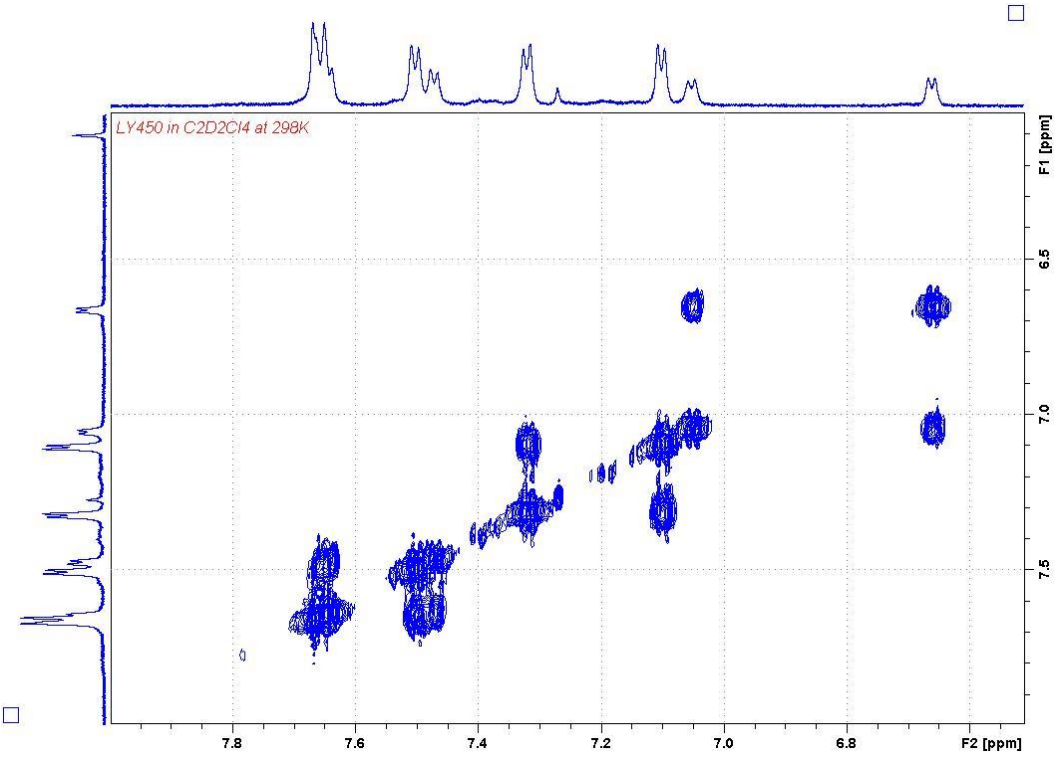

Figure 4-7. ^{2}D COSY spectrum of phenylene biscyclophane **4-13** in $C_2D_2Cl_4$ under 298 K.

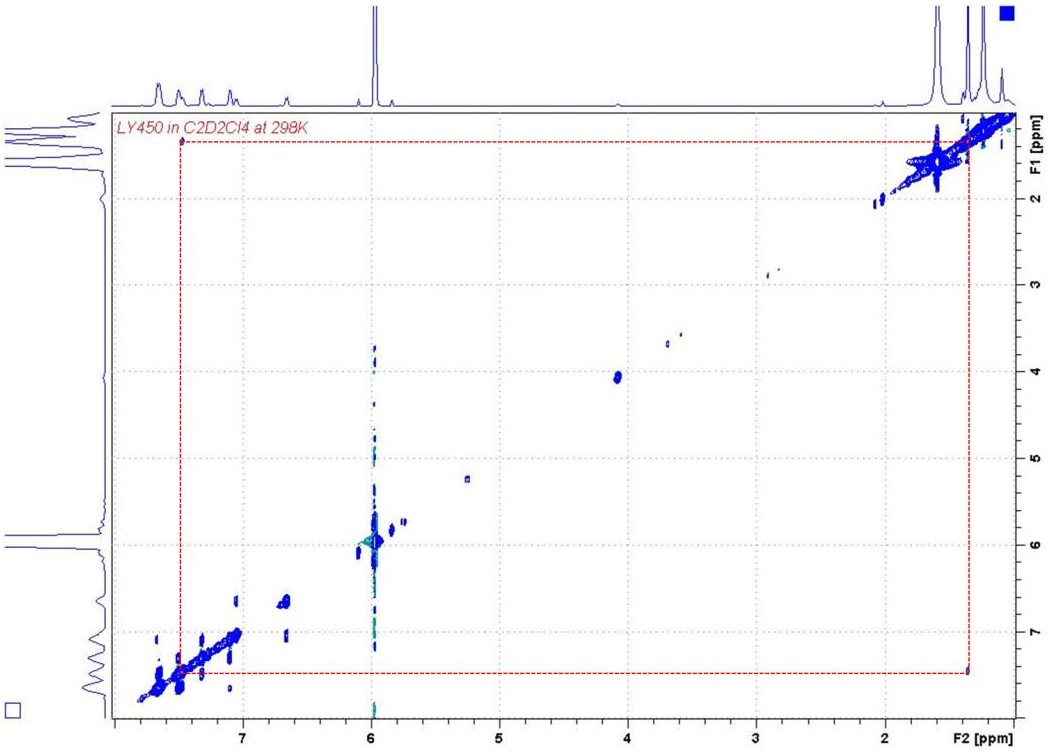

Figure 4-8. ^{1}H-^{1}H NOESY spectrum of phenylene biscyclophane **4-13** in $C_2D_2Cl_4$ under 298 K.

To verify the structure of the phenylene biscyclophane **4-13**, ^{1}H NMR (Figure 4-6)

together with correlation spectroscopy (Figure 4-7, and Figure 4-8) spectra provided further structural proof for phenylene bicyclophane **4-13**, and the signals of every aromatic proton could be assigned. After increasing the temperature to 373 K, the signals from most protons (in particular H_c, H_d, and H_h) showed a down-field shift of 0.03 ppm. In such a constrained structure, these protons are under the shielding effect from the adjacent benzene rings due to the high dihedral angles and strained geometry. Parallel with raising temperature, the strain will be more relaxed which will attenuate the shielding effect from neighboring benzene rings, and thus lead to the down-field shift. However, the pair of central benzene rings where H_h and H_i are located, are almost parallel with each other according to the simulated geometry of **4-13** (Figure 4-12). After increasing the temperature, the more free rotation of these benzene rings will lead to the increased dihedral angle between these two rings, and thus result in the shielding effect on proton H_c from adjacent benzene ring and up-field shift. Additionally, there are some subtle unindentified peaks observed in the NMR spectrum which are probably attributed to the presence of contaminants. However, the poor solubility of the phenylene biscyclophane **4-13** makes it difficult for further purification by chromatography and recrystalization.

Considering the strong trendency of **4-12** to intramolecular coupling, we have further modulated the structure of the tetraiodos derivative **4-12** by adding one more phenyl unit to tune the spatial position of the aryl-iodide units in the tetraiodo precursor. After altering the structure in precursor **4-16**, intermolecular transmetalation is expected to be more favorable against the competing intramolecular closure, and thus the formation of polyphenylene chains will be dominant.

The synthesis of **4-16** is following a similar strategy based on the oligophenylene **4-10** over 3 steps with the overall yield around 78% (scheme 4-3). Transformation of TMS groups in **4-10** into iodide units after treatment of ICl solution, and subsequent Suzuki coupling reaction with 4-(trimethylsilyl)phenylboronic acid gives rise to the compound **4-14** with the yield of 82%. Then tetraiodo precursor **4-16** is directly obtained *via* Yamamoto homocoupling of the oligophenylene **4-14**, and quantitative

conversion of TMS groups in **4-15** to iodide units. However, due to the low solubility of **4-16** in solvent like THF, chloroform, and dichloromethane, the precursor **4-16** was used directly after precipitation in methanol without further purification.

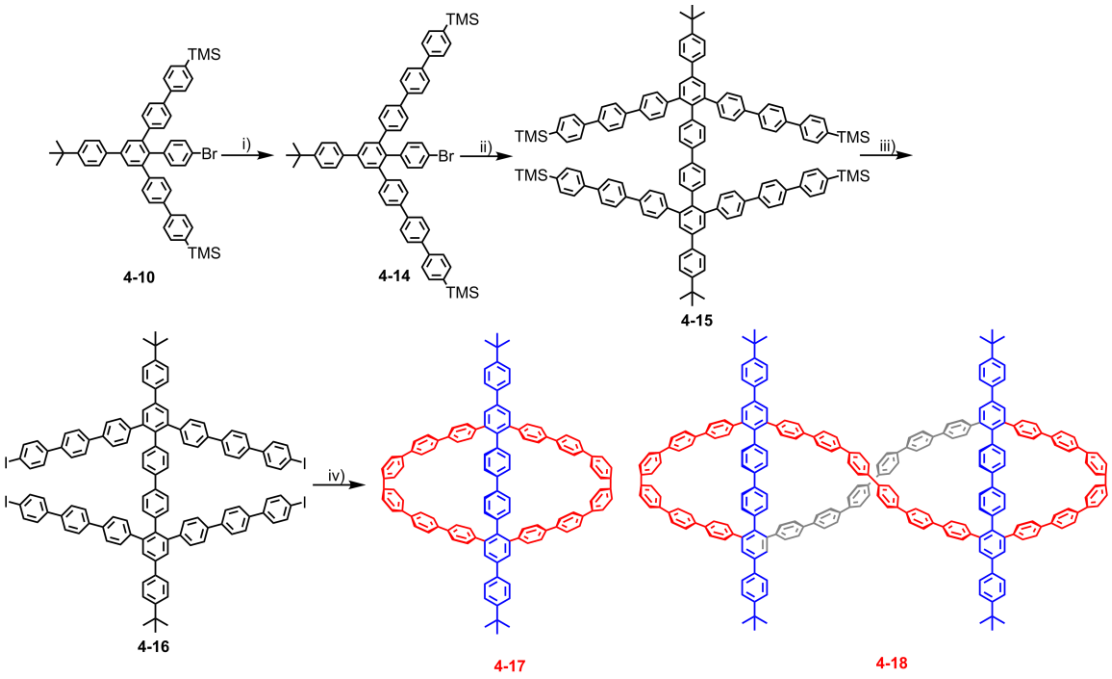

Scheme 4-3. Synthetic routes to phenylene biscyclophane **4-17** and its "figure-eight" cyclic oligophenylene **4-18**. Conditions: (i) a). ICL, DCM, rt, overnight; b) $Pd(PPh_3)_4$, K_2CO_3, 4-(Trimethylsilyl)phenylboronic acid, THF, 12 h, 60 ℃, 82%; (iv) $Ni(COD)_2$, Bipyridine, COD, Toluene/DMF, 100 ℃, 96%. (v) ICl (1.0 M in DCM), DCM, 0 ℃, 99%; (iv) $Ni(COD)_2$, Bipyridine, COD, THF, 120 ℃, microwave reactor, 54% for **4-17**, and 2% for **4-18**.

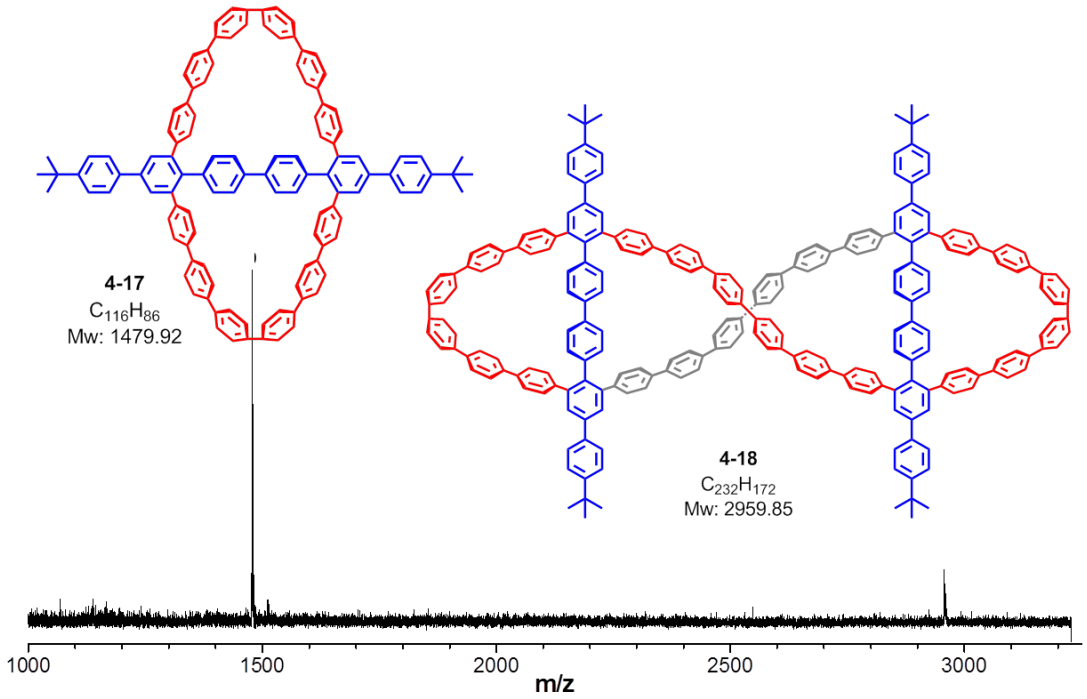

Figure 4-9. MALDI-TOF MS spectrum of the crude product from Yamamoto coupling of **4-16** in THF.

The Yamamoto coupling of precursor **4-16** toward the double-helical polymer was also attempted in the microwave oven with the concentration of 1.26 mM at the temperature of 120 ℃. However, the MALDI-TOF MS spectrum (Figure 4-9) of the crude product exhibited a similar trendency as precursor **4-12**. One dominant peak (m/z = 1480) directly verified the overwhelming intramolecular ring closure toward phenylene bicyclophane **4-17**. Another small peak with m/z = 2960.0 correponding to the "figure-eight" macrocycle **4-18** also indicated that the intermolecular transmetalation was still suppressed, and construction of highly strained polymer chain was too difficult via Yamamoto coupling.

After purification of the crude product via preparative GPC, one portion with elution time at 61 mins was collected to give rise to a colorless solid with the yield of 54%. Its MALDI-TOF MS spectrum suggested one single peak (m/z = 1749.8), which was consistent with the molar mass of compound **4-17** (1749.96 g/mol), and the experimental isotopic distribution also agreed well with the simulated distribution of the phenylene cyclophane **4-17** (Figure 4-10). Additionally, the other portion with

elution at 53 mins was also collected to yield a colorless solid with the yield of 2%, which will be studied later in the next section.

To further validate the chemical identity of **4-17** and elucidate its congested phenylene bicyclophane structure, we measured the ^{1}H NMR of compound **4-17.** However, the NMR spectrum demonstrated that the sample was contaminated with other unidentified impurities. And due to its poor solubility, it was quite difficult to purify the sample further.

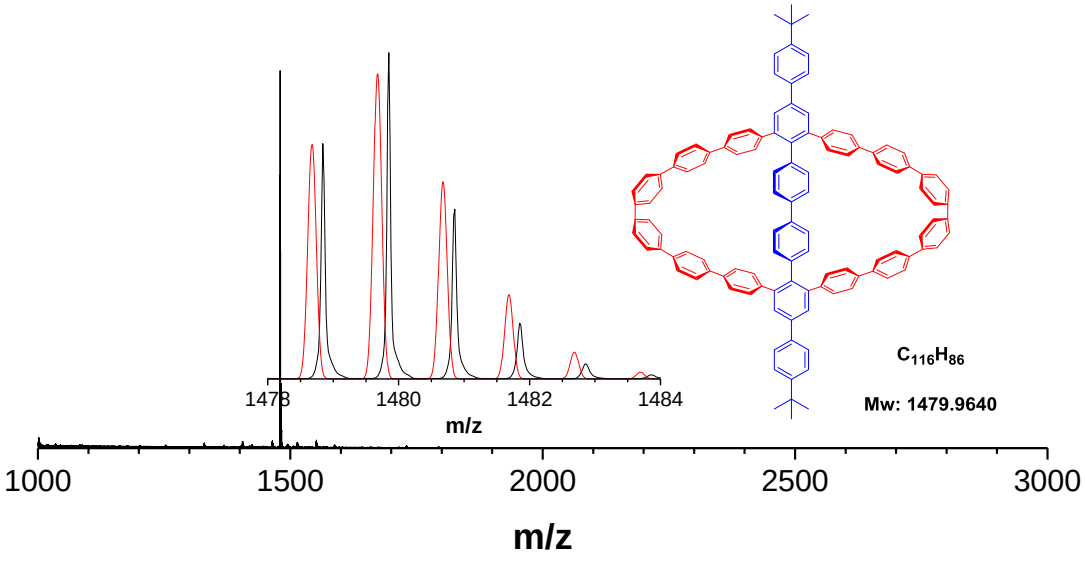

Figure 4-10. MALDI-TOF MS spectrum of the phenylene biscyclophane **4-17**. Inset: black line indicated the experimental distribution, and red line indicated the simulated distribution for compound **4-17**.

Additionally, in order to investigate the strains and geometry of the phenylene bicyclophane, the molecular geometry of compound **4-13** and **4-17** was simulated via Gaussian 9.0[18] on the basis level of B3LYP/6-31G(d). (figure 4-11) For **4-13**, the structural formula can directly suggest the highly curved geometry instead of linear geometry for the two [4]paraphenylene units. To measure the degree of molecular strain in the molecule, an imaginary line through the bridging carbon atoms of phenylene ring C and the adjacent carbon atom in phenyl ring D (Figure 4-11a) encloses a dihedral angle $\measuredangle_1$ of 151.3 °, while another counterpart dihedral angle $\measuredangle_2$

between the bridging carbon atoms of D and the neighboring carbon atom in benzene ring C is 151.4 °. Compared with the family of cycloparaphenylene, the strain between ring C and ring D in phenylene bicyclophane **4-13** is comparable with that in [9]CPP [19,20], in which the average dihedral angle between adjacent phenylene rings is around 149.3 °. And contrasted with the highly strained phenylene bicyclophene **4-5** (with a dihedral angle 142.5 °) reported by Höger, the intramolecular strain in compound **4-13** is much less attenuated indicated by the increase dihedral angles.

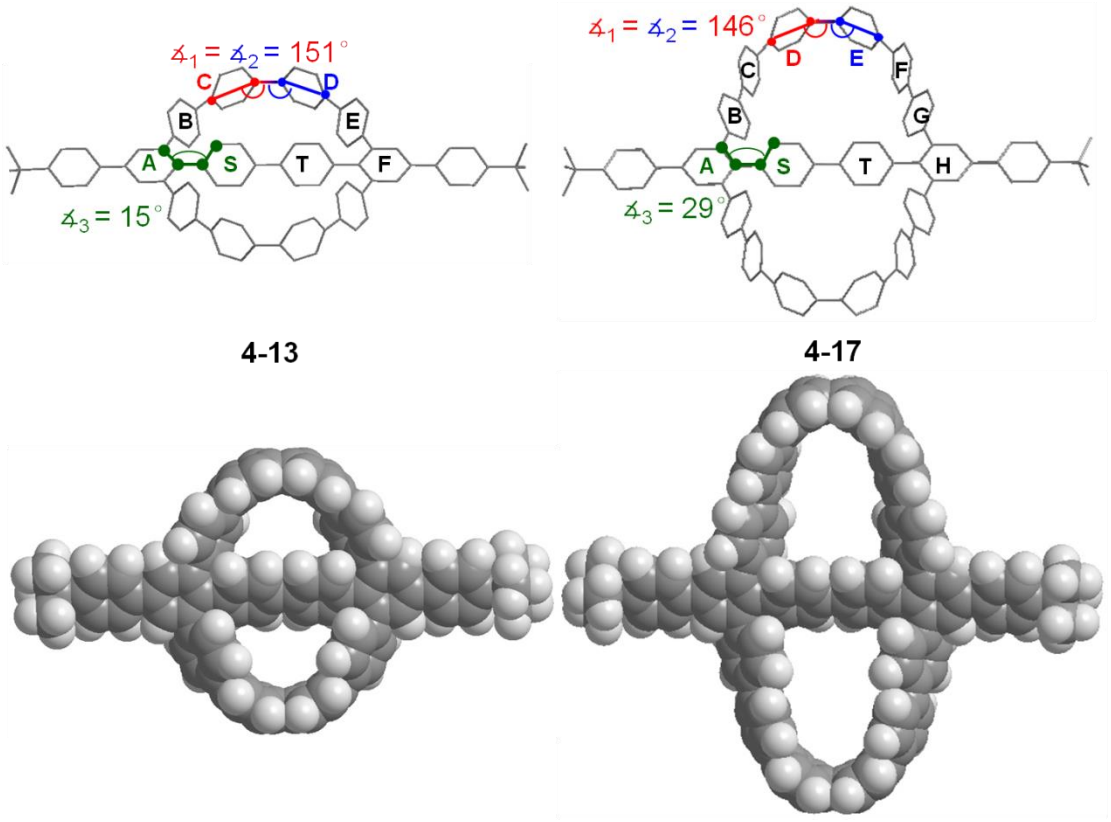

Figure 4-11. Molecular geometry of phenylene bicyclophane **4-13** and **4-17** on the basis level of B3LYP/6-31G(d). a) tube model of phenylene bicyclophane **4-13** with the angles ∢$_1$ and ∢$_2$, and ∢$_3$which are measures of the high strain of the bicyclophane system; a) tube model of phenylene bicyclophane **4-17** with the angles ∢$_1$, ∢$_2$, and ∢$_3$, which are measures of the high strain of the bicyclophane system; c) space-filling model of phenylene bicyclophane **4-13**; d) space-filling model of phenylene bicyclophane **4-17**.

In the case of reported phenylene bicyclophene **4-5**, the central biphenylene moiety is nearly perpendicular to the macrocycle plane. The central biphenylene segments

(benzene ring S and T, in Figure 4-11a) are clamped between the two peripheral [4]paraphenylene bridges and tilted out of the cyclophane surface. However, the significantly decreased dihedral angle $\measuredangle_3$ (approximate 14.9 °) between ring A and ring T in compound **4-13** also indicated the relaxed strain compared with **4-5**. The impressive space-filling model for **4-13** also straightforwardly suggested the tilting of the central biphenylene unit and the distinctive curve orientation of the two surrounding [4]paraphenylene segments which help minimize the steric hindrance inside the molecule.

As for phenylene bicyclophane **4-17**, the 3D geometry is nearly identical with that of **4-13** (Figure 4-11d). However, the increased dihedral angles $\measuredangle_1$ and $\measuredangle_2$ (146.1 ° and 146.3 ° in Figure 4-11b) of **4-17** at the center of the outer [6]paraphenylene segment clearly verified the increased strain in this compound when compared with that of **4-13**. The central biphenylene units (benzene ring S and T) are also clamped between the peripheral [6]paraphenylene segments with a dihedral angle $\measuredangle_3$ between ring A and ring S around 29.0 °, which also further confirmed the increased strain inside the macrocycle.

4.2.2 Characterization of highly twisted oligophenylene macrocycles with "figure-eight" conformation

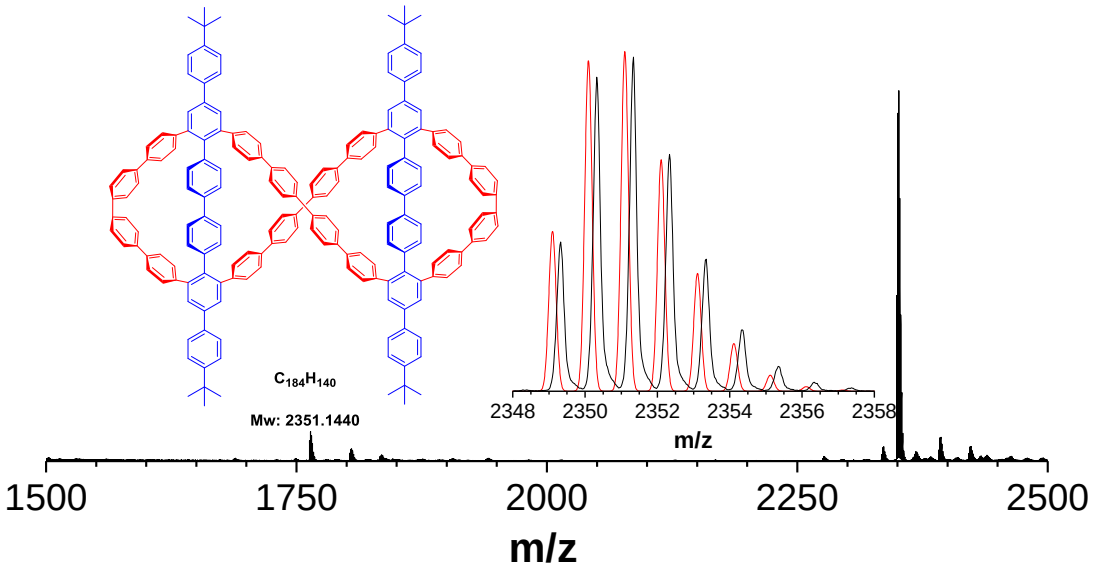

Figure 4-12. MALDI-TOF spectrum of the figure-eight-structured macrocycle **4-7**.

In the attempt to synthesize the double-helical polymer **4-6**, we have collected another portion with a very low yield *via* preparative GPC, which is probably figure-eight-structured macrocycle **4-7** and **4-18**. The MALDI-TOF MS spectrum of **4-7** indicated one major peak with m/z = 2351.1 (Figure 4-12), which is consistent with its molar mass of 2351.14g/mol. The experimental isotopic distribution also agree well with the simulated one for compound **4-7** (figure 4-12). However, the NMR spectrum of compound **4-7** is too complicated to assign each signals, even after raising the temperature to 373K (Figure 4-13). It seems that some contaminates are incoporated inside and lead to the existence of some unidentified small peaks in the NMR spectrum. And due to the low yield, the accumulation and further purification of the sample is quite challenging.

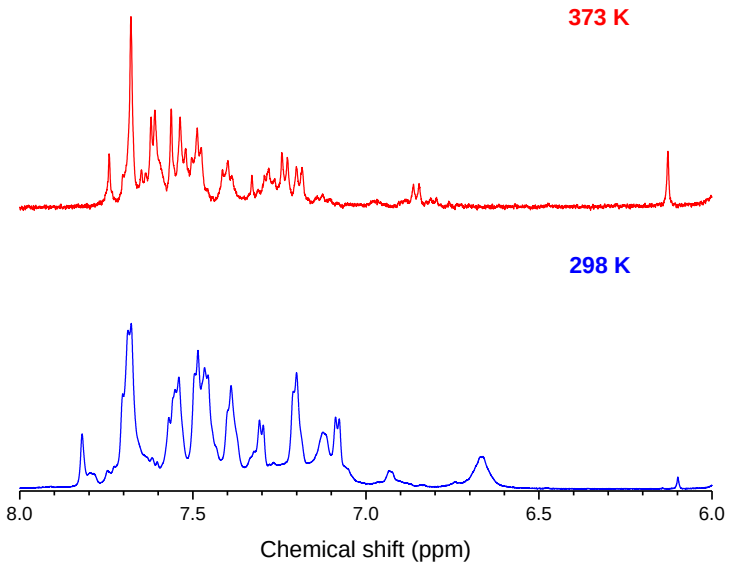

Figure 4-13. ^{1}H NMR spectra of compound **4-7** under different temperature.

Therotical calculation of the geometry for the compound **4-7** on the level of B3LYP/6-31G(d) clearly indicated a "figure-eight" conformation. Regarding a distorted molecule with figure-eight knotted topology, there probably exist two possible distinctive geometries [21], double-sided twisted *Hückel* cycle, and single-sided *Möbius* strip as shown in Figure 4-14.

As one of the most fascinating topological chemistry, the Möbius strip was firstly

proposed by August Ferdinand Möbius, and Johann Benedict Listing in 1858 [22]. This intruguing concept has fascinated the community from different fields, ranging from art and architecture, to science and engineering. However, in contrast to the already realized artifacts in the macroscopic world, the chemical synthesis of molecules with such topology still remains rare with only a few reported examples, due to the strained single-sided structrue and difficulty of identifing such a gerometry. Since the advent of the first synthetic Möbius aromatic hydrocarbon[24], several annulene derivatives[25,26] with Möbius geometry have been disclosed, and provide the molecular platform for experimentally testing the theoretical prediction on Möbius aromaticity proposed by Heilbronner in 1964 [27].

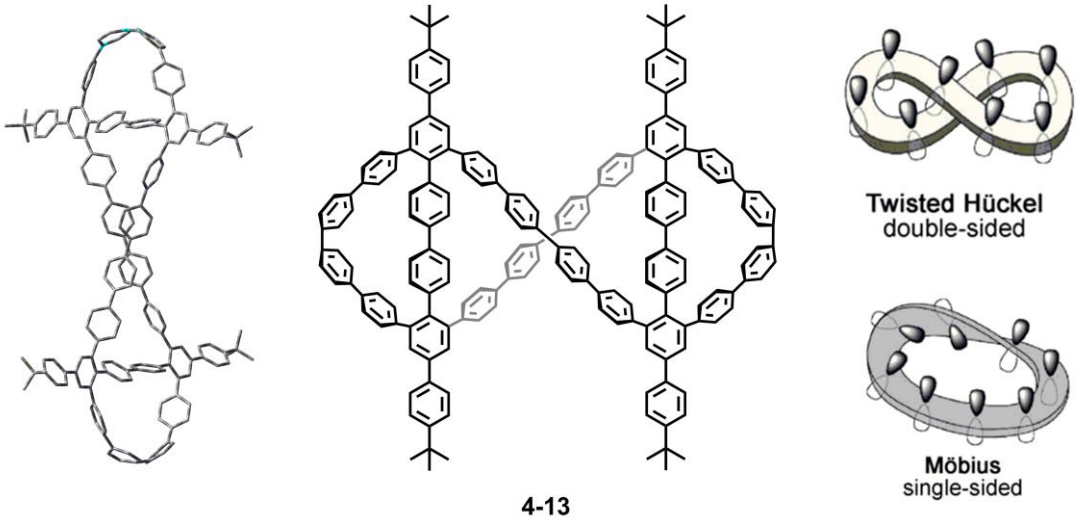

Figure 4-14. Calculated geometry of figure-eight-structured macrocycle **4-7** and its structure with two possible conformations: double-sided twisted Hückel cycle, and single-sided Möbius strip.

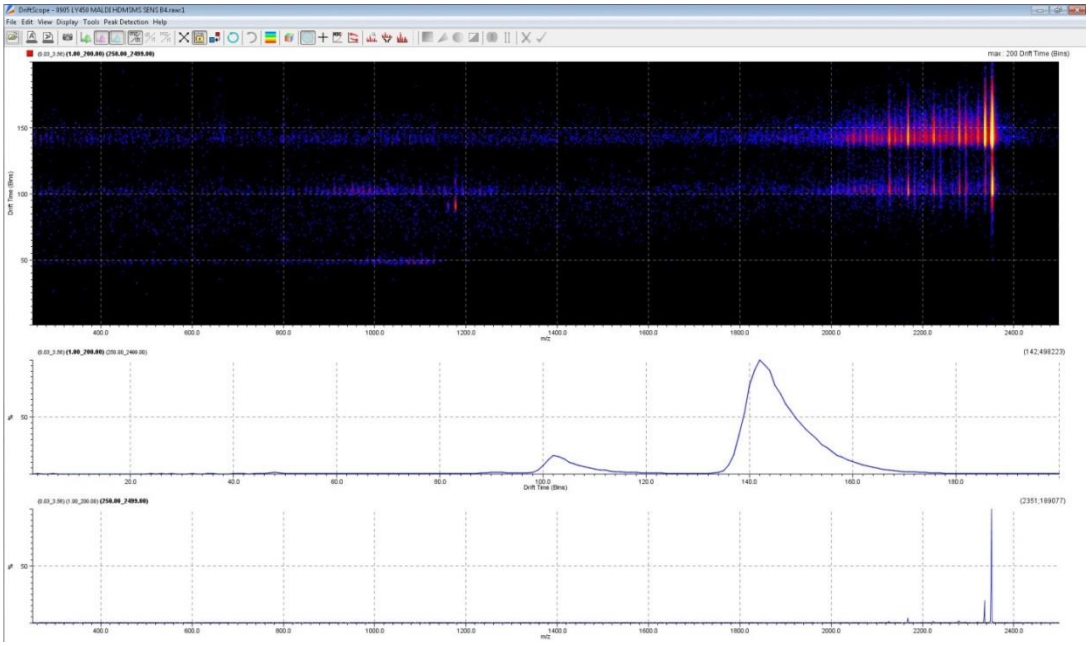

Figure 4-15. Ion-Mobility MS Spectrum (IM-MS) of figure-eight-structured macrocycle **4-7**.

In order to identify the composition of the obtained sample **4-7**, the drift tube ion-mobility mass spectrum measuremnt (IM-MS), which is an ideal method to study the molecular shape in the gas phase and determine the molecular diameter from collision cross section value[29], was applied to **4-7**. The ion mobilograms (Figure 4-15) clearly show two peaks with the drift time around 102 ms and 143 ms, which can be attributed to two conformers of the same molecular weight, or two molecules with similar molar mass.

For compound **4-18** with longer surrounding [6]paraphenylene segments on the cyclophane structure, the MALDI-TOF MS spectrum (Figure 4-16) also indicated one peak at m/z = 2959.6 agreeing well with the molar mass of 2959.93 g/mol, and the experimental isotopic distribution is also consistent with the calculated distribution. And only one conformer was observed in the ion mobilograms of the IM-MS spectrum with the drift time around 13.9 ms (Figure 4-17). However, the NMR spectrum of **4-18** is also too complicated for assignment, which still requires lots of efforts for in-depth analysis.

In summary, the extremely low yield of these two compounds with “figure-eight” conformation has hindered the identification of the exact topology in solution or solid

state. Thereore, continuous efforts are still required to optimize the synthetic routes toward figure-eight-structured oligophenylenes.

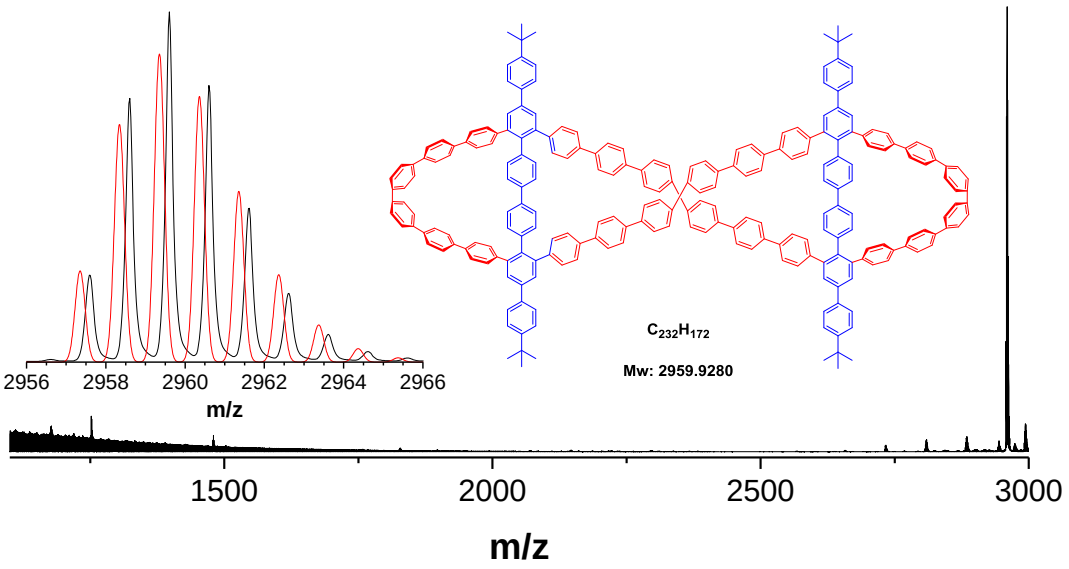

Figure 4-16. MALDI-TOF MS spectrum of the figure-eight-structured macrocycle **4-18**.

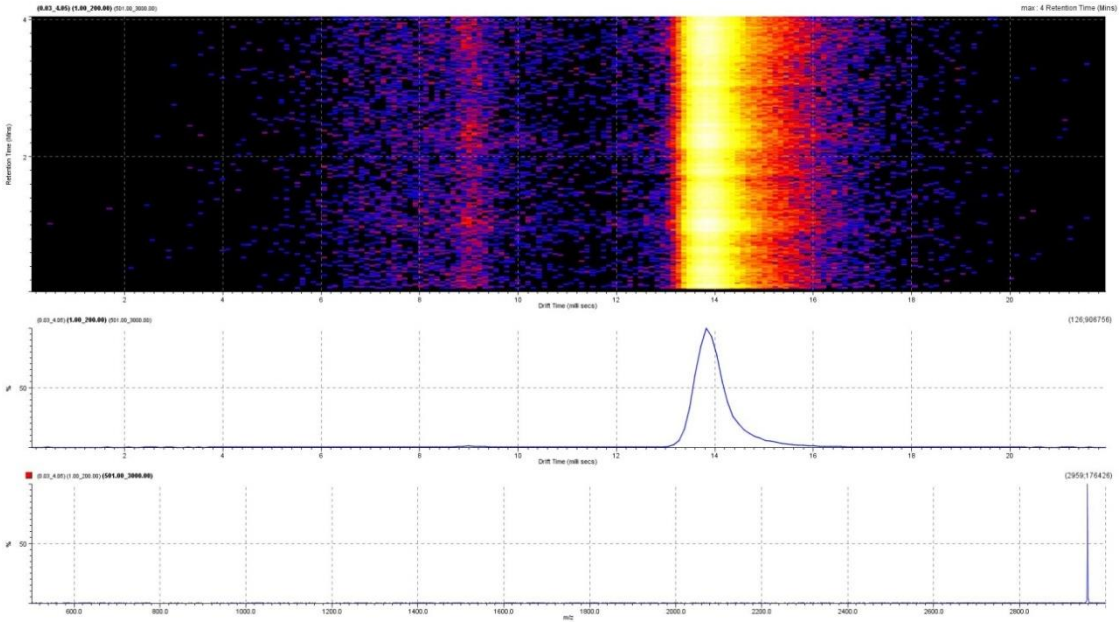

Figure 4-17. Ion-Mobility MS spectrum of the figure-eight-structured macrocycle **4-18**.

4.2.3 Synthesis and structural chracterization of cyclic oligophenylene with "figure-eight" conformation

Taking into account the extremely low yield of synthesizing the

figure-eight-structured macrocycle **4-7** and **4-18**, a more straightforward synthetic route (scheme 4-4) toward the corresponding cyclic oligophenylene **4-24** or **4-25** was designed. The formation of twisted figure-eight topology (from **4-21** to **4-23**) and conformation locking (from **4-23** to **4-24/4-25**) were realized in two-steps. The entire synthetic strategy was based on the asymmetric dibromo substituted precursor **4-21**, which was obtaiend via the condensation of an asymmetric pyrylium salt **4-20** with readily synthesized sodium 2,2'-(1,4-phenylene)diacetate in refluxing acetic anhydride in the yield of 29%. The asymmetric pyrylium salt **4-20** was produced by the Lewis acid catalyzed condensation reaction between commercial available 4-bromooacetophenone and 4'-methoxychalcone **4-19**, which could be easily synthesized via the aldol condensation between 4-mehtoxy-acetopheone and benzaldehyde. Then, Yamamoto coupling of dibromo precursor **4-21** was accomplished in refluxing THF under microwave irradiation, in which phenylene monocyclophane **4-22**, cyclic oligophenylene **4-23** with "figure-eight"conformation, are both expected.

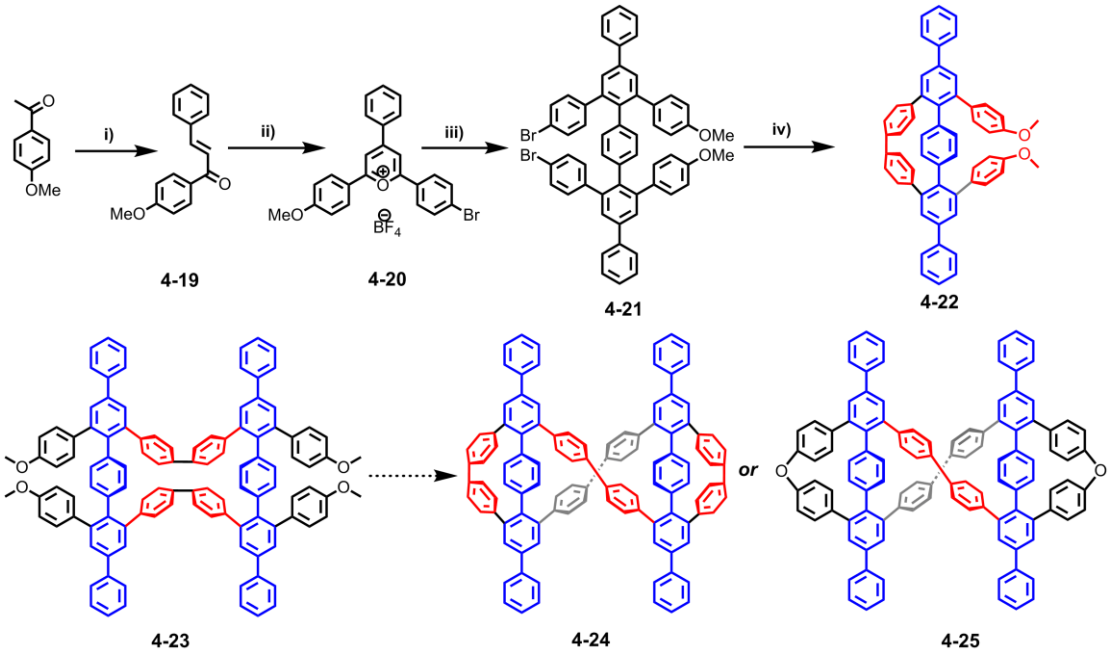

Scheme 4-4. Synthetic routes toward the figure-eight-structured cyclic oligophenylene **4-23** from an asymmetric precursor **4-21**. Conditions: (i) benzaldehyde, NaOH, MeOH, rt, 12h, 78%. (ii) 4-bromoacetophenone, BF_3-Et_2O, 100 ℃, 12h, 33%; (iii)

2,2'-(1,4-phenylene)diacetate sodium, Ac_2O, 150 ℃, 12h, 12%; (iv) $Ni(COD)_2$, Bipyridine, COD, THF, 120 ℃, microwave reactor, 32% for **4-22**, and 28% for **4-23**.

After removing the catalyst by flash chromatography with THF as eluent, the crude product is purified via preparative GPC in which compound **4-22** and **4-23** can both be obtained as a white solid with the yiled of 32%, and 28%, respectively. Although the overall yield of "figure eight" compound **4-23** over 4 steps is approximate 2.5%, all the precursors can be readily synthesized and obtained in large quantity. Additionaly, the reaction condition for the Yamamoto coupling can still be improved by increasing the concentration to enhance the inramolecular coupling, and thus increase the chance of dimer formation.

MALDI-TOF mass measurements were applied to validate the existence of the phenylene monocyclophane **4-22** and cyclic oligophenylene with "figure-eight" topology **4-23**. (figure 4-18) For the compound **4-22**, one single peak appeared at m/z = 744.2, which is consistent with its molar mass of 744.92 g/mol and the experimental isotopic distribution is also identical with the theoretical one. For the compound **4-23**, we can also observe one single peak on the MS spectrum (m/z = 1490.4) agreeing well with its molar mass (1489.83 g/mol), and the experimental isotopic distribution is also consistent with the simulated one.

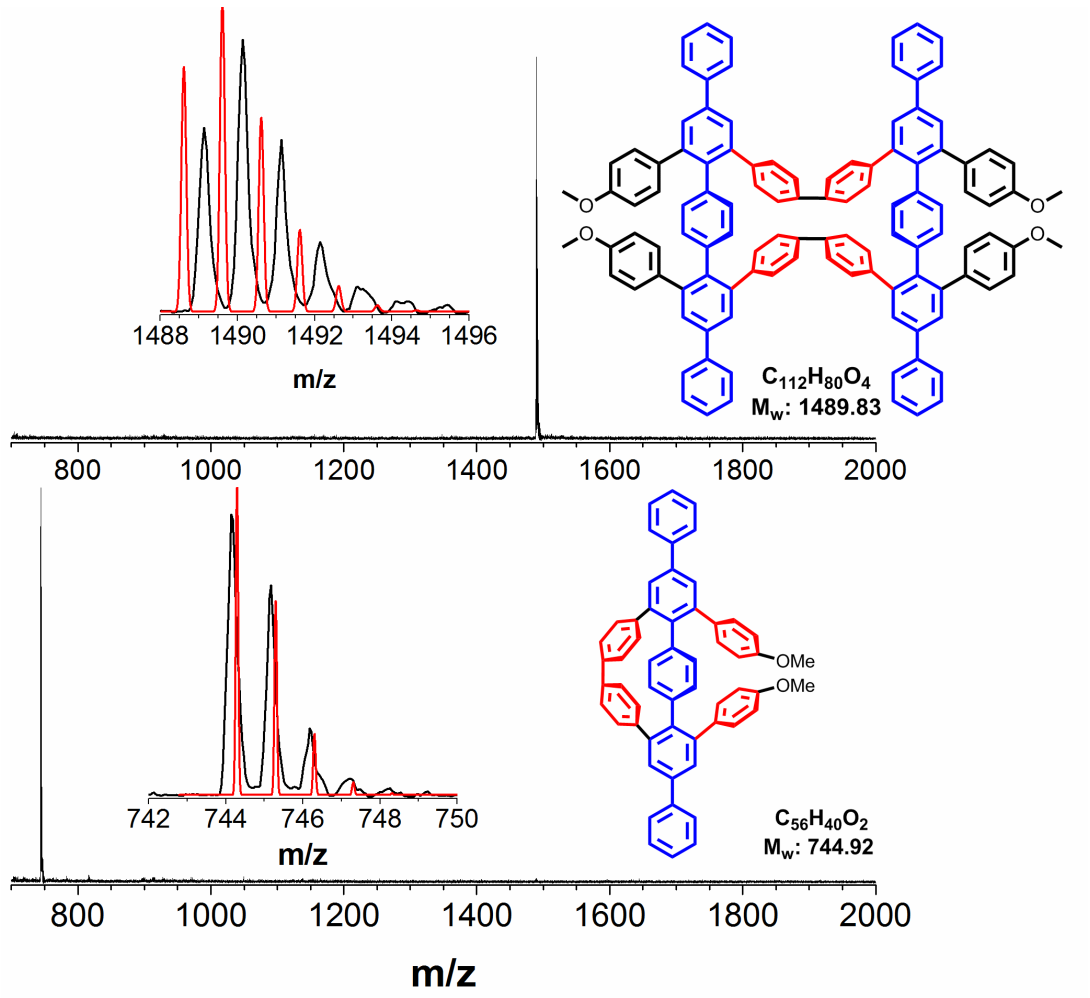

Figure 4-18. MALDI-TOF MS spectra of phenylene monocyclophane **4-22** and figure-eight-structured cyclic oligophenylene **4-23**. Inset: black curve is the experimental isotopic distribution, red line is the calculated isotopic distribution.

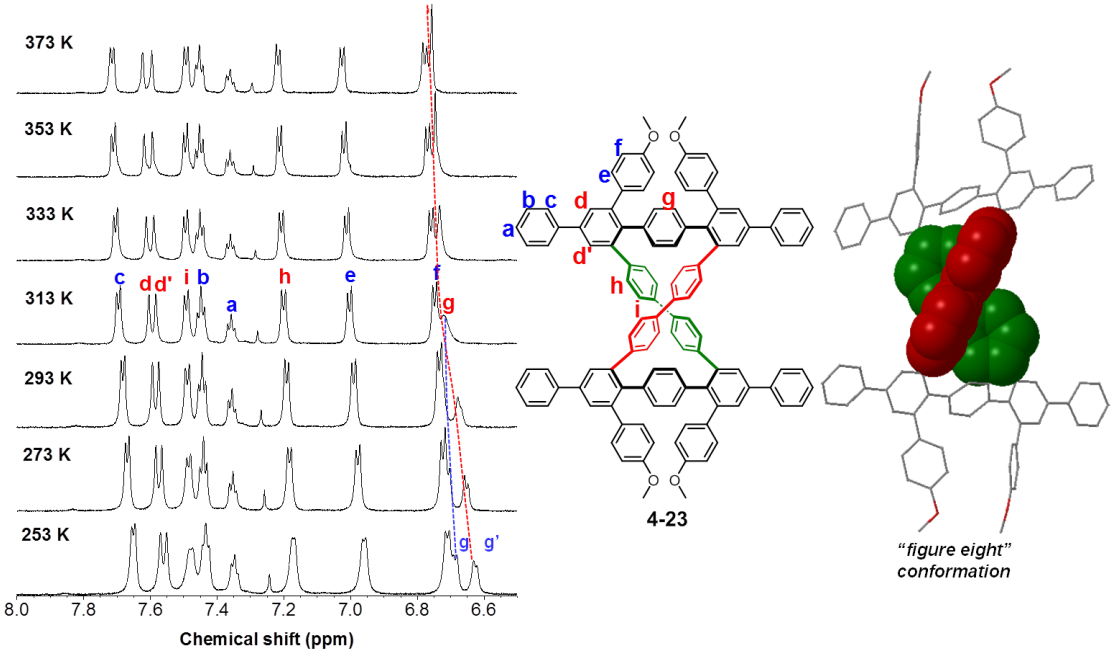

Figure 4-19. Temperature-dependent ^{1}H NMR spectra of **4-23** in $C_2D_2Cl_4$ ranging from 253 K to 373K, as well as the "figure-eight" conformation supported by the DFT calculation. Peaks were assigned on the basis of 2D correlation spectra.

The ^{1}H NMR spectrum and 2D COSY and NOESY spectra provide further structural proof for cyclic oligophenylene **4-23**, and every signal could be assigned to the aromatic protons in the molecule. (Figure 4-19) For the cyclic oligophenylene **4-23**, the compound is more likely to adopt a twisted conformation, namely the "figure-eight" conformation, to minimize the strain in the molecule. Otherwise, there would exist extremely high steric hindrance in the distorted macrocycle. This fascinating conformtion is further supported by the DFT calculation on the basis level of B3LYP/6-31G(d), in which the cyclophenylene **4-23** adopts a figure-eight conformation with the two biphenylene rings at the intersection. (green and red segments in Figure 4-19)

To investigate the cyclic conformation of compound **4-23**, ^{1}H NMR spectra are measured at various temperature ranging from 253K to 373 K. At room temperature (293 K), two peaks (6.72 and 6.68 ppm) corresponding to proton H_g are observed. Upon increasing the temperature (above 313K), the two peaks emerge into one singlet peak for the aromatic proton H_g, indicating that both bridging *para*-phenylene units of

4-23 are equivalent on the NMR timescale and rotate freely at high temperature. However, when the solution is cooled down below 293 K, the splitted peak appearing at 6.68 ppm shows an up-field shift gradually from 6.68 ppm at 293 K, to 6.66 ppm at 273 K, and to 6.63 ppm at 253 K, while another peak of proton H_g at 6.72 ppm exhibits a smooth up-field shift similar to other proton signals. And the integrities of both peaks crooresponding to proton H_g are in the ratio of 1:1. This is presumably because the rotation of these two bridging *para*-phenylene rings in cyclophenylene **4-23** will be frozen under low temperature. The protons H_g tilting into the figure-eight cycle and outward the cycle will split into two distinctive peaks because of their different chemical enviroments, and free rotation under high temperature will lead to the coalescence of the two phenylene signals into one singlet peak. (Figure 4-19)

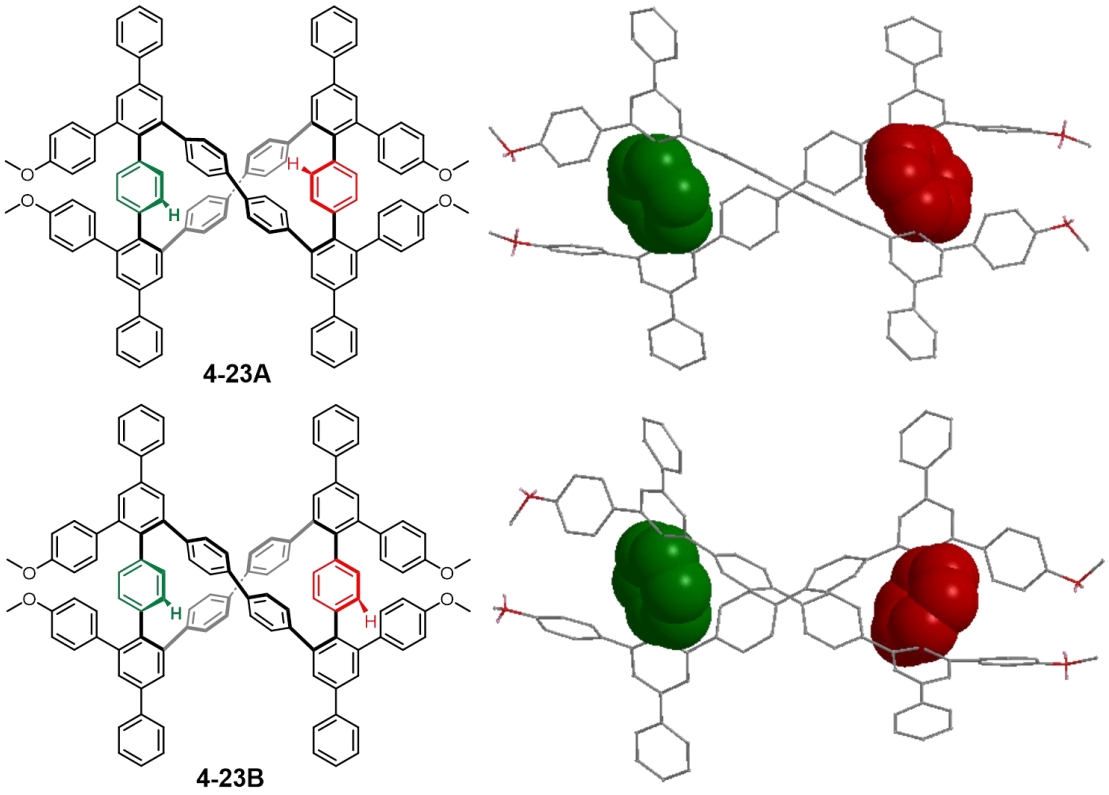

Figure 4-20. Two possible "figure-eight" conformers of cyclic oligophenylene **4-23** with distinctive orientation (**4-23A** with perpendicular alighment, and **4-23B** with parallel alignment) of the bridging *para*-phenylene rings based on the DFT theoretical calculation.

Paralleling the geometry optimization, two distinctive conformers with "figure-eight"

conformation are found for cyclic oligophenylene **4-23** with different orientation of the bridging para-phenylene rings. When incorporated into the macrocyclic backbones, the para-phenylene units enabling partial π-conjugation and retainig free rotation can give rise to various conformers via rotating these "topological selector". [30,31] Theoretical calculation suggests that the conformer **4-23A** is more stable than **4-23B**, and energy estimation on the basis of B3LYP/sto-3g reveals conformer **4-23A** to be ca. 5.7 KJ mol^{-1} more stable than **4-23B**. According to the simulated geometry, the conformer 4-23A appears to adopt a one-sided Möbius topology and the conformer **4-23B** adopts a double-sided cyclic topology. This still requests further works and proofs in the future.

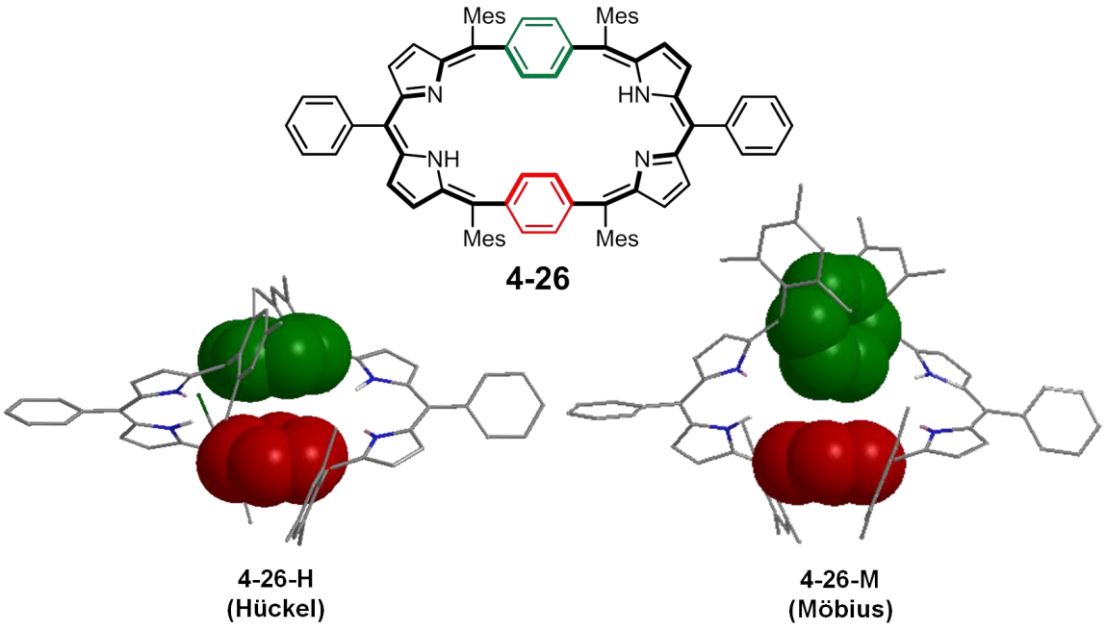

Figure 4-21. Expanded porphyrin 4-26 with a split personality: aromaticity switch between Hückel conformer **4-26-H** and Möbius conformer **4-26-M**.

This topological selection behavior from the rotation of the bridging units in macrocycle have been already studied in the case of expanded porphyrins featured with mutiple conformations.[32,33] For example, the phenylene ring can function as a "topology selector" in a expanded porphyrin compound **4-26** (Figure 4-21), and realize the conversion between Huckel and Möbius aromatic system after altering the temperature or solvent polarity.[34] Under high temperature, the two bridging

phenylene units will be parallel with each other, and lead to a conformer (**4-26-H**) with Hückel aromaticity, whereas another conformer (**4-26-M**) with "edge-to-face" arrangement of the two bridging phenylene rings will exihbt a unique Möbius topology at low temperature.

Compared with expanded porphyrins, the highly distorted cyclophenylene species are featured with higher barriers between different conformers due to the rigid phenylene units. However, the crucial conformation-property relationships make it necessary to study the conformational motion inside the figure-eight-structured cyclophenylene like **4-23**, which may provide new insight into the strategy of construction polyphenylene Möbius strips.

4.3 Summary

In this chapter, the work was focused on the synthesis of the double-stranded helical polyphenylene chians (**4-6**) and related figure-eight-structured subunits (**4-7**), and construction of carbon backbones with novel topology.. The synthetic strategy toward the highly twisted carbon structures was based on the Yamamoto coupling of a tetraiodo substituted monomer with pre-organized geometry (**4-12**). Once the intermolecular coupling is disclosed, the helical structure will appear as a consequence of minimizing the steric repulsion.

However, the MALDI-TOF mass spectrum of the crude product unambiguously indicated that the intramolecular coupling toward phenylene bicyclophane **4-13** is overwhelming, although a trace of dimer with "figure-eight" conformation can be also separated *via* preparative GPC. The detailed NMR investigation of **4-13** has verified the structure of highly congested bicyclophane conformation, while a DFT calculation on the level of B3lYP/6-31G(d) was also accomplished to elucidate the details about the geometry in such strained cyclophenylene species. Through calculating the dihedral angles in the peripheral [4]paraphenylene segments and comparing with the well-studied [*n*]cycloperaphenylene, the intramolecular strain of **4-13** is comparable with [9]CPP. To increase the chance of intermolecular coupling, a structural modulation on the precursor **4-12** was made to give the new precursor **4-16** with a less favored conformation for intramolecular coupling. However, the intramolecular ring closure toward phenylene bicyclophane **4-17** still overwhelmed in the reaction.

In order to study the double-helical structure of the targeted carbon networks, trace amounts of figure-eight-strutured cyclophenylene (**4-7**, and **4-18**) after Yamamoto coupling have been obtained with careful preparative GPC. Although the chemical identity of these two dimers has been validated by the MALDI-TOF mass spectrum and ion-mobility mass spectrum, the NMR investigation for conceivable structural characterization failed due to the existence of contaminants in the sample and extremely low yield.

The last part of this work is designing another synthetic approach toward the cyclic oligophenylene with “figure eight” conformation, which is based on an asymmetric dibromo precursor **4-21**. After Yamamoto coupling in a microwave oven, the partially opened cyclic oligophenylene **4-23** can be obtained with a satisfactory yield of 30% after purification *via* preparative GPC, and its molecular structure is confirmed by the detailed NMR investigation, and MALDI-TOF mass spectrum. The cyclic oligophenylene **4-23** has adopted a highly twisted “figure eight” conformation to minimize the steric repulsion, which is further supported by the theoretical DFT calculation. Additionally, the temperature-dependent NMR measurements suggest a dynamic conformational motion for the “figure-eight” cyclophenylene **4-23**, which can be controlled by raising or decreasing the temperature. Detailed geometry analysis of **4-23** also demonstrated the existence of two conformers with a distinct arrangement of the two bridging phenylene rings, which probably exhibits a Möbius topology.

In summary, this chapters describes the synthesis of cyclophenylene with “figure eight” conformation and probably Möbius topology, which are studied by NMR measurement and computational methods, However, a lot of effort are still needed to optimize the structure of figure-eight-structured cyclophenylene and investigate the thermodynamics of the conformational motion, for example, locked cyclophenylene **4-24** and **4-25**. (Scheme 4-2)

Reference:

[1] J. Gibson, M. Holohan. H. L. Riley, *J. Chem. Soc.* **1946,** 456.

[2] H. L. Riley, *J. Chim. Phys. Phys. Chim. Biol*. **1950**, *47*, 565.

[3] M. Yamaguchi, M. Shigeno, N. Saito, K. Yamamoto, *Chem. Rec*. **2014**, *14*, 15–27

[4] E. Yashima, K. Maeda, H. Iida, Y. Furusho, K. Nagai, *Chem. Rev*. **2009**, *109*, 6102.

[5] A. Rajca, A. Safronov, S. Rajca, R. Shoemaker, *Angew. Chem. Int. Ed. Engl.* **1997,** *36*, 488.

[6] Y. Furusho, E. Yashima, *J. Polym. Sci., Part A: Polym. Chem.*, **2009**, *47*, 5195.

[7] T. Maeda, Y. Furusho, S. I. Sakurai, J. Kumaki, K. Okoshi, E. Yashima, *J. Am. Chem. Soc.*, **2008**, *130*, 7938.

[8] G. Ohlendorf, C. W. Mahler, S.-S. Jester, G. Schnakenburg, S. Grimme, S. Höger, *Angew. Chem. Int. Ed*. **2013**, *52*, 12086.

[9] R. Katoono, Y. Tanaka, K. Kusaka, K. Fujiwara, T. Suzuki, *J. Org. Chem.* **2015**, *80*, 7613.

[10] R. Katoono, S. Kawai, K. Fujiwara, T. Suzuki, *Chem. Sci.*, **2015**, *6*, 6592.

[11] Z. Zhang, W. Y. Cha, N. J. Williams, E. L. Rush, M. Ishida, V. M. Lynch, D. Kim, J. L. Sessler. *J. Am. Chem. Soc*. **2014**, *136*, 7591.

[12] S. Saito, A. Osuka, *Angew. Chem. Int. Ed.* **2011**, *50*, 4342.

[13] Z. S. Yoon, A. Osuka, D. S. Kim, *Nat. Chem.* **2009**, *1*, 113.

[14]Y. Tanaka, S. Saito, S. Mori, N. Aratani, H. Shinokubo, N. Shibata, Y. Higuchi, Z. S. Yoon, K. S. Kim, S. B. Noh, J. K. Park, D. Kim, A. Osuka,, *Angew. Chem. Int. Ed.* **2008**, *47***,** 681.

[15] R. Herges, *Chem. Rev*. **2006,** *106*, 4820.

[16] T. Yamamoto, A, Morita, Y. Miyazaki, T. Maruyama, H. Wakayama, Z. H. Zhou, Y. Makamura, S. Sasaki, K. Kubota, *Macromoleculaes*. **1992,** *25*, 1214.

[17] T. Yamamoto, A, Yamamoto, *Chem, Lett*. **1977,** *4*, 353.

[18] Gaussian 09, Revision D.01, M. J. Frisch, G. W. Trucks, H. B. Schlegel, G. E. Scuseria, M. A. Robb, J. R. Cheeseman, G. Scalmani, V. Barone, B. Mennucci, G. A. Petersson, H.

Nakatsuji, M. Caricato, X. Li, H. P. Hratchian, A. F. Izmaylov, J. Bloino, G. Zheng, J. L. Sonnenberg, M. Hada, M. Ehara, K. Toyota, R. Fukuda, J. Hasegawa, M. Ishida, T. Nakajima, Y. Honda, O. Kitao, H. Nakai, T. Vreven, J. A. Montgomery, Jr., J. E. Peralta, F. Ogliaro, M. Bearpark, J. J. Heyd, E. Brothers, K. N. Kudin, V. N. Staroverov, T. Keith, R. Kobayashi, J. Normand, K. Raghavachari, A. Rendell, J. C. Burant, S. S. Iyengar, J. Tomasi, M. Cossi, N. Rega, J. M. Millam, M. Klene, J. E. Knox, J. B. Cross, V. Bakken, C. Adamo, J. Jaramillo, R. Gomperts, R. E. Stratmann, O. Yazyev, A. J. Austin, R. Cammi, C. Pomelli, J. W. Ochterski, R. L. Martin, K. Morokuma, V. G. Zakrzewski, G. A. Voth, P. Salvador, J. J. Dannenberg, S. Dapprich, A. D. Daniels, O. Farkas, J. B. Foresman, J. V. Ortiz, J. Cioslowski, and D. J. Fox, Gaussian, Inc., Wallingford CT, 2013.

[19] S.E. Lewis, *Chem. Soc. Rev.*, **2015**, *44*, 2221.

[20] B. M. Wong, *J. Phys. Chem. C*, **2009**, *113*, 21921.

[21] Y. Tanaka, S. Saito, S. Mori, N. Aratani, H. Shinokubo, N. Shibata, Y. Higuchi, Z. S. Yoon, K. S. Kim, S. B. Noh, J. K. Park, D. Kim, A. Osuka, *Angew. Chem. Int. Ed.*, **2008**. *47*, 681.

[22] I. M. James, (ed.) *History of Topology*, 909–924 (North-Holland, **1999**).

[24] D. Ajami, O. Oeckler, A. Simon, R. Herges, *Nature* **2003**, *426*, 819.

[25] H. S. Rzepa, *Org. Lett.* **2005**, ***7,*** 4637.

[26] C. Castro, Z. Chen, C. S. Wannere, H. Jiao, W. L. Karney, M. Mauksch, R. Puchta, N. J. R. v. E. Hommes, P. v. R. Schleyer, *J. Am. Chem. Soc*. **2005**, *127*, 2425.

[27] Heilbronner, E. *Tetrahedron Lett*. **1964**, 1923.

[29] P. Bonakdarzadeh, F. Topić, E. Kalenius, S. Bhowmik, S. Sato, M. Groessl, R. Knochenmuss, K. Rissanen, *Inorg. Chem.*, **2015**, *54*, 6055.

[30] M. Stepien , L. Latos-Grazynski, *J. Am. Chem.Soc*. **2002**, *124*, 3838.

[31] K. Müllen, H. Unterberg, W. Huber, O. Wennerstroem, U. Norinder, D. Tanner, *J. Am. Chem.Soc*. **1984**, *106*, 7514..

[32] S. Saito, A. Osuka, *Angew. Chem. Int. Ed*. **2011**, *50*, 4342.

[33] Z. S. Yoon, A. Osuka, D. Kim, *Nature Chem.*, **2009**, *1*, 113.

[34] M. Stepien , L. Latos-Grazynski, N. Sprutta, P. Chwalisz, L. Szterenberg, *Angew. Chem. Int. Ed.* **2007**, *46*, 7869.

5. Derivatizing sulfur-incorporated hexa-*peri*-hexabenzocoronenes with tunable optoelectronic properties

5.1 Introduction

Polycyclic aromatic hydrocarbons (PAHs) and their derivatives, such as triphenylenes, pyrene, corannulene, coronene, and hexa-*peri*-hexabenzocoronenes[1] (HBCs, figure 5-1), are structurally conceived as the substructures of the 2D graphene materials. Owing to their unique optoelectronic properties [2,3] and supramolecular behavior [4,5,6], these intriguing nanographene moieties have attracted enormous attention in the fields of synthetic chemistry and organic semiconducting materials. For example, HBCs bearing long aliphatic side chains can self-organize into 1D columnar superstructures in the solid state, which is highly promising for organic field-effect transistors (OFET) and organic light emitting diode (OLED).

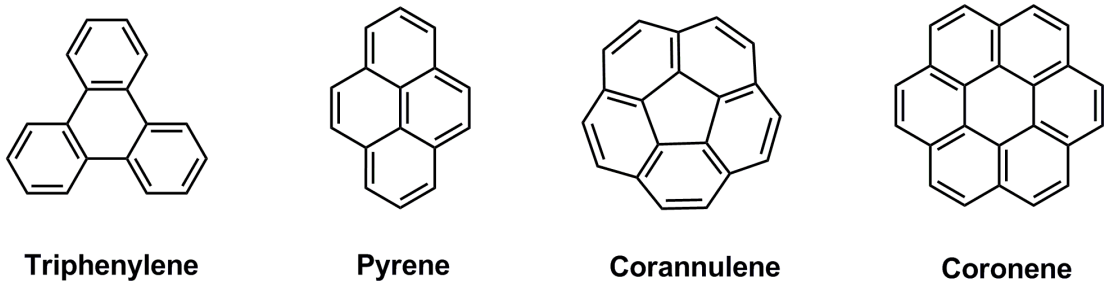

Figure 5-1. Structural represetentives of polycyclic aromatic hydrocarbons.

The fusion and incorporation of thiophene rings into PAHs and polyphenylene derivatives offers the opportunity for tuning their electronic energy levels, packing motifs and charge transport properties, [7,8,9] which is widely used in the design of novel organic semiconductors.[10,11,12] Therefore, by combining these two types of fascinating π-conjugated structures, the compound tribenzo[b,b',b"]tribenzo[2,3:6,7:10,-11]coroneno[1,12-fg:5,4-f'g':9,8-f"g"]tris[1]benz

othiophene (trisbenzothieno[1,2:7,8:13,14]hexa-peri-hexabenzocoronene, TTC, Figure 5-2)[13] has been synthesized in our group, in which three benzothiophene rings are fused to the HBC periphery with a C3 symmetric architecture. However, the poor solubility of unsubstituted TTC has hindered detailed studies of its optoelectronic properties, and supramolecular behavior. Except for rendering the possibility of extended π-conjugation systems and intramolecular donor-acceptor structures, the fusion with benzothiophene moieties also offers the potential for further chemical modification of S atoms, such as selective oxidation of the thiophene rings of TTC into thiophene-*S*,*S*-dioxide moieties of TTOC [14, 15, 16] (trisbenzothieno-*S*,*S*-dioxide[1,2:7,8:13,14]hexa-*peri*-hexabenzocoronene, Figure 5-2).

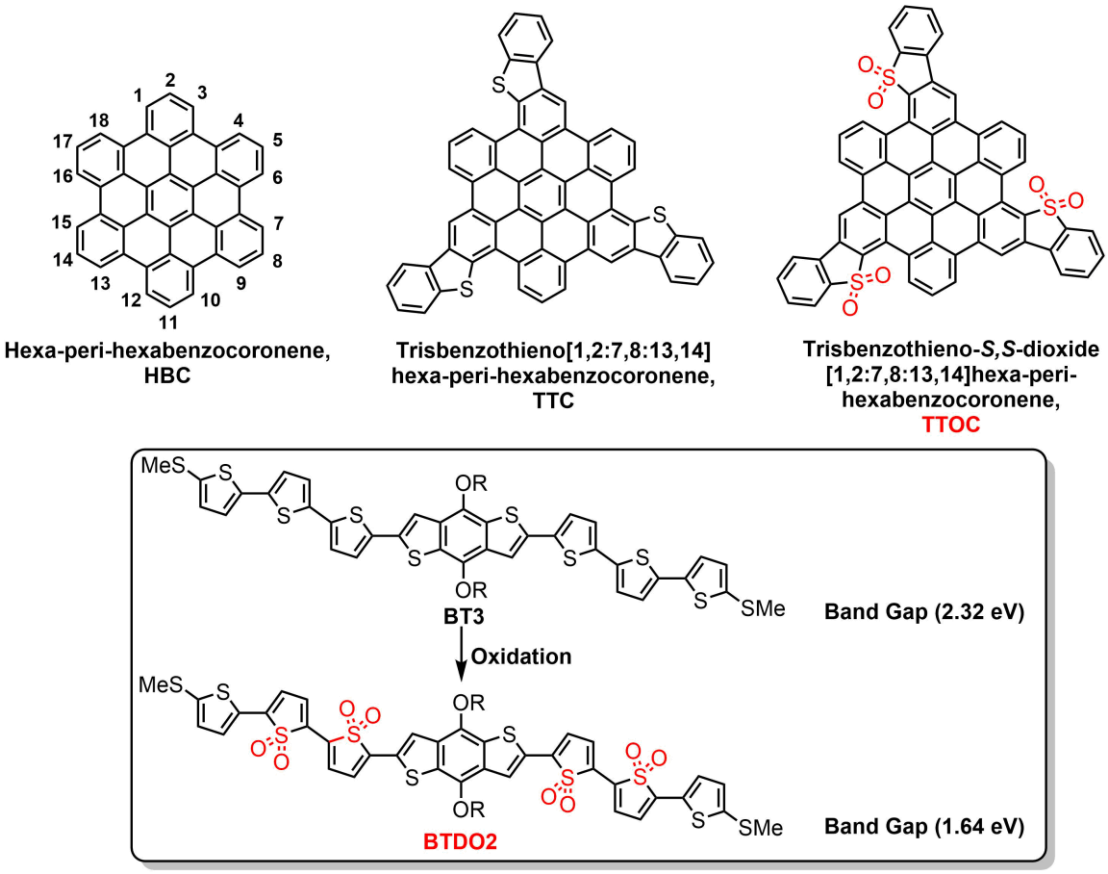

Figure 5-2. Representative molecular structure of hexa-*peri*-hexabenzocoronene, trisbenzothieno[1,2:7,8:13,14]hexa-*peri*-hexabenzocoronene (TTC), its oxidized derivative trisbenzothieno-*S*,*S*-dioxide[1,2:7,8:13,14]hexa-*peri*-hexabenzocoronene (TTOC), and

illustrative example of band gap engineering in oligothiophene derivatives (from BT3 to BTDO2).

In attempts to manipulate and engineer the band gap pf organic semiconductors, it is well known that the highest occupied molecular orbital (HOMO) is mainly affected by the "push" building blocks and the lowest unoccupied molecular orbital (LUMO) is determined by the "pull" units.[17,18] The oxidation of electron-rich thiophene units into electron-poor thiophene- *S,S* -dioxide proven to be a very promising strategy to modulate the electronic properties and develop stable n-type semiconductors.[19] For example, the band gap of BT3 can be effectively decreased from 2.32 eV to 1.64 eV *via* oxidation of "push" thiophene rings into "pull" thiophene- *S,S* -dioxide units, in which the change of the band gap primarily comes from the stabilization of LUMO due to the "pull" units.

In this chapter, the synthesis of various TTCs derivatives decorated with alkoxyl and alkyl substitutions will be presented. Furthermore, the transformation of the π-conjugated benzothiophene units into thiophene-*S,S*-dioxide moieties will also be investigated as an approach to modulate the optical, and electronic properties of TTCs. The assembling behavior of these TTCs will also be investigated via 2D-WAXS.

5.2 Results and Discussion

5.2.1 Synthesis of alkoxyl decorated TTCs and their oxidation

Herein, a series of TTC derivatives bearing alkoxyl chains was successfully synthesized, and showed good solubility in common organic solvents (like dichloromethane, and THF). Both the decoration of electron-donating alkoxy chains and conversion from electron-rich thiophene ring into electron-poor thiophene-*S,S*-dioxide units would be capable of tuning the highest occupied molecular orbital (HOMO) and lowest unoccupied molecular orbital (LUMO).

The synthesis of TTCs **5-6** bearing linear or branched alkoxy chains was based on the key building block, 1,3,5-tris-(2'-bromo-4'-methoxylphenyl)benzene (**5-2**) [20], which could be readily obtained via acid-catalyzed condensation of 2-bromo-4-methoxyacetophenone (**5-1**, scheme 3-1). The synthetic route consisted of Suzuki coupling of **5-2** with the commercially available 4-dibenzothiophenylboronic acid, subsequent BBr_3 induced deprotection of the methoxyl group, and then the substitution reaction with the desired alkyl bromide to afford the oligophenylene precursor (**5-5**) with various alkoxyl chains (from linear alkyl chains in **5-5b** and **5-5d**, to branched alkyl chains in **5-5a**, **5-5c** and **5-5e**). An intramolecular oxidative cyclodehydrogenation reaction (*Scholl* coupling) of **5-5**(**a-e**) was then performed with $FeCl_3$ as the Lewis acid and oxidant to provide targeted compounds **5-6**(**a-e**) substituted with different alkoxyl chains (from linear alkyl chains in **5-5b** and **5-5d**, to branched alkyl chains in **5-5a**, **5-5c** and **5-5e**) as orange powder. The products were well soluble in common organic solvents, including dichloromethane, toluene, and tetrahydrofuran. And the MALDI-TOF MS spectrometry (figure 5-3) of **5-6**(**a-e**) all indicated a single species with desired molar mass, and the experimental isotopic distributions are also consistent with the theoretical calculations. These results clearly support the successful synthesis of targeted benzothiophene-fused nanographenes substituted with various alkoxy chains. Furthremore, the investigation of the ^{1}H NMR spectra of these TTCs **5-6**(**a-e**) also validated the chemical identity of corresponding TTC compounds **5-6**(**a-e**).

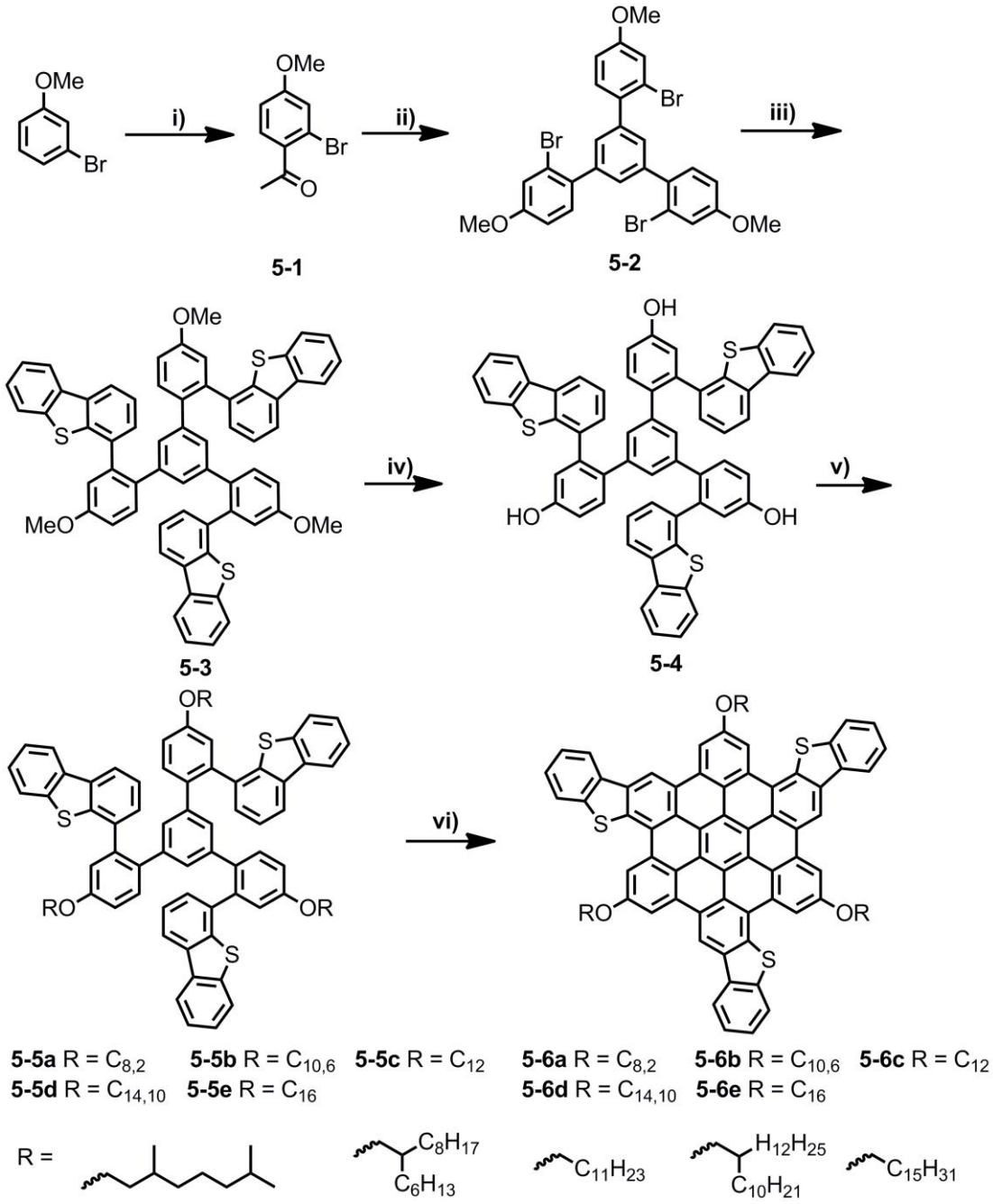

Scheme 5-1. Synthetic route towards TTCs **5-6**(**a-e**) derivatives bearing various alkoxy substitutions. Conditions: i) AcCl. $AlCl_3$, DCM, RT, 16h, 56%; ii) $SiCl_4$, EtOH, 70 ℃, 12h, 76%; iii) $Pd(PPh_3)_4$(10%mol), K_2CO_3, Tol/MeOH/H_2O, 100 ℃, 24h, 96%; iv) BBr_3, DCM, RT, 12h, 96%; v) RBr, K_2CO_3, DMF, 120 ℃, 24h, 35% (**5-5a**), 44% (**5-5b**), 47% (**5-5c**), 58% (**5-5d**), 40% (**5-5e**); vi) $FeCl_3$, DCM/CH_3NO_2, RT, 40mins, 95% (**5-6a**), 70% (**5-6b**), 67% (**5-6c**), 78% (**5-6d**), 68% (**5-6e**).

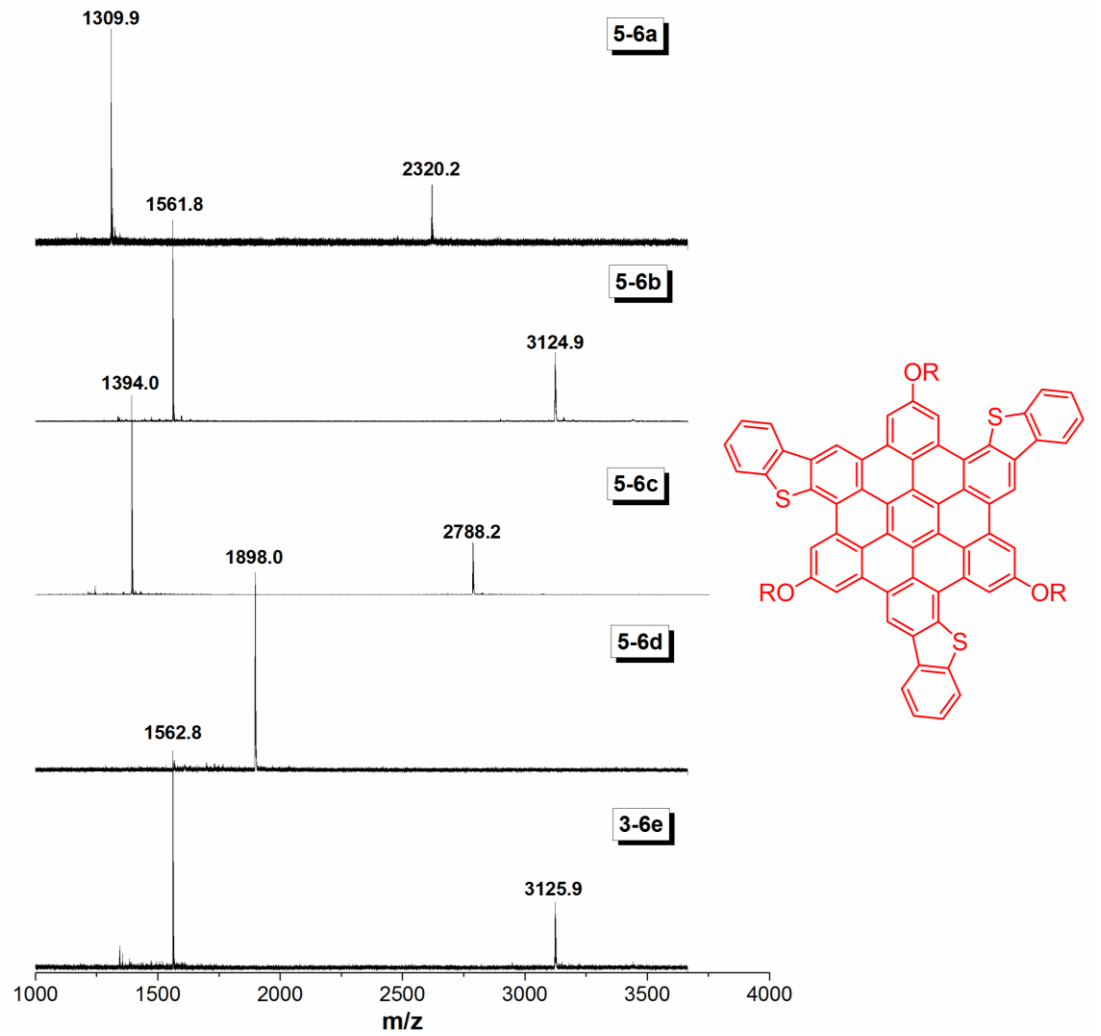

Figure 5-3. MALDI-TOF MS spectra of TTCs derivatives **5-6**(**a-e**) with various alkoxy chains substitutions.

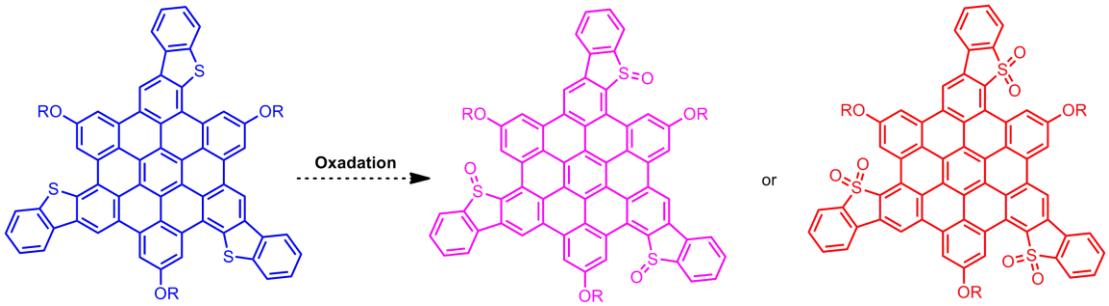

Scheme 5-2. Oxidation reaction of TTCs **5-6** derivatives bearing various alkoxy substitutions. Conditions: *m*-CPBA (8.0 eq), THF, RT, 12h.

To modulate the electronic structure of TTCs **5-6**(**a-e**), oxidation of the *S* atoms of TTC derivative **5-6a** (scheme 5-2) was initially conducted. After oxidation from

electron-donating benzothiophene units to electron-accepting thiophene-*S*,*S*-dioxide units, obvious intramolecular donor-acceptor conjugation structure was expected in the corresponding compound which could remarkably tune the electronic property of the corresponding PAH derivatives.

However, in the oxidation reaction of TTCs **5-6a** derivative using an oxidant like *meta*-chloroperoxybenzoic acid (*m*-CPBA) under room temperature in THF solution overnight and quenching with MeOH, the decomposition of the alkoxy substitutions and incomplete oxidation were observed in the MALDI-TOF MS spectrum (Figure 5-4) of the obtained product. The MALDI-TOF mass spectrum also indicated the incomplete oxidation even after usage of excess amount of oxidants. Therefore, synthesis of the desired TTOC derivatives substituted with alkoxyl side groups failed due to its suspecibility to oxidation conditions.

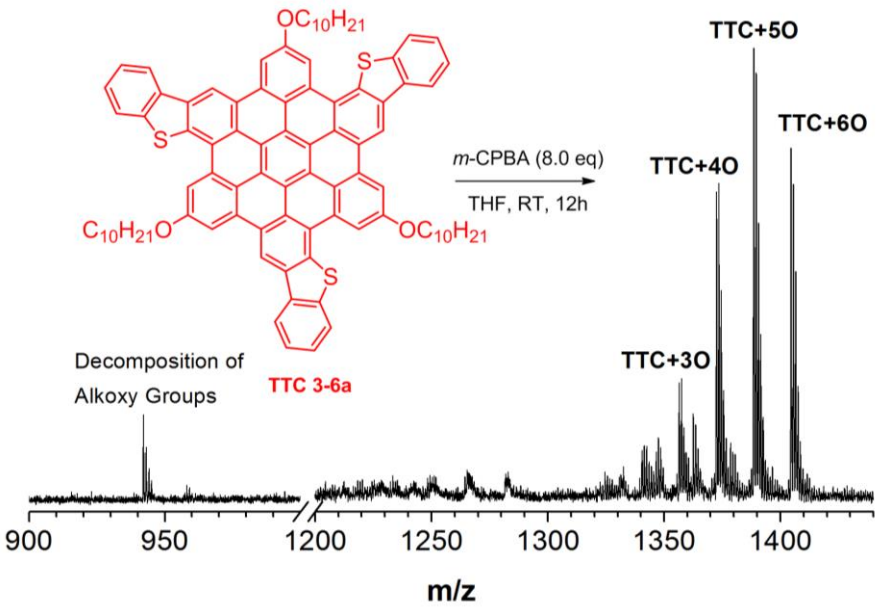

Figure 5-4. MALDI-TOF mass spectrum of oxidization product of TTC derivative **5-6a**.

5.2.2 Synthesis of alkyl chains decorated TTCs and their chemical modification

Taking into account the incomplete oxidation of TTC **5-6**(**a-e**) derivatives, we turned to the synthesis of TTC **5-10** which is substituted with alkyl substitutions based on the same synthetic strategy described above(scheme 5-3). After conversion of the phenol

group of compound **5-4** to corresponding aryl triflate units in compound **5-7**, the subsequent introduction of the alkyl chain on compound **5-7** via *Sonagashira* coupling, and the hydrogenation reaction of **5-8** in an autoclave, and the *Scholl* cyclodehydrogenation reaction of oligophenylene precursor **5-9**, a tridodecyl-chains substituted TTC 5-**10** as an orange powder could be obtained with an overall yield of 41% in just 4 steps.

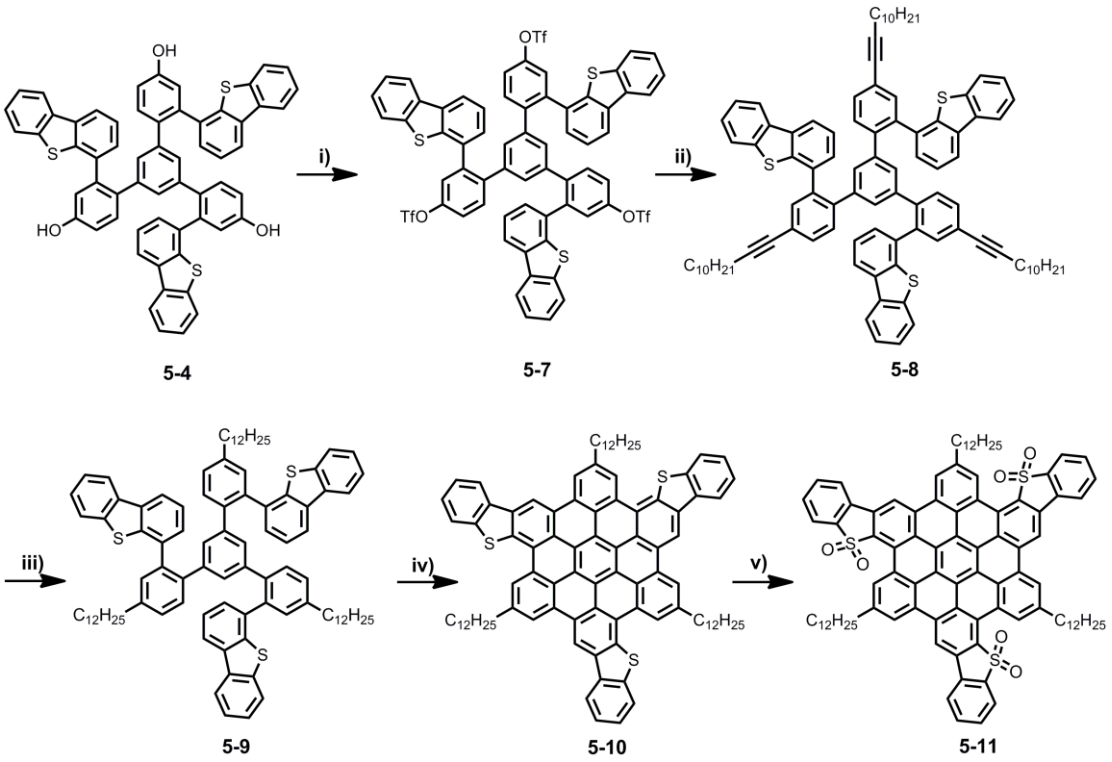

Scheme 5-3. Synthetic routes toward tridodecyl chain-substituted TTC **5-10** and TTOC **5-11**. Conditions: i) Tf_2O, TEA, DCM, 0 ℃, 2h, 67%; ii) $Pd(PPh_3)_2Cl_2$, CuI, PPh_3, i-Pr_2EtN, DMF, 80 ℃, 12h, 78%; iii) Pd/C (10 wt%), H_2,EtOAc, RT, 10 bar, 12h, 97%; iv) $FeCl_3$, DCM/$MeNO_2$, RT, 40mins, 80%; v) *m*-CPBA, THF, RT, 60mins, 85%.

MALDI-TOF MS spectrometry of **5-10** revealed a single species with the isotopic distribution, which was consistent with the theoretical distribution. The peak m/z of 1345.5 was also in good agreement with its molar mass of 1345.98 g/mol (Figure 5-5). Compound **5-10** was subsequently subjected to the oxidation reaction with *m*-CPBA in THF at room temperature. After quenching the reaction with MeOH, filtration, and thoroughly washing with MeOH, compound **5-11** was obtained as a red powder in

high yield (85%). MALDI-TOF MS spectrometry of **5-11** showed a single peak at 1442.5, consistent with the targeted molar mass of 1441.98 g/mol (Figure 5-5).

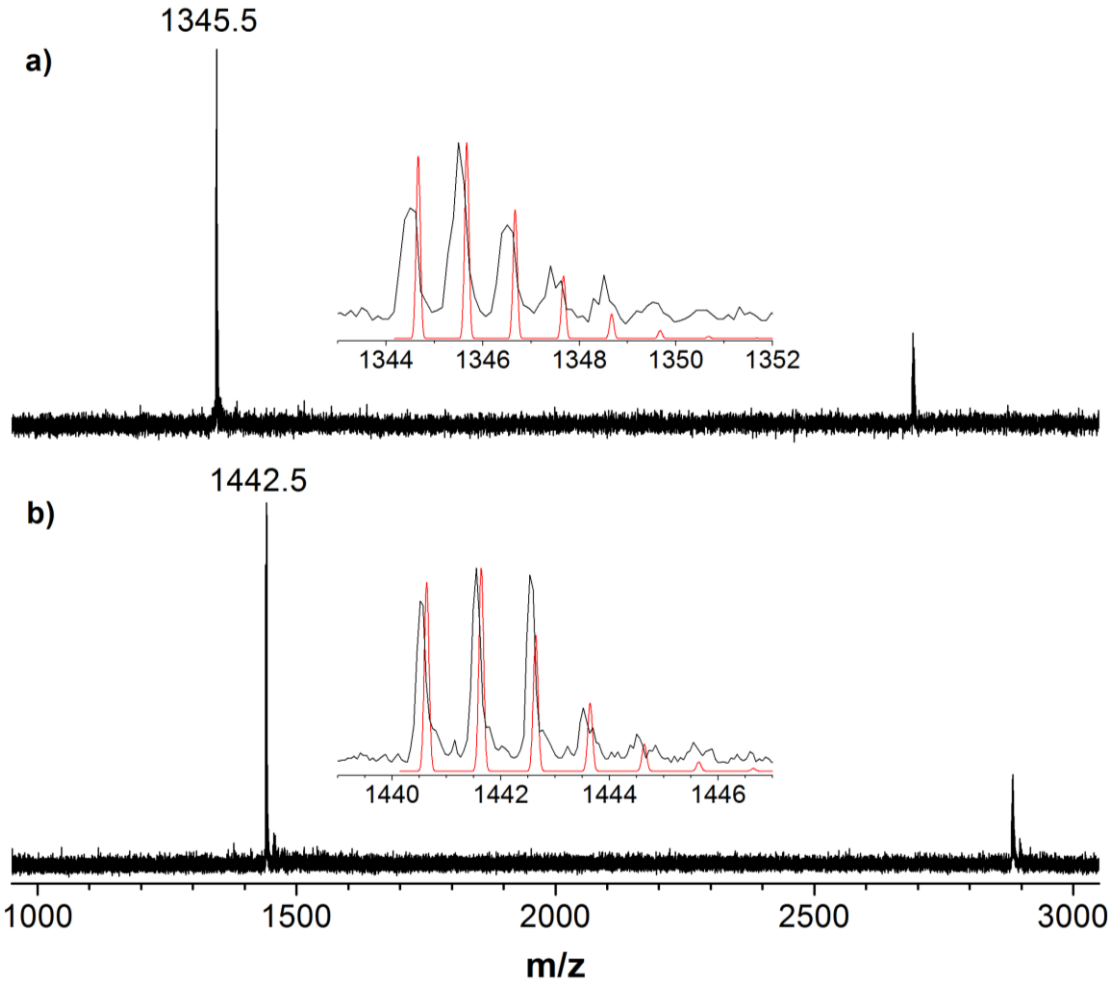

Figure 5-5. MALDI-TOF MS spectra of TTC **5-10** (a) and TTOC 5-**11** (b). Inset: Experimental (dark line) and simulated (red line) isotopic distribution.

To further elucidate the successful conversion from TTC **5-10** to TTOC **5-11** and its impact on the electronic structure of the HBC cores, detailed proton NMR measurement and 2D NMR were conducted. In the ^{1}H NMR spectra of **5-10** and **5-11** in $C_2D_2Cl_4$ at 403 K (Figure 5-6), every aromatic proton signals could be assigned with the assistance of the correlation 2D NMR spectra. (Figure 5-7 and Figure 5-8 for TTC **5-11**; Figure 5-9 and Figure 5-10 for TTOC **5-11**)

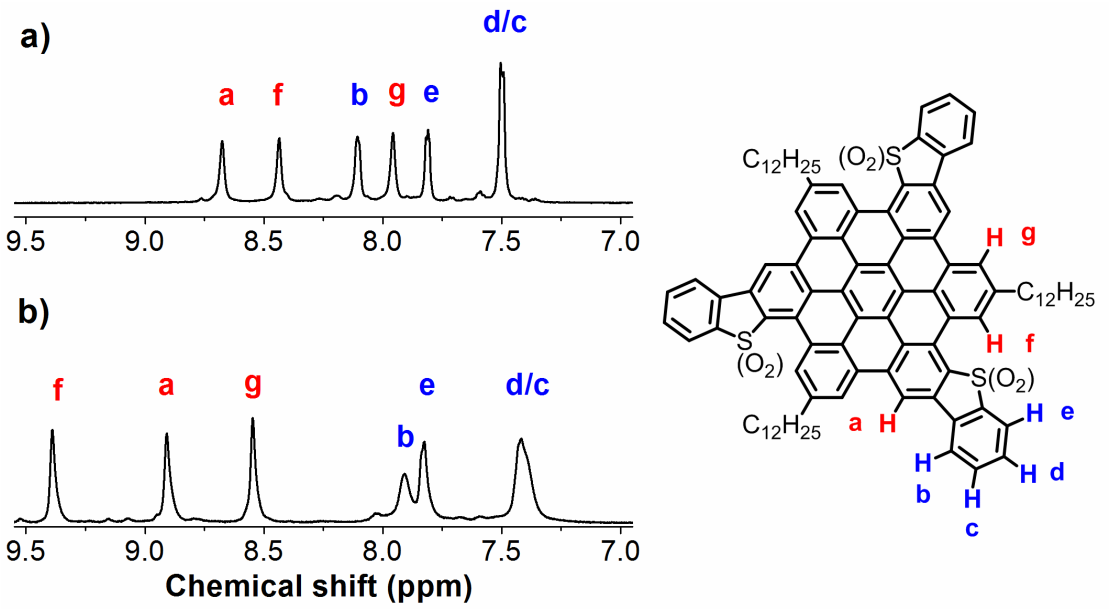

Figure 5-6. Detailed ^{1}H NMR spectra of TTC **5-10** (a) and TTOC **5-11** (b) in $C_2D_2Cl_4$ at 403K.

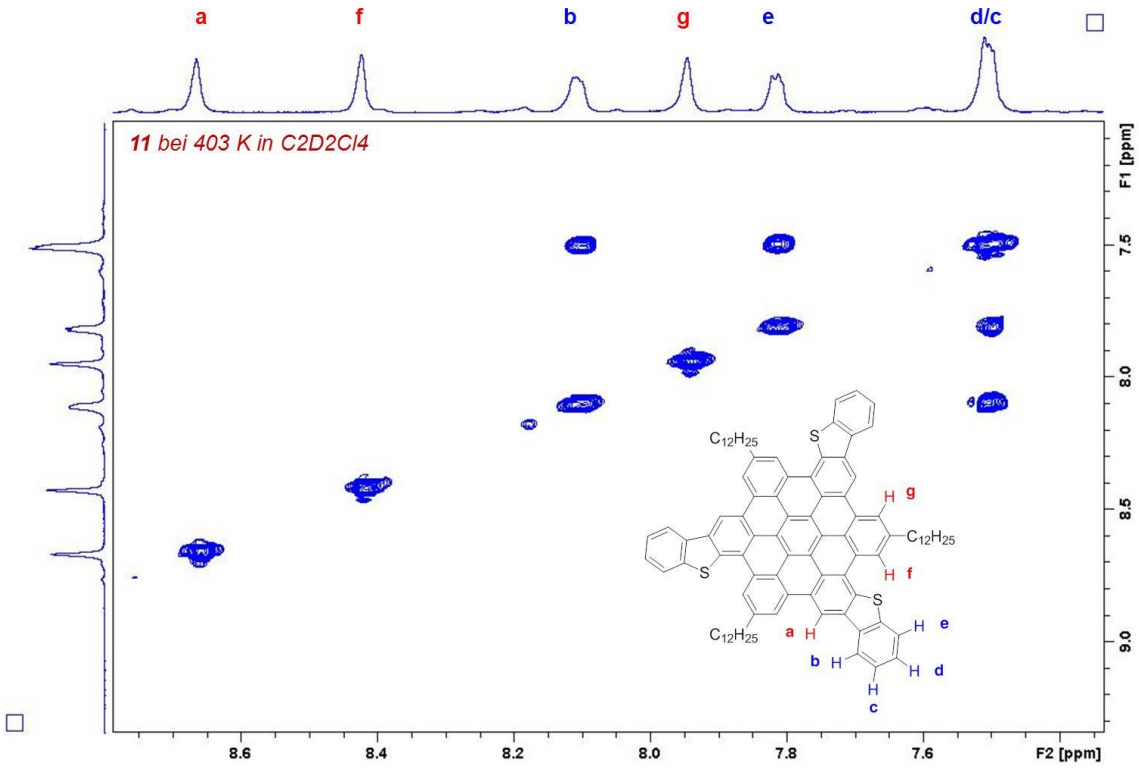

Figure 5-7. 2D ^{1}H-^{1}H COSY spectrum of TTC **5-10** in $C_2D_2Cl_4$ at 403 K.

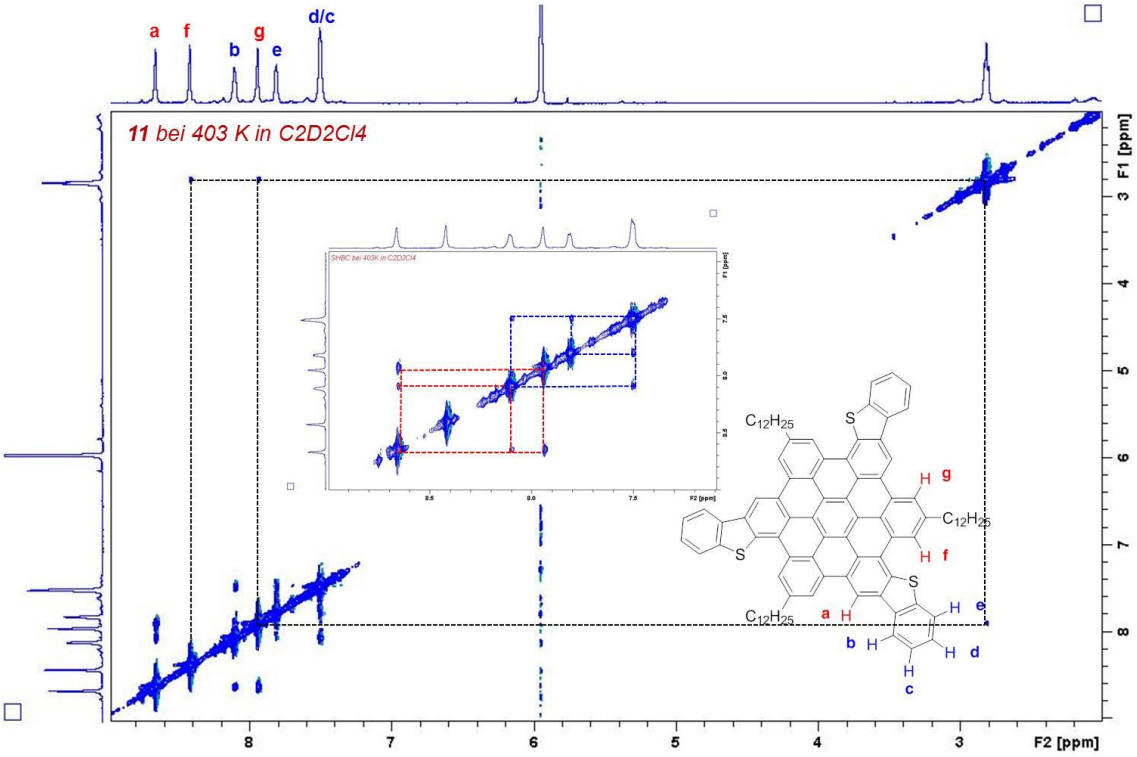

Figure 5-8. 2D ^{1}H-^{1}H NOESY spectrum of TTC **5-10** in $C_2D_2Cl_4$ at 403 K.

Through comparison of the signals of aromatic protons of TTC **5-10** and TTOC **5-11** (figure 5-6), obvious downfield shifts were observed for the three types of peripheral protons (H_a, H_f, H_g) on the HBC cores after oxidation of the *S* atoms. The signal of the proton H_a located at the phenyl ring where the benzothiophene units are fused showed a downfield shift from 8.67 (for **5-10**) to 8.91 (for **5-11**) after oxidation. And the peak corresponding to two aromatic protons (H_f/H_g) adjacent to the substituted dodecyl chain also shifted from 8.43/7.96 (for **5-10**) to 9.31/8.55 (for **5-11**), respectively. This down-field shift can be probably attributed to decreased electron density on the HBC cores after oxidation, and the resulting attenuated deshielding effect on these three protons (H_a, H_f, H_g) from the nanographene segments. It is also well consistent with our proposal of modulating the electron density of the HBC cores through the chemical modification on the incorporated heteroatoms.

Additonally, for the aromatic protons located on the peripheral benzothiophene ring, a slight downfield shift could be observed for the signal of the *ortho* proton H_e from 7.81 (for **5-10**) to 7.83 (for **5-11**), which is presumably because of the enhanced

deshielding effect from the electron-withdrawig thiophene-*S*,*S*-dioxide group. The signals of other two peripheral phenyl protons H_c and H_d merged into one broad peak, and exhibited an upfield shift from δ = 7.50 for **5-10** to δ = 7.42 for **5-11** after oxidation. In addition, the proton H_b located at the bay region displayed a more pronounced upfield shift from 8.11 (for **5-10**) to 7.91 (for **5-11**) after oxidation.

As we know, thiophene is a 6π-aromatic system. After the oxidation, the sulfur's lone electron pairs will be removed from this conjugated system, and thus the electron-delocalization between the HBC core and peripheral benzene rings will be disrupted.[21] In addition, the tri(sulfuryl) groups in TTOC can withdraw the electron clouds from the nanographene cores to the peripheral benzene rings and decrease the electron density in the HBC core.[22] After oxidation into thiophene-*S*,*S*-dioxide units, the strong electron-withdrawing sulfone moieties will enrich the electron density on the pristine thiophene rings, and thus reinforce the shielding effects which lead to the resulting upfield shifts for protons H_b, H_c/H_d, and H_e. However, the proton H_e will also be under the direct impact of the neighboring sulfone moieties, the strong electron-withdrawing property of the adjacent sulfone units will overcome the shielding effects, and thus result in the slight down-field shift for proton H_e.

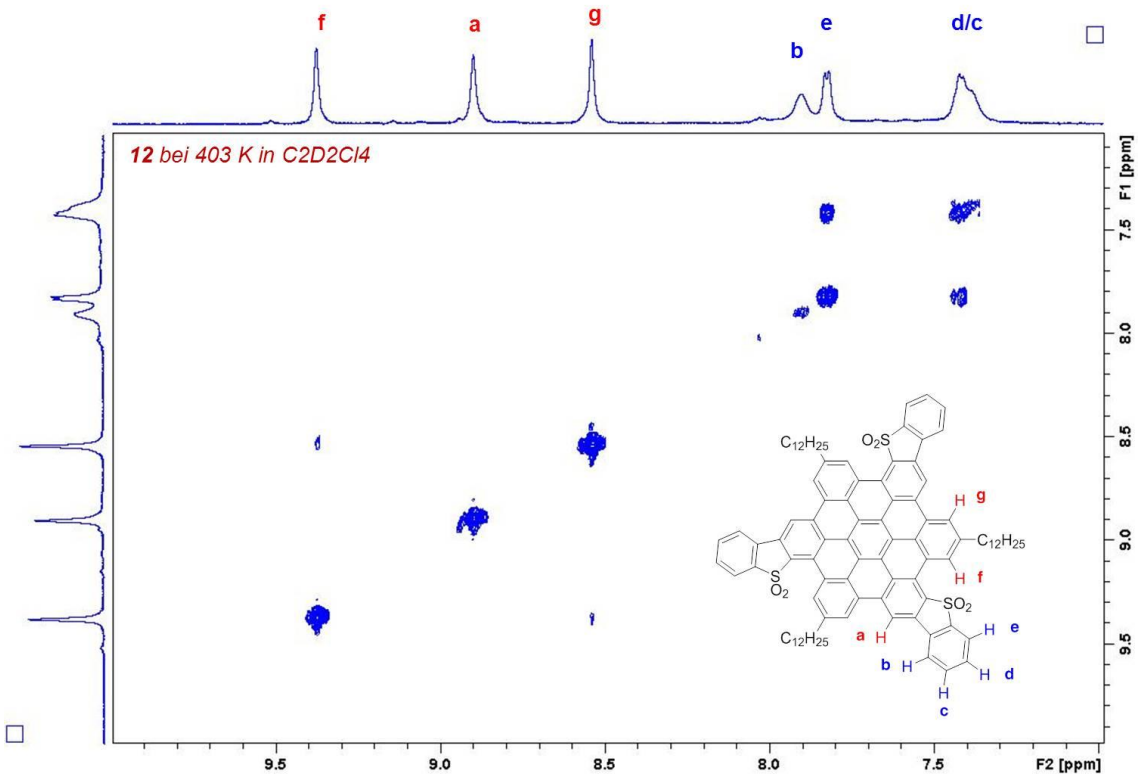

Figure 5-9. 2D ^{1}H-^{1}H COSY spectrum of TTOC **5-11** in $C_2D_2Cl_4$ at 403 K.

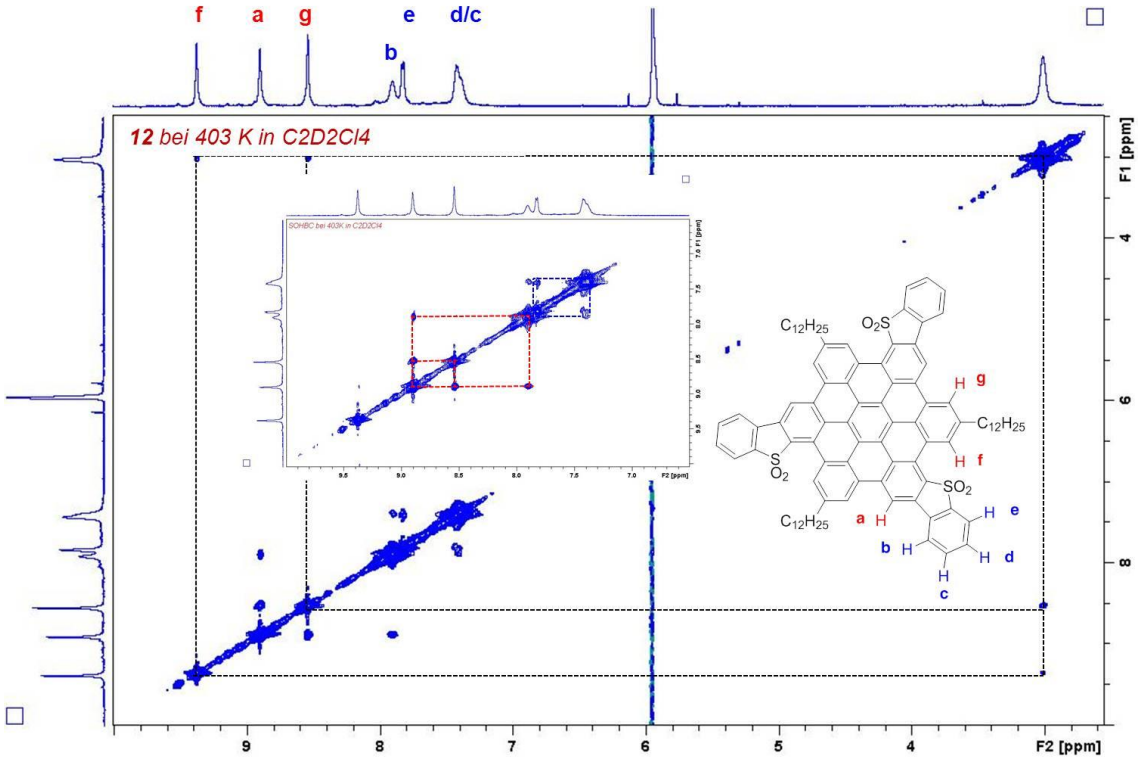

Figure 5-10. 2D ^{1}H-^{1}H NOESY spectrum of TTOC **5-11** in $C_2D_2Cl_4$ at 403 K.

5.2.3 Optical and electronic properties of TTC and TTOCs

To further investigate the impact of the oxidation of the *S* atom and substitution with electron-donating alkoxyl chains on the photophysical properties of TTC derivatves, UV/Vis absorption and fluorescence spectra of **5-6**(**a-e**), **5-10**, and **5-11** were measured in THF (Figure 5-11 and Figure 5-12).

The UV-Vis spectra of TTC derivatives **5-6** (**a-e**) exhibited the typical β, and p bands which were characteristic of the large polycyclic aromatic hydrocarbons,[23,24] while the detection of the α band was too difficult due to the extremely low intensity of tha band. As for the TTC derivatives (**5-6b** and **5-6d**) substituted with branched alkoxy chains, the β band at 392 nm and the p band as shoulder at 424 and 434 nm could be clearly resolved. And for the analoguous TTC derivatives (**5-6a**, **5-6c** and **5-6e**), the β band appeared at 390 nm with and the p band at 435 nm. In comparision with the parent HBC which are featured with β band at 360 nm and p band at 390 nm,[25,26] the UV-Vis spectra of TTC **5-6** had exhibited a red-shift of approximate 30 nm attributed to the extended π-conjugation with electron rich thiophene ring.

Addtionlly, compared with the the pristine TTC (λ_{abs} = 350 nm) reported at 2007,[13] the absorbance maxima of **5-6** showed a significant bathochromic shift of 40 nm due to the magnified solubility. And this relationship between the optical properties and processbility was also confirmed in the comparison between **5-6b**/**d** and **5-6a**/**c**/**e**. The branched and sterically demanding substitutions on **5-6b**/**d** gave these two TTCs better solubility and less tendency toward aggregate formation. Therefore, the UV-Vis spectra of TTCs **5-6a**/**c**/**e** had also obviously broadened and less resolved in comparison with that of TTCs **5-6b**/**d**.

Table 5-1. Optoelectronic properties of TTC **5-6(a-e)**.

	5-6a ($C_{8,2}$)	**5-6b($C_{10,6}$)**	**5-6c (C12)**	**5-6d ($C_{14,10}$)**	**5-6e (C_{16})**
$\lambda_{max,\ abs}$ / nm[a]	389	392	390	392	389
ε / 10^5 $M^{-1}cm^{-1}$[a]	0.844	1.394	0.963	1.455	0.990
$\lambda_{max,\ lum}$ / nm[a]	535	523	539	520	537

[a] Maximum absorption wavelength in THF solution (1.0×10^{-5} M). [b] Molar extinction coefficient at $\lambda_{abs,\ max}$. [c] Maximum photoluminescence wavelength in THF solution (1.0×10^{-5} M).

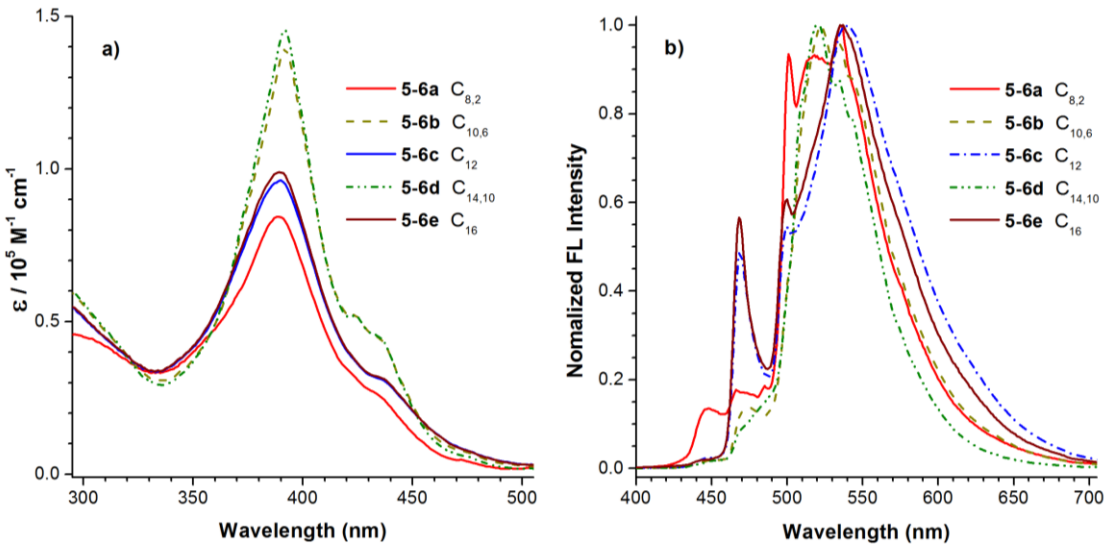

Figure 5-11. UV-Vis (a) and photoluminescence (b) spectra of TTC **5-6** (**a-e**) (1.0×10^{-5} M in THF).

In the case of photoluminescence spectra, the fluorescence maxima for TTCs substituted with linear alkoxyl chains (λ_{lum} = 537 nm for **5-6a**, **5-6c** and **5-6e**) showed an obvious red shift when comparing with TTCs substituted with sterically demanding substitutions (λ_{lum} = 520 nm for **5-6b**, and **5-6d**) due to the formation of aggregates driven by strong π-π stacking. The PL spectra of the TTCs **5-6** also revealed many sharp shoulder bands, which is due to the existence of different vibronic levels of the ground state S_0 for the TTCs or their aggreagtes. Therefore, the

radiative relaxation from the excited state S_1 to the various vibronic levels of S_0 led to a set of distinct peaks as observed.

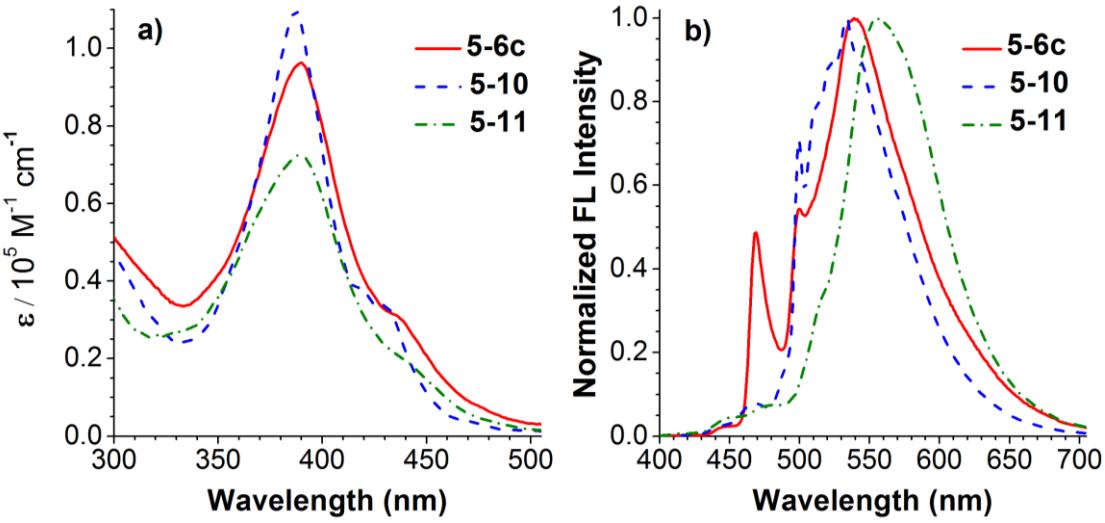

Figure 5-12. UV/Vis (a) and photoluminescence (b) spectra of TTC **5-6c**, **5-10** and TTOC **5-11** (1.0×10^{-5} M in THF).

Meanwhile, in order to study the impact of electron donating/accepting substitution on the optical properties of TTCs, the UV-Vis spectra of TTC **5-6c**, **5-10** and TTOC **5-11** were compared in detail (Figure 5-12). The absorption maximum of **5-6c** (λ_{abs} = 390 nm, $\varepsilon = 0.96 \times 10^5$ $M^{-1}cm^{-1}$) exhibited a subtle bathochromic shift compared to that of **5-10** (λ_{abs} = 387 nm, $\varepsilon = 1.10 \times 10^5$ $M^{-1}cm^{-1}$), which was attributed to the electron-donating dodecyloxy chains that extends the conjugation. Compound **5-11** (λ_{abs} = 389 nm, $\varepsilon = 0.73 \times 10^5$ $M^{-1}cm^{-1}$) also displayed a slightly red shift of the absorption maximum with respect to that of compound **5-10** due to integration of the electron-withdrawing thiophene-*S*,*S*-dioxide units into the large π-system. For the photoluminescence spectra, the bathochromic shift was more obvious after introduction of the electron-donating alkoxy chains (λ_{lum} = 539 nm for **5-6c**) or electron-withdrawing thiophene-*S*,*S*-dioxide units (λ_{lum} = 557 nm for **5-11**) when compared with alkyl chain-substituted TTC **5-10** (λ_{lum} = 534 nm).

On the other hand, in order to determine the energy levels of TTCs (**5-6c**, and **5-10**) and TTOC **5-11**, cyclic voltammetry measurements for **5-6c**, **5-10**, and **5-11** in DCM were recorded to measure the oxidation potential (Figure 5-13, and Table 5-2).

Probably due to the poor solubility of TTCs and TTOC and their tendancy to form aggregates under high concentration (1.0 mM), the quality of the cyclic voltammetry is very poor. Thereby, the HOMO levels could only be roughly calculated from the first oxidation potential to be -4.90 eV, -4.91 eV and -5.46 eV for **5-6c**, **5-10**, and **5-11** respectively, which was also well consistent with the values calculated based on DFT calculation. No reversible reduction peaks were observed in the CV spectra. However, with the combination of the HOMO level determined from CV spectra and optical band gap from the UV-Vis spectra, the LUMO level could be roughly estimated. (Table 5-2)

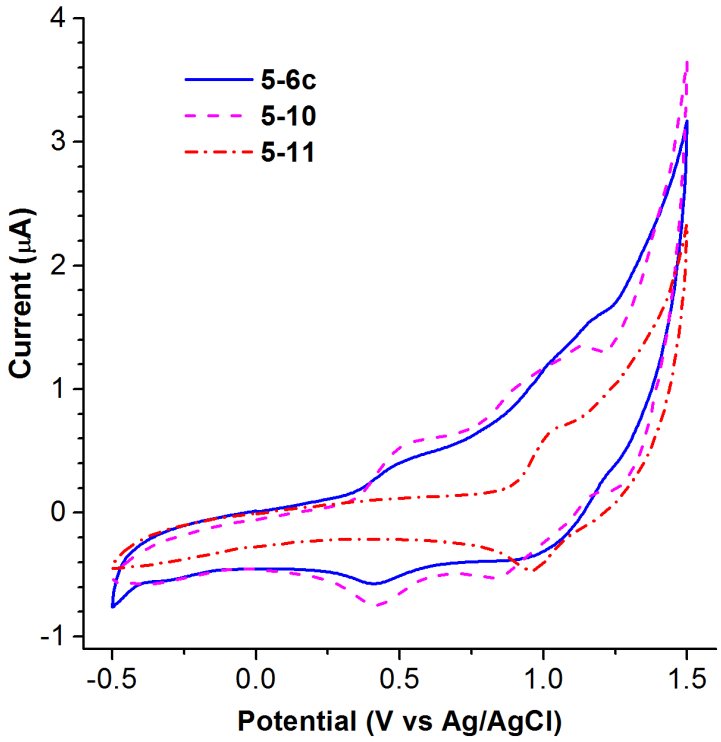

Figure 5-14. Cyclic voltametry spectra of TTCs **5-6c**, TTC **5-10**, and TTOC **5-11** in DCM (1 mM) measured with [*n*-Bu_4N][PF_6] (0.1 M) as a supporting electrolyte.

The energy levels of model compounds for **5-6c**, **5-10**, and **5-11** were calculated by the density functional theory (DFT) method at the B3LYP/6-31G(d) level of theory (Figure 5-14).[27] After introduction of the alkoxy chains, the HOMO level of **5-6c** increased to -4.99 eV compared to its alkyl-substituted analogue **5-10** (-5.08 eV), while the LUMO level also increased from -1.80 eV (**5-10**) to -1.75 eV (**5-6c**) due to the electron-donating behavior of the alkoxyl substitutions.

Table 5-2. Optoelectronic properties of TTC **5-6c**, TTC **5-10**, and TTOC **5-11**.

	UV/Vis Solutions		Cyclic Voltammetry			DFT Calculations[f]		
	λ_{max} [nm][a]	E [10^5 M^{-1} cm^{-1}][b]	HOMO [ev][c]	LUMO [ev][d]	$E_{g,opt}$ [ev][e]	HOMO [ev]	LUMO [ev]	E_g [ev]
5-6c	390	0.963	-4.90	-2.29	2.61	-4.99	-1.75	3.24
5-10	387	1.099	-4.91	-2.18	2.73	-5.08	-1.80	3.28
5-11	389	0.725	-5.46	-2.86	2.60	-5.59	-2.35	3.24

Energy levels are referenced to vacuum. [a] Maximum absorption wavelength in THF solution. [b] Molar extinction coefficient at λ_{max}. [c] HOMO level calculated from the onset of the first oxidation wave and the half-wave potential of the ferrocene as an internal potential standard. [d] LUMO level calculated by adding the optical band gap from the electrochemical HOMO level [f] Optical band gap calculated from the absorption onset in THF solution. [g] DFT calculations of tribenzothiophene fused HBCs.

Notably, the HOMO/LUMO level (-5.59/-2.35 eV) of TTOC **5-11** markedly decreased compared with that of TTC **5-10** (-5.08/-1.80 eV) after converting the electron-rich benzothiophene ring into an electron-poor thiophene-*S,S*-dioxide unit. The effect of oxidation of the sulfur atom on the band gap was subtle (from 3.28 eV in TTC **5-10** to 3.24 eV in TTOC **5-11**), which was also supported by the similar absorption spectra for **5-10** and **5-11**. By contrast, the oxidation of thiophene into thiophene-*S,S*-dioxide could dramatically stabilize the LUMO level of polythiophene and effectively lower its band gap, while the HOMO level was retained.[28]. In our work, the thiophene-*S,S*-dioxide fused PAH **5-11** had a markedly low-lying LUMO level (0.55 eV) and parallelly low-lying HOMO energy (0.51 eV), consequently exhibiting a similar band gap. In the normal "push-pull" chromophore, the HOMO level was usually defined by the electron-rich ("push") units, such as the hexa-*peri*-benzocorenene core in TTOC. In our work, the electron-withdrawing

thiophene-*S*,*S*-dioxide units were directly conjugated to the HBC core, and thus the electron density on the HBC core would be reduced remarkably which led to the lower HOMO level. Additionally, the introduction of the bulky *S*,*S*-dioxide units onto TTOC **5-11** would distorted the conjugation backbone (Figure 5-15), and interrupted the π-conjugation.

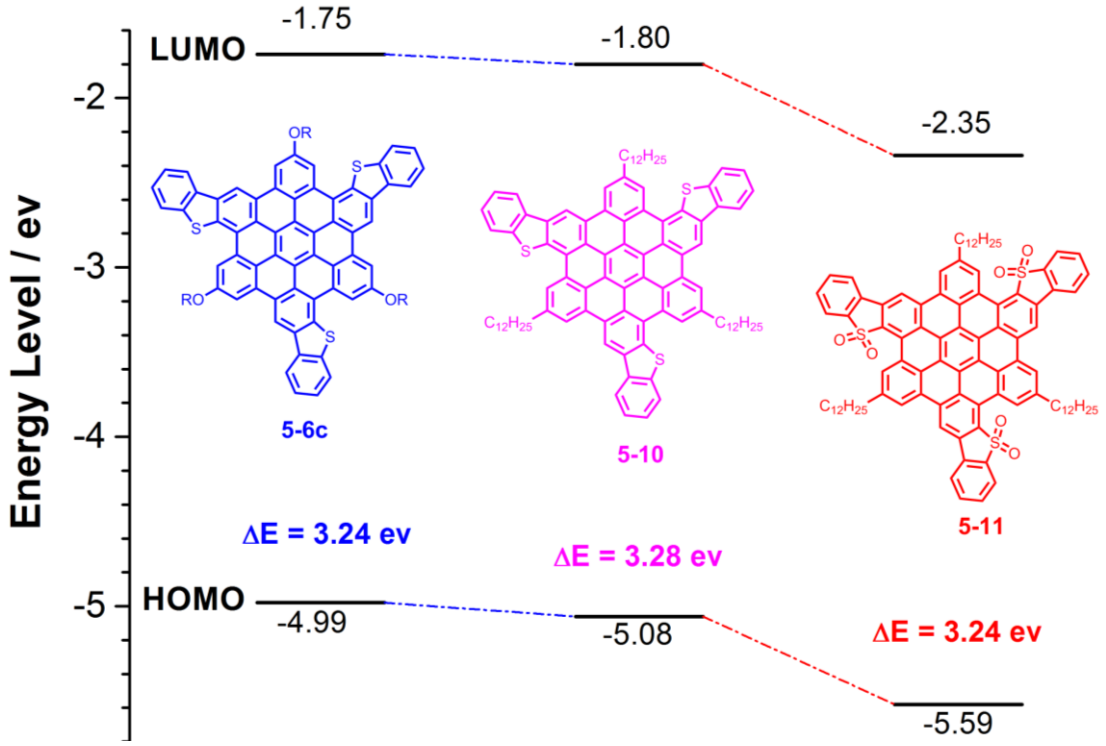

Figure 5-14. Molecular energy level of model compounds for TTC **5-6c**, **5-10**, and TTOC **5-11,** respectively, based on B3LYP/6-31G(d) level via DFT calculation (dodecyl chain was substituted with a methyl group to reduce the calculation time).

In addition, the geometry of compounds TTCs **5-6c** (Figure 5-15a), TTC **5-10** (Figure 5-15b), and TTOC **5-11** (Figure 5-15c) was optimized on the basis level of B3LYP/6-31G(d). (Figure 5-15). The peripheral benzothiophene rings were clearly observed to be slightly tilted out of the HBC plane to a certain degree with C3h symmetry, which was probably due to the strong steric repulsion between the proton H_f (Figure 5-6) with the substituted benzothiophene ring. For TTC **5-6c** and TTC **5-10**, the benzothophene rings were distorted out of the HBC surface with an identical degree, which was identified by the dihedral angles $\measuredangle_1$ (approximate 8.3°) and $\measuredangle_2$ (approximate 15.0°) between the benzothiophene ring and the HBC core.(Figure 5-15)

However, after converting the thiophene ring in TTC **5-10** to thiophene-*S*,*S*-dioxide moiety in TTOC **5-11**, the benzothiophene ring was tilted out of the HBC plane with a more pronounced degree indicated by the increased dihedral angles $\measuredangle_1$ and $\measuredangle_2$ (11.0 ° and 16.1 °, respectively) as a result of the more bulky *S*,*S*-dioxide groups. This subtle conformational change not only had disrupted the π-conjugation, but also would have an impact on the supramolecular self-assembling behavior of these compounds in the solide state, which will be discussed in the following section.

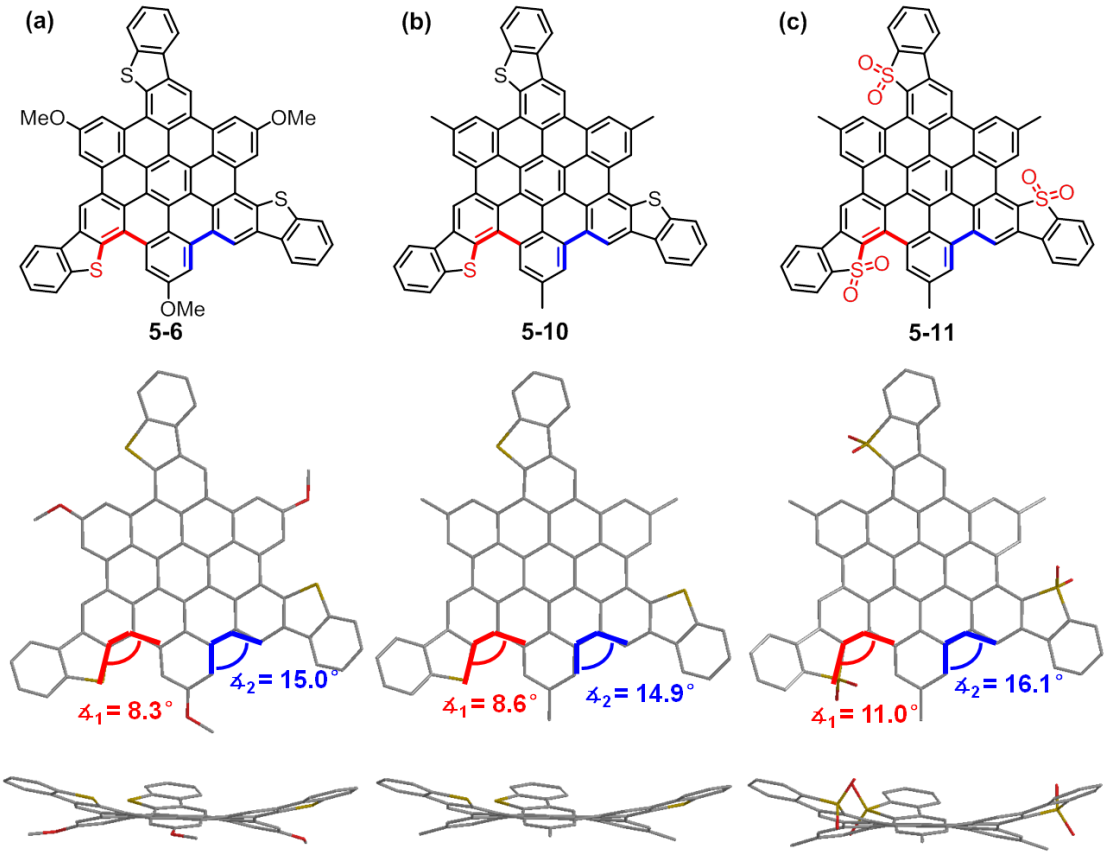

Figure 5-15. Molecular structure and sticks-like models of sulfur-incoporated HBCs TTCs **5-6c** (a), TTC **5-10** (b), and TTOC **5-11** (c) on the basis level of B3LYP/6-31G(d) with the angles $\measuredangle_1$ and $\measuredangle_2$ which are measures of the out-of-plane degree for the peripheral benzothiophene rings.

5.2.4 Bulk property and self-assembling behavior of TTCs and TTOC

For the application of organic semiconductors and fabrication of electronic devices (like OFET, and OLED), the solid-state organization of these organic semiconductors

has a critical impact on the performance of these devices when these molecules are processed from solution into solid-state devices. Therefore, the investigation of their bulk property and self-assembling behaviors is of great significane.

The bulk thermotropic behavior of TTCs **5-6c**, **5-10**, and TTOC **5-11** was investigated by thermogravimetric analysis (TGA) and differential scanning calorimetry (DSC). The TGA measurement exposed a decomposition temperature under inert atmosphere (corresponding to 5% weight lost) of about 423 ℃, 455 ℃ and 422 ℃ for **5-6c**, **5-10**, and **5-11**, respectively. The DSC analyses exhibited no obvious phase transition over the investigated temperature range between 20 ℃ and 300 ℃.

In the attempts to elucidate the supramolecular organization of the varieties of TTCs and its oxadized derivative **5-11**, the 2D-wide angle X-ray scattering (2D-WAXS) patterns of these molecules are measured using their extruded fibers. The 2D-WAXS pattern of extruded fibers for TTC **5-6c** in Figure 5-16 indicates a typical discotic columnar organization, which is observed for a broad range of PAHs in their liquid crystalline phase.[29] In this state, the columns are characteristically arranged in a hexagonal unit cell with a packing parameter of a_{hex} = 2.88 nm, determined based on the positions of the equatorial reflections. This value is consistent with the molecular size of **5-6c**. The position of reflections in the meridional axis of the pattern is attributed to the π-stacking distance of 0.34 nm of the non-tilted disc. After thermal annealing (190 ℃) and subsequent cooling (30 ℃), there is no obvious change of the solid-state organization over wide temperature range.

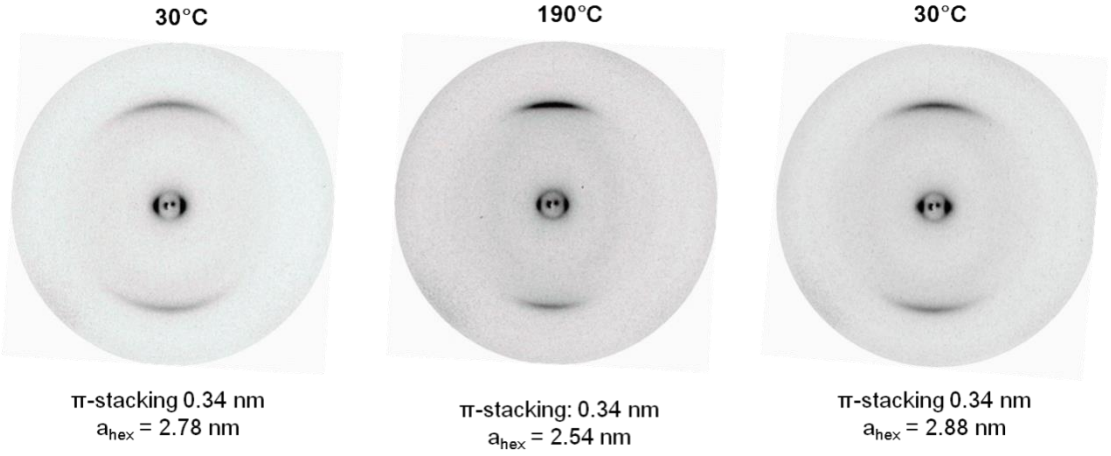

Figure 5-16. 2D-WAXS results of TTCs **5-6c** under different temperature.

For the other four kinds of TTCs **5-6** (**a-e**) decorated with sterically demanding, long, branched alkoxyl chains, the 2D-WAXS measurements (Figure 5-17) indicated identical hexagonal intercolumnar arrangement patterns with the same π-stacking distance of 0.34 nm, which is well consistent with the typical distance for π-π interaction. The formation of these liquid crystallines at ambient temperature can be correlated with the C_3 symmetry of these triangular shaped molecules **5-6** (**a-e**)**,** and the attachment of the relatively flexible alkoxy side chains. [30]

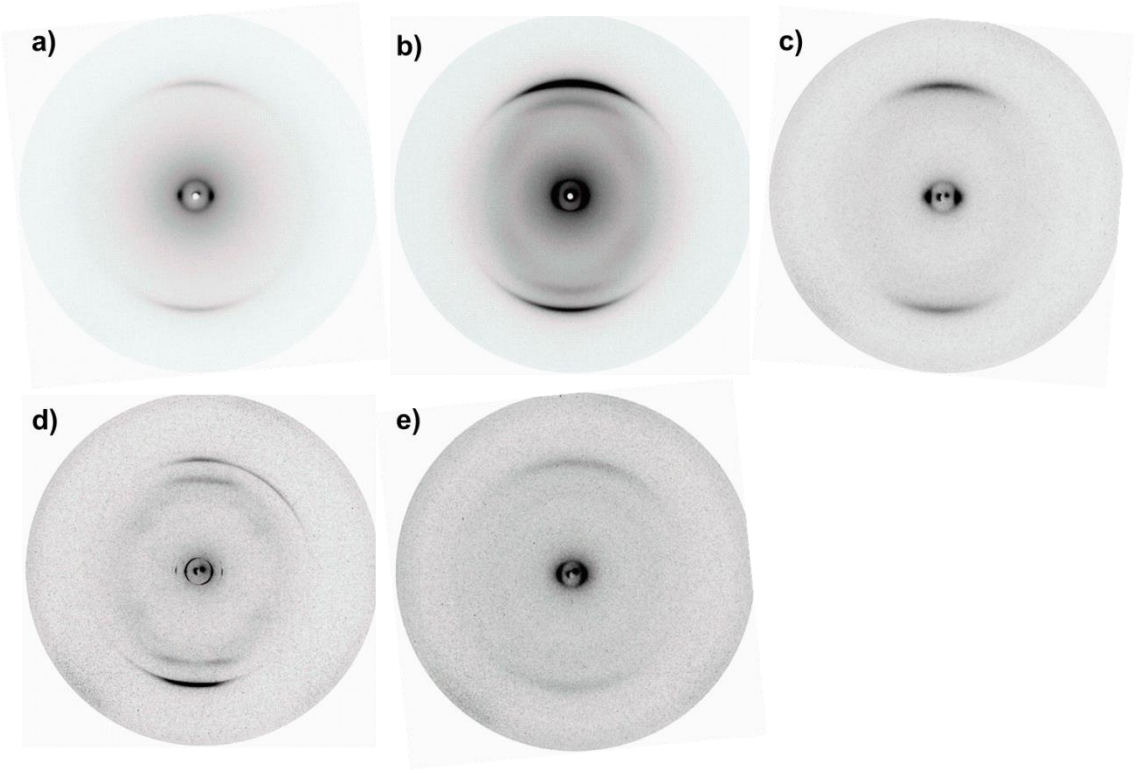

Figure 5-17. 2D-WAXS results of TTCs **5-6**(**a-e**).

Replacing these dodecyloxy substituents by dodecyl chains in **5-10** can obviously strengthen the solid-state supramolecular organization order (Figure 5-18). Although the molecules are also assembled in stacks (with π-stacking distance 0.35 nm, and orthogonal unit cell a = 3.25 nm and b = 1.92 nm), the multiple wide-angle meridional and small-angle off-meridional scattering intensities suggest the formation of a complex organization within the columns (Figure 5-18a). Typically, such scattering patterns are characteristic of helical packing with a relatively long pitch.[31] In the case

of **3-10**, the pitch length of 3.4 nm was derived from the position of the first scattering line (hk1). Taking into account the simple intermolecular distance of 0.35 nm and the C3 symmetry of the molecule, a rotation angle of 12 °between neighboring discs can be concluded (Figure 5-18b). Simulations by Cerius2 suggested a 2D pattern, which are in good agreement with the experimental data, and thus confirme the proposed helical packing model. We assume that the slight helical rotation in the column is triggered by the three out-of-plane benzothiophene units, which are sticking out into the core periphery due to the steric hindrance.

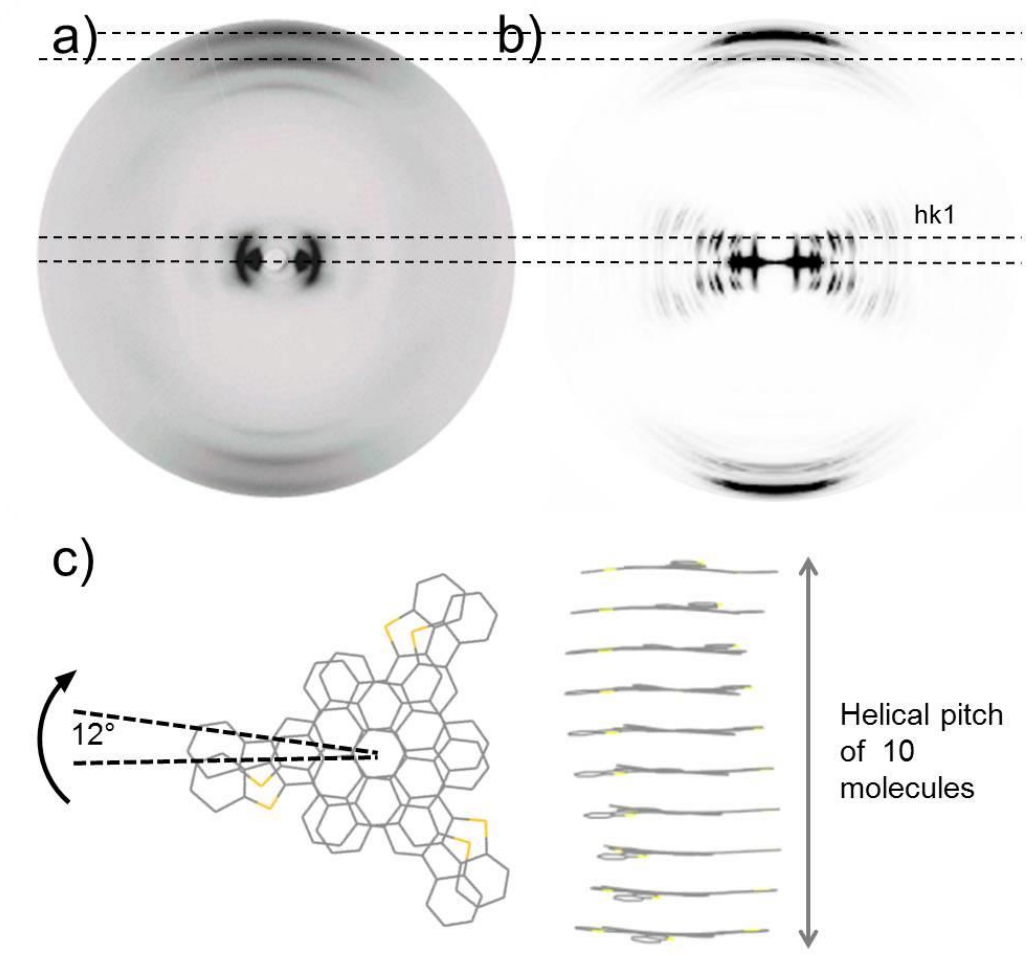

Figure 5-18. a) 2D-WAXS and b) Cerius2 simulation of TTC **5-10**, c) packing model for TTC **5-10** at the top and side view of a column.

At last, the impact of the oxidation on the *S* atoms is also investigated by measuring the 2D-WAXS of the extruded fibers of TTOC **5-11** (Figure 5-19). The recorded

result indicates that the conversion of the benzothiophene moieties for **5-10** into more bulky benzothiophene-*S*,*S*-dioxide units for **5-11** slightly increases the π-stacking distance to 0.36 nm, which can be attributed to the increased dihedral angles between the out-of-plane benzothiophene rings and HBC cores in TTOC **5-11** (Figure 5-15). Meanwhile a liquid crystalline phase identical to that of TTC **5-6c**, but with a cubic intercolumnar arrangement (a = 2.45 nm) as the best fit, was also recorded for TTOC **5-11** after the chemical modification on the benzothiophene units.

Figure 5-19. 2D-WAXS results of TTOC **5-11**.

5.3 Summary

In summary, a variety of benzothiopene π-conjugated HBC derivatives **5-6**(**a-e**) and **5-10** (trisbenzothieno[1,2:7,8:13,14]hexa-peri-hexabenzocoronenes, TTC) substituted with flexible alkyl or alkoxyl chains, were readily synthesized by the *Scholl* reaction of the corresponding oligophenylene precursor. Furthermore, a new HBC derivative conjugated with the strongly electron-withdrawing thiophene-*S,S*-dioxide units **5-11** (trisbenzothieno-*S,S*-dioxide[1,2:7,8:13,14]hexa-*peri*-hexabenzocoronene, TTOC) was synthesized *via* oxidation of thiophene rings in the TTC **5-10**.

The detailed NMR investigation of the TTC **5-10** and its oxidized counterpart TTOC **5-11** verified the successful conversion from the electron-rich thiophene rings to the "electron-poor" thiophene-*S,S*-dioxide units. The remarkable downfield shift of the protons on the HBC cores in TTOC **5-11** confirmed the decreased electorn density on of the HBC cores due to the electron-withdrawing effects of thiophene-*S,S*-dioxide units. The impact of the oxidation of *S* atoms on the electron structure and energy level of TTC derivatives had also been investigated through the UV-Vis and fluorescence spectroscopy, and the cyclic voltammetry measurement. The red-shift of aborbance maxima and emission maxima of TTOC **5-11**, and its reduced oxidation potential in CV meaxurements further supported the decreased energy level.

In order to further elucidate the energy levels of TTCs **5-10** and TTOC **5-11**, the theoretical calculation of the HOMO and LUMO levels of TTC **5-6**(**a-e**), **5-10**, and TTOC **5-11** was conducted on the basis of B3LYP/6-31G(D). Notably, TTOC **5-11** manifested a markedly lowered LUMO level (approximate 0.55 eV) due to the existence of strong "pull" unit thiophene-*S,S*-dioxide, and a parallelly lowered HOMO level (c.a. 0.51 ev). Although the change of band gap is trival, the significantly lowered energy levels suggested that the chemical modification of the thiophene units could effectively modulate the electronic property.

At last, the bulk properties and self-assembling behaviors of TTC derivatives (**5-6** and **5-10**) and TTOC **5-11** were studied by the DSC and 2D-WAXS measurement. The 2D-WAXS results indicated that a unique helical packing in bulk with a relatively long pitch (3.4 nm), while the 2D-WAXS results of TTC **5-6** and TTOC **5-11** showed distinctive patterns in comparison with that of TTC **5-10**.

In conclusion, this chapter has reported a strategy of incorporating thiophene units into the PAH frameworks and subsequent oxidation on *S*-atoms for developing new nanographene derivatives with tunable electronic properties.

Reference

[1] L. Chen, Y. Hernandez, X. Feng, K. Müllen, *Angew. Chem. Int. Ed.* **2012**, *51*, 7640.

[2] W. Pisula, X. Feng, K. Müllen, *Chem. Mater.* **2011**, *23*, 554.

[3] W. Pisula, X. Feng, K. Müllen, *Adv. Mater.* **2010**, *22*, 3634.

[4] F. J. M. Hoeben, P. Jonkheijm, E. W. Meijer, A. P. H. J. Schenning, *Chem. Rev.* **2005**, *105*, 1491.

[5] T. Aida, E. W. Meijer, S. I. Stupp, *Science* **2012**, *335*, 813.

[6] S. S. Babu, S. Prasanthkumar, A. Ajayaghosh, *Angew. Chem. Int. Ed.* **2012**, *51*, 1766.

[7] C-Y. Chiu, B. Kim, A. A. Gorodetsky, W. Sattler, S. Wei, A. Sattler, M. Steigerwald, C. Nuckolls, *Chem. Sci.* **2011**, *2*, 1480.

[8] L. Zöphel, V. Enkelmann, R. Rieger, K. Müllen, *Org. Lett.* **2011**, *13*, 4506.

[9] L. Chen, S. R. Puniredd, Y-Z. Tan, M. Baumgarten, U. Zschieschang, V. Enkelmann, W. Pisula, X. Feng, H. Klauk, K. Müllen, *J. Am. Chem. Soc.* **2012**, *134*, 17869.

[10] A. A. Gorodetsky, C-Y. Chiu, T. Schiros, M. Palma, M. Cox, Z. Jia, W. Sattler, I. Kymissis, M. Steigerwald, C. Nuckolls, *Angew. Chem. Int. Ed.* **2010**, *49*, 7909.

[11] W. Jiang, Y. Zhou, H. Geng, S. Jiang, S. Yan, W. Hu, Z. Wang, Z. Shuai, J. Pei, *J. Am. Chem. Soc.* **2011**, *133*, 1.

[12] C. Wang, H. Dong, W. Hu, Y. Liu, D. Zhu, *Chem. Rev.* **2011**, *112*, 2208.

[13] X. Feng, J. Wu, M. Ai, W. Pisula, L. Zhi, J. P. Rabe, K. Müllen, *Angew. Chem. Int. Ed.*

2007, *46*, 3033.

[14] K. C. Moss, K. N. Bourdakos, V. Bhalla, K. T. Kamtekar, M. R. Bryce, M. A. Fox, H. L. Vaughan, F. B. Dias, A. P. Monkman, *J. Org. Chem.* **2010**, *75*, 6771.

[15] E. Tedesco, F. D. Sala, L. Favaretto, G. Barbarella, D. Albesa-Jové, D. Pisignano, G. Gigli, R. Cingolani, K. D. M. Harris, *J. Am. Chem. Soc.* **2003**, *125*, 12277.

[16] S. Wei, J. Xia, E. J. Dell, Y. Jiang, R. Song, H. Lee, P. Rodenbough, A. L. Briseno, L. M. Campos, *Angew. Chem. Int. Ed.* **2014**, *53*, 1832.

[17] H. A. M.van Mullekom, J. A. J. M. Vekemans, E. E. Havinga, E. W. Meijer, *Mater. Sci. Eng., R* **2001**, *32*, 1.

[18] L. Pandey, C. Risko, J. E. Norton, J. L. Brédas, *Macromolecules* **2012**, *45*, 6405.

[19] E. Busby, J. Xia, J. Z. Low, Q. Wu, J. Hoy, L. M. Campos, M. Y. Sfeir, *J. Phys. Chem. B* **2015**, 119,7644

[20] J. Luo, Y. Zhou, Z-Q. Niu, Q-F. Zhou, Y. Ma, J. Pei, *J. Am. Chem. Soc.* **2007**, *129*, 11314.

[21] E. J. Dell, L. M. Campos, *J. Mater. Chem.*, **2012**, *22*, 12945.

[22] Y. Yang, J. Liang, L. Hu, B. Zhang, W. Yang, *New J. Chem.*, **2015**, *39*, 6513.

[23] E. Clar, *Polycyclic Hydrocarbons*; Academic Press and Springer-Verlag: London, 1964; Vols. I+II

[24] J. C. Fetzer, *Large (C>)24) Polycyclic Aromatic Hydrocarbons*; John Wiley & Sons: New York, 2000..

[25] R. Riegera, K. Müllen, *J. Phys. Org. Chem.* **2010**, *23*, 315.

[26] M. Kastler, J. Schmidt, W. Pisula, D. Sebastiani, K. Müllen, *J. Am. Chem. Soc.* **2006**, *128*, 9526.

[27] Gaussian 09, Revision D.01, M. J. Frisch, G. W. Trucks, H. B. Schlegel, G. E. Scuseria, M. A. Robb, J. R. Cheeseman, G. Scalmani, V. Barone, B. Mennucci, G. A. Petersson, H. Nakatsuji, M. Caricato, X. Li, H. P. Hratchian, A. F. Izmaylov, J. Bloino, G. Zheng, J. L. Sonnenberg, M. Hada, M. Ehara, K. Toyota, R. Fukuda, J. Hasegawa, M. Ishida, T. Nakajima, Y. Honda, O. Kitao, H. Nakai, T. Vreven, J. A. Montgomery, Jr., J. E. Peralta, F. Ogliaro, M. Bearpark, J. J. Heyd, E. Brothers, K. N. Kudin, V. N. Staroverov, T. Keith, R. Kobayashi, J. Normand, K. Raghavachari, A. Rendell, J. C. Burant, S. S. Iyengar, J. Tomasi, M. Cossi, N. Rega, J. M. Millam, M. Klene, J. E. Knox, J. B. Cross, V. Bakken, C. Adamo,

J. Jaramillo, R. Gomperts, R. E. Stratmann, O. Yazyev, A. J. Austin, R. Cammi, C. Pomelli, J. W. Ochterski, R. L. Martin, K. Morokuma, V. G. Zakrzewski, G. A. Voth, P. Salvador, J. J. Dannenberg, S. Dapprich, A. D. Daniels, O. Farkas, J. B. Foresman, J. V. Ortiz, J. Cioslowski, and D. J. Fox, Gaussian, Inc., Wallingford CT, 2013.

[28]. S. Wei, J. Xia, E. J. Dell, Y. Jiang, R. Song, H. Lee, P. Rodenbough, A. L. Briseno, L. M. Campos, *Angew. Chem. Int. Ed.* **2014**, *53*, 1832.

[29] X. Feng, W. Pisula, K. Müllen, *Pure Appl. Chem.* **2009**, *81*, 2203.

[30] X. Feng, M. Liu, W. Pisula, M. Takase, J. Li, K. Müllen, *Adv. Mater.* **2008**, *20*, 2684.

[31] J. Shu, D. Dudenko, M. Esmaeili, J. H. Park, S. R. Puniredd, J. Y. Chang, D. W. Breiby, W. Pisula, M. R. Hansen, *J. Am. Chem. Soc.* **2013**, *135*, 11075.

6. Synthesis of molecular building blocks for bottom-up fabrication of graphene nanoribbon

6.1 Introduction

Due to its zero band-gap, the potential of graphene for electronic applications is severely undermined. Fabrication of graphene nanoribbons (GNRs) appears to be a feasible and promising route for opening a controllable band gap in graphene films, which is strongly dependent on the ribbon width. Herein, a new approach for the fabrication of GNRs is proposed by our colleagues, which is the research subject of UPGRADE project (bottom-UP blueprinting GRAphene baseD Electronics). This approach consists of two steps. (Figure 6-1) Firstly, the molecular building blocks (MBBs) bearing directing units are self-assembling to achieve a controlled and ordered physisorption on graphene. Secondly, the preorganized MBBs are covalently bonded to the graphene surface by *in-situ* activation (by either light , current or temperature) of the chemically reactive sites of the MBBs, which will convert the sp^2 carbons of graphene to sp^3 defects, and thus open an atomically precise band gap and generate semiconducting domains for electronic devices.

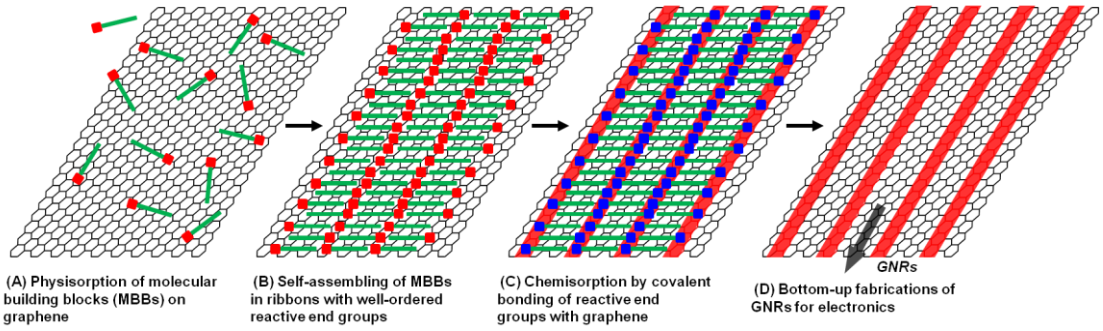

Figure 6-1. Schematic representation of graphene nanoribbons (GNRs) fabrication by alkanes self-assembling at solid-liquid interface and controllable chemical modification on graphene.

In this approach, chemical modification on the basal plane of the pristine graphene materials is the prerequisite for generation of defects. However, the most commonly

utilized reactions for graphene functionalization are the amide or ester formation on the edge structure of the carbon sheet,[1] and C-C bond formation *via* radical attack.[2,3] However, these dominating modification approaches mostly happens at the more reactive "edge-structure" on graphene, or located at the peripheral oxo-groups[4] (such as carboxyl and hydroxyl groups on the edge of graphite) for amide/ester formation. This leaves the major and relatively inert "basal plane" regions of the graphene untouched. Among these methods, the radical attacking generated from the decomposition of phenyldiazonium salt,[5] is the most viable approach for the covalent functionalization on the inert basal plane of graphitic materials. In this context, another two new types of modifier are also chosen for this purpose, according to the wall modification of CNTs by [2+1] pericyclic cycloadditions with nitrene or carbene intermediates, which can be generated from azide and diazirine derivatives (Figure 6-2). [6,7,8]

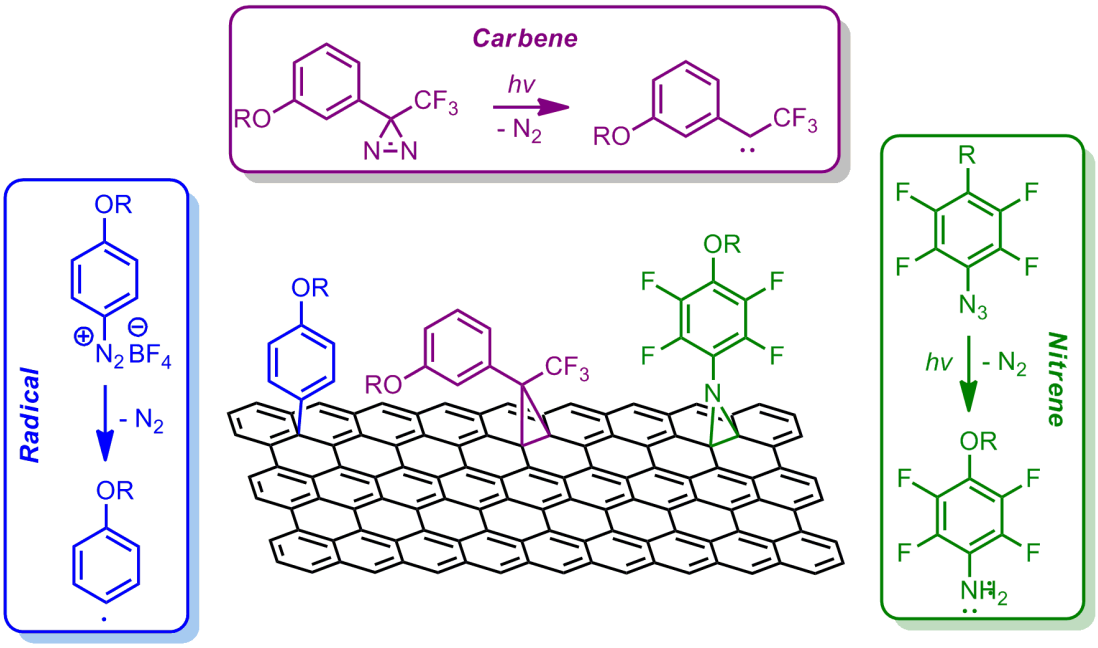

Figure 6-2. Schematic illustration for three different chemical reactions for the "basal-plane" modification on pristine graphene.

However, for the chemical modification methods described above, they all have the major flaws of random distribution of the reacting sites and thus surpressing the electronic conducting of graphene. To surmount this problem, one promissing solution

is to improve the efficiency of the chemical modification by spatially controlling the generation of defects on the graphite, as depicted in the UPGRADE approach (Figure 6-1). Therefore, the attachment of long and linear alkyl chains onto the reactive moieties is suggested to realize the well-ordered organization of MBBs on graphene surface.[9,10,11]

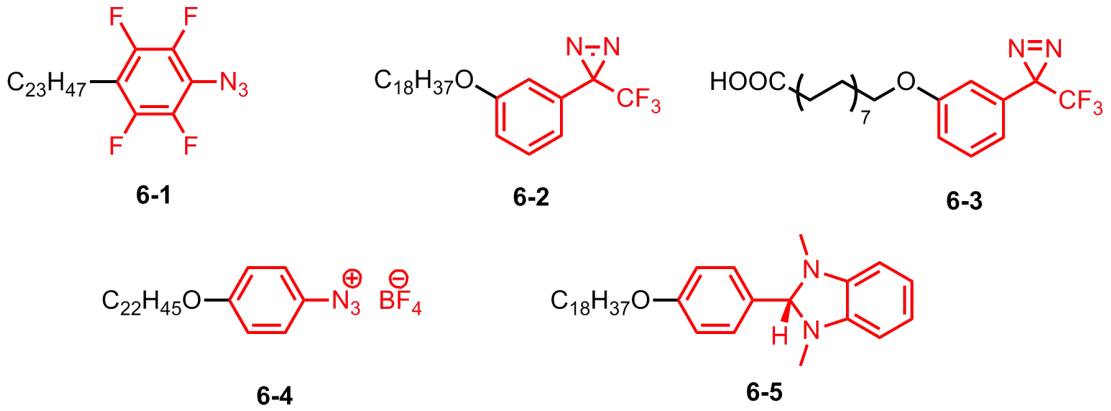

Scheme 6-1. Proposed molecular building blocks (MBBs) for GNR engineering, red part indicated the reactive moieties toward graphene network.

To fulfill these requirements for MBBs design, we had proposed and synthesized five different MBBs in this chapter following the protocol described above (Scheme 6-1). All these MBBs are composed of a long alkyl chain for self-assembling monolayer formation on graphene, and a reactive head (azide in **6-1**, diazirine in **6-2**/**6-3**, phenyldiazonium in **6-4**, organic dopant in **6-5**) for defects generation.

6.2 Results and discussions

6.2.1 Synthesis of MBBs with lazide reactive group

The phenylazide and its derivatives have been widely utilized as the photoaffinity labeling agents in biochemistry for a long time because of their high reaction efficiency, fast kinetics, and ease of preparation. [12,13,14] Upon light irradiation, the azide unit will decompose by releasing a molecule of nitrogen to yield the singlet phenylnitrene, which is an extremely reactive intermediate capable of undergoing numerous reactions (Figure 6-3). According to the mechanism,[15,16] the singlet

phenylnitrene can expand to the corresponding seven-membered ketenimine (path i in Figure 6-3), or relax *via* intersystem crossing to the triplet phenylnitrene for bimolcular homocoupling (path iii in Figure 6-3). However, the second route (path ii in Figure 6-3) appears to be the most interesting reaction in modification of carbon materials, namely the CH or NH insertion, and C=C [2+1] cycloaddition reactions. After introducing fluoride atoms on the aromatic ring, the ring expansion (path i) of the initially liberated phenylnitrene intermediate can be extremely suppressed, and thus the yield of insertion/addition reaction (path iii) will be greatly enhanced. Therefore, perfluorophenylazide had been widely utilized in the chemical functionalization of carbons materials.[17,18,19] In this section, a perfluorophenylazide **6-1** substituted with long alkyl chains (-$C_{23}H_{47}$) is synthesized to realize the controllable functionalization of graphene (Scheme 6-2).

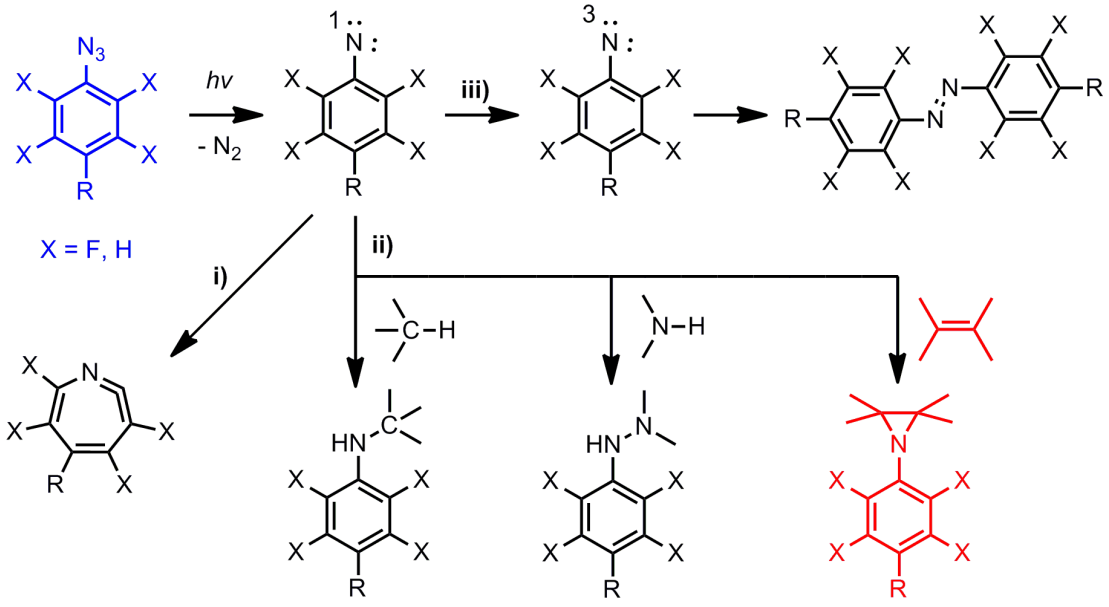

Figure 6-3. Schematic illustration of phenylazide photochemistry: (i) ring expansion, (ii) insertion and addition reactions, and (iii) intersystem crossing.

To introducing a long alkyl chain onto the perfluorophenylazide unit, tricos-1-yne **6-8** ($C_{23}H_{44}$) was first synthesized *via Seyferth-Gilbert* homologation reaction on docosanal **6-7** which can be readily obtained by the direct oxidation of docosan-1-ol. Then the *Yamamoto* coupling between tricos-1-yne **6-8** and pefluoroiodobenzene

could yield the desired 1,2,3,4,5-pentafluoro-6-(tricos-1-yn-1-yl)benzene **6-9**, which can be converted to 1,2,3,4,5-pentafluoro-6-tricosylbenzene **6-10** via hydrogenation in autoclave under H_2 gas. At last, the targeted molecular **6-1** was obtained as a colorless solid by refluxing the mixture of sodium azide with **6-10** in DMF after the addition of catalytic amount of tetrabutylammonium azide.[20] In summary, the desired MBB 1-azido-2,3,5,6-tetrafluoro-4-tricosylbenzene **6-1** can be obtained with the yield of 12% over 5 steps.

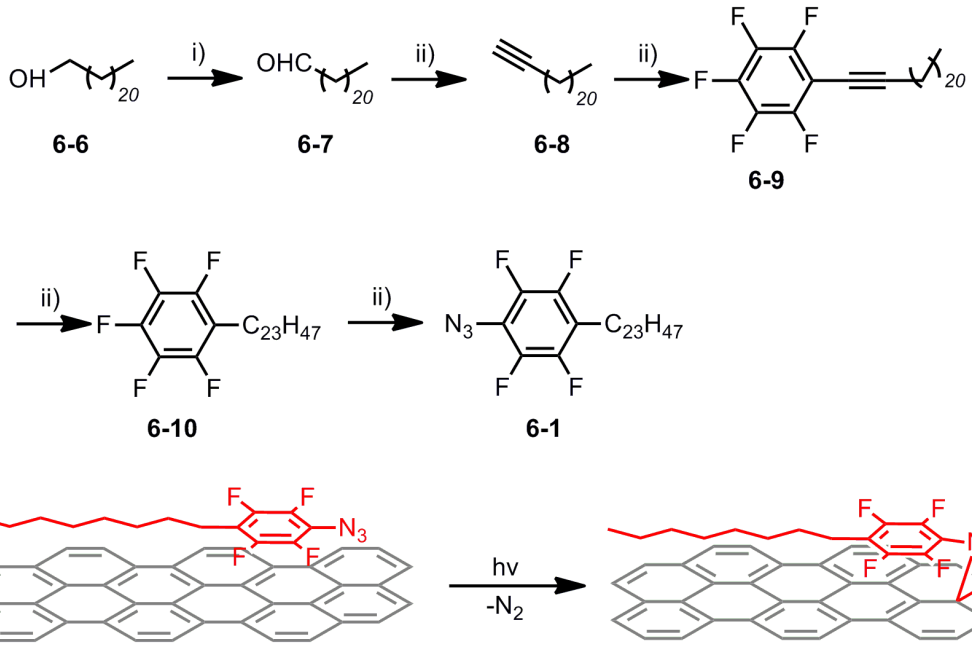

Scheme 6-2. Synthetic routes toward *p*-tricosyl perfluorophenyl azide **6-1**. Conditions: i) SO_3-pyridine complex, *i*Pr_2NEt, DMSO/DCM, from 0 ℃ to RT, 68%; ii) dimethyl (1-diazo-2-oxopropyl)phosphonate, K_2CO_3, MeOH, RT, 78%; iii) perfluoroiodobenzene, $Pd(PPh_3)_2Cl_2$, CuI, Diisopropylamine, THF, RT, 60%; iv) Pd/C (10 wt%), H_2 (10 bar), EtOAc, RT, 100%; v) *t*-Bu_4N N_3, NaN_3, DMF, 40 ℃, 39%.

The chemical identity of the MBB **6-1** was then confirmed by the NMR and FD MS spectra. The FD-MS spectrum of **6-1** clearly indicated one single peak around *m/z* = 513.2, which is consistent with its molar mass of 513.7 g/mol. To further check the purity of the MBB **6-1**, the ^{19}F NMR was utilized to investigate the ^{19}F signals of the precursor **6-10** and MBB **6-1** (Figure 6-4). The result unambiguously indicated that the signal corresponding to the F_c (δ = -163.2 ppm) at *para*- position had completely

disappeared in the ^{19}F NMR of MBB **6-1** in comparison with that of precursor **6-10**. The signals of another F_b at the *meta*- position had up-field shifted from -158.5 ppm in **6-10** to -152.9 ppm in **6-1** after the substitutions due to the deshielding effect of adjacent azido group.

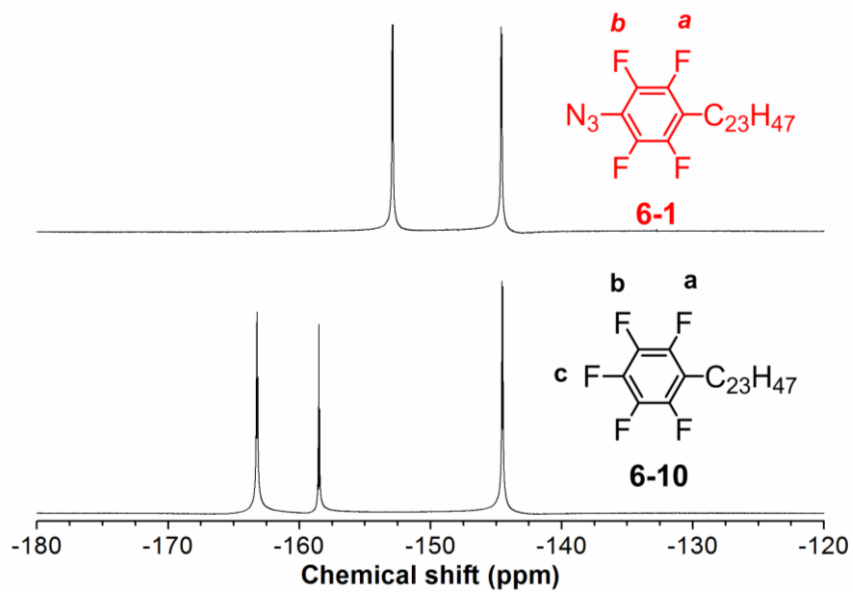

Figure 6-4. ^{19}F NMR spectrum of *p*-tricosyl perfluorophenyl azide **6-1** in $CDCl_3$.

Then, the optical properties of MBB **6-1** were investigated by measuring the UV-Vis absorption spectrum in THF at the concentration of 1.0×10^{-5} M (Figure 6-5). The absorption maximum was determined to be 256 nm, which was well consistent with the absorption band of the tetrafluorophenylazide chromophore reported in previous literature.[24]

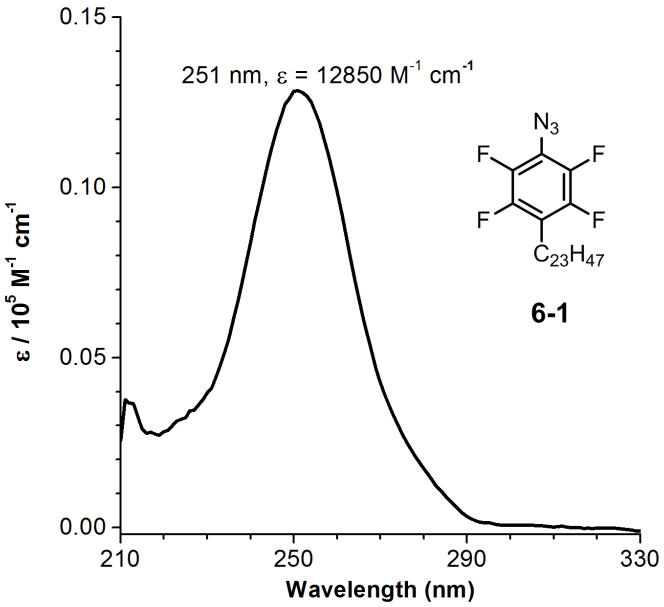

Figure 6-5. UV-Vis spectrum of *p*-tricosyl perfluorophenyl azide **6-1** (1.0×10^{-5} M in THF).

At last, to fulfill the aim of well-ordered organization of the compound on the graphene surface, the scanning tunneling microscopy technique was applied to investigate the self-assembling monolayer (SAM) formation of MBB **6-1** at the interface of 1-nonanoic acid/HOPG. The STM images suggested that the functional heads (perfluorophenyl azide group) of **6-1** lay closely to each other with a "head-to-tail" alignment and the alkyl chains forming an interdigitated structure, exhibiting a unit cell: a = (1.13 ± 0.2) nm, b = (3.41 ± 0.2) nm, α = (90 ± 2)° leading to an area A = (3.85 ± 0.71) nm^2, with each unit cell containing one molecule (Figure 6-6). Four perfluorophenyl azide head was located at the four vertices of each rectangle.

In order to check the possibility of transforming SAM covered graphene into GNRs, the Raman spectra and electronic device of the graphene with spin-coated thin films of MBB **6-1** after photoirradiation were investigated in the group of our colleagues at the University of Strassbourg. However, the result suggested extremely low reactivity of the physisorbed MBB **6-1** on graphene, although the reactive heads were well-aligned in the SAM layer as anticipated.

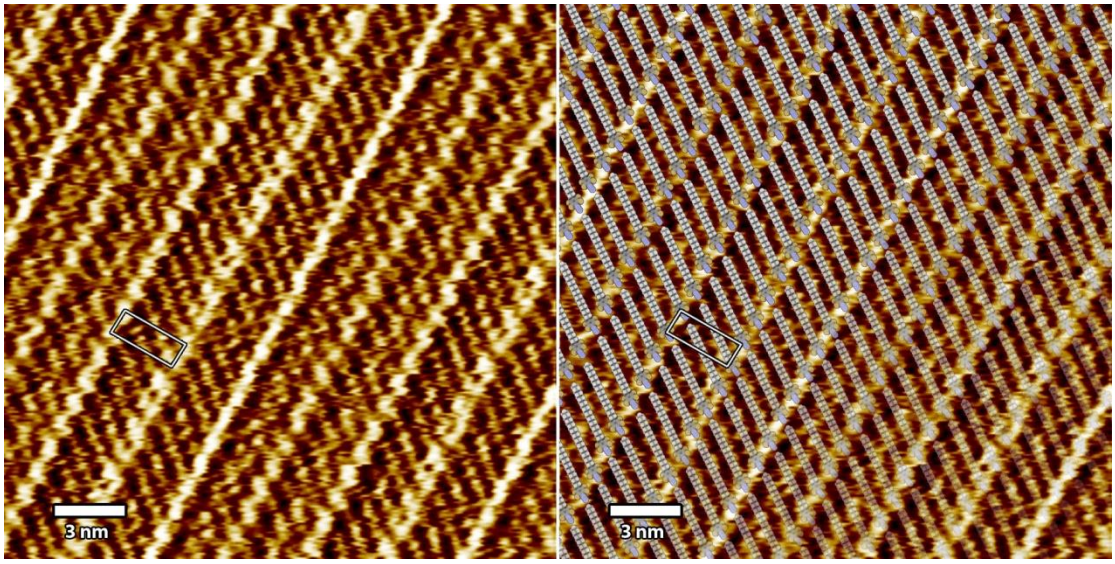

Figure 6-6. STM images of a self-assembled monolayer of p-tricosyl perfluorophenyl azide **6-1** at the interface of 1-nonanoic acid/HOPG. The Unit cell parameters: a = (1.13 ± 0.2) nm, b = (3.41 ± 0.2) nm, α = (90 ± 2) °, A = (3.85 ± 0.71) nm ².

This low reactivity is probably due to the pointing-out orientation of the reactive azido group with the graphene surface, and the difficulty of the physisorbed nitrene intermediates to approach the C=C bond on the graphene surface. Therefore, lots of works are still in demand on modulating the structure of MBBs bearing azide moieties, for example altering the *para*-substituted perfluorophenylazide to *meta*-substituted analogue. In addition, searching for photoreactive agents with appropriate substitution and suitable orientation on grapheme appears to be another promising solution, which will be discussed in the next section.

6.2.2 Synthesis and investigation of molecules with diazirine reactive group

For the perfluorophenylazide-based MBB **6-1** studied above, the *para*-substituted alkyl chain regarding to reactive azide unit has locked an unsuitable orientation for in-situ chemical modification. To solve this problem, another photoaffinity agent with *meta*-substituted reactive sites, named 3-aryl-3-(trifluoromethyl)diazirine, is chosen in this section.

Featured as the strained three-membered heterocyclic ring containing an azo group

bonded with a sp^3-hybridized carbon atom, diazirines can readily form extremely reactive carbene species by liberating N_2 upon exposure to the exterior stimulus such as light irradiation and heating. The formed carbene is capable to undergo a [2+1] cycloaddition with C=C bonds, such as the sidewall region and edge-plane end region of CNTs, and other targeted structure as a photoaffinity labeling agent. [21,22,23] Due to the highly strain of the three-membered ring, normal diazirines are quite reactive and unstable. Therefore, a wide variety of diazirine derivatives have be developed to render them the chemical stability under a broad range of reaction conditions. Among them, the derivatives based on 3-aryl-3-(trifluoromethyl)diazirines are the most promissing families which prove to be stable under room temperature and are capable of producing carbenes after phtolysis,[24,25] which have been used as a functional modifier on CNT and glassy carbons in a previous report.[26]

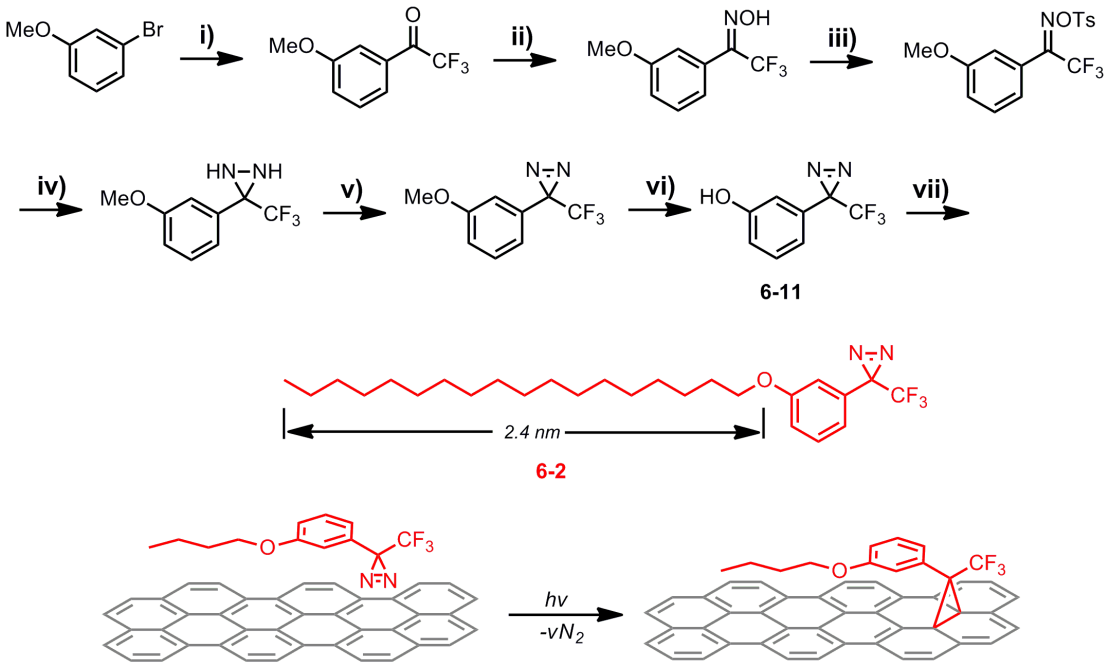

Scheme 6-3. Synthetic routes toward the molecular building block **6-2** diazirine derivative substitued with long alkoxyl chain. Conditions were as follows: i) *n*-BuLi, Et_2NCOCF_3, THF, -78 ℃, 3 h; ii) NH_2OH-HCl, EtOH, 70 ℃, 4 h; iii) TsCl, NEt_3, DMAP, DCM, RT, 24 h; iv) NH3, DCM, -78 ℃, 12 h; v) Ag_2O, Et_2O, RT, 20 h; vi) BBr_3, DCM, RT, 12 h; vii)C18H37Br, K_2CO_3, Acetone, 60 ℃, 12h, 65%.

To realize the well-ordered SAM formation for the diazirine derivatives on the

graphene substrate, a diazirine derivative **6-2** substituted with long and linear alkoxyl chain ($C_{18}H_{37}$-) was designed. The synthesis of MBB **6-2** was based on a previously reported compound 3-(trifluoromethyl)-3-(3-hydroxyphenyl)diazirine (**6-11**)[27] by S_N2 substitution reaction with 1-bromooctadecane. The synthesis of diazirine precursor (**6-11**) was exactly following the reported literature over 6 steps with the overall yield around 40% (Scheme 6-4). ^{1}H NMR spectrum of **6-2** clearly validated the existence of diazirine group, and its chemical identity was also confirmed by the FD-MS spectrum.

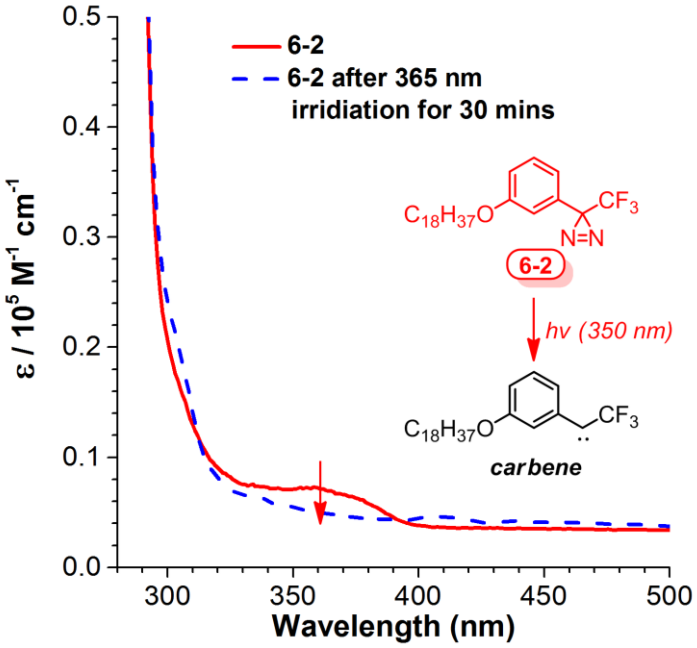

Figure 6-7. UV-Vis spectra of the solution of the diazirine derivative **6-2** in THF (1.0×10^{-5} M) before and after UV irridation.

UV-Vis spectroscopy of the diazirine derivative **6-2** suggested the presence of an absorption peak around 356 nm (Figure 6-7), which was indicative of the presence of the diazirine unit corresponding to π-to-π* transitions in the *azo* moiety of the diazirine molecule. After irradiating the solution of MBB **6-2** in THF at ambient condition with UV light for 30 minutes, the characteristic absorption peak of diazirine obviously disappeared, which indicated the photolysis of MBB **6-2** by releasing a nitrogen gas and generating a reactive carbene intermediate.

In order to study the potential of this diazirine derivative **6-2** for GNR engineering,

the SAM of MBB **6-2** on HOPG and CVD graphene was investigated by STM. Driven by the *van der Waals* force between the neighboring alkyl chains, these alkane derivatives were physisorbed on graphite surface and form a well-defined crystalline lamellar structure. The STM images of diazirine molecule **6-2** revealed that the reactive diazirine heads lay close to each other with a "head-to-head" arrangement, and the alkyl substitutions ($C_{18}H_{37}$) were adsorbed on the surface with a parallel conformation by forming an interdigitated structure. These results exhibited a unit cell: a = (0.9 ± 0.1) nm, b = (3.8 ± 0.1) nm, α = (84 ± 2)°, A = (3.4 ± 0.1) nm^2, and each unit cell contained two molecules (Figure 6-8). On the basis of the STM observations, the angle between the molecular axis and direction of the lamella alignment was quite close to 90 °, which could be attributed to the maximized van der Waals force between adjacent alkyl chains for largest contact area. These results directly validated the existence of well-ordered alignment of the reactive units on the graphene surface, which was a prerequisite for the controllable defect generation of graphene..

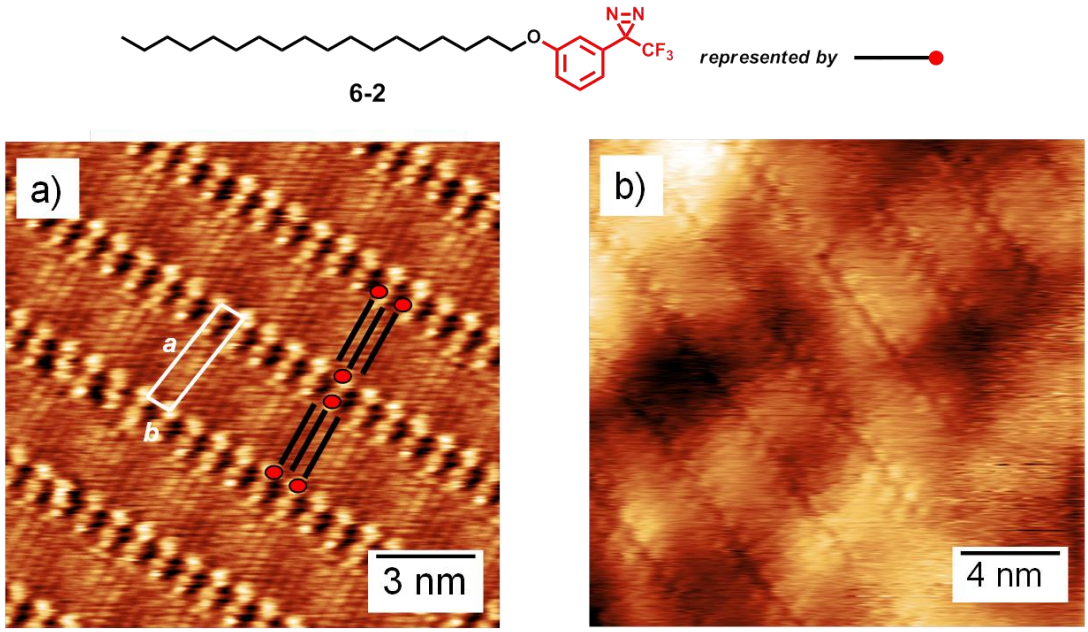

Figure 6-8. STM images of SAMs of the diazirine derivative **6-2** on HOPG (a), and on CVD graphene on SiO_2 (b).

To obtain well-ordered defect, the reaction between diazirine derivative **6-2** and graphene materials had also been studied, in which Raman spectroscopy was utilized

to monitor the appearance of the defects after chemical modification. The solution of MBB **6-2** in anhydrous chloroform was spin-coated on the monolayer CVD graphene substrate, then the thin film was irradiated with UV-light. Raman spectroscopy was used to confirm the reactivity of diazirine toward the basal plane of graphene. The Raman spectrum of pristine CVD graphene clearly revealed the presence of the G-peak (~1580 cm^{-1}), and the absence of the D-peak (~1350 cm^{-1}). This result directly suggested the defect-free structure of the pristine CVD-graphene before photochemical modification. After photo-irradiating the film of **6-2** on CVD graphene for 30 minutes, two new shoulder peaks (~1268 cm^{-1}, and ~1335 cm^{-1}) appeared which could be attributed to the expected chemical modification and sp^3-defect formation on graphene (Figure 6-9).

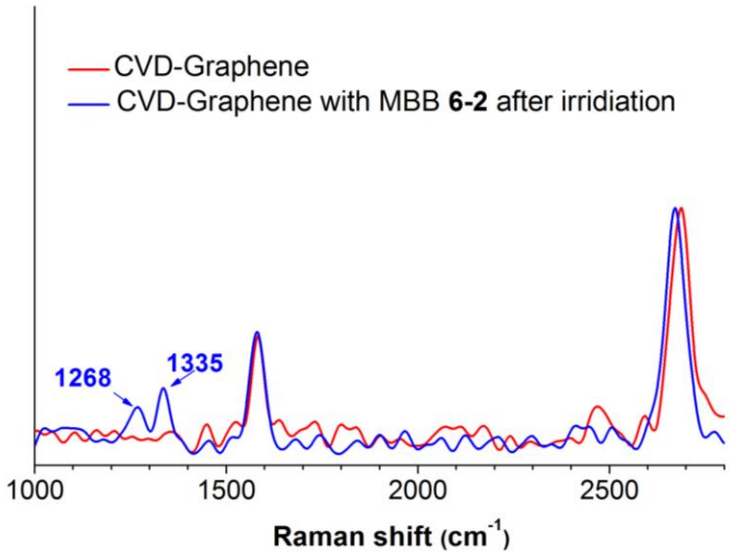

Figure 6-9. Raman spectra of CVD graphene and CVD graphene modified with diazirine **6-2** after UV irradiation.

In order to check the wet chemistry between MBB **6-2** and graphene, we also investigated the chemical modification of MBB **6-2** on the electrochemically exfoliated graphene (EEGs), which could be dispersed in solvents. The high quality EEGs were prepared by our colleague by organic radical-assisted electrochemical exfoliation of graphite.[28]

Firstly, 10 mg EEGs were suspended in 10 mL solution of MMB **6-2** in anhydrous

and degassed DMF (2.5 mg/mL), then the EEGs were collected *via* filtration after irradiating the mixture in a UV reactor (360 nm) for 24 hours. The Raman spectra of the pristine EEGs, EEGs after UV irradiation, and EEGs after photochemical modification with MBB **6-2** were measured respectively, in which the ratio (I_D/I_G) of the intensity of D peak (I_D) to that of G peak (I_G) was applied as a measure for the degree of defects on the carbon materials. However, the I_D/I_G values remained nearly the same even after photochemical modification with **6-2** for 24 fours, which suggested a low reactivity of diazirine **6-2** toward the inert "basal-plane". Therefore, the reactivity of these MBBs still required to be enhanced in the future works for fulfilling the goal of well-patterned defect generation.

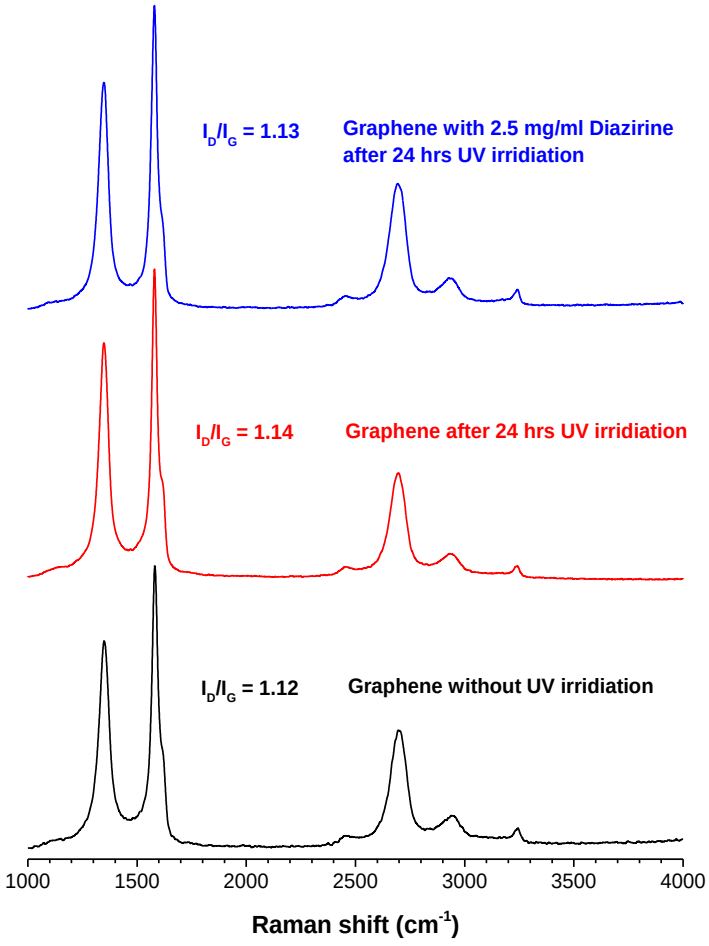

Figure 6-10. Raman spectra of electrochemical exfoliated graphene (EEGs), and EEGs modified with diazirine 6-2 after UV irradiation.

Suggested by the STM images of **6-2** on graphene, the "head-to-head" arrangement of

6-2 had determined in advance the distribution pattern of the anticipated defects on the modified graphene surface. In an attempt to further modulate the distribution and density of the generated defects, a new diazirine derivative **6-3** substituted with long and linear alkyl chain and terminated with carboxylic acid group, which could form dimer via hydrogen bonding, was proposed and synthesized.

The synthesis routes toward **6-3** started from the same precursor **6-11**, which was then substituted with methyl 16-bromohexadecanoate to produce the diazirine compound with a terminal ester group (**6-12**). Then the desired compound **6-3** could be readily obtained by the hydrolysis of ester **6-12** in the mixture of methanol and aqueous solution of NaOH at elevated temperature in quantitative yield, which was confirmed by the disappearing of the Me group on the ^{1}H NMR spectrum of **6-3**.

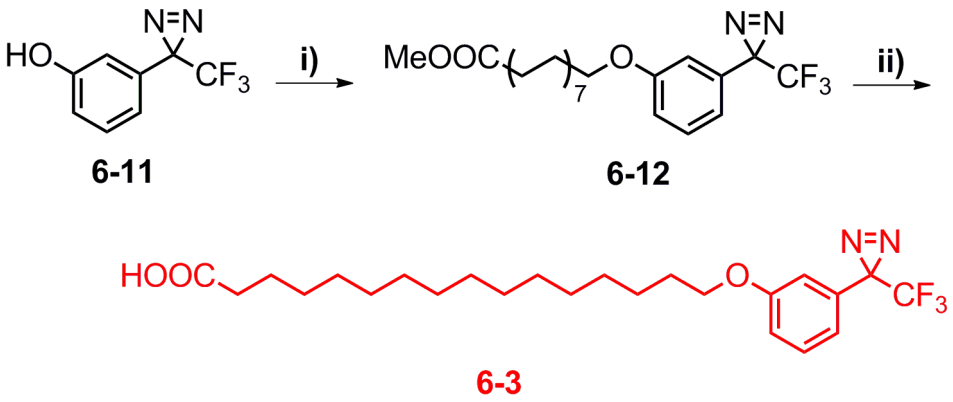

Scheme 6-4. Synthetic routes toward diazirine derivative **6-3** substituted with long alkoxyl chain with terminal carboxylic acid group. Conditions: i) Methyl 16-bromohexadecanoate, K_2CO_3, Acetone, 60 ℃, 12h, 65%; ii) NaOH, MeOH/H_2O, 50 ℃, 4h, 98%.

During the photochemical grafting of MBB **6-2** on the graphene, the generated reactive carbene species from the photolysis of **6-2** might undergo side reaction with the solvent (for example chloroform, methanol, or residual water) to yield some by-products. Therefore, one structural analogue **6-14** was also synthesized to as a model compound for the photolysis of **6-2** in presence of waer. (Scheme 6-5).

In conclusion, similar to the described perfluorophenelazide based MBB **6-1**, MBB **6-2** with diazirine also suffered from low reactivity toward the inert graphene surface and undesired side reaction with solvents.[29] Hence, searching for more reactive

groups was still required to fulfill the goal of controllable chemical modification on graphene and bottom-up fabrication of GNRs.

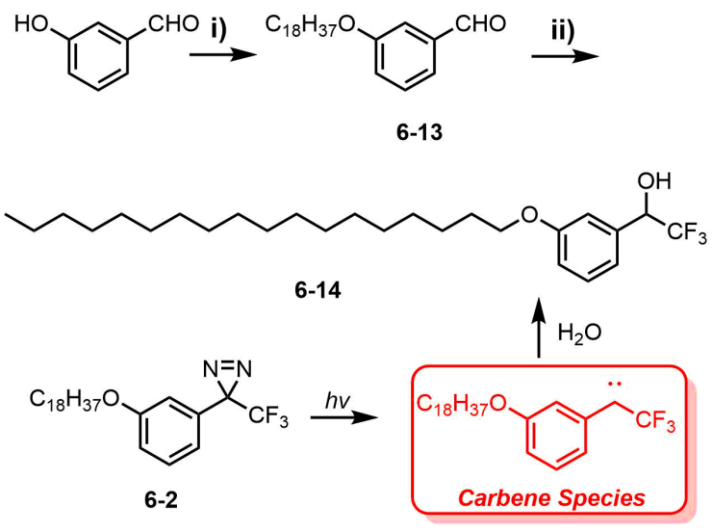

Scheme 6-5. Synthetic routes toward the analogue **6-14** of diazirine. Conditions: i) $C_{18}H_{37}Br$, K_2CO_3, Acetone, 60 ℃, 89%; ii) (a)$TMSCF_3$, K_2CO_3, DMF, RT, 12h (b) HCl(1.0 M, aqu), RT, 1h, 85%;

6.2.3 Synthesis and study of MBBs with diazonium reactive group

Among functionalization methods of graphene described above, precise control of the chemical modification (like the density and spatial order of the defect sites) is relatively difficult to be accomplished due to the long reaction time up to several hours and high heating temperature. Although the heating issues can be solved by the attachment of the light-sensitive perfluorophenylazide and diazirine units which can be trigged and controlled by the UV-irradiation, the extremely low reactivity hinders the effective modification on graphene which is supported by the Raman investigation presented above. By contrast, the electrochemical grafting using the aryl diazonium salt is well-known as a powerful approach for graphene functionalization due to its high reactivity, and the whole grafting process can also be precisely controlled by applying an electronic bias in the electrochemical cell to trigger the generation of reactive radical species. [30,31]

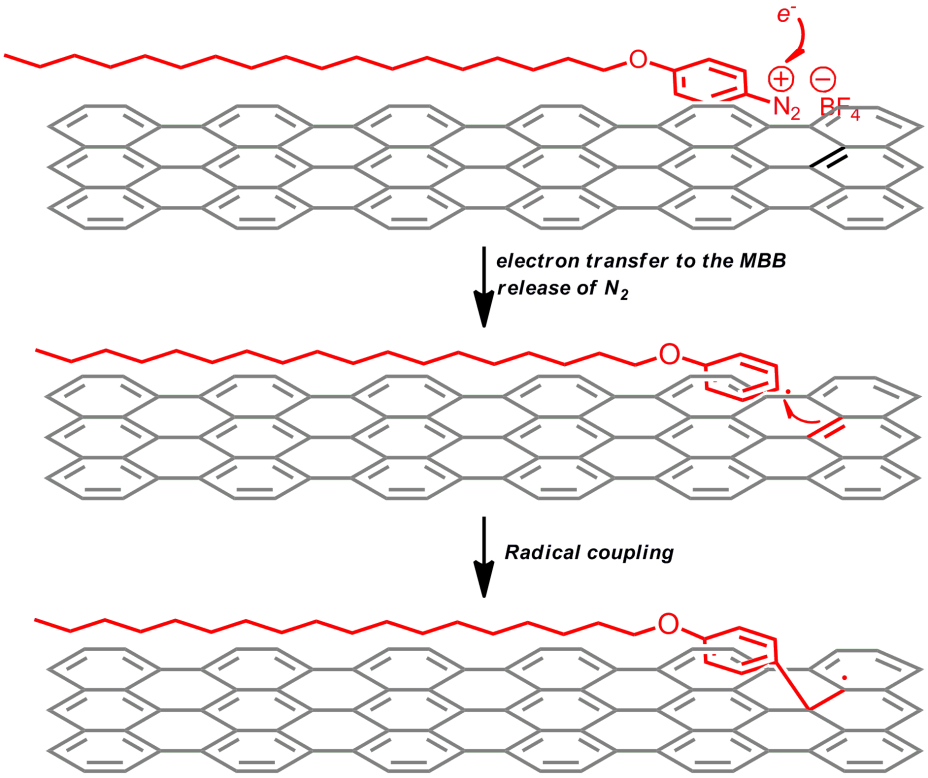

Figure 6-11. Reaction mechanism between aryl diazonium cation and graphene lattice.

The mechanism of covalent functionalization on graphene with aryl diazonium salts is illustrated in Figure 6-11. [32] Firstly, a delocalized electron (from the electrodes in the electrochemical cell or the pristine graphene) is transferred to the aryl diazonium cation, which releases a molecule of N_2 and thus produces a reactive aryl radical. Then, a covalent bond with a sp^2-hybridized carbon atom on the graphene lattice is generated by the coupling of the aryl radical. Meanwhile, the attachment of a phenyl group leads to another delocalized, unpaired electron which would induce the further aryl modification.

To render the aryl diazonium salt the ability of self-assembling on the graphene surface, an aryl diazonium derivative **6-4** substituted with linear and long alkoxyl chain ($C_{22}H_{45}$) was synthesized. The synthesis toward the targeted diazonium salt was accomplished over three steps with the overall yield around 30% (Scheme 6-7). Firstly, the long alkoxyl chain substituted arylamine precursor **6-16** was prepared via substitution of 4-fluoronitrobenzene with docosanol in DMF, and then hydrogenation of the nitrobenzene derivative **6-15** into amine under hydrogen atmosphere in the

autoclave. Finally, the arylamine precursor **6-16** was treated with *t*-BuONO in the presence of Lewis acid BF_3 to yield the targeted aryl diazonium salt **6-4**. The final product **6-4** was fully characterized by NMR and MS measurement, and showed good solubility in the polar solvent (like chloroform, DMSO). The long alkyl tail was approximate 3.3 nm with the reactive diazonium head.

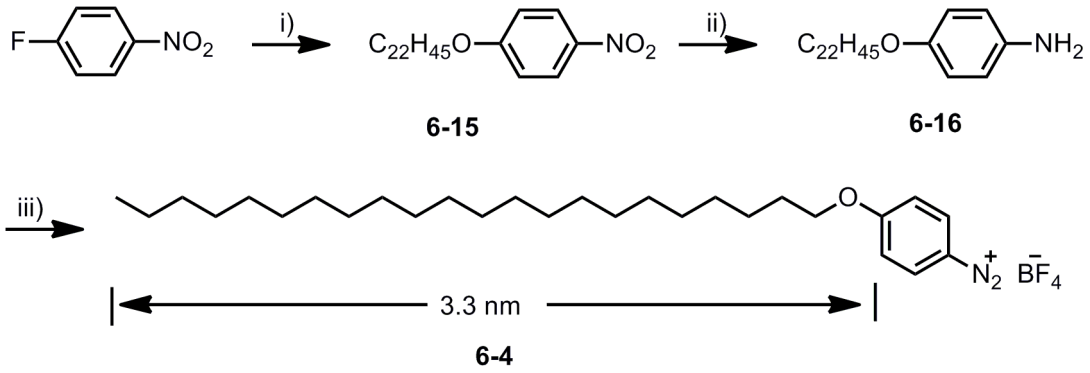

Scheme 6-6. Synthetic routes toward the 4-(docosyloxy)benzenediazonium tetrafluoroborate **6-4**. Condition: i) docosanol, K_2CO_3, DMF, 100 ℃, 24hs, 36%; ii) Pd/C (20 wt%), H_2(5 bar), THF, RT, 12hrs, 96%; iii) BF_3-Et_2O. *t*-BuONO, THF, 0 ℃ to RT, 30 min, 94%.

To investigate the self-assemblying behavior of MBB **6-4** on a graphene surface with the assistance of the long linear alkoxyl chains, scanning tunneling microscopy (STM) was utilized to monitor the lamellar structure formation on graphite and CVD graphene of MBB **6-4** in the group of our colleague in the University of Strassbourg. (Figure 6-12) It was found that the quality of the images on graphite was much better than that measured with the CVD graphene as substrate, which could be attributed to the natural roughness of the underlying SiO_x surface of CVD graphene. However, both images measured on graphite and graphene substrate exhibited a similar morphology, which also confirmed that the molecule **6-4** could self-assemble into physisorbed monolayers on graphite and graphene substrate with the same way.

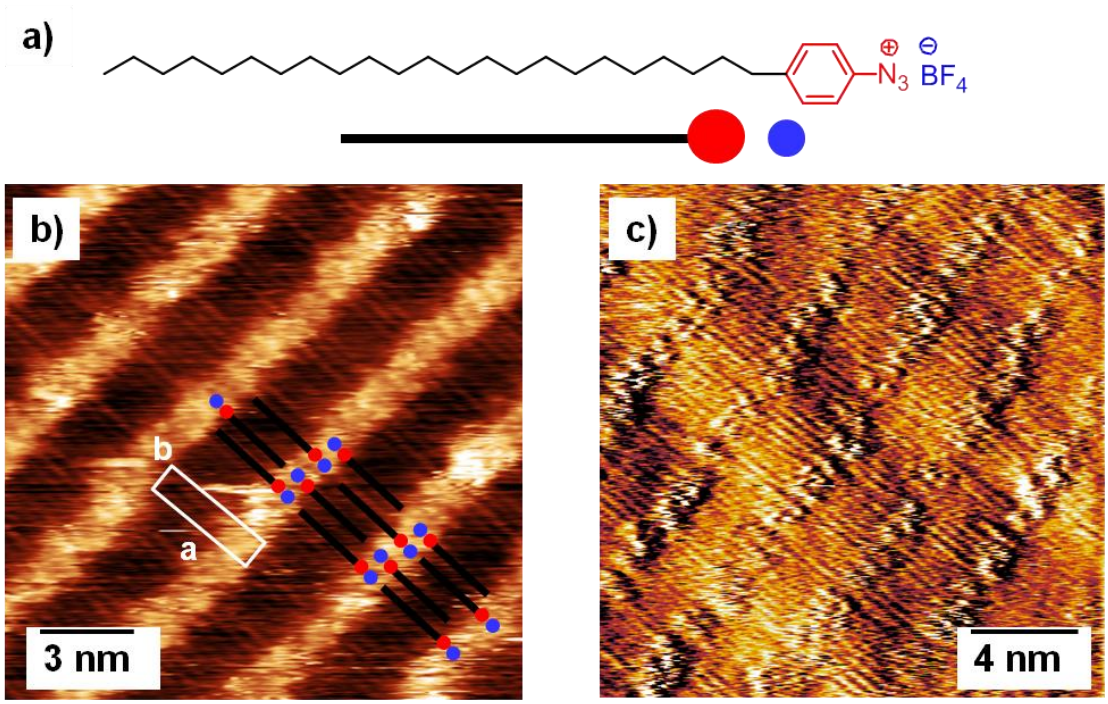

Figure 6-12. a) Molecular structure of MBB **6-5**. b) STM image of **6-5** assembly on graphite, showing also the unit cell; the possible molecular packing is also schema1zed. The posi1on of negative charged BF_4^- counter-ion is just indicative. Lattice parameters: a=3.9±0.1 nm: b=1.0±0.1 nm: a=89°±2°: A=3.9±0.1 nm^2. c) Current images of **6-5** self-assembled on graphene. The images were recorded by using the following tunneling parameters: (b) tip voltage (V_t) = -1200 mV and average tunneling current (I_t) = 60 pA; (c) (V_t) = -1200 mV, (I_t) = 20 pA.

In the observed STM images, the strip-like bright part could be ascribed to the alignment of those aromatic reactive head groups (phenyldiazonium salts), while the darker regions were attributed to the docosyl chains which were densely packed in a side-to-side manner. This 2D pattern could be characterized by a rectangular unit cell of a= (3.9±0.1) nm, b= (1.0±0.1) nm and α= (89±2°), with a unit cell area A= 3.9±0.2 nm^2 containing tswo molecules per cell. The fuzzy appearance of those bright domains, where the reactive head units were located, might be caused by the presence of the BF_4^- counterions. The interaction between these small counterions and the graphite surface was so weak that the ions were capable of moving on a timescale faster than the STM imaging. Therefore, we failed to observe the bright regions with better resolutions. The presence of the BF_4 anions neighboring the cationic reactive

head group was necessary to attenuate the mutual electrostatic repulsion between adjacent diazonium salts in neighboring molecules, which were also observed in the previous literatures. [33,34] Additionally, the identical brightness of the neighboring strip-like bright domains suggests that the adjacent molecules assemble with a head-to-tail arrangement (Figure 6-12b), which was driven by the minimization of the electrostatic repulsion and the maximization of the electrostatic attraction both at the intra- and inter-lamellar level.

The STM results described above were quite promising for the well-ordered defect generation on graphene materials, which also led to a new approach to engineering the graphene nanoribbons via lithography. The chemical modification of the self-assembling monolayers of MBB **6-4** on graphene had also been investigated by our colleague in the Consiglio Nazionale delle Ricerche, Italy.[35] The result suggested that an electrochemical impulse could successfully transform the physisorption into a covalent chemisorptions for the monolayer of MBB **6-4** with retaining well-ordered packing formed upon self-assembly. Therefore, the two-step approach for controllable chemical modification was proved to be feasible on graphene substract, and paved a new approach toward versative functional graphene-based materials.

Compared with the MBBs comprising azide (**6-1**) or diazirine moieties (**6-2**), MBB **6-4** with diazonium reactive head was featured with two advantages: the ease for thermal motion on the graphene surface and high yield of reactive radical intermediate after electrochemical stimulus. To realize the controllable covalent chemisorptions, optimization of the reactivity and molecular motion was obviously a necessity in the future works.

6.2.4 Synthesis of MBBs with *n*-type doping moieties

In contrast to the three types of covalent chemistry methods for graphene functionalization described above, there is another approach to introduce defects and alter the electronic properties of the graphene materials, namely electron doping. 1,3-Dimethyl-2-phenyl-2,3-dihydro-1*H*-benzoimidazole (DMBI) derivatives [36, 37]

have been reported as effective organic electron donors (OEDs) with the corresponding redox potentials (E = +0.33V), that can reduce substrates and organic compounds by single electron transfer.[38,39,40] The reactions of these OED materials are also well known to involve the hydride-transfer and/or electron-transfer reactions *via* radical intermediate formation. Therefore, these varieties of OED molecules present an ideal class of *n*-type dopants, and can readily form radicals and transfer the electron to targeted substrate. However, the normal doping by simply mixing is a random process in nature, and the distribution of doped domains on the substrate is difficult to control.

In order to obtain spatially controlled doping of graphene, a long alkoxyl chain was substituted on the *para*-position of DMBI, and the synthetic routes toward the desired *n*-type dopant **6-5** was also proposed. (Scheme 6-8). Firstly, the benzaldehyde precursor **6-17** was readily synthesized *via* the S_N2 substitution between alkyl halide and *p*-hydroxybenzaldehyde, and the condensation between **6-17** and N^1,N^2-dimethylbenzene-1,2-diamine under sonication directly yielded the targeted long alkyl chain substituted organic dopant **6-5**.

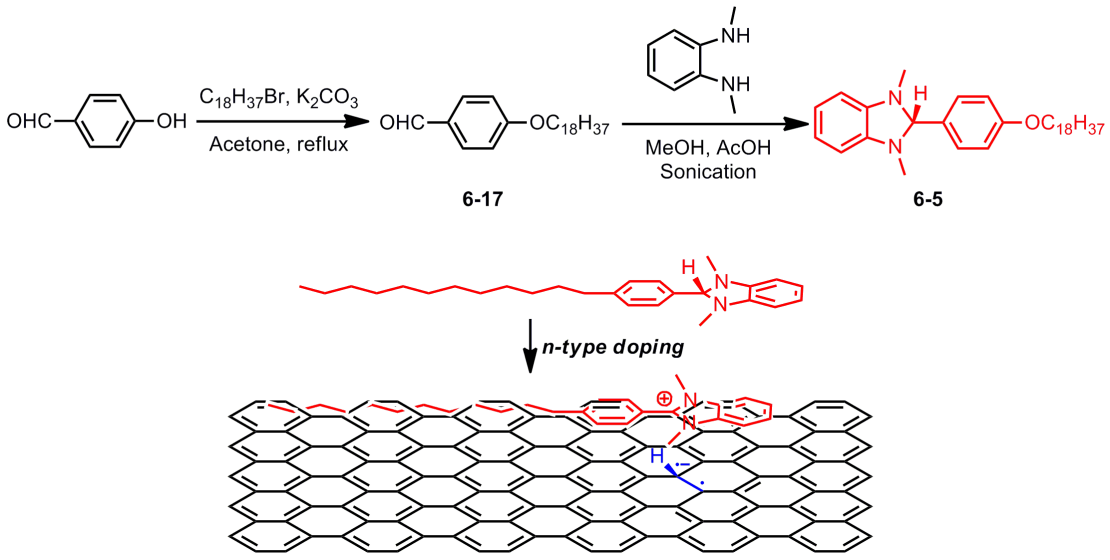

Scheme 6-7. Synthetic routes toward long alkoxyl chain substituted organic dopant **6-5**.

The doping experiment of octadecyloxy substituted N-DMBI molecule **6-5** on the CVD graphene was carried out in the nitrogen gas filled glove box to avoid the

contamination of water and oxygen, and high temperature was applied to activate the film of dopants **6-5**. Firstly, the solution of **6-5** in dry chlorobenzene (20 mg/mL) was spin-coated onto the CVD-graphene (on Cu substrate), and then the samples were heating at specific temperature for 30 minutes (temperature in choice: RT, 40 ℃. 60 ℃, and 80 ℃) in glove box under inert atmosphere before Raman measurement.

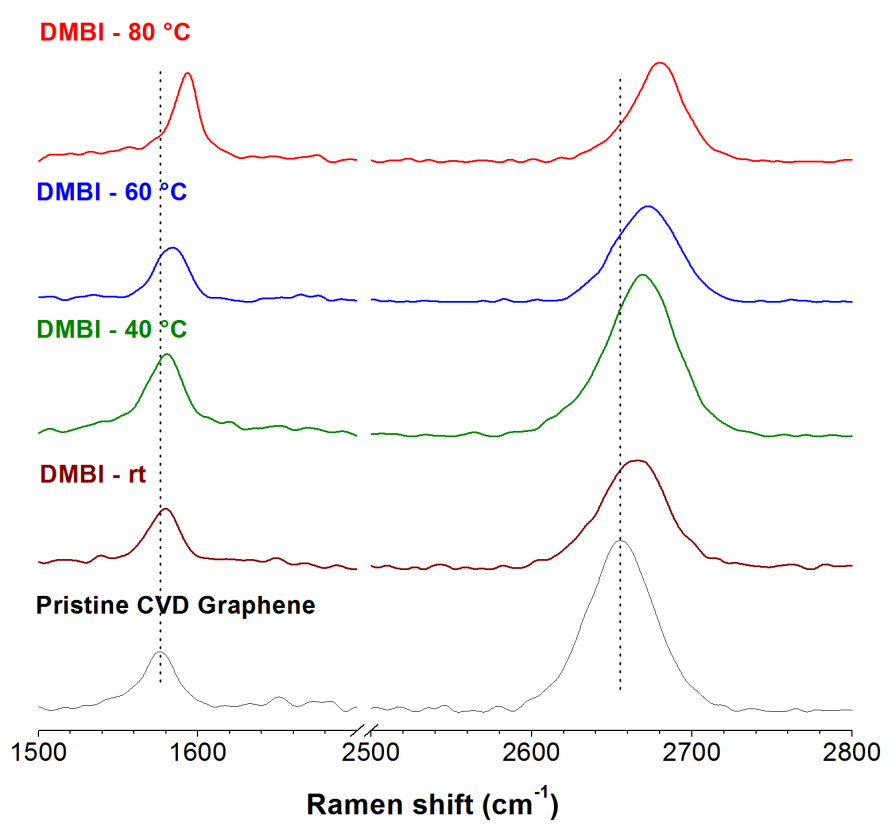

Figure 6-13. Raman spectra of CVD-Graphene sheets on Cu foil doped with **6-5** after annealing at different temperature.

Then the Raman spectra of these four samples and the control sample were measured under ambient condition. The Raman results clearly indicated that the G-peak of the CVD graphene samples upshift gradually with simultaneous shape stiffening when the reaction temperature increased from RT to 80 ℃. This phenomenon suggested that the graphene became *n*-type after the electric doping of MBB **6-5**, which was also consistent with the reported literature [41] The upshifted 2D band and lowered I_{2D}/I_G ratio also confirmed the evolution toward *n*-type graphene. Based on the temperature-dependent shift of G and 2D band (Figure 6-13), it was found that

heating the sample at high temperature was necessary to achieve high doping degree.

Furthermore, to realize spatially controlled doping on the graphene substrate, the STM images of the molecule **6-5** on graphite were studied. The molecule **6-5** was firstly dissolved in 1-phenyloctane with concentration of 0.1 mM, 1 mM and 10 mM, and then the solution was deposited onto the graphite substrate before STM imaging. However, it was found that no SAMs of MBB **6-5** could be observed on the surface, which was probably due to the non-planar structure of MBB **6-5** and its susceptbility to electric currents. The fast doping reaction between MBB **6-5** and graphene substrate might also contribute to the failure of SAM formation. Therefore, efforts in optimizing the structure and geometry of organic dopants were necessary for realizing the spatially-controlled doping on the graphene substrate.

6.3 Summary

In summary, a two-step appraoch of self-assembling assisted controllable chemical modification on graphene was proposed in this chapter to fulfill the goal of opening up the band gap of graphene and bottom-up fabrication of GNRs. To fulfill this goal, a series of molecular building blocks (compound **6-1** to **6-5** in Scheme 6-2) had been successfully synthesized. These molecules were all composed by reactive functional groups, and long alkyl chains which had extremely high affinity to the graphene surface. In the attempt to facilitate the modification process and avoid the disturbance of thermodynamic motions in the self-assembling monolayer structure, the reactive groups included phenylazide, diazirine, aryldiazonium salts, and organic dopants, which could be triggered by light irradiation, or electrochemical bias at room temperature. These functional modifiers were all structurally characterized *via* NMR measurement and MS spectra.

Firstly, scanning tunneling microscopy was utilized to investigate the formation of self-assembling monolayer of those functional modifiers on graphite and CVD graphene surface. Fortunately, nice STM images with well-patterned structures had been observed for the MBBs comprising long aliphatic chain and reactive units (from compound **6-1** to **6-4**). In these structures, the reactive groups were all well-ordered immobilized on the graphene surface in the "head-to-head" (MBB **6-2**) or "head-to-tail" (MBB **6-1** and **6-4**) alignment within a defined unit cell, and the cell parameters could be efficiently tuned by the length of the alkyl chains. However, for the MBB **6-5** containing *n*-type dopant, the non-planar structure of reactive moieties hindered the SAM formation as suggested by STM images.

Secondly, the reactivity of MBBs with graphene surface was studied by Raman spectroscopy and conductivity measurement. It was found that the reactivity of photo-responsive MBBs, including azide (**6-1**) and diazirine (**6-2**), had been greatly attenuated after physisorbed on the graphene surface. This is probably due to the low efficiency of photo-initiation for these reactive moieties, and confinement of the

motions of those reactive groups which thereby hindered the attacks of reactive intermediate toward the graphene surface. In the case of MBB **6-4** with diazonium functionality, covalent chemisorption of the MBB on graphene surface with retained well-ordered alignment was obtained after electrochemical impulse, which was ascribed to the high efficiency of radical generation in electrochemical cell and the ease of thermal motion for the pristine phenyldiazonium head on the graphene surface.

In summary, spatially confined covalent tethering of MBBs on graphene surface for periodic defect generation and GNR fabrication was proved to be feasible via the two-step approach in this chapter, and still required to be improved by optimizing the reactivity and motion.

Reference

[1] A. Bellunato, H. A. Tash, Y. Cesa, G. F. Schneider, *ChemPhysChem*, **2016**, *17*, 785.

[2] J. Park, M. D. Yan, *Acc. Chem. Res.*, **2013**, *46*, 181.

[3] W. Yang, H. Grennberg, *ECS. Trans.*, **2009**, *17*, 211.

[4] S. Eigler, *Chem. Eur. J.*, **2016**, *22*, 7012.

[5] G. L. C. Paulus, Q. H. Wang, M. S. Strano, *Acc. Chem. Res.*, **2013**, *46*, 160.

[6] Y. P. Sun, K .F. Fu, Y. Lin, W. J. Huang, *Acc. Chem. Res.*, **2012**, *35*, 1096.

[7] C. Liu, Q. Zhang, F. Stellacci, N. Marzari, L. Zheng, Z. Zhan, S*mall*, **2011**, *7*, 1257.

[8] K. Balasubramanian, M. Burghard, S*mall*, **2005**, *2*, 180.

[9] Q. H. Wang, M. C. Hersam, M. C, *Nat. Chem.* **2009**, *1*, 206.

[10] A. Deshpande, C. H. Sham, J. M. P. Alabonson, J. M. Mullin, G. C. Schaz, M. C. Hersam, *J. Am. Chem. Soc.* **2012**, *134*, 16759.

[11] M. C. Prado, R. Nascimento, L. C. Moura, M. J. S. Matos, M. S. C. Mazzoni, L. G. Cacado, H. Chacham, B. R. A. Neves, *ACS Nano*, **2011**, *5*, 394.

[12] H. Bayley, J. R. Knowles, *Biochemistry*, **1978**, *17*, 2414.

[13] K.A. Schnapp, R. Poe, E. Leyva, N. Soundararajan, M. S. Platz, *Bioconjugate Chem.* **1993**, *4*, 172.

[14] J. F. W. Keana, S. X. Cai, *J. Org. Chem.* **1990**, *55*, 3640.

[15] R. Poe, K. Schnapp, M. J. T. Young, J. Grayzar, M. S. Platz, *J. Am. Chem. Soc.* **1992**, *114*, 5054.

[16] N. P. Gritsan, M. S. Platz, *Chem. Rev.* 2006, *106*, 3844–3867.

[17] L.H. Liu, M. D. Yan, *Acc. Chem. Res.*, **2010**, *43*, 1434.

[18] L.H. Liu, M. D. Yan, *J. Mater. Chem.*, **2011**, *21*, 3273.

[19] L. H. Liu, M. M. Lerner, M. D. Yan, *Nano Lett.* **2010,** *10*, 3754.

[20] Y. Xia, F. Q. Qu, A. Maggiani, K. Sengupta, C. Liu, L. Peng, *Org. Lett.*, **2011**, *13*, 4248.

[21] A. Blencowe, W. Hayes, *Soft Matter* **2005**, *1*, 178.

[22] H. Nakashima, M. Hashimoto, Y. Sadakane, T. Tomohiro, Y. Hatanaka, *J. Am. Chem. Soc.* 2006, *128*, 15092.

[23] M. Hashimoto, Y. Hatanaka, *Eur. J. Org. Chem.* **2008**, 2513.

[24] J. Brunner, H. Senn, F. M. Richards, *J. Biol. Chem.* **1980**, *255*, 3313.

[25] J. Brunner, G. Semenza, *Biochemistry* **1981**, *20*, 7174.

[26] H. Ismaili, F. Lagugne-Labarthet, M. S. Workentin, *Chem. Mater*. **2011**, *23*, 1519.

[27] E. J. Lawrence, G. G. Wildgoose, L. Aldous, Y. A. Wu, J. H. Warner, R. G. Compton, P. D. McNaughter, *Chem. Mater*. **2011**, *23*, 3740.

[28] S. Yang, S. Brüller, Z. Wu, Z. Liu, K. Parvez, R. Dong, F. Richard, P. Samorì, X. Feng, K. Müllen, *J. Am. Chem. Soc.*, **2015**, *137*, 13927.

[29] M. Gobbi, S. Bonacchi, J. Lian, Y. Liu, X, Wang, M.-A. Stoeckel, M. A. Squillaci, G. D'Avino, A. Narita, K. Müllen, X. Feng, Y. Olivier, D. Beljonne, E. Orgiu, P. Samorì "Periodic potentials in hybrid van der Waals heterostructures formed by supramolecular lattices on graphene." *Nat. Commun. (Accepted)*

[30] P. M. Kirkman, A. G. Guell, A. S. Cuharuc, P. R. Unwin, *J. Am, Chem. Soc*., **2014**, 136, 36.

[31] P. Huang, L. Jing, H. Zhu, X. Gao, *Acc. Chem. Res*., **2013**, *46*, 43.

[32] A. A. Mohamed, Z. Salmi, S. A. Dahoumane, A. Mekki, B. Carbonnier, M. M. Chehimi, *Adv. Colloid Interface Sci*., **2015**, *225*, 16.

[33] S. De Feyter, F. C. De Schryver, *Chemical Society Reviews* **2003**, *32*, 139.

[34] S. Haar, A. Ciesielski, J. Clough, H. Yang, R. Mazzaro, F. Richard, S. Conti, N. Merstorf, M. Cecchini, V. Morandi, C. Casiraghi, P. Samorì, *Small,* **2015**, *11*, 1691.

[35] Z. Xia, F. Leonardi, M. Gobbi, Y. Liu, V. Bellani, A. Liscio, A. Kovtun, R. Li, X. Feng, E. Orgiu, P. Samori, E. Treossi, V. Palermo, *ACS Nano,* **2016**, *10*, 7125.

[36] H. Chikashita, H. Ide, K. Itoh, *J. Org. Chem.*, **1986**, *51*, 5400.

[37] D. D. Tanner, J. J. Chen, *J. Org. Chem.*, **1989**, *54,* 3842.

[38] J. Broggi, T. Terme, P. Vanelle, *Angew. Chem. Int. Ed*. **2014**, *53*, 384.

[39] E. Doni, J. A. Murphy, *Chem. Commun.*, **2014**, *50*, 6073.

[40] J. A. Murphy, *J. Org. Chem.*, **2014**, *79*, 373.

[41] P. Wei, N. Liu, H. R. Lee, E. Adijanto, L. Ci, B. D. Naab, J. Q. Zhong, J. Park, W. Chen, Y. Cui, Z. N. Bao, *Nano Lett.*, **2013**, *13*, 1890.

7. Conclusion and outlook

Two differnet carbon networks with distintive bonding patterens and dimensions which are structurally related to the elusive carbon allotrope “cubic graphite”, are theoretically proposed. These two carbon networks are featured with 2D polyphenylene networks in chapter 3, and 1D double helical polyphenylene in chapter 4. (Figure 7-1) Considering the difficulty to directly furnish the final carbon networks, substructures of these proposed cabon frameworks are synthesized and investigated in chapter 3 and 4.

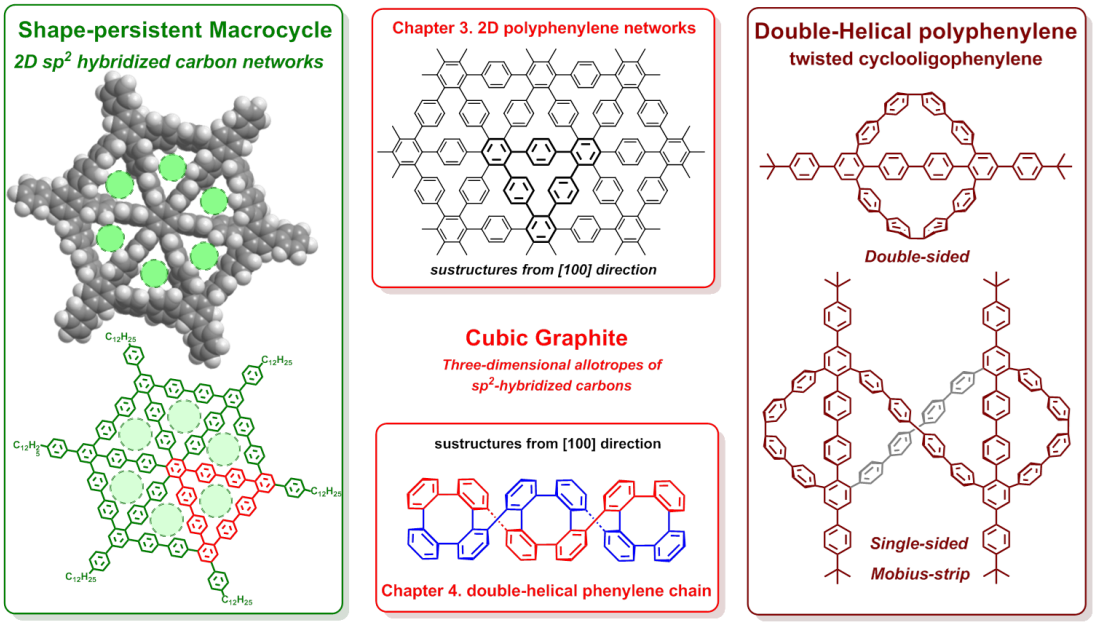

Figure 7-1. Theoretically proposed carbon networks which are structurally related to the “cubic graphite”, the purely sp^2-hybridized 2D carbon structures with hexagonal symmetry and extremely distorted double helical polyphenylenes, and their substructures.

In chapter 3, two purely sp^2-hybridized 2D carbon structures with hexagonal symmetry had been conceived by replacing ethynylene groups of γ-graphyne and graphdiyne with *para*-phenylene units, which we named graphenylene-1 and graphenylene-2, respectively. Notably, graphenylene-1 corresponded to a single-layer substructure of the hypothetical carbon allotrope “cubic graphite”. Herein, two shape-persistent polyphenylenes spoked wheels (**3-1** and **3-2**), consisting of 22 and 37

benzene rings, were proposed as the nanosized substructure of the 2D carbon networks. Toward synthesis of subunits **3-1** and **3-2**, two dendritic oligophenylene precursors (**3-6**, and **3-13**) were designed with twelve bromo groups at appropriate positions for forming the rims of the wheellike molecules by six-fold aryl-aryl coupling reactions. The hexaphenylbenzene core in **3-6**, and **3-13** was expected to serve as a shape-persistent template that facilitates the ring closure.

Upon cobalt-catalyzed cyclotrimerization of corresponding acetylene derivatives (**3-5** and **3-12**), these two precursors **3-6** and **3-13** had been successfully synthesized and unambiguously characterized by NMR, mass spectrometry. However, Yamamoto coupling of the two dendritic polyphenylene precursors with diluted concentration under microwave treatment, failed to give the desired subunit **3-1**. Fortunately, another targeted substructure **3-2**, was obtained as a white solid after purification via recycling GPC with the yield of 56%. In order to verify the chemical structure of the nanosized macrocyclic compound **3-2**, scanning tunneling microscope (STM) technique was applied to directly visualize the molecular structure of nanometer sized macrocycle besides the normal NMR and MS measurements. The STM images clearly show a hexagonal packing pattern with the unit cell parameters of $a = b = 4.7 \pm 0.2$ nm and $\alpha = 60 \pm 3°$, which perfectly matched the size of the macrocycle **3-2**. In addition, the hexagonal shape of the macrocycle **3-2** could also be clearly observed in the STM images with higher resolution, while six adjacent pores appearing in each hexagon in the STM images also clearly demonstrated the shape-persistent structure of the spoked wheel **3-2**. Such molecular structure with six internal pores (approximately 4A in diameter as measured both in models and STM images) could be highly interesting for studying supramolecular interactions with other guest molecules or ions, since they were expected to accommodate e.g. methyl groups or Br^- and I^- anions.

Chapter 4 studied the double-helical tetraphenylene chains **4-1**, which could be envisoned as a subunit in the “cubic graphite”. The double helical structure and its intrinsic highly distorted “figure eight” conformation had attracted lot of attentions

due to the unique topology and property. In the attempt to synthesize polyphenylene chain **4-6** with double helical structure, and cyclic oligophenylene with "figure eight" conformation, a synthetic route *via* Yamamoto polymerization of tetraiodo precursor **4-12** was proposed.

Through the *Yamamoto* coupling of the corresponding tetraiodo precursors (**4-12** and **4-16**), the extremely strained oligophenylene bicyclophanes **4-13** and **4-17**, were obtained exclusively with high yield. Only a trace of dimers with locked "figure eight" geometry (**4-7** and **4-18**) could been observed on the MALDI-TOF spectra of the crude product, and purified *via* preparative GPC with the approximate yield of 2%. Although this synthetic method toward double helical polyphenylene **4-6** had failed, the structural investigation on the strained geometry of the oligophenylene bicyclophane **4-13**, had shed some light on the distorted structure of the targeted double helical backbone.

In the last section of chapter 4, another synthetic route toward the cyclic oligophenylene with "figure eight" geometry was proposed via stepwise ring closure of asymmetric dibromo precursor (**4-21**). The *Yamamoto* coupling of precursor **4-21** had both yielded the half-cyclized oligophenylene cyclophane **4-22**, and the intriguing cyclic oligophenylene **4-23** with "figure-eight" conformation in a satisfactory yield of c.a. around 28%. The chemical identify of **4-23** was easily established by NMR measurements and further confirmed by MALDI-TOF MS spectrum. Theoretical calculation of the geometry of **4-23** had revealed two distinctive conformers with different orientations of the two bridging phenylene rings, in which one conformer was probably adopting a Möbius topology. As indicated by temperature dependent NMR of **4-23** in solution, the free rotation of the bridging phenylene rings could be frozen at low temperature, which provided the possibility of driving the formation and isolation for the conformers with Möbius geometry. Furthermore, the residual four methoxyl groups on **4-23**, also furnished possible sites for intramolecular locking of the relative flexible "figure eight" conformations in **4-23**.

In conclusion, carbon networks composed entirely of phenylene units have been proposed in this part, which are structurally related to the fascinating carbon allotrope "cubic graphite". Although the ultimate carbon networks remain elusive until now, a series of substructures with identical geometry have been prepared in this part, and their unique structures, like shape-persistent geometry in **3-2** and "figure eight" conformation in **4-23** have been investigated in depth. These results also opened up a new avenue for designing and synthesizing a further variety of unprecedented carbon structures and their subunits.

In the second part of this work, we focus on the modulation of the energy levels of the nanographene and graphene by chemical modification. Represented as the most outstanding carbon materials, graphene-related materials with diverse energy level have attracted lots of efforts. Herein, we propose two alternative approaches to modulate the nanographene (chapter 5) and graphene (chapter 6) via controllable chemical modification methods.

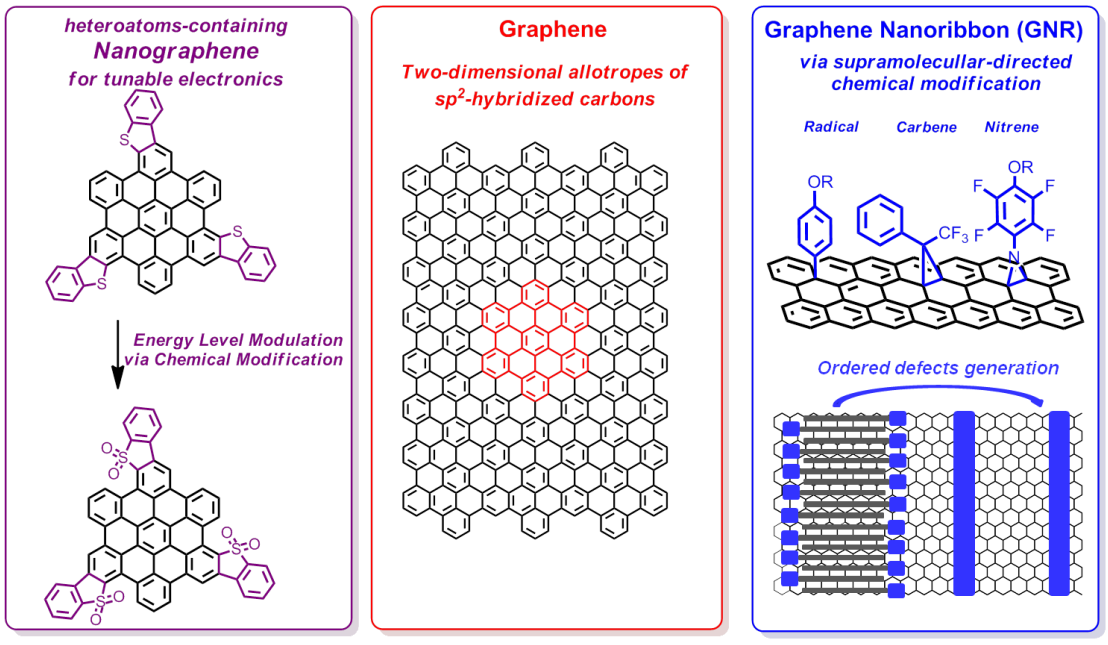

Figure 7-2. Modulation of the energy levels of the nanographene and graphene via controllable chemical modification.

In chapter 5, a series of sulfur-incorporating nanographene derivatives (**5-6** and **5-10**) had been prepared via *Scholl* reaction of the corresponding oligophenylene precursors.

Then by converting the electron-donating thiophene rings on the nanographene motif into electron-withdrawing thiophene-*S*,*S*-dioxide units via controllable oxidation of sulfur atoms, another new nanographene derivative **5-11** π-conjugated with strong electron-withdrawing groups had been successfully obtained via chemical modification on PAH **5-10**. The chemical structures of both **5-10** and **5-11** had been validated by NMR and MALDI-TOF MS spectra.

Then UV-Vis spectra, fluorescent spectra, cyclic voltammetry, and theoretical simulation eludicated the modulation of energy levels via chemical mofication. The thiophene-*S*,*S*-dioxide fused PAH **5-11** had a markedly low-lying LUMO level (0.55 eV) and parallelly low-lying HOMO energy (0.51 eV), and consequently exhibiting a similar band gap in comparison with nanographene **5-10**. The decresed HOMO and LOMO levels in **5-11** after oxidation have clearly manifested that oxidation of thiophene was a powerful approach to tune the optolectronic properties of the thiophene incorporated nanographene semiconductors. In addition, a unique helical packing in solid state with a long pitch (3.4 nm) was observed for TTC **5-10** as indicated by the 2D-WAXS results.

In chapter 6, we were aiming to engineer the band gap of pristine graphene via self-assembly assisted chemical modification. To accomplish this proposal, a series of molecular building blocks composed of long alkyl chain, which were capable of forming ordered self-assembled monolayers on the interface of graphene and solution, and diverse reactive groups (like perfluorophenylazide in **6-1**, diazirine in **6-2** and **6-3**, diazonium in **6-4,** and organic dopant in **6-5**), were successfully synthesized and carefully characterized via NMR and MS spectra.

Additionally, STM imaging was utilized to invertigate their self-assembling behavior on the graphene surface, and Raman spectra were applied to monitor the defect generation on the graphene materials. In the case of MBBs with perfluorophenylazide unit (MBB **6-1**) and diazirine moiety (MBB **6-2**), well-ordered monolayer could be envisioned in the STM images with “head to tail” and “head to head” alignment in the unit cell, respectively. However, the nearly invisible D band in the Raman spectra of

graphene after photochemical modification indicated the extremely low degree of modification and inert reactivity for these physisorbed molecules. The diazonium salt MBB **6-4** exhibted extremely high reactivity toward the basal plane of graphene with retaining ordered packing by electrochemical modification approach. However, MBB **6-5** bearing n-type doping moiety was found to be unsuitable for SAM formation on graphene due to the non-planar structure.

In summary, controllable chemical modification methods, either atomically (chapter 5) and spatially (chapter 6), had been successfully utilized to tune the energy level of the graphene-related molecules and materials. These findings paved the new way toward a versatile and well-controlled route to functionalize graphene-related materials. Besides the sulfur atoms and aliphatic chains used in this work, this concept of controllable modification could also be extended to other heteroatoms incorporation and more complex 2D paterns on graphene.

Throughout all chapters, it was demonstrated that bottom-up approach to carbon networks and functional graphene materials represented a longstanding challenge for chemists, and remained as a necessity for getting in-sights into the structure-property relationship for emerging carbon materials. The synthesis of 2D polyphenylene networks and 1D highly-twisted polyphenylene chains was aimed towards structurally defined synthetic carbon networks, which would driven the construction of new carbon materials. The controllable modification on nanographene and graphene was exploring the miximum usage of carbon allotropes, which could enrich the variety of existing carbon materials. All these studies could contribute to the development of improved carbon materials in the future.

8. Experiment part

8.1 General methods

Chemicals and solvents

The commercially available chemicals and solvents were obtained from the companies Acros Organics, Alpha-Aesar, Sigma-Aldrich, Strem Chemicals and TCI Europe and they were used as received without further purification.

Inert atmosphere

Standard Schlenk techniques were used for oxygen- or moisture-sensitive reactions, using argon (grade 4.8, Westfalen AG) as inert gas. A stream of argon was purged through the reac-tion mixture to degas the reaction.

Chromatography

Preparative column chromatography was performed on silica gel from Macherey-Nagel with a grain size of 0.063−0.200 mm (silica gel) or 0.040−0.063 mm (flash silica gel). Analytical thin layer chromatography (TLC) plates “Alugram Sil G/UV254” from Macherey-Nagel with a 0.2 mm silica gel coating and a fluorescence indicator were used. Compounds were detected by fluorescence quenching at 254 nm or self-fluorescence at 366 nm. Pure solvents (p.a. or technical grade) were used as eluents. Preparative thin layer chromatography was performed with PLC silica gel 60, F254, 2 mm sheets on glass from Merck.

Microwave-assisted synthesis

Microwave-assisted reactions were performed in a microwave oven (CEM GmbH, Kamp-Lintfort, Germany, model: Discover). The microwave was equipped with a pressure and tem-perature sensor and the reaction vessels could hold a pressure of up to 12 bars. 122 7 Experimental Part

Size-exclusion chromatography

Preparative size-exclusion chromatography (SEC) was performed on SEC facility from Shi-madzu, pump series LC20AD, a SPD20A UV-detector (λ = 320 nm) with JAIGEL 2.5H col-umns and chloroform as eluting solvent at 298 K.

8.2 Analytical methods

NMR spectroscopy

1D proton and carbon NMR spectra were measured on a 250, 300, 500, and 700 MHz system. The ^{1}H NMR experiments were performed with a 5 mm probes on different Bruker AVANCE III systems (TOPSPIN 3.1 software version), and referenced to residual signals of the deuterated solvent. Abbreviations: s = singlet, d = doublet, t = triplet, m = multiplet, b = broad. The spectra were obtained with π/2-pulse lengths of around 10 μs (^{1}H) and mostly 128 number of scans were required for sufficient signal to noise ratio. The carbon measurements were made with a J-modulated (coupling constant of 145 Hz ^{1}H-^{13}C was used) spin-echo for C-nuclei coupled to protons to determine the number of attached protons and proton decoupling during acquisition. The 90 °pulse for carbon was 14 μs long and with a relaxation delay of 2 s.

The assignment of the aromatic proton signals was accomplished by 2D ^{1}H,^{1}H COSY and 2D ^{1}H,^{1}H NOESY (nuclear overhauser enhancement spectroscopy) methods. The spectroscopic widths of the homo-nuclear NOESY experiments were typically 13600 Hz in both dimension (f1 and f2) and the relaxation delay 2 s. The mixing time used in the 2D NOESY was kept at 350 ms.

The diffusion (DOSY, Diffusion Ordered Spectroscopy) experiments were done with a 5 mm BBFO z-gradient probe and a gradient strength of 5.350 [G/mm] on the 500 MHz system. For the calibration of the gradient strength, a sample of $^{2}H_2O/^{1}H_2O$ was measured at a defined temperature and compared with the literature diffusion coefficient of $^{2}H_2O/^{1}H_2O$. The used temperature of 298.3 K was approved with a standard ^{1}H methanol NMR sample. In this work, the gradient strength was varied in

16 steps from 2 to 100%. The diffusion time d20 was optimised at 60 ms and the gradient length p30 of 1.8 ms.

The calculation of the diffusion value was automatically done with the mono exponential function[z]:

$$\ln\left(\frac{I(G)}{I(0)}\right) = -\gamma^2\delta^2G^2\left(\Delta - \frac{\delta}{3}\right)D,$$

where I(G) and I(0) are the intensities of the signals with and without gradient, γ the gyromagnetic ratio of the nucleus (^{1}H in this measurements), G is the gradient strength, δ the duration of the pulse field gradient (PFG), D the diffusion value in m^2/s and Δ the "diffusion time" between the beginning of the two gradient pulses.

The experiments were conducted between 298 K and 393 K, regulated by a standard 1H methanol (low temperature) and glycol (high temperature) NMR sample. As an internal standard the deuterated solvent was used: for $CHDCl_2$ δ(1H) = 5.32 ppm, CD_2Cl2 δ(13C) = 54.00 ppm; for $CHCl_3$ δ(1H) = 7.24 ppm, $CDCl_3$ δ(13C) = 77.23 ppm: for THF-d_7H δ(1H) = 3.58 ppm, THF-d_8 δ(13C) = 67.57 ppm; for C_2DHCl_4 δ(1H) = 5.91 ppm, $C_2D_2Cl_4$ δ(13C) = 74.20 ppm.

Mass spectrometry

Field desorption (FD) mass spectra were measured on VG Instruments ZAB 2 SE-FPD. MALDI-TOF mass spectra were recorded on a Bruker Reflex II-TOF spectrometer High resolution (HR) MALDI-TOF mass spectrometry measurements were performed on a Solarix ESI-/MALDI-ICR (9.4T) system (Bruker Daltonics, Germany), with a SmartBeam laser II. The system was internally calibrated in positive mode using sodium tri-fluoroacetate (Fluka, >99 %) or sodium perfluoroheptanoate (Fluka, >99 %) on quadratic cal-ibration mode. A total of 10-400 shots were accumulated for each mass spectrum. The results were calculated using Data Analysis software (Bruker Daltonics, Germany). HR-ESI mass spectra were measured on a QTof Ultima 3 Fa. Micromass/Waters. Ion mobility measure-ments and tandem mass spectrometry were performed on a SYNAPT G2 Si instrument (Wa-ters

Corp., Manchester, UK) with matrix-assisted laser desorption/ionization (MALDI) source.

UV-Vis spectroscopy

Solution UV-Vis absorption spectra were recorded at 298 K on a Perkin-Elmer Lambda 900 spectrophotometer.

Emission spectroscopy

Solution emission spectra were recorded at 298 K on a J&M TIDAS spectrofluorometer, us-ing Quartz cuvettes from Hellma with 1 cm thickness.

Electrochemical measurements

All electrochemical measurements were carried out in a conventional three-electrode cell, using a Wave Driver 20 bipotentiostat (Pine Instrument Company, USA) controlled at room temperature. An Ag/AgCl (4 M KCl) and a platinum wire were used as reference and counter electrodes, respectively. All potentials in this study refer to that of the Ag/AgCl electrode. A RRDE electrode with a Pt ring (6.25 mm inner-diameter and 7.92 mm outer-diameter) and a glassy carbon disk (5.61 mm diameter) served as the substrate for the working electrode for evaluating the ORR activity and selectivity of various catalysts. Prior to use, the glassy carbon electrode was polished using aqueous alumina suspensions on felt polishing pads.

For preparing the catalyst ink, 1.0 mg of [MN4]-complex was first dissolved in DCM to get a clear solution, and then 4.0 mg carbon black (Ketjenblack EC300J) was added to obtain a 20 wt% [MN4] mixture. This mixture was first ultrasonicated for 30 min and stirred overnight to dry at room temperature. Finally, the catalyst ink was obtained by blending the dried powder with a 50 µL Nafion solution (0.5 wt%) and 950 µL ethanol in an ultrasonic bath. 9.9 L of the catalyst ink was then pipetted onto the GC surface, leading to a catalyst loading of 0.2 mg·cm-2. For comparison, a commercially available catalyst of 20 wt% Pt supported on car-bon black (BASF) was used and 5 mg·mL-1 Pt/C suspension was also prepared with the same procedure as

mentioned above. 4.95 L of the catalyst ink was then pipetted onto the GC sur-face, leading to a Pt loading of 20 g·cm-2. 7

STM imaging

For STM measurements, a solution of macrocycle **3-2** was prepared in 1,2,4-trichlorobenzene (TCB) at a concentration of 10^{-4} mol·L^{-1}. A droplet of this solution was then drop-cast on the surface of a piece of freshly cleaved highly oriented pyrolytic graphite (HOPG, grade ZYB, Advanced Ceramics Inc., Cleveland, USA). Although the molecules of **3-2** were deposited from a TCB solution onto the substrate, at longer times after deposition (when most of the TCB evaporated), a droplet of 1-phenyloctane was added to the sample to ensure the presence of liquid on top the monolayer. STM measurements were performed with a PicoSPM (Agilent) instrument operating in constant current mode using a mechanically cut Pt/Ir (80/20) tip. The data were analyzed with the WsXM (Nanotec Electronica, Spain)[1] and Scanning Probe Image Processor (SPIP, Image Metrology ApS) softwares.

7.3. Synthesis

7.3.1 A shape-persistent polyphenylene macrocycle composed with all *sp*^{2}-carbons

2,6-Bis(4-bromophenyl)-4-(4-(methoxycarbonyl)phenyl)pyrylium tetrafluorobor-ate (3-3)

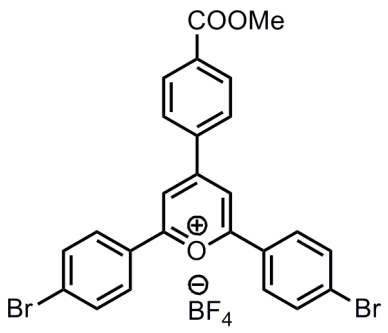

3-3

To a flask containing methyl 4-formylbenzoate (1.0 eq, 4.68 g, 28.5 mmol) and

1-(4-bromophenyl)ethan-1-one (2.0 eq, 11.5 g, 57.8 mmol) was added BF_3-Et_2O (4.0 eq, 15.0 mL, 115 mmol). The reaction mixture was heated to 100 ℃ with vigorous stirring overnight. After cooling the mixture to room temperature, 100 mL of Et_2O was added into the flask with vigorous stirring to precipitate the desired pyrylium salt. After filtration and washing with Et_2O, 4.40 g of the title compound was obtained as a red solid (25% crude yield). Because of the poor solubility in normal organic solvents, this compound was used directly in the next step without further purification. ^{1}H NMR (300 MHz, DMSO-d_6): δ ppm 9.29 (s, 2H), 8.70 (d, 2H, J = 8.6 Hz), 8.55 (d, 4H, J = 8.7 Hz), 8.28 (d, 2H, J = 8.4 Hz), 8.02 (d, 4H, J = 8.7 Hz), 3.96 (s, 3H). ^{13}C NMR (75 MHz, DMSO-d_6): δ ppm 132.94, 131.71, 130.65, 130.30, 129.99, 129.28, 116.42, 52.65.

Methyl 4''-bromo-5'-(4-bromophenyl)-4'-(4-iodophenyl)-[1,1':3',1''-terphenyl]-4-carboxylate (3-4)

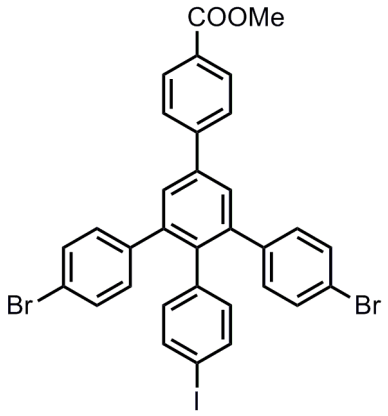

3-4

To a two-necked round-bottom flask containing 2,6-bis(4-bromophenyl)-4-(4-(methoxycarbonyl)phenyl)pyrylium tetrafluoroborate (**3-3**) (1.0 eq, 4.30 g, 7.0 mmol) and sodium 2-(4-iodophenyl)acetate (2.6 eq, 4.8 g, 18 mmol) was added 40 mL of acetic anhydride. After stirring at 150 ℃ for 12 h, the reaction mixture was cooled to room temperature, and then poured into 200 mL of MeOH. The precipitates were collected by filtration and washed with MeOH. The crude product was further purified by silica gel column chromatography with dichloromethane (DCM)/hexane = 1/4 as eluent to yield 2.40 g of the title compound as a white solid (47% yield).

FD-MS (8 kV): *m*/*z* calcd. for $C_{32}H_{21}Br_2IO_2$: 724.2 [M^+]; found: 723.9. ^{1}H NMR (250 MHz, CD_2Cl_2): δ ppm 8.16 (d, 2H, *J* = 8.6 Hz), 7.81 (d, 2H, *J* = 8.4 Hz), 7.72 (s, 2H), 7.45 (d, 2H, *J* = 8.6 Hz), 7.40 (d, 4H, *J* = 8.6 Hz), 7.05 (d, 4H, *J* = 8.2 Hz), 6.67 (d, 2H, *J* = 8.4 Hz), 3.96 (s, 3H). ^{13}C NMR (75 MHz, CD_2Cl_2): 137.16, 133.73, 131.92, 131.36, 13048, 128.91, 127.41, 100.38, 52.43

Methyl 4''-bromo-5'-(4-bromophenyl)-4'-(4-((2',6'-dibromo-[1,1'-biphenyl]-4-yl)-ethynyl)phenyl)-[1,1':3',1''-terphenyl]-4-carboxylate (3-5)

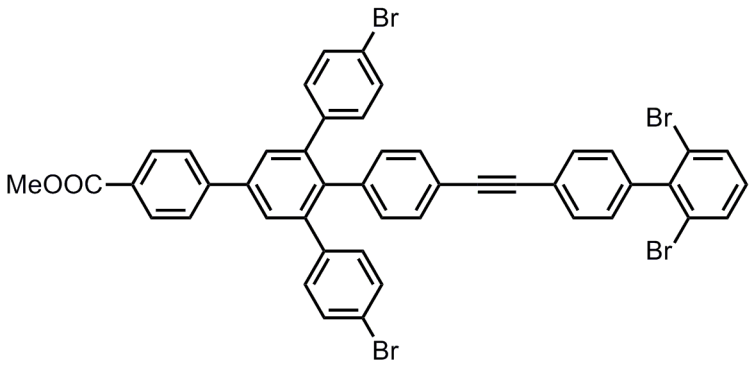

3-5

A two-necked 250-mL round-bottom flask containing methyl 4''-bromo-5'-(4-bromophenyl)-4'-(4-iodophenyl)-[1,1':3',1''-terphenyl]-4-carboxylate (**3-4**) (1.0 eq, 2.73 g, 3.77 mmol), 2,6-dibromo-4'-ethynyl-1,1'-biphenyl **17** (1.0 eq, 1.27 g, 3.77 mmol), $Pd(PPh_3)_2Cl_2$ (0.05 eq, 130 mg, 0.18 mmol), and CuI (0.05 eq, 36 mg, 0.18 mmol) was evacuated and refilled with argon gas for three times. Then, 60 mL of anhydrous THF was added into the flask, followed by 10 mL of degassed trimethylamine. The reaction mixture was stirred under room temperature overnight. After evaporating the solvent, the crude product was purified via silica gel column chromatography with DCM/hexane = 1/3 as eluent to obtain 2.50 g of the title compound as a white solid (71% yield). FD-MS (8 kV): *m*/*z* calcd. for $C_{46}H_{28}Br_4O_2$: 932.3 [M^+]; found: 932.1. ^{1}H NMR (250 MHz, CD_2Cl_2): δ ppm 8.17 (d, 2H, *J* = 8.7 Hz), 7.84 (d, 2H, *J* = 8.7 Hz), 7.75 (s, 2H), 7.71 (d, 2H, *J* = 8.1 Hz), 7.64 (d, 2H, *J* = 8.4 Hz), 7.42 (d, 4H, *J* = 8.6 Hz), 7.32 (d, 2H, *J* = 8.6 Hz), 7.25 (d, 2H, *J* = 8.5 Hz), 7.6 (t, 1H, *J* = 8.3 Hz), 7.09 (d, 4H, *J* = 8.3 Hz), 6.93 (d, 2H, *J* = 8.3 Hz), 3.96 (s, 3H).

^{13}C NMR (175 MHz, CD_2Cl_2): δ ppm 160.60, 144.26, 142.23, 141.55, 141.15, 140.32, 139.38, 139.06, 138.09, 131.93, 131.62, 131.56, 131.33, 130.95, 130.87, 130.20, 130.10, 129.45, 128.47, 127.04, 124.17, 122.92, 121.20, 120.92, 89.75, 89.36, 52.03.

Star-shaped polyphenylene precursor (3-6):

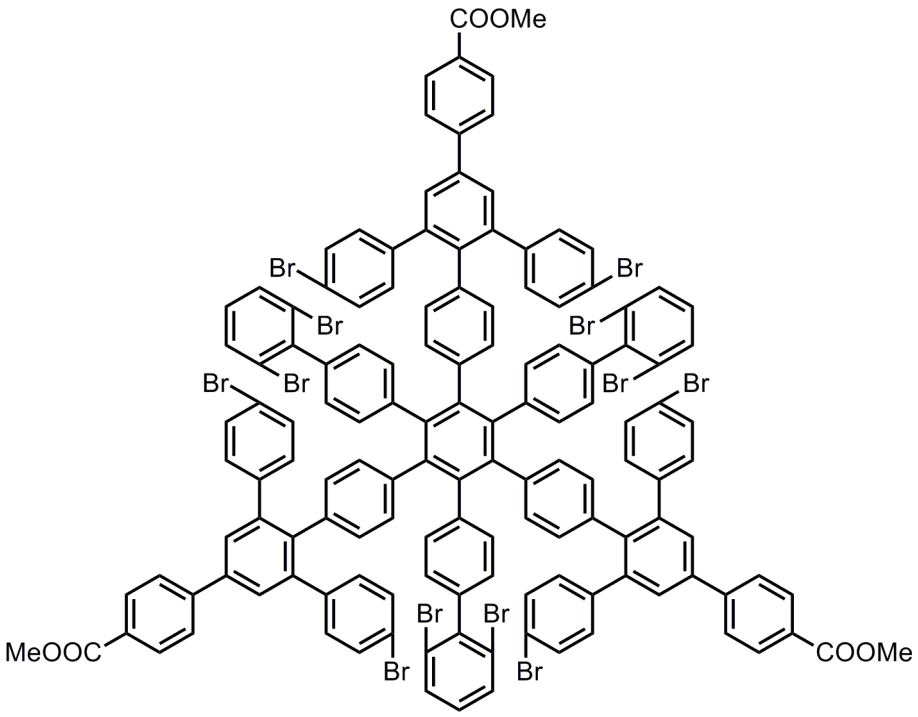

3-6

A two-necked 250-mL flask containing methyl 4''-bromo-5'-(4-bromophenyl)-4'-(4-((2',6'-dibromo-[1,1'-biphenyl]-4-yl)ethynyl)phenyl)-[1,1':3',1''-terphenyl]-4-carboxylate **(3-5)** (1.0 eq, 932 mg, 1.0 mmol) was evacuated and refilled with argon gas for three times. Dioxane (50 mL) was added into the flask, and the solution was further degassed by bubbling with argon gas for 15 min. Dicobalt octacarbonyl (0.5 eq, 171 mg, 0.500 mmol) was then added into the mixture under argon atmosphere. The reaction was kept under refluxing with vigorous stirring overnight. Evaporation the solvent and removal the catalyst via filtration through a pad of silica gel with dichloromethane as eluent gave 700 mg of crude product. Purified by silica gel column chromatography with dichloromethane/hexane = 3/1 as eluent provided 210 mg of the title compound as a white solid (23% yield). MALDI-TOF MS: m/z calcd. for $C_{138}H_{84}Br_{12}O_6$: 2797.0 [M^+]; found: 2796.4. ^{1}H

NMR (700 MHz, CD_2Cl_2): δ ppm 8.07 (d, 6H, J = 7.7 Hz), 7.66 (d, 6H, J = 8.4 Hz), 7.49 (m, 12H), 7.14 (d, 12H, J = 8.5 Hz), 6.97 (t, 3H, J = 8.0 Hz), 6.88 (d, 12H, J = 7.8 Hz), 6.69 (s, 12H), 6.49 (d, 6H, J = 7.3 Hz), 6.30 (d, 6H, J = 8.3 Hz), 3.83 (s, 9H). ^{13}C NMR (175 MHz, CD_2Cl_2): δ ppm 166.67, 144.38, 142.80, 141.52, 140.58, 140.08, 138.67, 138.40, 138.30, 131.96, 131.79, 131.56, 130.62, 130.42, 130.05, 129.38, 128.54, 127.63, 126.96, 124.44, 120.58, 51.99.

Shape-persistent polyphenylene macrocycle (3-1)

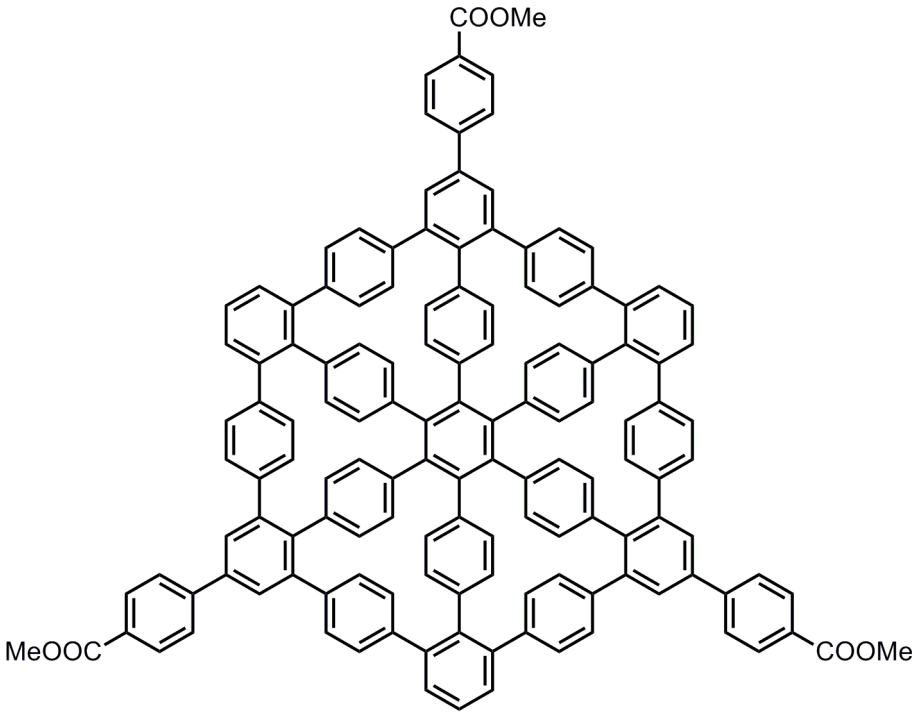

3-1

$Ni(COD)_2$ (24 eq, 24 mg, 86 μmol), dendritic polyphenylene precursor **3-6** (1.0 eq, 10 mg, 3.6 μmol), COD (24 eq, 10 mg, 86 μmol), and 2,2'-bipyridine (24 eq, 13 mg, 86 μmol) were added into a dried microwave tube in a glove box under the protection of argon gas. After addition of anhydrous THF (20 mL), the microwave tube was sealed with a microwave cap. The mixture in the tube was protected with aluminum foil against light before putting it into the microwave reactor. The heating program was started with pre-stirring of 1 min and heating at 120 ℃ for 4 hours under microwave irradiation with maximum power of 200 W and activated cooling. After cooling to room temperature, the reaction mixture was passed through a pad of silica gel with

THF as eluent to remove the catalyst. MALDI-TOF MS measurement analysis of the resulting product indicated the absence of the desired compound **3-1**.

Table S1. Reaction condition for Yamamoto coupling based cyclization

Solvent	Time (hr)	Temperature	Equivalent (per Bromide)	MS Results
THF	4	120	1.1	NONE desired product
THF	4	120	2	NONE desired product
DMF/Tol (1/4)	4	170	1.1	NONE desired product
DMF/Tol (1/4)	4	170	2	NONE desired product
DMF/Tol (1/1)	4	170	1.1	NONE desired product
DMF/Tol (1/1)	4	170	2	NONE desired product

4-Dodecylbenzaldehyde (3-8)

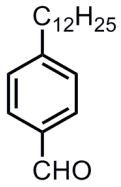

3-8

The compound was synthesized following a reported procedure.[2] FD-MS (8 kV): *m*/*z* calcd. for $C_{19}H_{30}O$: 274.5 [M^+]; found: 274.3. ^{1}H NMR (250 MHz, $CDCl_3$): δ ppm 9.90 (s, 1H), 7.73 (d, 2H, J = 8.3 Hz), 7.27 (d, 2H, J = 8.3 Hz), 2.61 (t, 2H, J = 7.8 Hz), 1.57 (m, 2H), 1.18 (m, 18H), 0.81 (t, 2H, J = 7.2 Hz).

2,6-Bis(4-bromophenyl)-4-(4-dodecylphenyl)pyrylium tetrafluoroborate (3-9)

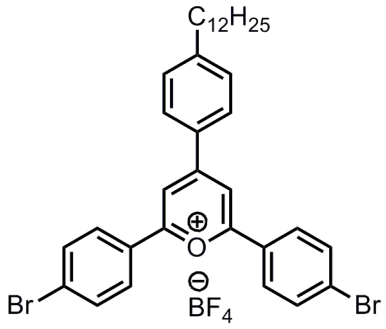

3-9

To a flask containing 4-dodecylbenzaldehyde (3-**8**) (1.0 eq, 4.72 g, 17.2 mmol) and 1-(4-bromophenyl)ethan-1-one (2.0 eq, 6.85 g, 34.4 mmol) was added 8.50 mL of BF_3-Et_2O (4.0 eq, 68.8 mmol). The reaction mixture was heated to 100 ℃ with vigorous stirring overnight. After cooling the mixture to room temperature, 100 mL of Et_2O was added into the flask with vigorous stirring to precipitate the desired pyrylium salt. After filtration and washing with Et_2O, 5.80 g of the title compound was obtained as a orange solid (46% crude yield). Because of the poor solubility of this salt in normal organic solvents such has chloroform, dichloromethane, and tetrahydrofuran, this compound was used directly in the next step without further purification. ^{1}H NMR (300 MHz, CD_2Cl_2): δ ppm 8.46 (s, 1H), 8.11 (m, 6H), 7.78 (d, 4H, J = 8.9 Hz), 7.36 (d, 2H, J = 8.4 Hz), 2.56 (t, 2H, J = 7.5 Hz), 1.52 (m, 2H), 1.19 (m, 18H), 0.80 (t, 2H, J = 6.9 Hz). ^{13}C NMR (75 MHz, CD_2Cl_2): δ ppm 134.07, 131.63, 130.98, 130.47, 130.27, 130.08, 114.86, 114.34, 36.67, 32.32, 31.14, 30.07, 30.05, 29.96, 29.83, 29.79, 29.76, 23.09, 14.28.

4-Bromo-3'-(4-bromophenyl)-5'-(4-dodecylphenyl)-4''-iodo-1,1':2',1''-terphenyl (3-10)

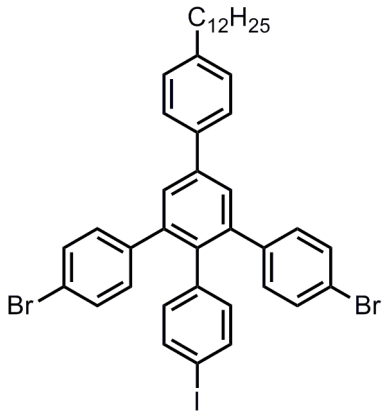

3-10

To a 100-mL flask containing 2,6-bis(4-bromophenyl)-4-(4-dodecylphenyl)pyrylium tetrafluoroborate (3-**9**) (1.0 eq, 5.77 g, 8.0 mmol) and sodium 2-(4-iodophenyl)acetate (2.5 eq, 5.68 g, 20 mmol) was added 30 mL of acetic anhydride. The reaction mixture was stirred at 150 ℃ for 12 h. After cooling to room temperature, the solution was poured into 100 mL of methanol, and the precipitates were collected by filtration and thoroughly washing with methanol. The crude product was further purified via silica gel column chromatography with dichloromethane/hexane = 1/4 as eluent to yield 2.60 g of the title compound as a white solid (39% yield). FD-MS (8 kV): *m*/*z* calcd. for $C_{42}H_{43}Br_2I$: 834.5 [M^+]; found: 833.9. ^{1}H NMR (250 MHz, CD_2Cl_2): δ ppm 7.67 (s, 2H), 7.64 (d, 2H, *J* = 8.2 Hz), 7.44 (d, 2H, *J* = 8.4 Hz), 7.39 (d, 4H, *J* = 8.6 Hz), 7.33 (d, 2H, *J* = 8.2 Hz), 7.04 (d, 4H, *J* = 8.8 Hz), 6.67 (d, 2H, *J* = 8.6 Hz), 2.69 (t, 3H, *J* = 8.0 Hz), 1.68 (b, 2H), 1.31 (m, 18H), 0.92 (t, 3H, *J* = 6.4 Hz). ^{13}C NMR (75 MHz, CD_2Cl_2): δ ppm 137.09, 133.85, 132.36, 131.96,131.28, 129.41, 129.31, 128.58, 127.20, 35.93, 32.32, 31.91, 30.06, 30.04, 30.03, 29.99, 29.89, 29.75, 29.72, 23.09, 14.28.

1,2-Bis(4-bromo-3'-(4-bromophenyl)-5'-(4-dodecylphenyl)-[1,1':2',1'':4'',1'''-quaterphenyl]-4'''-yl)acetylene (3-11)

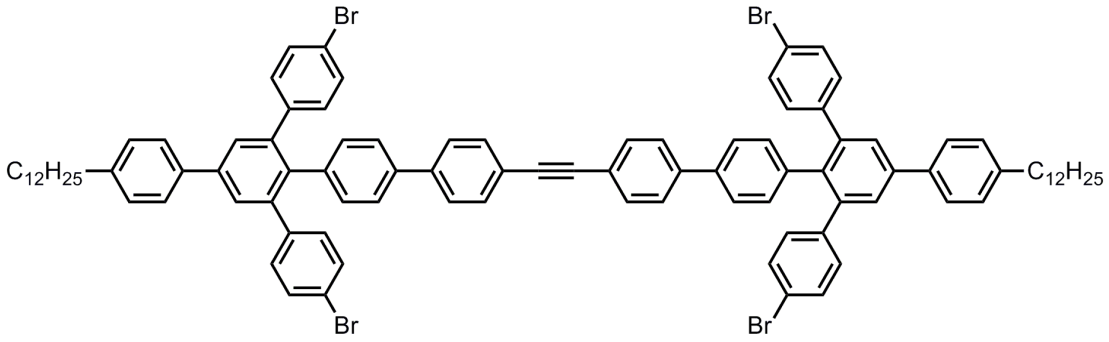

3-11

To a 250-mL two-necked round-bottom flask containing 4-bromo-3'-(4-bromophenyl)-5'-(4-dodecylphenyl)-4"-iodo-1,1':2',1"-terphenyl (3-**10**) (2.0 eq, 2.55 g, 3.06 mmol), 4,4′-(acetylene-1,2-diyl)bis(phenylboronic acid pinacol ester) (1.0 eq, 660 mg, 1.53 mmol), $Pd(PPh_3)_4$ (0.06 eq, 106 mg, 0.09 mmol), and K_2CO_3 (6.0 eq, 1.27 g, 9.17 mmol), was added 80 mL of degassed THF and 20 mL of a degassed mixture of ethanol and H_2O (1:1) under argon atmosphere. The reaction mixture was further degassed by three "freeze-pump-thaw" cycles, and then vigorously stirred at 60 ℃ overnight. After cooling to room temperature, the reaction mixture was extracted with dichloromethane (3 × 50 mL), and the combined organic layers were dried in vacuo. The crude product was purified by silica gel column chromatography with dichloromethane/hexane = 1/4 as eluent to yield 1.42 g of the title compound as a white solid (58% yield). MALDI-TOF MS (TCNQ as matrix): *m*/*z* calcd. for $C_{98}H_{94}Br_4$: 1590.4 [M^+]; found: 1588.8. ^{1}H NMR (250 MHz, CD_2Cl_2): δ ppm 7.64 (s, 4H), 7.57 (m, 12H), 7.38 (b, 2H), 7.32 (d, 12H, J = 8.8 Hz), 7.27 (b, 2H), 7.05 (d, 8H, J = 8.15 Hz), 6.95 (d, 4H, J = 8.27 Hz), 2.65 (t, 4H, J = 7.62 Hz), 1.63 (m, 4H), 1.25 (m, 36H), 0.86 (t, 6H, J = 6.84 Hz). ^{13}C NMR (75 MHz, CD_2Cl_2): δ ppm 132.54, 132.29, 132.02, 131.20, 129.41, 128.56, 127.21, 127.06, 126.25,35.94, 32.31, 31.92, 30.06, 30.05, 30.03, 29.99, 29.89, 29.74, 23.08, 14.28.

Star-shaped polyphenylene precursor (3-12):

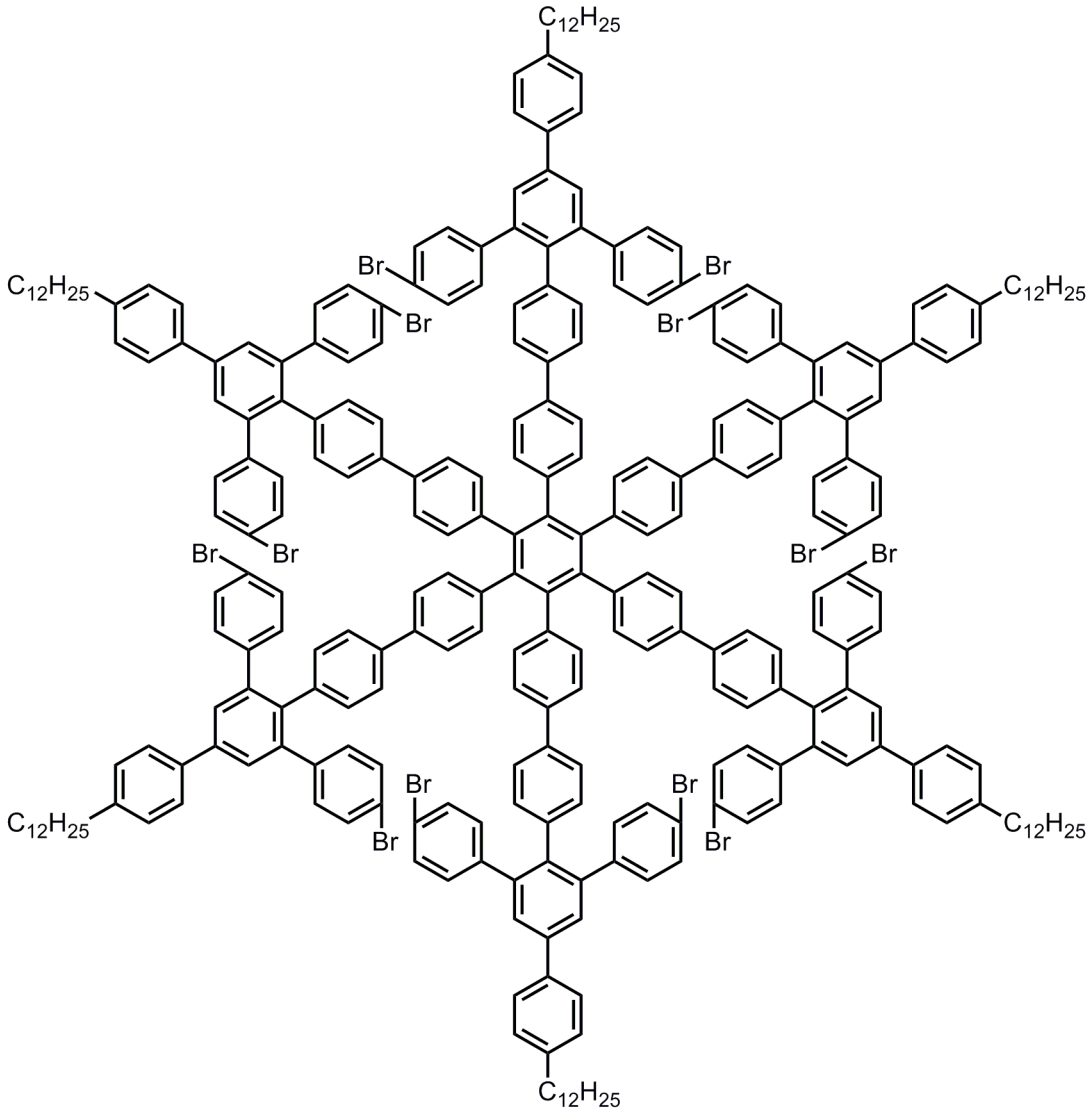

3-12

A solution of 1,2-bis(4-bromo-3'-(4-bromophenyl)-5'-(4-dodecylphenyl)-[1,1':2',1":4",1"'-quaterphenyl]-4"'-yl)acetylene (**3-11**) (1.0eq, 920 mg, 0.58 mmol) in 100 mL of toluene was degassed by argon bubbling for 15 min, and then dicobalt octacarbonyl (0.6 eq, 118 mg, 0.35 mmol) was added under argon atmosphere. After refluxing with vigorous stirring overnight, the solution was cooled to room temperature and passed through a pad of silica gel with tetrahydrofuran as eluent to remove the catalyst. Purification by recycling preparative GPC afforded 300 mg of the title compound as a white sold (34% yield). MALDI-TOF MS (TCNQ as matrix): *m*/*z* calcd. for $C_{294}H_{282}Br_{12}$: 4774.3 [M^+]; found: 4774.1. ^{1}H NMR (250 MHz, CD_2Cl_2):

δ ppm; 7.54 (m, 24H), 7.20 (d, 36H, J = 6.5 Hz), 7.08 (m, 24H), 6.94 (d, 24H, J = 8.2 Hz), 6.87 (b, 12H), 6.77 (d, 12H, J = 8.2 Hz), 2.56 (t, 12H, J = 8.0 Hz), 1.55 (m, 12H), 1.18 (m, 108H), 0.79 (t, 18H, J = 6.8 Hz) ^{13}C NMR (125 MHz, CD_2Cl_2): δ ppm 142.89, 141.38, 140.89, 140.20, 139.86137.98, 137.59, 137.24, 137.16, 136.93, 133.31, 131.98, 131.93, 131.66, 130.84, 129.54, 129.00, 128.22, 127.51, 126.82, 125.75, 124.95, 120.63, 35.53, 31.91, 31.51, 29.65, 29.63, 29.59, 29.50, 29.35, 22.69, 13.93.

Shape-persistent polyphenylene macrocycle (3-2)

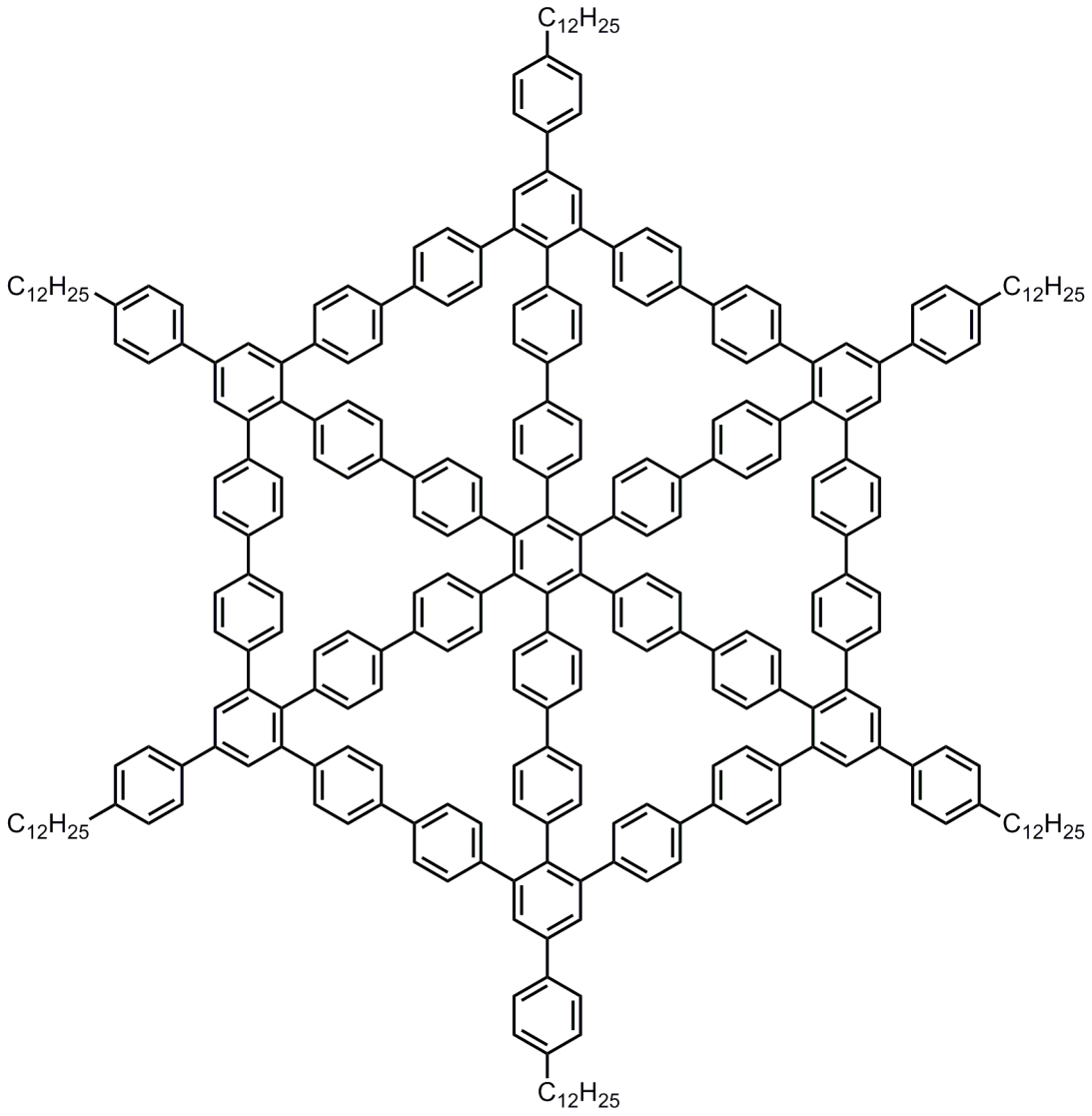

3-2

$Ni(COD)_2$ (24 eq, 70 mg, 0.25 mmol), dendritic polyphenylene precursor **3-12** (1.0 eq,

50 mg, 0.010 mmol), COD (24 eq, 27 mg, 0.25 mmol), and 2,2'-bipyridine (24 eq, 40 mg, 0.25 mmol) was added into a dried microwave tube in the glove box under the protection of argon gas. After addition of anhydrous THF (20 mL), the microwave tube was sealed with a microwave cap. The mixture was protected with aluminum foil against light before putting it into the microwave reactor. The heating program was started with pre-stirring of 1 min and heating at 120 ℃ for 8 h under microwave irradiation with maximum power of 200 W and activated cooling. After cooling to room temperature, the reaction mixture was passed through a pad of silica gel with tetrahydrofuran as eluent to remove the catalyst. The solution was concentrated in vacuo and poured into methanol to precipitate the resulting products. Purified by recycling preparative GPC with chloroform as eluent provided 23 mg of the title compound as a white solid (58% yield). MALDI-TOF MS (TCNQ as matrix): *m*/*z* calcd. for $C_{294}H_{282}$: 3815.5 [M^+]; found: 3815.5. ^{1}H NMR (500 MHz, $C_2D_2Cl_4$): δ ppm; 7.73 (s, 12H), 7.64 (d, 12H, J = 8.1 Hz), 7.48 (d, 24H, J = 8.2 Hz), 7.27 (d, 12H, J = 8.2 Hz), 7.23 (d, 12H, J = 8.3 Hz), 7.20 (d, 12H, J = 8.4 Hz), 7.16 (d, .24H, J = 7.7 Hz), 6.92 (d, 12H, J = 7.7 Hz), 6.79 (d, 12H, J = 7.5 Hz), 2.63 (b, 12H), 1.62 (m, 12H), 1.22 (m, 108H), 0.84 (t, 18H, J = 6.6 Hz) ^{13}C NMR (125 MHz, CD_2Cl_2): δ ppm 142.60, 141.90, 141.08, 137.51, 136.70, 135.09, 133.33, 131.60, 130.38, 129.05, 127.60, 127.00, 125.23, 124.54, 123.87, 35.68, 31.99, 31.51, 29.77, 29.73, 29.70, 29.61, 29.50, 29.44, 22.80, 14.33.

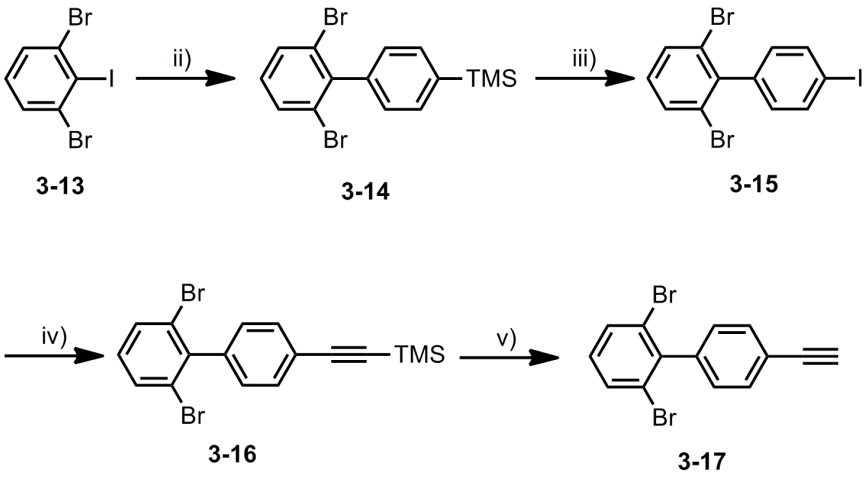

Scheme 8-1. Synthetic routes to the precursor **3-17**.

(2',6'-Dibromo-[1,1'-biphenyl]-4-yl)trimethylsilane (3-14)

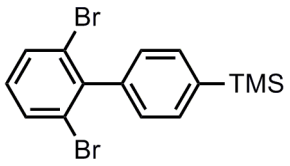

3-14

To the 250 mL two-necked round flask containing 5.60 g 1,3-dibromo-2-iodobenzene **3-13** (1.0 eq, 15.5 mmol), 3.02 4-TMS-phenylboronic acid (1.0 eq, 15.5 mmol), 800 mg $Pd(PPh_3)_4$ (0.05 eq, 0.78 mmol), and 6.44 g K_2CO_3 (3.0 eq, 46.6 mmol), was added 80 mL degassed toluene, 20 mL degassed EtOH/H_2O (1/1) under Argon atmosphere. The reaction mixture was further degassed by three "freeze-pump-thaw"cycles, and then heated to 100 ℃ with vigorous stirring overnight. After standard work-up and purification by column chromatography (Silica gel, with Hexane as eluent), 4.02 g white solid was obtained with the yield of 67.5%. FD-MS (8 KV): m/z 383.9, calcd.: 384.2 (M+). ^{1}H NMR (250 MHz, CD_2Cl_2): δ ppm 7.55 (dd, 4H, J= 7.05 Hz), 7.11 (d, 2H, J= 8.03 Hz), 7.01 (t, 1H, J= 7.83 Hz), 0.24 (s, 9H). ^{13}C NMR (175 MHz, CD_2Cl_2): δ ppm 145.20, 143.83, 142.78, 135.46, 134.24, 132.26, 130.69, 126.69, 0.90.

2,6-Dibromo-4'-iodo-1,1'-biphenyl (3-15)

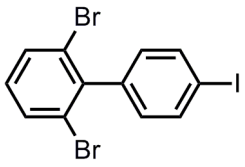

3-15

To the solution of 4.0g 2',6'-dibromo-[1,1'-biphenyl]-4-yl)trimethylsilane **3-14** (1.0 eq, 10.4 mmol) in 50 mL anhydrous DCM under Argon atmosphere was added 16 mL ICl (1.0 M in DCM) solution (1.5 eq, 15.6 mmol) at -78 ℃. Remove the acetone/dry ice bath, and keep stirring under room temperature for 2 hrs. After quenching the reaction with aqueous solution of $Na_2S_2O_3$, the mixture was extracted with DCM (50 mL for 3 times). The combined organic solution was evaporated, and the obtained crude

product was further purified on the silica gel column chromatography with Hexane as eluent. 4.55 g white solid was obtained with t yield of 98.9%. FD-MS (8 KV): m/z 438.2, calcd.: 437.90 (M+). ^{1}H NMR (300 MHz, CD_2Cl_2): δ ppm 7.85 (d, 2H, J= 8.41 Hz), 7.69 (d, 2H, J= 7.89 Hz), 7.15 (s, 1H), 7.02 (d, 2H, J = 8.39 Hz). ^{13}C NMR (75 MHz, CD_2Cl_2): δ ppm 142.22, 141.05, 137.84, 132.36, 131.59, 130.68, 124.48, 94.31.

((2',6'-Dibromo-[1,1'-biphenyl]-4-yl)ethynyl)trimethylsilane (3-16)

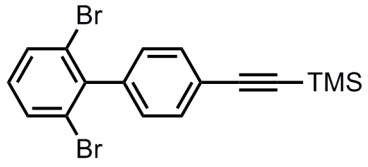

3-16

To the 250 mL two-necked round flask was added 880 mg 2,6-dibromo-4'-iodo-1,1'-biphenyl **3-15** (1.0 eq, 2.0 mmol),42 mg $Pd(PPh_3)_2Cl_2$ (0.03 eq, 0.06 mmol), and 12 mg CuI (0.03 eq, 0.06 mmol) , and then evacuated and refilled with Argon for three times. 50 mL anhydrous THF was added into the flask to dissolve the reagent, and followed by the addition of 10 mL degassed triethylamine. After addition of 0.42 mL ethynyltrimethylsilane (1.5 eq, 3.0 mmol) into the reaction mixture, the reaction continued with stirring under room temperature overnight. After evaporating the organic solvent, the crude product was purified via silica column chromatograpy with Hexane as eluent. 810 mg white solid was obtained with t yield of 99.2%. FD-MS (8 KV): m/z 407.9, calcd.: 408.20 (M+). ^{1}H NMR (300 MHz, $CDCl_3$): δ ppm 7.60 (d, 2H, J= 8.00 Hz), 8.54 (d, 2H, J= 8.17 Hz), 7.14 (d, 2H, J= 8.51 Hz), 7.05 (t, 1H, J = 8.15 Hz), 0.24 (s, 9H). ^{13}C NMR (175 MHz, CD_2Cl_2): *δ* ppm 143.57, 142.64, 133.24, 133.00, 131.54, 130.73, 130.67, 125.47, 124.29, 105.86, 96.32, 0.90.

2,6-Dibromo-4'-ethynyl-1,1'-biphenyl (3-17)

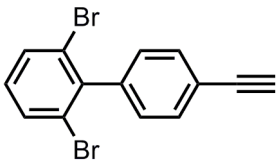

3-17

To the flask containing the THF solution of 810 mg ((2',6'-dibromo-[1,1'-biphenyl]-4-yl)ethynyl)trimethylsilane **3-16** (1.0 eq, 2.0 mmol) was added dropwise 2.5 mL TBAF solution (1.0 M in THF, 2.5 eq, 2.5 mmol). Keep stirring under room temperature with bubbling Argon gas for 30 mins. After evaporating the organic solvent, the crude product was purified via silica column chromatograpy with Hexane as eluent. 618 mg white solid was obtained with the yield of 92.0%. FD-MS (8 KV): m/z 335.1, calcd.: 336.02 (M+). ^{1}H NMR (300 MHz, $CDCl_3$): δ ppm 7.56 (d, 2H, J= 7.99 Hz), 7.52 (d, 2H, J= 8.34 Hz), 7.11 (d, 2H, J= 8.17 Hz), 7.01 (t, 1H, J = 8.09 Hz), 3.06 (s, 1H). ^{13}C NMR (175 MHz, CD_2Cl_2): δ ppm 142.11, 141.63, 131.94, 131.93, 130.25, 129.41, 124.09, 121.88, 83.12, 77.70.

7.3.2 Synthesis of oligophenylene macrocycles with “figure eight” conformations

4-(4-(Tert-butyl)phenyl)-2,6-bis(4-iodophenyl)pyrylium tetrafluoroborate (4-8)

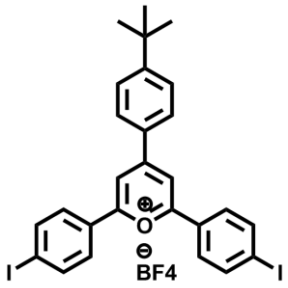

4-8

To a flask containing methyl 4-tert-Butylbenzaldehyde (1.0 eq, 4.86 g, 30 mmol) and 1-(4-iodophenyl)ethan-1-one (2.0 eq, 14.76 g, 60 mmol) was added BF_3-Et_2O (4.0 eq, 15.0 mL, 115 mmol). The reaction mixture was heated to 100 ℃ with vigorous stirring overnight. After cooling the mixture to room temperature, 100 mL of Et_2O

was added into the flask with vigorous stirring to precipitate the desired pyrylium salt. After filtration and washing with Et_2O, 8.2 g of the title compound was obtained as a red solid (39% crude yield). Because of the poor solubility in normal organic solvents, this compound was used directly in the next step without further purification. ^{1}H NMR (300 MHz, DMSO-d_6): δ ppm 9.15 (s, 2H), 8.55 (d, 2H, J = 8.87 Hz), 8.31 (d, 4H, J = 8.87 Hz), 8.19 (d, 4H, J = 8.57 Hz), 7.79 (d, 2H, J = 8.37 Hz), 1.30 (s, 9H). ^{13}C NMR (75 MHz, DMSO-d_6): δ ppm 138.74, 130.19, 129.98, 126.81, 114.95, 30.90, 30.61.

4''-Bromo-5'-(4-(tert-butyl)phenyl)-4-iodo-3'-(4-iodophenyl)-1,1':2',1''-terphenyl (4-9)

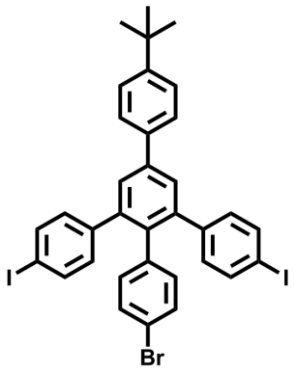

4-9

To a two-necked round-bottom flask containing 4-(4-(tert-butyl)phenyl)-2,6-bis (4-iodophenyl)pyrylium tetrafluoroborate (**4-8**) (1.0 eq, 7.8 g, 11.0 mmol) and sodium 2-(4-bromophenyl)acetate (2.0 eq, 5.2 g, 22 mmol) was added 40 mL of acetic anhydride. After stirring at 150 ℃ for 12 h, the reaction mixture was cooled to room temperature, and then poured into 200 mL of MeOH. The precipitates were collected by filtration and washed with MeOH. The crude product was further purified by silica gel column chromatography with dichloromethane (DCM)/hexane = 1/4 as eluent to yield 2.96 g of the title compound as a white solid (35% yield). ^{1}H NMR (250 MHz, CD_2Cl_2): δ ppm 7.54 (s, 2H), 7.53 (d, 2H, J = 8.32 Hz), 7.47 (d, 4H, J = 8.47 Hz), 7.41 (d, 2H, J = 8.55 Hz), 7.11 (d, 2H, J = 8.40 Hz), 6.78 (d, 4H, J = 8.55 Hz), 6.67 (d, 2H, J = 8.47 Hz), 1.27 (s, 9H). ^{13}C NMR (75 MHz, CD_2Cl_2): 137.30, 133.63, 132.18,

132.12, 131.12, 128.57, 127.01, 126.33, 31.44.

(2''-(4-Bromophenyl)-5''-(4-(tert-butyl)phenyl)-[1,1':4',1'':3'',1''':4''',1''''-quinquephenyl]-4,4''''-diyl)bis(trimethylsilane) (4-10)

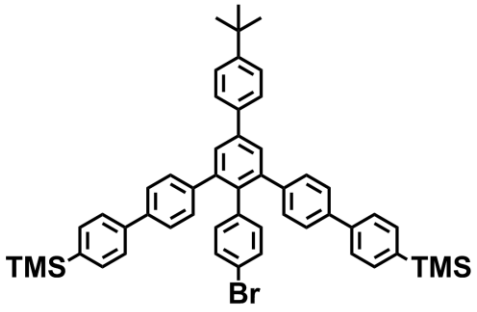

4-10

To a 250-mL two-necked round-bottom flask containing 4''-bromo-5'-(4-(tert-butyl)phenyl)-4-iodo-3'-(4-iodophenyl)-1,1':2',1''-terphenyl (**4-9**) (1.0 eq, 2.5 g, 3.25 mmol), 4-(Trimethylsilyl)phenylboronic acid (2.0 eq, 1.26 g, 6.5 mmol), $Pd(PPh_3)_4$ (0.08 eq, 300 mg, 0.26 mmol), and K_2CO_3 (6.0 eq, 2.7 g, 19.5 mmol), was added 100 mL of degassed THF and 30 mL of a degassed mixture of ethanol and H_2O (1:1) under argon atmosphere. The reaction mixture was further degassed by three "freeze-pump-thaw" cycles, and then vigorously stirred at 60 °C overnight. After cooling to room temperature, the reaction mixture was extracted with dichloromethane (3 × 50 mL), and the combined organic layers were dried in vacuo. The crude product was purified by silica gel column chromatography with dichloromethane/hexane = 1/4 as eluent to yield 2.01 g of the title compound as a white solid (76% yield). MALDI-TOF MS (TCNQ as matrix): *m*/*z* calcd. for $C_{52}H_{53}BrSi_2$: 814.0 [M^+]; found: 813.8. ^{1}H NMR (300 MHz, CD_2Cl_2): δ ppm 7.64 (s, 2H), 7.59 (d, 2H, J = 8.57 Hz), 7.51 (b, 8H), 7.42 (m, 6H), 7.13 (m, 6H), 6.78 (d, 2H, *J* = 8.25 Hz), 1.28 (s, 9H), 0.21 (s, 18H). ^{13}C NMR (75 MHz, CD_2Cl_2): δ ppm 135.31, 134.91, 132.01, 131.86, 129.68, 128.14, 127.76, 127.54, 127.39, 32.54, 0.

Tetra(trimethylsilyl)-sustituted oligophenylene precursor (4-11)

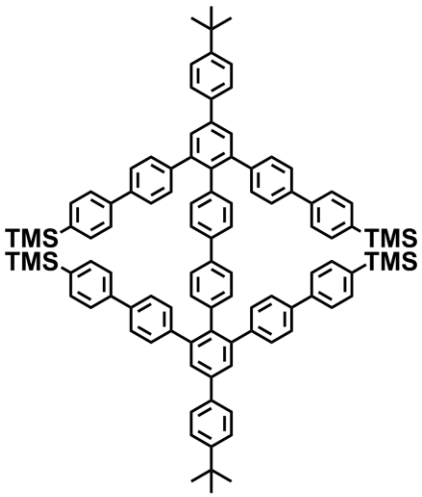

4-11

To a dry 250-mL two-necked round-bottom flask was added Ni(COD)2 (2.3 eq, 550 mg, 2.0 mmol), 4,4'-bipyridine (2.3 eq, 320 mg, 2.0 mmol), and COD (2.3 eq, 0.3 mL, 2.0 mmol) in the glove box. And then 20 mL anhydrous toluene and 20 mL anhydrous DMF was added into the flask. Before taking the flask out of the glove box, the flask was protected against light by covering with aluminium foil. The catalyst mixture was heated at 60 ℃ for 1 hour, and then the solution of the oligophenylene precursor (2"-(4-bromophenyl)-5"-(4-(tert-butyl)phenyl)-[1,1':4',1":3",1"':4"',1""-quinquephenyl] -4,4""-diyl)bis(trimethylsilane) (**4-10**) (1.0 eq, 700 mg, 0.86 mmol) in 20 mL toluene was added into the flask. The reaction mixture was then vigorously stirred at 80 ℃ overnight. After cooling to room temperature, the reaction mixture was dried in the rotary evaporator to remove the toluene, and then 100 mL MeOH was added into the residue DMF solution to precipitate the product. After filtration, the crude product was purified by silica gel column chromatography with dichloromethane/hexane = 1/4 as eluent to yield 600 mg of the title compound as a white solid (95% yield). MALDI-TOF MS (TCNQ as matrix): *m/z* calcd. for $C_{104}H_{106}Si_4$: 1468.3 [M^+]; found: 1468.2. ^{1}H NMR (300 MHz, CD_2Cl_2): δ ppm 7.63 (m, 8H), 7.50 (s, 16H), 7.39 (m, 16H), 7.14 (m, 8H), 6.92 (d, 4H, J = 8.204 Hz), 1.29 (s, 18H), 0.20 (s, 36H). ^{13}C NMR (75 MHz, CD_2Cl_2): δ ppm 135.28, 135.09, 132.57, 131.85, 129.65, 128.96, 128.14, 127.64, 127.54, 127.36, 32.55, 26.17, 0.

Tetra-iodo-sustituted oligophenylene precursor (4-12)

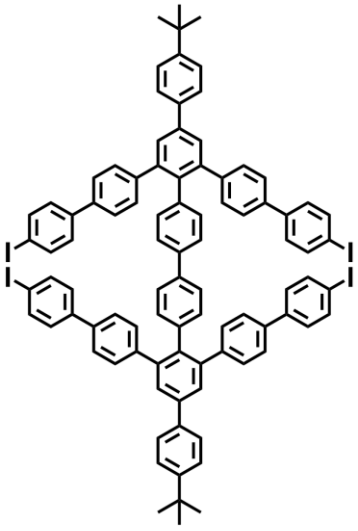

4-12

To the 100 mL two-necked flask containing tetra-TMS-sustituted Oligophenylene precursor (**4-11**) (1.0 eq, 367 mg, 0.25 mmol) was added 60 mL anhydrous THF under Argon gas, and then followed by the addition of the solution of ICl in DCM (8.0 eq, 2g/mL in DCM, 0.4 mL) under ice bath. The reaction mixture was kept under vigorous stirring at room temperature overnight. Finally, 100 mL MeOH was added into the mixture to precipitate the product. After filtration and washing with MeOH and DCM, 412 mg of the titled compound was obtained as a white solid (95% yield). Because of the poor solubility of this compound in common organic solvent, the compound is directly used without further purification and characterization.

Oligophenylene bicyclophane (4-13)

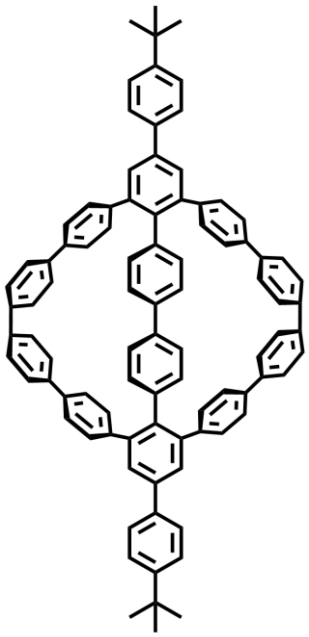

4-13

$Ni(COD)_2$ (8.0 eq, 70 mg, 0.25 mmol), Tetra-Iodo-sustituted Oligophenylene precursor (**4-12**) (1.0 eq, 50 mg, 0.03 mmol), COD (8.0 eq, 27 mg, 0.25 mmol), and 2,2'-bipyridine (8.0 eq, 40 mg, 0.25 mmol) was added into a dried microwave tube in the glove box under the protection of argon gas. After addition of anhydrous THF (20 mL), the microwave tube was sealed with a microwave cap. The mixture was protected with aluminum foil against light before putting it into the microwave reactor. The heating program was started with pre-stirring of 1 min and heating at 120 ℃ for 8 h under microwave irradiation with maximum power of 200 W and activated cooling. After cooling to room temperature, the reaction mixture was passed through a pad of silica gel with tetrahydrofuran as eluent to remove the catalyst. The solution was concentrated in vacuo and poured into methanol to precipitate the resulting products. Purified by recycling preparative GPC with chloroform as eluent provided 19 mg of the title compound as a white solid (53% yield). MALDI-TOF MS (TCNQ as matrix): *m*/*z* calcd. for $C_{92}H_{70}$: 1175.6 [M^+]; found: 1175.7. ^{1}H NMR (700 MHz, $C_2D_2Cl_4$): δ ppm; 7.65 (m, 16H), 7.50 (d, 8H, J = 8.18 Hz), 7.48 (d, 4H, J = 7.55 Hz), 7.32 (d, 8H, J = 7.55 Hz), 7.10 (d, 8H, J = 7.90 Hz), 7.05 (d, 4H, J = 7.62 Hz), 6.66 (d, 4H, J = 7.65 Hz), 1.35 (s, 18H).

Oligophenylene bicyclophane fimer (4-7)

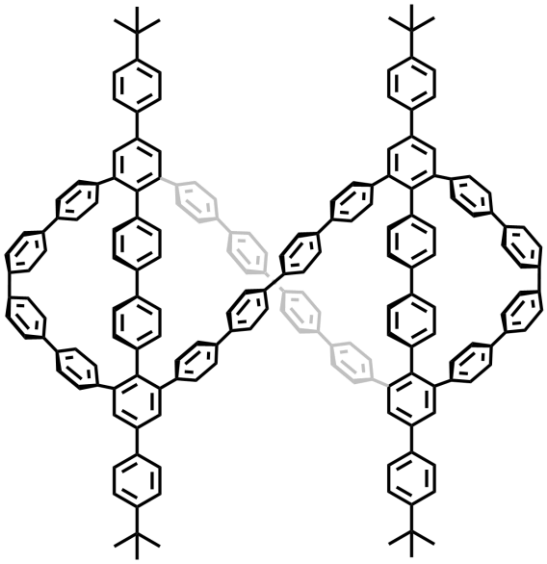

4-7

The same procedure with Oligophenylene bicyclophane (**4-13**). Purified by recycling preparative GPC with chloroform as eluent provided 1.1 mg of the title compound as a white solid (3% yield). MALDI-TOF MS (TCNQ as matrix): *m*/*z* calcd. for $C_{184}H_{140}$: 2351.1 [M^+]; found: 2351.1. Due to the absence of some contaminants inside the sample, the NMR spectra of this compound is quite complicated, and thus no accurate data can be provided here.

(2'''-(4-Bromophenyl)-5'''-(4-(tert-butyl)phenyl)-[1,1':4',1'':4'',1''':3''',1'''':4'''',1''''':4''''',1''''':4''''',1''''''-sepiphenyl]-4,4''''''-diyl)bis(trimethylsilane) (4-14)

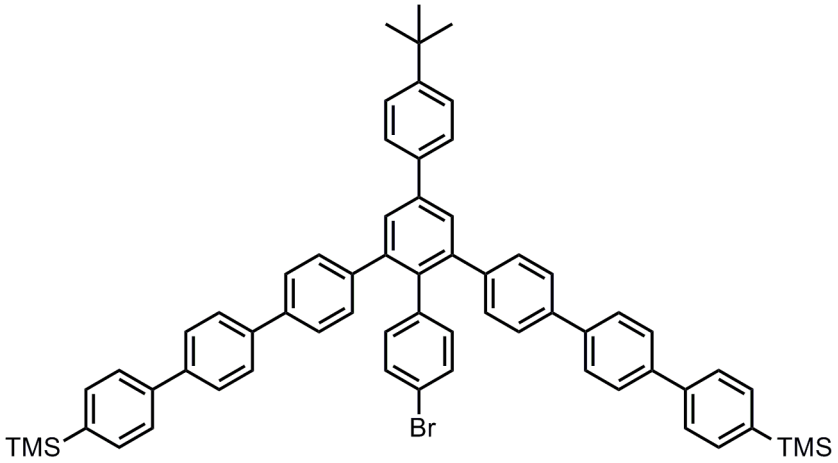

4-14

Firstly, the trimethylsilyl protecting group in the oligphenyleen precursor (2"-(4-bromophenyl)-5"-(4-(tert-butyl)phenyl)-[1,1':4',1":3",1"':4"',1""-quinquephenyl] -4,4""-diyl)bis(trimethylsilane) (**4-10**) (1.0 q, 940mg, 1.15 mmol) is converted to iodo atoms by treating with the solution of ICl (3.0 eq, 560mg, 3.46 mmol) in 10 mL DCM under ice bath following the same strategy toward **4-12**. After keeping stirring overnight, the reaction was quenched by addition of 100 mL MeOH into the mixture, and 940 mg white solid was filtrated and repeatedly washed with MeOH. Secondly, to a 250-mL two-necked round-bottom flask containing the obtained white solid (1.0 eq, 940 mg, 1.02 mmol), 4-(Trimethylsilyl)phenylboronic acid (2.0 eq, 400 mg, 2.04 mmol), $Pd(PPh_3)_4$ (0.08 eq, 94 mg, 0.08 mmol), and K_2CO_3 (6.0 eq, 846 mg, 6.12 mmol), was added 100 mL of degassed THF and 30 mL of a degassed mixture of ethanol and H_2O (1:1) under argon atmosphere. The reaction mixture was further degassed by three "freeze-pump-thaw" cycles, and then vigorously stirred at 60 °C overnight. After cooling to room temperature, the reaction mixture was extracted with dichloromethane (3 × 50 mL), and the combined organic layers were dried in vacuo. The crude product was purified by silica gel column chromatography with dichloromethane/hexane = 1/4 as eluent to yield 910 mg of the title compound as a white solid (82% yield). MALDI-TOF MS (TCNQ as matrix): *m*/*z* calcd. for $C_{64}H_{61}BrSi_2$: 966.3 [M^+]; found: 966.2. ^{1}H NMR (250 MHz, CD_2Cl_2): δ ppm 7.64 (m, 20H), 7.47 (t, 6H, J = 7.29 Hz), 7.16 (t, 6H, J = 8.20 Hz), 6.83 (d, 2H, J = 8.20 Hz), 1.30 (s, 9H), 0.24 (s, 18H). ^{13}C NMR (75 MHz, CD_2Cl_2): δ ppm 135.41, 135.03, 134.85, 132.47, 132.02, 131.56, 129.96 128.33, 127.66, 127.54, 127.38, 32.33, 28.29.

Tetra-(trimethylsilyl)-sustituted oligophenylene precursor (4-15)

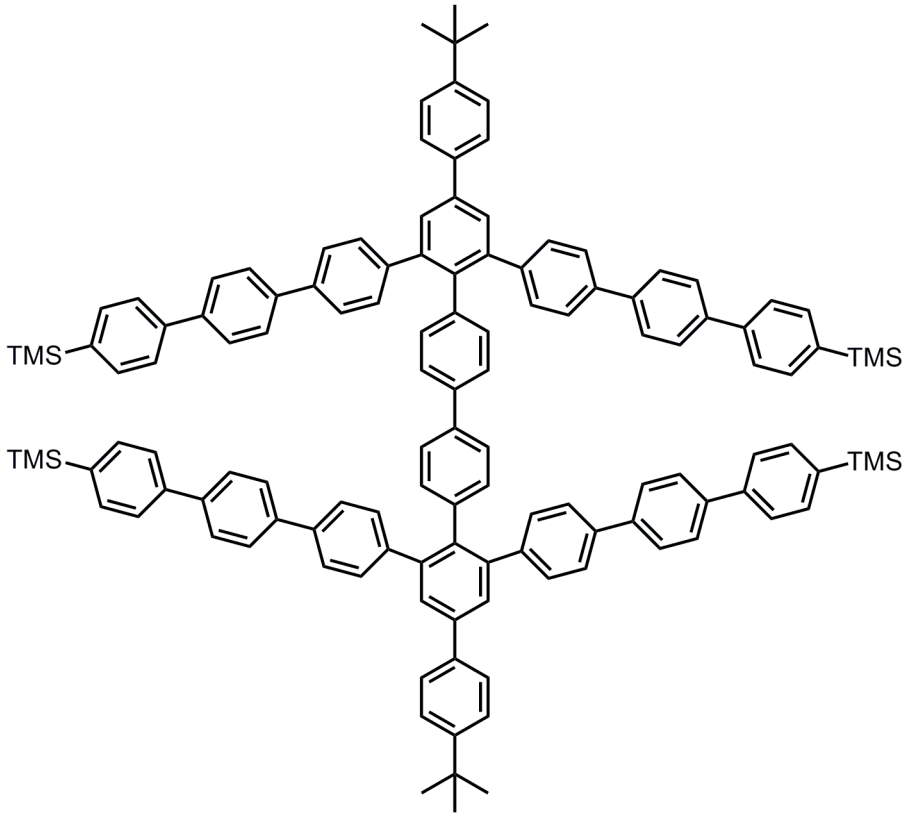

4-15

$Ni(COD)_2$ (2.05 eq, 114 mg, 0.41 mmol), oligophenylene precursor (**4-14**) (1.0 eq, 200 mg, 0.2 mmol), COD (2.05 eq, 45 mg, 0.41 mmol), and 2,2'-bipyridine (2.05 eq, 65 mg, 0.41 mmol) was added into a dried microwave tube in the glove box under the protection of argon gas. After addition of anhydrous toluene (20 mL) and anhydrous DMF (5 mL), the microwave tube was sealed with a microwave cap. The mixture was protected with aluminum foil against light before putting it into the microwave reactor. The heating program was started with pre-stirring of 1 min and heating at 120 ℃ for 8 h under microwave irradiation with maximum power of 200 W and activated cooling. After cooling to room temperature, the reaction mixture was passed through a pad of silica gel with tetrahydrofuran as eluent to remove the catalyst. The solution was concentrated in vacuo and poured into methanol to precipitate the resulting products. The crude product was then purified by silica gel column chromatography with dichloromethane/hexane = 1/3 as eluent to yield 170 mg of the title compound as

a white solid (96% yield). MALDI-TOF MS (TCNQ as matrix): *m*/*z* calcd. for $C_{128}H_{122}Si_4$: 1772.7 [M^+]; found: 1772.3. ^{1}H NMR (300 MHz, CD_2Cl_2): δ ppm 7.64 (m, 40H), 7.45 (m, 12H), 7.12 (m, 12H), 6.92 (d, 4H, J = 8.22 Hz), 1.28 (s, 18H), 0.23 (s, 36H). ^{13}C NMR (75 MHz, CD_2Cl_2): δ ppm 136.58, 136.01, 135.59, 135.21, 133.87, 132.02, 130.01, 129.11, 128.44, 128.13, 127.53, 127.36, 33.13, 28.02, 0.

Tetra-iodo-sustituted oligophenylene precursor (4-16)

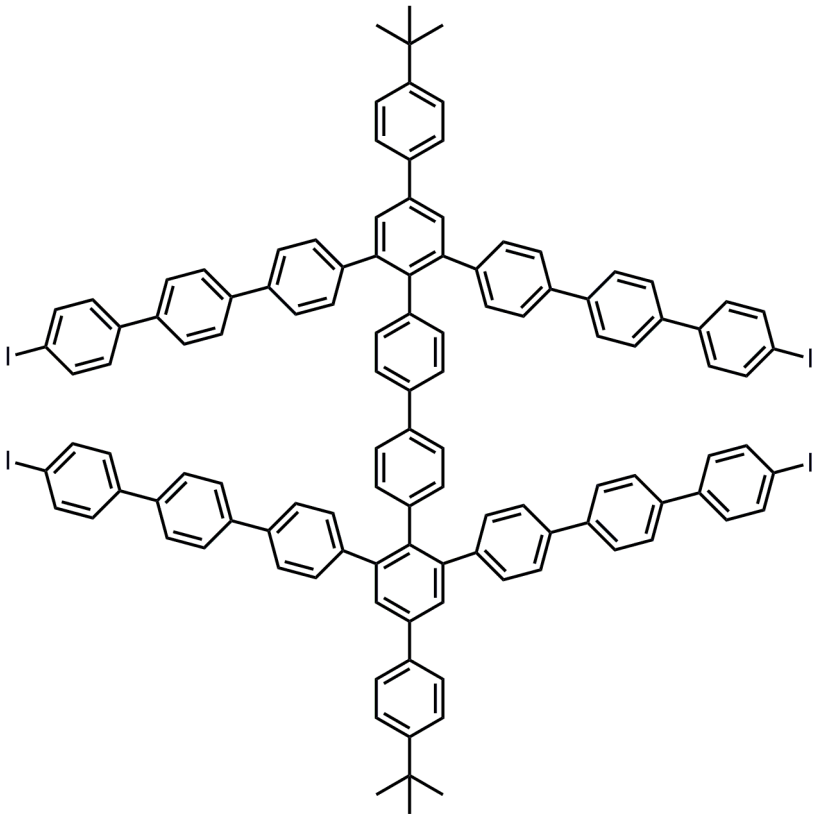

4-16

To the 100 mL two-necked flask containing tetra-TMS-sustituted oligophenylene precursor (**4-15**) (1.0 eq, 160 mg, 0.09 mmol) was added 50 mL anhydrous DCM under Argon gas, and then followed by the addition of the solution of ICl (8.0 eq, 120 mg, 0.72 mmol) in 10 mL DCM under ice bath. The reaction mixture was kept under vigorous stirring at room temperature overnight. Finally, 100 mL MeOH was added into the mixture to precipitate the product. After filtration and washing with MeOH and DCM, 175 mg of the titled compound was obtained as a white solid (99% yield). Because of the poor solubility of this compound in common organic solvent, the

compound is directly used without further purification and characterization.

Oligophenylene bicyclophane (4-17)

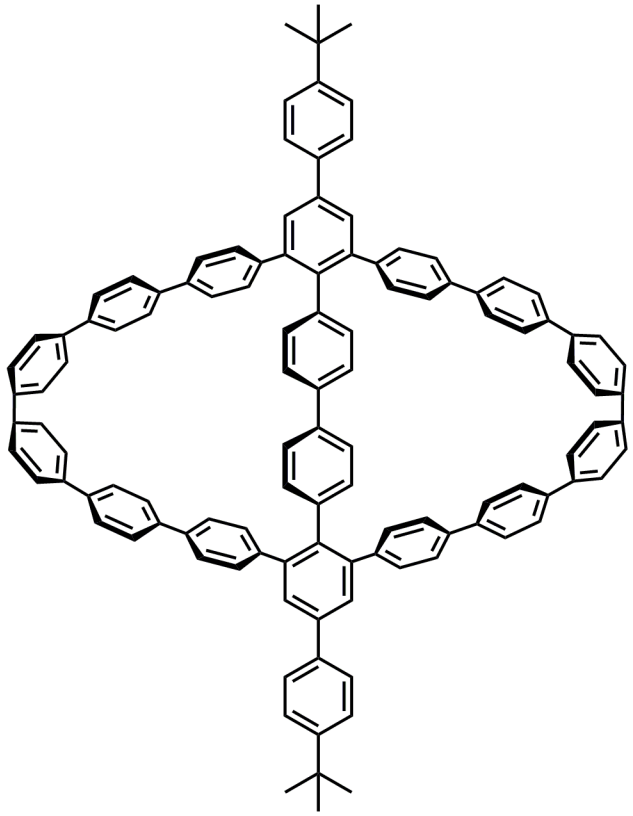

4-17

$Ni(COD)_2$ (8.0 eq, 55 mg, 0.2 mmol), Tetra-Iodo-sustituted Oligophenylene precursor (**4-16**) (1.0 eq, 50 mg, 0.025 mmol), COD (8.0 eq, 22 mg, 0.2 mmol), and 2,2'-bipyridine (8.0 eq, 32 mg, 0.2 mmol) was added into a dried microwave tube in the glove box under the protection of argon gas. After addition of anhydrous THF (20 mL), the microwave tube was sealed with a microwave cap. The mixture was protected with aluminum foil against light before putting it into the microwave reactor. The heating program was started with pre-stirring of 1 min and heating at 120 ℃ for 8 h under microwave irradiation with maximum power of 200 W and activated cooling. After cooling to room temperature, the reaction mixture was passed through a pad of silica gel with tetrahydrofuran as eluent to remove the catalyst. The solution was concentrated in vacuo and poured into methanol to precipitate the resulting products. Purified by recycling preparative GPC with chloroform as eluent provided

20 mg of the title compound as a white solid (54% yield). MALDI-TOF MS (TCNQ as matrix): *m*/*z* calcd. for $C_{116}H_{86}$: 1479.9 [M^+]; found: 1479.9.

Oligophenylene bicyclophane dimer (4-7)

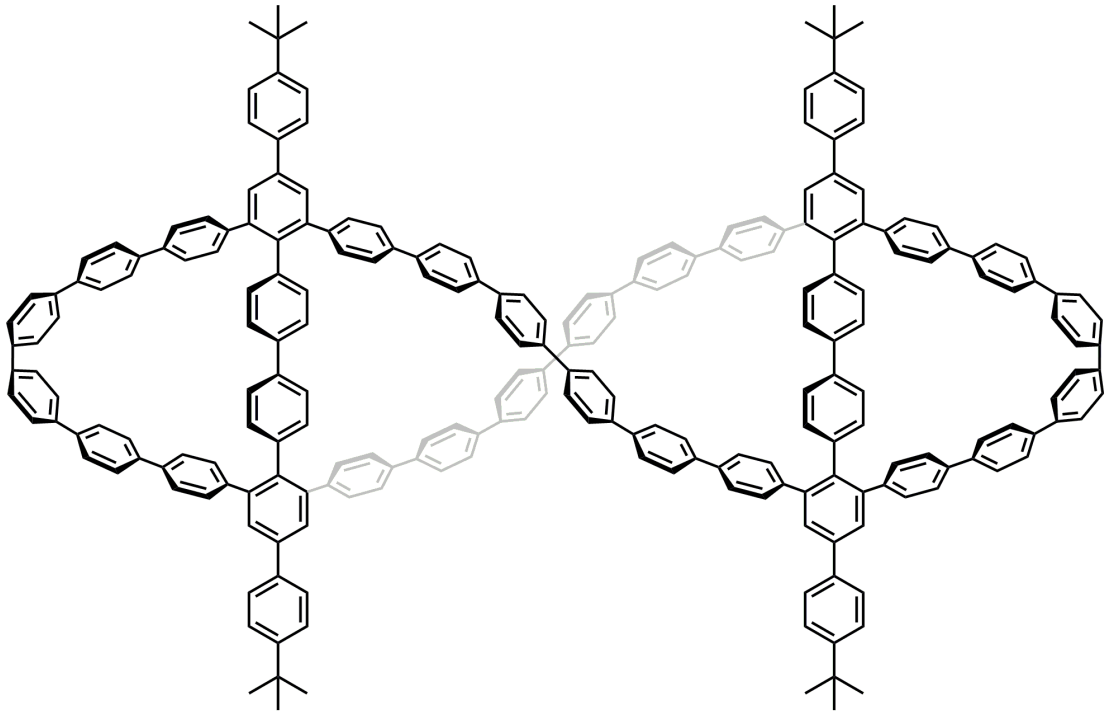

4-18

The same procedure with Oligophenylene bicyclophane (**4-17**). Purified by recycling preparative GPC with chloroform as eluent provided 0.7 mg of the title compound as a white solid (2% yield). MALDI-TOF MS (TCNQ as matrix): *m*/*z* calcd. for $C_{232}H_{172}$: 2959.9 [M^+]; found: 2959.8.

1-(4-Methoxyphenyl)-3-phenylprop-2-en-1-one (4-19)

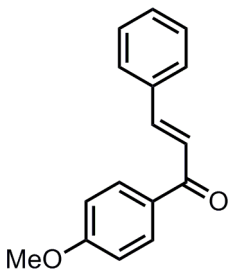

4-19

To a flask containing 4-methoxy-acetopheone (1.0 eq, 30 g, 0.2 mol) and

benzaldehyde (1.0 eq, 21.2 g, 0.2 mol)was added 200 mL MeOH, and followed by the dropwise addition of the aqueous solution of NaOH (16 g) in 40 mL. After stirring for 24 hrs, the precipitates were filtrated out and washing with MeOH and water. After drying in the oven, 37.0 g of the title compound is obtained as a white solid (78% yield). ^{1}H NMR (300 MHz, $CDCl_3$): δ ppm 7.96 (d, 2H, J = 9.37 Hz), 7.69 (d, 1H, J = 15.51 Hz), 7.59 (m, 2H), 7.50 (d, 1H, J = 15.51 Hz), 7.34 (m, 3H), 6.92 (d, 2H, J = 9.05 Hz), 3.80 (s, 3H). ^{13}C NMR (75 MHz, CD_2Cl_2): δ ppm 143.83, 131.59, 131.04, 130.67, 129.28, 128.70, 122.27, 55.92.

2-(4-Bromophenyl)-6-(4-methoxyphenyl)-4-phenylpyrylium tetrafluoroborate (4-20)

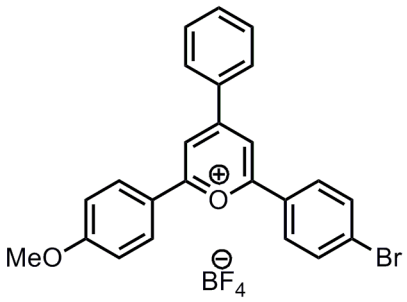

4-20

To a flask containing methyl (E)-1-(4-methoxyphenyl)-3-phenylprop-2-en-1-one (**4-19**) (1.0 eq, 36.3 g, 152 mmol) and 1-(4-bromophenyl)ethan-1-one (1.1 eq, 33.3 g, 167 mmol) was added BF_3-Et_2O (3.0 eq, 56 mL, 465 mmol) and 40 mL DCM. The reaction mixture was heated to 45 ℃ with vigorous stirring overnight. After cooling the mixture to room temperature, 100 mL of Et_2O was added into the flask with vigorous stirring to precipitate the desired pyrylium salt. After filtration and washing with Et_2O, 25.4 g of the title compound was obtained as a red solid (33% crude yield). This compound was used directly in the next step without further purification. ^{1}H NMR (300 MHz, DMSO-d_6): δ ppm 9.05 (d, 2H, J = 8.78 Hz), 8.60 (d, 2H, J = 8.78Hz), 8.55 (d, 2H, J = 7.88 Hz), 8.48 (d, 2H, J = 8.55 Hz), 8.0 (d, 2H, J = 8.34 Hz), 7.77 (m, 3H), 7.34 (d, 2H, J = 9.35 Hz), 3.99 (s, 3H). ^{13}C NMR (75 MHz, DMSO-d_6): δ ppm 134.86, 132.81, 131.60, 130.18, 129.77, 115.58, 56.17.

4,4''''-Dibromo-3',6'''-bis(4-methoxyphenyl)-4''',5'-diphenyl-1,1':2',1'':4'',1''':2''',1''''-quinquephenyl (4-21)

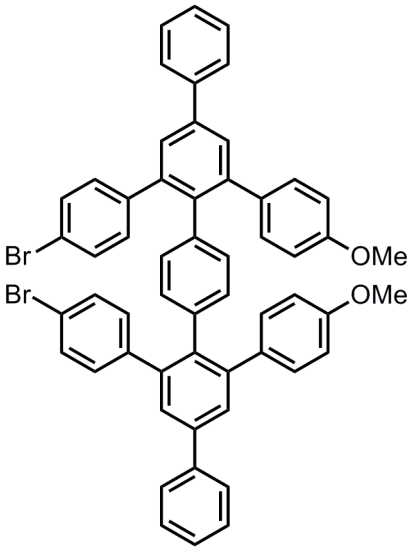

4-21

To a two-necked round-bottom flask containing 2-(4-bromophenyl)-6-(4-methoxyphenyl)-4-phenylpyrylium tetrafluoroborate (**4-20**) (2.5 eq, 20.8 g, 41.1 mmol) and sodium 2,2'-(1,4-phenylene)diacetate (1.0 eq, 3.92 g, 16.4 mmol) was added 80 mL of acetic anhydride. After stirring at 150 ℃ for 12 h, the reaction mixture was cooled to room temperature, and then poured into 400 mL of MeOH. The precipitates were collected by filtration and washed with MeOH. The crude product was further purified by silica gel column chromatography with dichloromethane (DCM)/hexane = 1/2 as eluent to yield 1.78 g of the title compound as a white solid (12% yield). ^{1}H NMR (300 MHz, CD_2Cl_2): δ ppm 7.60 (d, 4H, J = 7.58 Hz), 7.52 (d, 2H, J = 2.02 Hz), 7.46 (d, 2H, J = 1.86 Hz), 7.37 (t, 4H, J = 7.62 Hz), 7.28 (m, 6H), 6.90 (d, 8H, J = 8.63 Hz), 6.68 (d, 4H, J = 8.82 Hz), 6.52 (s, 4H), 3.72 (s, 6H). ^{13}C NMR (75 MHz, CD_2Cl_2): δ ppm 132.11, 131.42, 131.28, 131.01, 129.23, 129.13, 123.22, 127.97, 127.38, 113.39, 55.57.

Oligophenylene monocyclophane (4-22)

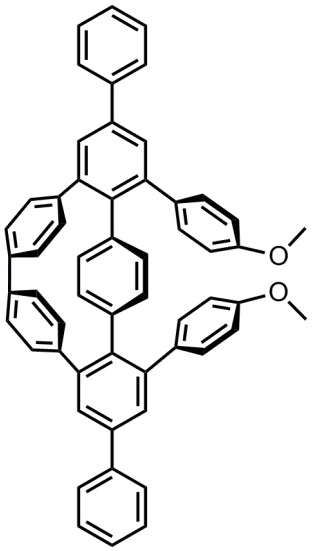

4-22

$Ni(COD)_2$ (4.6 eq, 70 mg, 0.25 mmol), 4,4''''-dibromo-3',6'''-bis(4-methoxyphenyl)--4''',5'-diphenyl-1,1':2',1'':4'',1''':2''',1''''-quinquephenyl (**4-21**) (1.0 eq, 50 mg, 0.055 mmol), COD (4.6 eq, 27 mg, 0.25 mmol), and 2,2'-bipyridine (4.6 eq, 40 mg, 0.25 mmol) was added into a dried microwave tube in the glove box under the protection of argon gas. After addition of anhydrous THF (20 mL), the microwave tube was sealed with a microwave cap. The mixture was protected with aluminum foil against light before putting it into the microwave reactor. The heating program was started with pre-stirring of 1 min and heating at 120 ℃ for 8 h under microwave irradiation with maximum power of 200 W and activated cooling. After cooling to room temperature, the reaction mixture was passed through a pad of silica gel with tetrahydrofuran as eluent to remove the catalyst. The solution was concentrated in vacuo and poured into methanol to precipitate the resulting products. Purified by recycling preparative GPC with chloroform as eluent provided 13 mg of the title compound as a white solid (32% yield). MALDI-TOF MS (TCNQ as matrix): *m*/*z* calcd. for $C_{56}H_{40}O_2$: 744.9 [M^+]; found: 744.7. ^{1}H NMR (500 MHz, CD_2Cl_2): δ ppm; 7.90 (d, 2H, *J* = 2.08 Hz), 7.77 (d, 4H, *J* = 7.72 Hz), 7.52 (t, 4H, *J* = 7.72 Hz), 7.48 (d, 2H, *J* = 2.05 Hz), 7.42 (d, 2H, *J* = 7.40 Hz), 7.37 (d, 4H, *J* = 8.82 Hz), 7.15 (d, 4H, *J* = 8.66 Hz), 6.89 (d, 4H, *J* = 8.66 Hz), 6.62 (d, 4H, *J* = 8.98 Hz), 6.39 (s, 4H), 3.81 (s,

6H). ^{13}C NMR (125 MHz, CD_2Cl_2): δ ppm; 158.05, 142.57, 142.27, 141.02, 140.56, 140.28, 139.04, 137.03, 136.23, 134.07, 130.54, 129.97, 129.63, 128.85, 128.80, 128.46, 127.51, 127.01, 124.10, 112.98, 54.89.

Twisted oligophenylene monocyclophane (4-23)

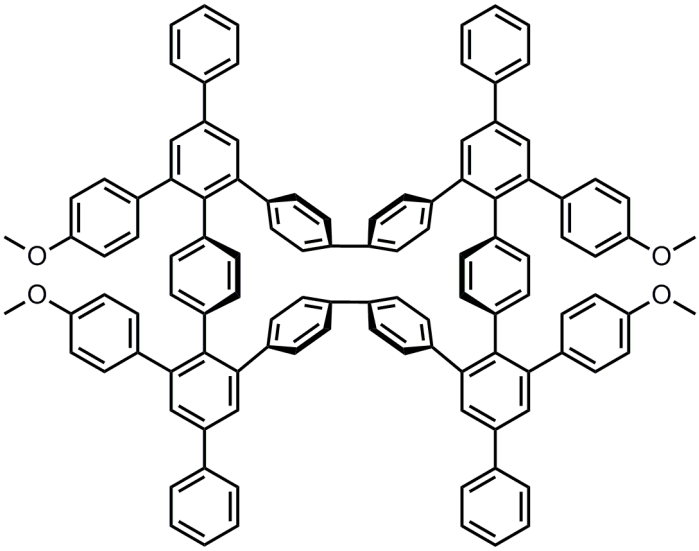

4-23

For the crude product of the Yamamoto reaction of compound **4-21**, purification by recycling preparative GPC with chloroform as eluent provided 10 mg of the title compound as a white solid (28% yield). MALDI-TOF MS (TCNQ as matrix): *m*/*z* calcd. for $C_{112}H_{80}O_4$: 1489.9 [M^+]; found: 1489.7. ^{1}H NMR (500 MHz, CD_2Cl_2): δ ppm; 7.74 (d, 8H, J = 8.24 Hz), 7.65 (d, 4H, J = 2.09 Hz), 7.63 (d, 4H, J = 1.95 Hz), 7.49 (m, 16H), 7.40 (t, 4H, J = 7.68 Hz), 7.23 (d, 8H, J = 8.31 Hz), 7.07 (d, 8H, J = 8.80 Hz), 6.80 (m, 16H), 3.86 (s, 12H). ^{13}C NMR (125 MHz, CD_2Cl_2): δ ppm; 158.27, 142.28, 141.77, 141.17, 140.34, 139.34, 137.54, 137.17, 134.17, 131.03, 130.67, 128.80, 127.0, 125.59, 113.01, 55.10.

7.3.3 Derivatizing sulfur incorporated hexa-*peri*-hexabenzocoronenes with tunable optoelectronic properties

2-Hexyl-decylbromide and 2-decyl-tetradecylbromide were prepared according to previous literature.[3]

1-(2-Bromo-4-methoxyphenyl)ethanone (5-1)

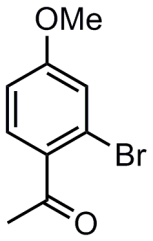

5-1

1-(2-bromo-4-methoxyphenyl)ethanone **5-1** was synthesized as formerly reported.[4]

2,2''-dibromo-5'-(2-bromo-4-methoxyphenyl)-4,4''-dimethoxy-1,1':3',1''-terphenyl (5-2)

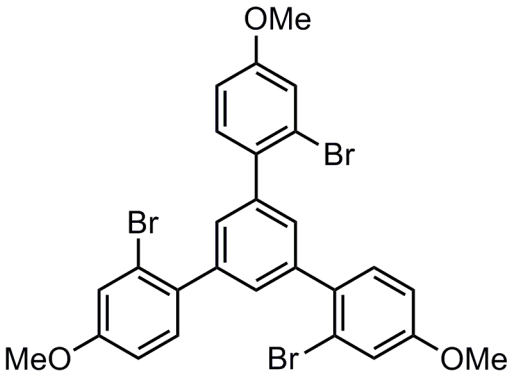

5-2

2,2''-dibromo-5'-(2-bromo-4-methoxyphenyl)-4,4''-dimethoxy-1,1':3',1''-terphenyl **5-2** was prepared as literature reported. [5]

1,1'-(5'-(2-(Dibenzo[b,d]thiophen-1-yl)-4-methoxyphenyl)-4,4''-dimethoxy-[1,1':3',1''-terphenyl]-2,2''-diyl)didibenzo[b,d]thiophene (5-3)

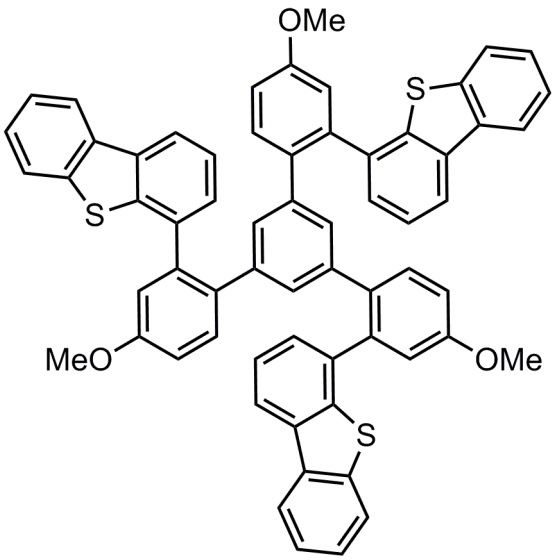

5-3

3.40 g (5.38 mmol) **5-2**, 4.65 g (19.36 mmol) 4-dibenzothiopheneboronic acid, 624 mg (10mol%) $Pd(PPh_3)_4$, 8.92 g K_2CO_3, 30 mL toluene, 6 mL EtOH and 6 mL H_2O were added into 250mL Schlenk flask. The mixture was degassed by four "freeze-pump-thaw"cycles and then heated to reflux overnight. After standard work-up and purification by column chromatography (Silica gel, PE/DCM =2/1), 4.85 g white solid was obtained (96.6%). FD-MS (8 KV): m/z 942.9, calcd.: 943.2 (M+). ^{1}H NMR (300 MHz, CD_2Cl_2): δ ppm 8.26 (d, 3H, J= 6.70 Hz), 8.09 (d, 3H, J= 7.84 Hz), 7.86 (d, 3H, J= 6.74 Hz), 7.54 (m, 6H), 7.06 (m, 6H), 6.51 (m, 12H), 3.77 (s, 9H). ^{13}C NMR (75 MHz, CD_2Cl_2): δ ppm 158.89, 140.19, 139.82, 139.63, 137.02, 136.12, 135.92, 133.46, 131.63, 128.89, 128.38, 127.10, 124.73, 123.14, 122.04, 120.20, 115.18, 114.06, 55.60.

2,2''-Bis(dibenzo[b,d]thiophen-4-yl)-5'-(2-(dibenzo[b,d]thiophen-4-yl)-4-hydroxy phenyl)-[1,1':3',1''-terphenyl]-4,4''-diol (5-4)

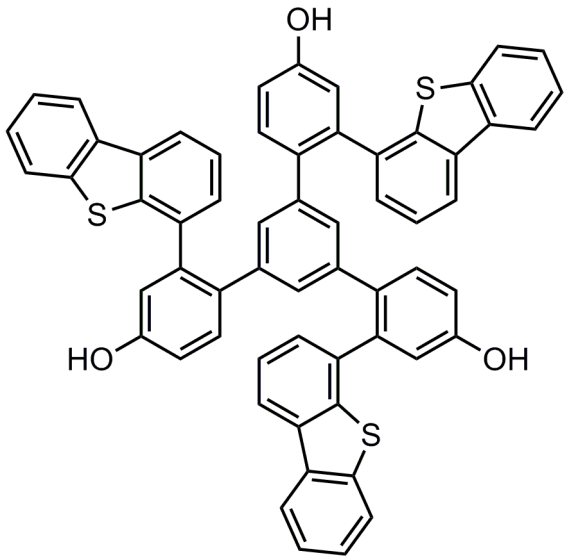

5-4

11 mL (4.5 eq, 11 mmol) BBr_3 solution (1 M) in DCM was added into the solution of **5-3** (2.33 g, 2.47 mmol) in 50 mL under liquid nitrogen/acetone bath with protection of argon gas. The mixture was kept stirring under room temperature overnight, and quenched with 40 mL 1 M HCl solution. The organic phase was separated, and the aqueous layer was washed with CH_2Cl_2 (3 × 40 mL). The combined organic phase was washed with H_2O (50 mL), brine (50 mL), dried over $MgSO_4$, and the solvent was removed in *vacuo*. 2.15 g pale white solid was obtained (96%). ^{1}H NMR (300 MHz, CD_2Cl_2): δ ppm 8.22 (m, 3H), 8.07 (d, 3H, J= 7.96 Hz), 7.81 (d, 3H, J= 7.25 Hz), 7.61 (m, 6H), 6.99 (m, 6H), 6.51 (m, 12H). ^{13}C NMR (75 MHz, CD_2Cl_2): δ ppm 153.89, 138.86, 134.94, 134.69, 132.42, 130.79, 127.73, 127.17, 125.96, 123.59, 121.98, 120.84, 119.06, 115.56, 114.49.

4,4'-(5'-(2-(Dibenzo[b,d]thiophen-4-yl)-4-(3,7-dimethyloctyloxy)phenyl)-4,4''-bis(3,7-dimethyloctyloxy)-[1,1':3',1''-terphenyl]-2,2''-diyl)didibenzo[b,d]thiophene (5-5a)

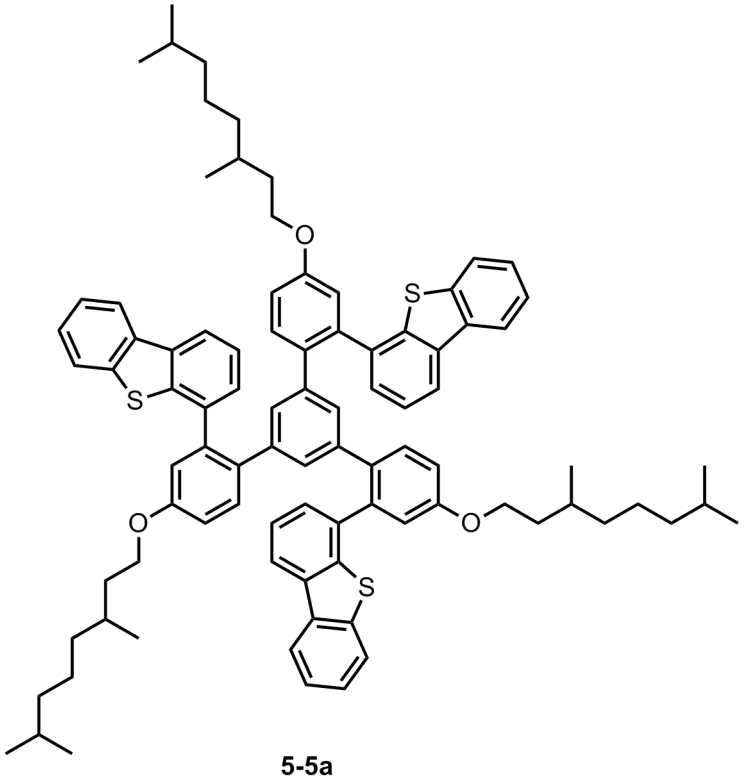

5-5a

730 mg (0.81 mmol) **5-4**, 1.8 g (10.0 eq, 8.1 mmol) 3,7-dimethyloctyl bromide, 2.24 g K_2CO_3,(20.0 eq, 16.2 mmol), and 40 mL anhydrous DMF were added into 100mL flask. The mixture was heated to 110 ℃ with stirring overnight. After standard work-up and purification by column chromatography (Silica gel, PE/DCM =4/1), 360 mg white solid was obtained (35%). FD-MS (8 KV): m/z 1321.5, calcd.: 1321.92 (M+). ^{1}H NMR (300 MHz, CD_2Cl_2): δ ppm 8.22 (d, 3H, J= 6.87 Hz), 8.05 (d, 3H, J= 7.94 Hz), 7.79 (d, 3H, J= 7.44 Hz), 7.49 (m, 6H), 7.00 (m, 3H), 6.92 (d, 3H, J= 2.62 Hz), 6.52 (m, 12H), 3.92 (m, 6H), 1.77 (m, 3H), 1.57 (m, 9H), 1.23 (m, 18H), 0.91 (d, 9H, J= 6.36Hz), 0.86 (d, 18H, J= 6.61Hz). ^{13}C NMR (75 MHz, CD_2Cl_2): δ ppm 158.21, 139.94, 139.49, 137.03, 135.97, 135.74, 133.24, 131.46, 128.77, 128.39, 126.90, 124.65, 123.03, 121.87, 120.07, 115.68, 114.52, 66.69, 39.54, 37.60, 36.38, 30.18, 28.33, 24.98, 22.81, 22.71, 19.69.

4,4'-(5'-(2-(Dibenzo[b,d]thiophen-4-yl)-4-(2-hexyl-1-decyloxy)phenyl)-4,4''-bis(2-hexyl-1-decyloxy)-[1,1':3',1''-terphenyl]-2,2''-diyl)didibenzo[b,d]thiophene (5-5b)

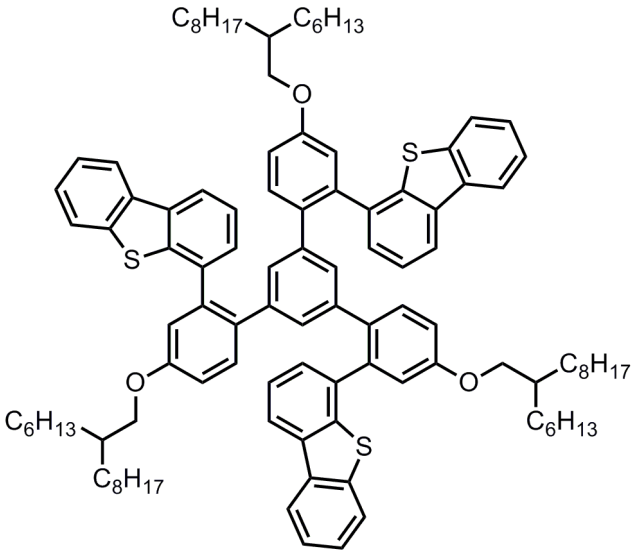

5-5b

360 mg (0.4 mmol) **5-4**, 1.2 g (10.0 eq, 4.0 mmol) 2-hexyl-1-decyl bromide, 1.10 g K_2CO_3,(20.0 eq, 8.0 mmol), and 20 mL anhydrous DMF were added into 100mL flask. The mixture was heated to 110 ℃ with stirring overnight. After standard work-up and purification by column chromatography (Silica gel, PE/DCM =4/1), 280 mg white solid was obtained (44%). FD-MS (8 KV): m/z 1574.2, calcd.: 1574.40 (M+). ^{1}H NMR (300 MHz, CD_2Cl_2): δ ppm 8.25 (d, 3H, J= 6.70 Hz), 8.09 (d, 3H, J= 7.84 Hz), 7.83 (d, 3H, J= 6.74 Hz), 7.53 (m, 6H), 7.00 (m, 6H), 6.52 (m, 12H), 3.80 (d, 6H), 1.76 (m, 3H), 1.31 (m, 72H), 0.91 (m, 18H). ^{13}C NMR (75 MHz, CD_2Cl_2): δ ppm 161.26, 158.67, 140.12, 139.62, 137.15, 136.13, 135.87, 133.21, 131.53, 128.92, 128.19, 126.95, 124.60, 123.09, 122.04, 120.15, 115.66, 114.74, 71.33, 66.64, 38.23, 37.60, 32.19, 31.62, 31.40, 30.33, 29.99, 29.63, 27.01, 22.96, 14.17.

4,4'-(5'-(2-(Dibenzo[b,d]thiophen-4-yl)-4-(dodecyloxy)phenyl)-4,4''-bis(dodecyloxy)-[1,1':3',1''-terphenyl]-2,2''-diyl)didibenzo[b,d]thiophene (5-5c)

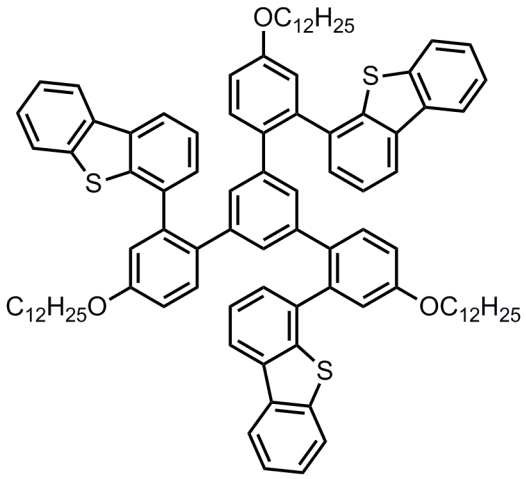

5-5c

360 mg (0.4 mmol) **5-4**, 1.0 g (10.0 eq, 4.0 mmol) dodecyl bromide, 1.10 g K_2CO_3,(20.0 eq, 8.0 mmol), and 20 mL anhydrous DMF were added into 100mL flask. The mixture was heated to 110 ℃ with stirring overnight. After standard work-up and purification by column chromatography (Silica gel, PE/DCM =4/1), 264 mg white solid was obtained (47%). FD-MS (8 KV): m/z 1406.5, calcd.: 1406.08 (M+). ^{1}H NMR (300 MHz, CD_2Cl_2): δ ppm 8.25 (d, 3H, J= 6.92 Hz), 8.08 (d, 3H, J= 7.82 Hz), 7.83 (d, 3H, J= 7.65 Hz), 7.53 (m, 6H), 7.04 (m, 3H), 6.97 (d, 3H, J= 2.66 Hz), 6.57 (m, 12H), 3.91 (t, 6H, J= 6.57 Hz), 1.76 (m, 6H), 1.34 (m, 60H), 0.88 (m, 9H). ^{13}C NMR (75 MHz, CD_2Cl_2): δ ppm 158.30, 140.14, 139.71, 136.91, 136.14, 135.89, 133.28, 131.60, 128.89, 128.23, 127.08, 124.61, 123.13, 122.05, 120.09, 115.65, 114.68, 68.41, 32.22, 30.01, 29.74, 29.58, 26.22, 22.98, 14.19.

4,4'-(5'-(2-(Dibenzo[b,d]thiophen-4-yl)-4-(2-decyl-1-tetradecyloxy)phenyl)-4,4''-bis(2-decyl-1-tetradecyloxy)-[1,1':3',1''-terphenyl]-2,2''-diyl)didibenzo[b,d]thiophene (5-5d)

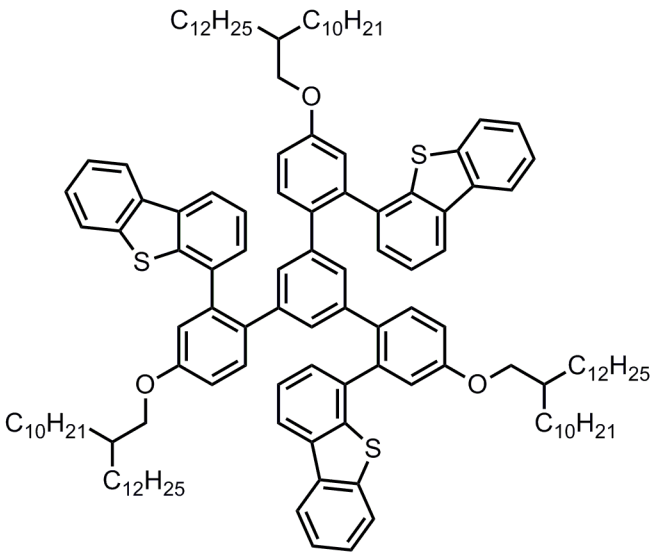

5-5d

360 mg (0.4 mmol) **5-4**, 2.0 g (10.0 eq, 4.0 mmol) 2-decyl-1-tetradecyl bromide, 1.10 g K_2CO_3,(20.0 eq, 8.0 mmol), and 20 mL anhydrous DMF were added into 100mL flask. The mixture was heated to 110 ℃ with stirring overnight. After standard work-up and purification by column chromatography (Silica gel, PE/DCM =4/1), 464 mg white solid was obtained (58%). FD-MS (8 KV): m/z 1910.4, calcd.: 1911.03 (M+). ^{1}H NMR (300 MHz, CD_2Cl_2): δ ppm 8.22 (d, 3H, J= 6.88 Hz), 8.05 (d, 3H, J= 8.28 Hz), 7.79 (d, 3H, J= 7.36 Hz), 7.49 (m, 6H), 7.20-6,20 (b, 15H), 3.77 (d, 6H, J= 5.59 Hz), 1.75 (b, 3H), 1.27 (b, 120H), 0.88 (m, 18H). ^{13}C NMR (75 MHz, CD_2Cl_2): δ ppm 158.71, 140.23, 139.70, 137.21, 136.18, 135.91, 133.26, 131.69, 129.00, 128.40, 127.09, 124.73, 123.19, 122.08, 120.18, 115.81, 114.76, 71.52, 38.28, 32.33, 31.70, 30.41, 30.07, 29.75, 27.19, 23.09, 14.28.

4,4''-(5'-(2-(Dibenzo[b,d]thiophen-4-yl)-4-(hexadecyloxy)phenyl)-4,4''-bis(hexadecyloxy)-[1,1':3',1''-terphenyl]-2,2''-diyl)didibenzo[b,d]thiophene (5-5e)

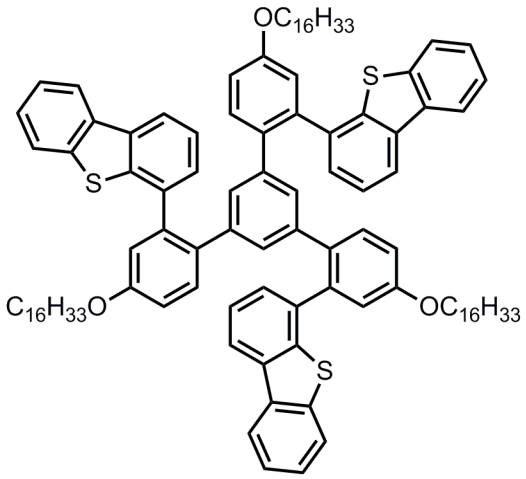

5-5e

360 mg (0.4 mmol) **5-4**, 1.2 g (10.0 eq, 4.0 mmol) hexadecyl bromide, 1.10 g K_2CO_3,(20.0 eq, 8.0 mmol), and 20 mL anhydrous DMF were added into 100mL flask. The mixture was heated to 110 ℃ with stirring overnight. After standard work-up and purification by column chromatography (Silica gel, PE/DCM =4/1), 250 mg white solid was obtained (40%). FD-MS (8 KV): m/z 1574.7, calcd.: 1574.40 (M+). ^{1}H NMR (300 MHz, CD_2Cl_2): δ ppm 8.25 (d, 3H, J= 6.79 Hz), 8.08 (d, 3H, J= 7.66 Hz), 7.83 (d, 3H, J= 7.66 Hz), 7.53 (m, 6H), 7.04 (m, 3H), 6.97 (d, 3H, J= 2.63 Hz), 6.51 (m, 12H), 3.91 (t, 6H, J= 6.53 Hz), 1.75 (m, 6H), 1.29 (m, 84H), 0.90 (m, 9H). ^{13}C NMR (75 MHz, CD_2Cl_2): δ ppm 158.32, 140.09, 139.60, 137.08, 136.05, 135.70, 133.02, 131.47, 128.80, 128.34, 126.70, 124.70, 122.99, 122.03, 120.13, 115.62, 114.62, 68.40, 32.28, 30.02, 29.75, 29.55, 26.30, 23.02, 14.22.

5,11,17-Tris(3,7-dimethyloctyloxy)-trisbenzothieno[1,2:7,8:13,14]hexa-peri-hexabenzocoronene (5-6a)

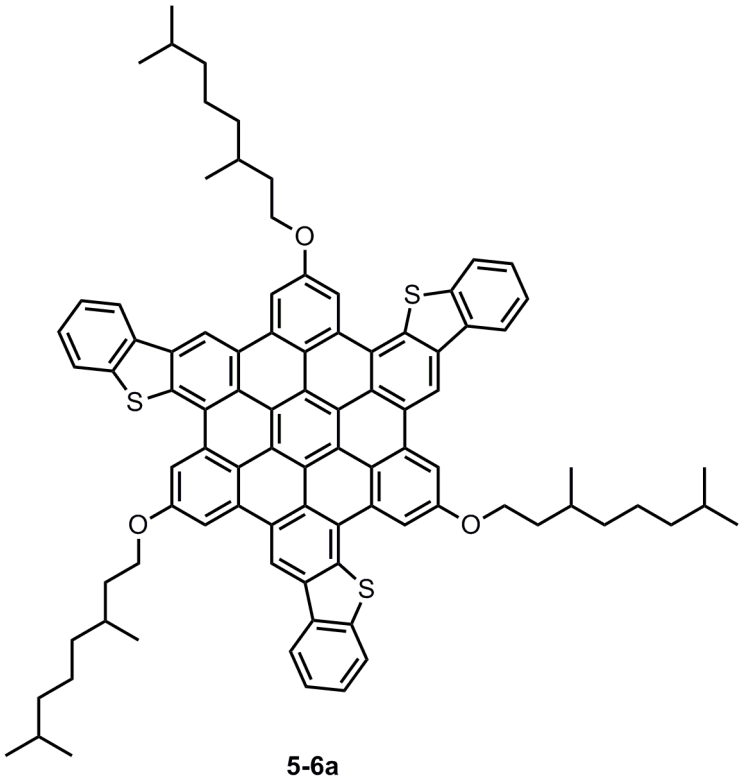

5-6a

212 mg (0.16 mmol) **5-5a** was dissolved in 60 mL anhydrous dichloromethane, the solution was then degassed by bubbling through argon for 30 min, and then 1.24 mg $FeCl_3$ in 4 mL CH3NO2 was added dropwise. After being stirred for 60 min, the reaction was quenched by adding 100mL methanol, the yellow precipitate was collected, washed by methanol and water repeatedly and dried under vacuum to afford 201 mg yellow powder (95%). MALDITOF-MS (TCNQ as matrix): m/z= 1309.9, calcd. 1309.82 for $C_{90}H_{84}O_3S_3$. ^1H NMR (500 MHz, $C_2D_2Cl_4$, 403K): 8.7-6.8 (b, 21H), 4,4-4,0 (b, 6H), 2,2-0.6 (b, 57H).

5,11,17-Tris(2-hexyl-1-decyloxy)-trisbenzothieno[1,2:7,8:13,14]hexa-peri-hexabenzocoronene (5-6b)

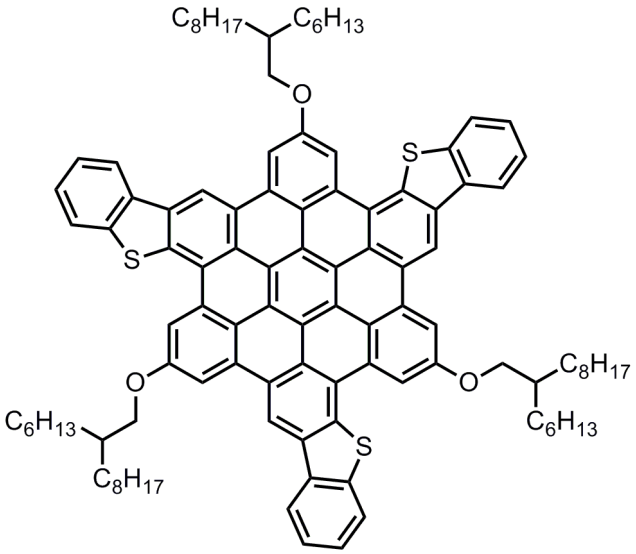

5-6b

340 mg (0.21 mmol) **5-5b** was dissolved in 100 mL anhydrous dichloromethane, the solution was then degassed by bubbling through argon for 30 min, and then 1.26 g $FeCl_3$ in 4 mL CH3NO2 was added dropwise. After being stirred for 60 min, the reaction was quenched by adding 100mL methanol, the yellow precipitate was collected, washed by methanol and water repeatedly and dried under vacuum to afford 238 mg yellow powder (70%). MALDITOF-MS (TCNQ as matrix): m/z= 1561.8, calcd. 1562.30 for $C_{108}H_{120}O_3S_3$. ^{1}H NMR (500 MHz, $C_2D_2Cl_4$, 403K): 8.90 (s, 3H), 8.43 (s, 3H), 8.27 (s, 3H), 8.01 (s, 3H), 7.85 (s, 3H), 7.59 (m, 6H), 4.34 (s, 6H), 2.24 (s, 3H), 1.56 (m, 72H), 1.01 (d, 18H)..

5,11,17-Tris-*n*-dodecyloxy-trisbenzothieno[1,2:7,8:13,14]hexa-peri-hexabenzocoronene (5-6c)

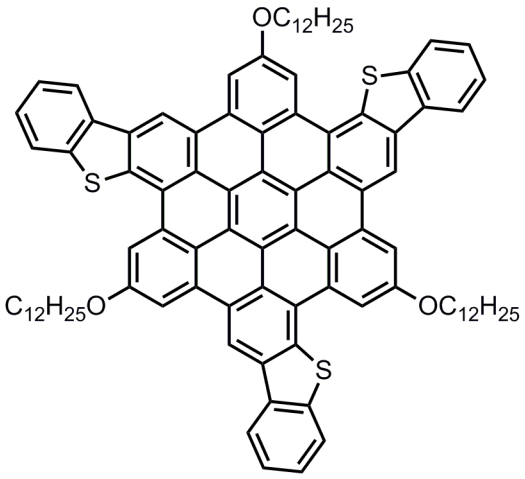

5-6c

216 mg (0.15 mmol) **5-5c** was dissolved in 60 mL anhydrous dichloromethane, the solution was then degassed by bubbling through argon for 30 min, and then 1.2 g $FeCl_3$ in 4 mL CH3NO2 was added dropwise. After being stirred for 60 min, the reaction was quenched by adding 100mL methanol, the yellow precipitate was collected, washed by methanol and water repeatedly and dried under vacuum to afford 144 mg yellow powder (67%). MALDITOF-MS (TCNQ as matrix): m/z= 1394.0, calcd. 1393.98 for $C_{96}H_{96}O_3S_3$. ^{1}H NMR (500 MHz, $C_2D_2Cl_4$, 403K): 8.25 (s, 3H), 7.92 (s, 3H), 7.68 (b, 6H), 7.40 (b, 9H), 3.93 (s, 6H), 1.97 (s, 6H), 1.56 (b, 54H), 0.98 (m, 9H).

5,11,17-Tris(2-decyl-1-tetradecyloxy)-trisbenzothieno[1,2:7,8:13,14]hexa-peri-hexabenzocoronene (5-6d)

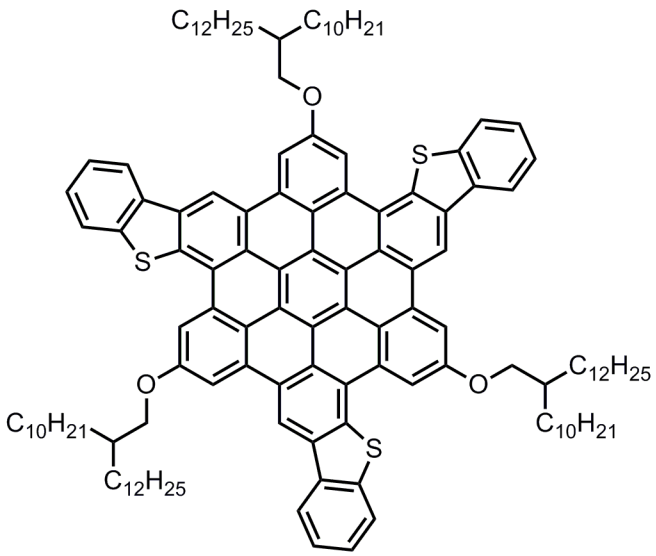

5-6d

309 mg (0.16 mmol) **5-5d** was dissolved in 100 mL anhydrous dichloromethane, the solution was then degassed by bubbling through argon for 30 min, and then 930 mg $FeCl_3$ in 4 mL CH3NO2 was added dropwise. After being stirred for 60 min, the reaction was quenched by adding 100mL methanol, the yellow precipitate was collected, washed by methanol and water repeatedly and dried under vacuum to afford 242 mg yellow powder (78%). MALDITOF-MS (TCNQ as matrix): m/z= 1898.0, calcd. 1898.94 for $C_{132}H_{168}O_3S_3$. ^{1}H NMR (500 MHz, $C_2D_2Cl_4$, 403K): 9.01 (s, 3H), 8.53 (s, 3H), 8.34 (s, 3H), 8.12 (s, 3H), 7.89 (s, 3H), 7.60 (m, 6H), 6.81 (b, 3H), 4.41 (s, 6H), 2.27 (s, 3H), 1.60 (m, 120H), 0.90 (s, 18H).

5,11,17-Tris-*n*-hexadecyloxy-trisbenzothieno[1,2:7,8:13,14]hexa-peri-hexabenzocoronene (5-6e)

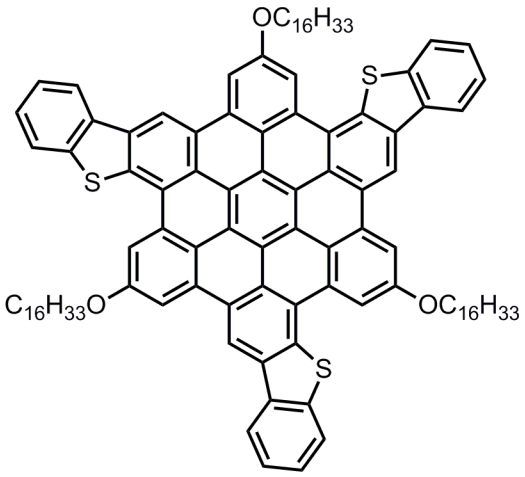

5-6e

224 mg (0.14 mmol) **5-5d** was dissolved in 60 mL anhydrous dichloromethane, the solution was then degassed by bubbling through argon for 30 min, and then 1.10 g $FeCl_3$ in 5 mL CH3NO2 was added dropwise. After being stirred for 60 min, the reaction was quenched by adding 100mL methanol, the yellow precipitate was collected, washed by methanol and water repeatedly and dried under vacuum to afford 153 mg yellow powder (68%). MALDITOF-MS (TCNQ as matrix): m/z= 1562.8, calcd. 1562.30 for $C_{108}H_{120}O_3S_3$. ^{1}H NMR (500 MHz, $C_2D_2Cl_4$, 403K): 8.46 (s, 3H), 8.04 (s, 3H), 7.94 (s, 3H), 7.76 (s, 3H), 7.50 (m, 9H), 4.10 (s, 6H), 2.05 (s, 6H), 1.52 (m, 78H), 0.94 (m, 9H).

2,2''-Bis(dibenzo[b,d]thiophen-4-yl)-5'-(2-(dibenzo[b,d]thiophen-4-yl)-4-(((trifluoromethyl)sulfonyl)oxy)phenyl)-[1,1':3',1''-terphenyl]-4,4''-diyl bis(trifluoromethanesulfonate) (5-7)

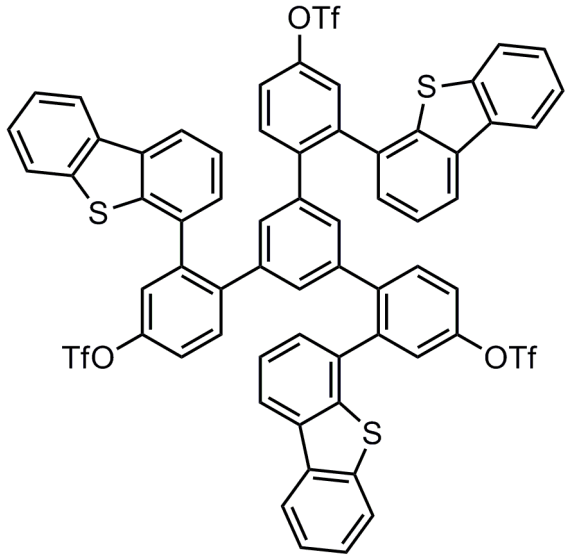

5-7

To the solution of 1.08 g (1.19 mmol) **5-4** and 1.3 mL (8.0 eq, 9.5 mmol) triethylamine in 50 mL DCM, was added 4.8 mL (4.0 eq, 4.8 mmol) trifluoromethylsufonyl anhydride (1 M in DCM) under ice bath. 50 mL H_2O was added to quench the reaction after 2 hours. After standard work-up and purification by column chromatography (Silica gel, PE/DCM =1/3), 1.04 g white solid was obtained (67%). MALDITOF-MS (in DCM): m/z 1296.5, calcd.: 1297.30 for $C_{63}H_{33}F_9O_9S_6$. ^1H NMR (250 MHz, CD_2Cl_2): 8.27 (m, 3H), 8.13 (d, 3H, J = 7.96 Hz), 7.86 (m, 3H), 7.57 (m, 6H), 7.41 (m, 3H), 7.2-6.4 (m, 15H).

4,4'-(5'-(2-(Dibenzo[b,d]thiophen-4-yl)-4-(dodec-1-yn-1-yl)phenyl)-4,4''-di(dodec-1-yn-1-yl)-[1,1':3',1''-terphenyl]-2,2''-diyl)didibenzo[b,d]thiophene (5-8)

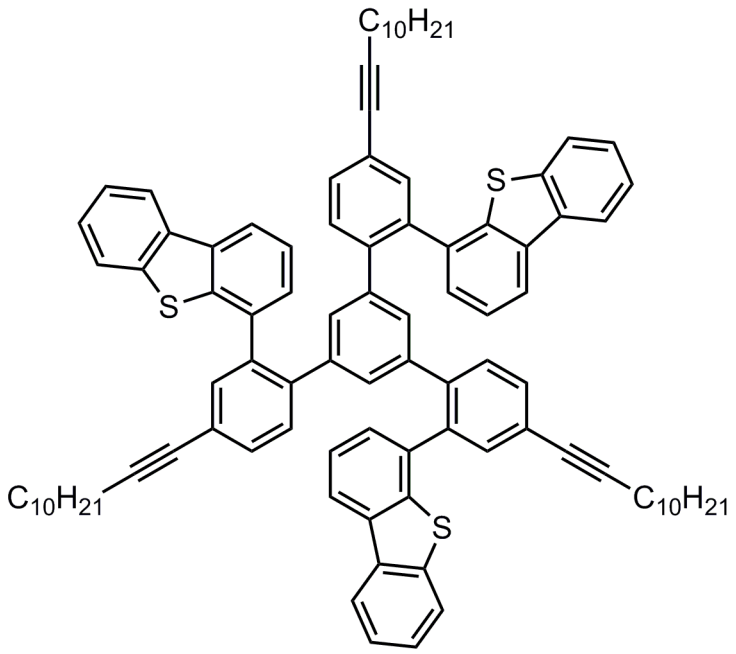

5-8

To the 250 mL Schlenk flask containing 1.03 g (0.79 mmol) **5-7**, 84 mg (0.22mmol, 15mol%) $Pd(PPh_3)_2Cl_2$, 23 mg (0.22mmol, 15mol%) CuI under protection of Argon gas was added 5mL triethylamine (bubbling with Argon for 30 minutes), and 50 mL anhydrous DMF. The mixture heated to 80 ℃ with stirring overnight after addition of 0.78 mL (3.57 mmol, 4.5eq) 1-Dodecyne. After standard work-up and purification by column chromatography (Silica gel, PE/DCM =5/1), 840 mg white solid was obtained (78.6%). MALDITOF-MS (TCNQ as matrix): m/z= 1345.9, calcd. 1345.98 for $C_{96}H_{96}S_3$. ^{1}H NMR (300 MHz, CD_2Cl_2): 8.20 (m, 3H), 8.03 (d, 3H, J = 7.69 Hz), 7.78 (d, 3H, J = 7.23Hz), 7.49 (m, 6H), 7.41 (d, 3H, J = 1.62 Hz), 7.4-6.4 (m, 15H), 2.37 (t, 6H, J = 6.94 Hz), 1.53 (m, 6H), 1.35 (m, 48H), 0.88 (m, 9H). ^{13}C NMR (300 MHz, CD_2Cl_2): 140.15, 140.10, 139.81, 138.82, 136.30, 136.06, 135.94, 133.20, 131.36, 130.46, 128.91, 128.77, 127.20, 124.86, 123.49, 123.17, 122.11, 120.41, 91.92, 80.12, 32.28, 29.97, 29.92, 29.70, 29.53, 29.28, 29.11, 23.06, 19.71, 14.26.

4,4'-(5'-(2-(Dibenzo[b,d]thiophen-4-yl)-4-(dodecyl)phenyl)-4,4''-bis(dodecyl)-[1,1':3',1''-terphenyl]-2,2''-diyl)didibenzo[b,d]thiophene (5-9)

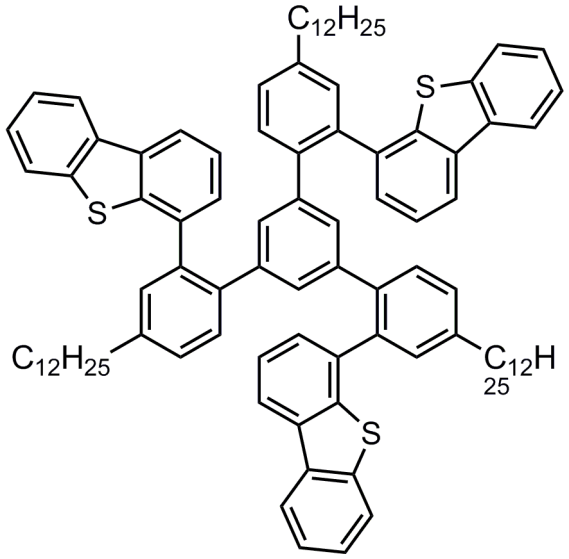

5-9

The solution of 400 mg compound **5-8** in 40 mL ethyl acetate was bubbled with argon gas for 30 minutes before addition of 10 wt% Pd/C (40 mg) in an open test tube held within a Parr bottle. The reaction solution was agitated using a Parr shaker under a hydrogen atmosphere (10 bar) for 12 hours. After removing the catalyst by the flask column chromatography (PE/DCM =5/1), 390mg white solid was obtained (96.6%). MALDITOF-MS (TCNQ as matrix): m/z= 1358.1, calcd. 1358.08 for $C_{96}H_{96}S_3$. ^{1}H NMR (300 MHz, CD_2Cl_2): 8.18 (m, 3H), 8.01 (d, 3H, J = 7.82 Hz), 7.74 (m, 3H), 7.45 (m, 6H), 7.20 (d, 3H, J = 1.61 Hz), 7.1-6.5 (m, 15H), 6.28 (m, 3H), 2.53 (t, 6H, J = 7.89 Hz), 1.51 (m, 6H), 1.35 (m, 54H), 0.83 (m, 9H). ^{13}C NMR (300 MHz, CD_2Cl_2): 142.38, 140.36, 140.21, 140.00, 138.50, 138.25, 137.34, 136.21, 135.91, 130.52, 130.11, 129.11, 128.69, 128.54, 127.06, 124.71, 123.11, 122.07, 120.06, 35.72, 32.32, 31.65, 30.97, 30.10, 30.08, 30.04, 30.01, 29.88, 29.76, 29.67, 23.08, 14.27.

5,11,17-Tris-*n*-dodecyl-trisbenzothieno[1,2:7,8:13,14]hexa-peri-hexabenzocorone ne (5-10)

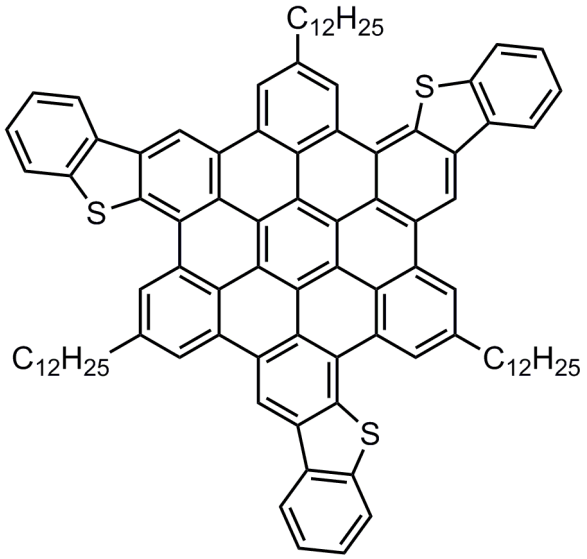

5-10

130 mg (0.095 mmol) **5-9** was dissolved in 60 mL anhydrous dichloromethane, the solution was then degassed by bubbling through argon for 30 min, and then 560 mg $FeCl_3$ in 3 mL CH3NO2 was added dropwise. After being stirred for 60 min, the reaction was quenched by adding 100mL methanol, the yellow precipitate was collected, washed by methanol and water repeatedly and dried under vacuum to afford 101 mg yellow powder (80%). MALDITOF-MS (TCNQ as matrix): m/z= 1345.5, calcd. 1345.98 for $C_{96}H_{96}S_3$. ^{1}H NMR (500 MHz, $C_2D_2Cl_4$, 403 K): 8.67 (s, 3H), 8.43 (s, 3H), 8.11 (s, 3H), 7.96 (s, 3H), 7.81 (m, 3H), 7.50 (m, 6H), 2.82 (m, 6H), 1.92 (m, 6H), 1.35 (m, 54H), 0.95 (t, 9H, J = 6.89).

5,11,17-Tris-*n*-dodecyl-trisbenzothieno-*S*,*S*-dioxide[1,2:7,8:13,14]hexa-peri-hexabenzocoronene (5-11)

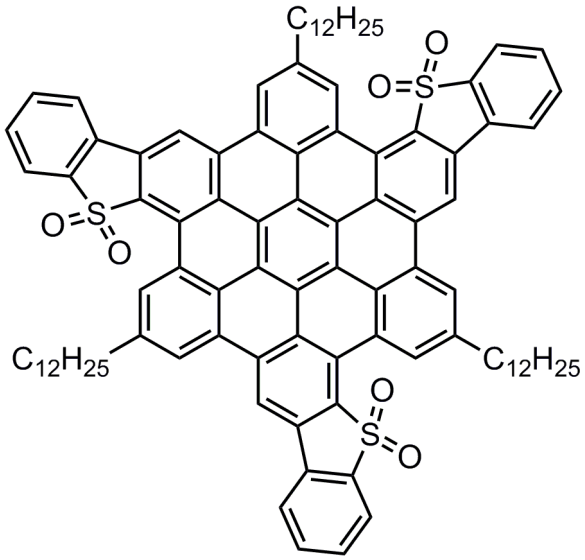

3-11

53 mg (0.095 mmol) **5-10** was dissolved in 4 mL anhydrous dichloromethane followed by addition of 245 mg *meta*-Chloroperoxybenzoic acid (55%). After being stirred for 60 min, the reaction was quenched by adding 20mL methanol, the orange precipitate was collected, washed by methanol and water repeatedly and dried under vacuum to afford 48 mg yellow powder (84.5%). MALDI TOF-MS (TCNQ as matrix): m/z= 1442.5, calcd. 1441.98 for $C_{96}H_{96}S_3O_6$. ^{1}H NMR (500 MHz, $C_2D_2Cl_4$, 403 K): 9.31 (s, 3H), 8.91 (s, 3H), 8.55 (s, 3H), 7.91 (s, 3H), 7.83 (b, 3H), 7.42 (b, 6H), 3.01 (b, 6H), 2.04 (m, 6H), 1.49 (m, 54H), 0.95 (b, 9H).

7.3.4 Synthesis of MBBs for bottom-up graphene nanoribbon fabrication

1-Azido-2,3,5,6-tetrafluoro-4-tricosylbenzene (6-1)

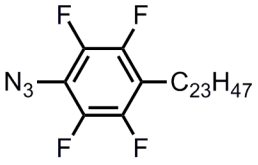

6-1

To a 100 mL round bottom flask containing 1,2,3,4,5-pentafluoro-6-methylbenzene (1.0 eq, 880 mg, 1.79 mmol), NaN3 (2.0 eq, 233.mg, 3.6 mmol), tetrabutylammonium azide (0.1 eq, 51 mg, 0.18 mmol) was added 20 ml anhydrous DMF. After keeping stirring at 80 ℃ for 24 hrs, the reaction mixture was cooled down to room temperature. The crude product was the purified by silica gel column chromatography with hexane as eluent to give 360mg the titled compound as a white solid. (39% yield). FD-MS (8 kV): *m*/*z* calcd. for $C_{29}H_{47}F_4N_3$: 513.7 [M^+]; found: 513.7. ^{1}H NMR (300 MHz, $CDCl_3$): δ ppm 2.58 (t, 2H, J = 7.62 Hz), 1.45 (m, 2H), 1.16 (b, 40H), 0.78 (t, 3H, J = 6.87 Hz). ^{13}C NMR (75 MHz, $CDCl_3$): δ ppm 31.93, 29.70, 29.66, 29.63, 29.59, 29.47, 29.36, 29.22, 29.13, 22.69, 14.11. ^{19}F NMR (658.9 MHz, $CDCl_3$): δ ppm -152.9, -144.6.

3-(3-(Octadecyloxy)phenyl)-3-(trifluoromethyl)-3H-diazirine (6-2)

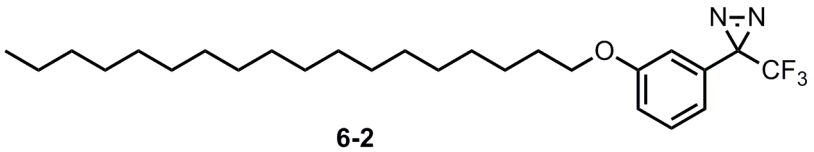

6-2

In the solution of 3-(3-(trifluoromethyl)-3H-diazirin-3-yl)phenol (1.0eq, 2.02 g, 10 mmol) in 60 mL acetone was added 1-bromooctadecane (1.2 eq, 4.0 g, 12.mmol) and K_2CO_3 (3.0 eq, 4.14 g, 30 mmol) in a round-bottom flask. After refluxing with vigorous stirring overnight, the reaction mixture was filtrated and thoroughly washed with dichloromethane. The combined organic solution was then evaporated to give the oil-like crude product. This crude product was purified by silica gel column chromatography by first using Hexane as eluent to wash away the excessive 1-bromooctadecane, and then using Haxane/DCM (10/1) to give compound **2** as a white solid. (3.20 g, yield: 65 %) FD-MS (8 KV): m/z 454.2, calcd.: 454.6 (M+). ^{1}H NMR (300 MHz, CD_2Cl_2): δ ppm 7.35 (t, 1H, J= 8.20 Hz), 6.98 (dd, 1H, J= 8.27 Hz), 6.80 (d, 1H, J= 7.84 Hz), 6.72 (s, 1H), 3.97 (t, 2H, J= 6.34 Hz), 1.80 (pentet, 2H, J= 8.42 Hz), 1.30 (m, 30H), 0.92 (t, 3H, J= 7.02 Hz). ^{13}C NMR (75 MHz, CD_2Cl_2): δ ppm 159.86, 130.67, 130.42, 118.73, 116.05, 113.14, 68.62, 32.32, 30.09, 30.05, 29.98, 29.95, 29.75, 29.50, 26.33, 23.09, 14.28.

16-(3-(3-(Trifluoromethyl)-3H-diazirin-3-yl)phenoxy)hexadecanoic acid (6-3)

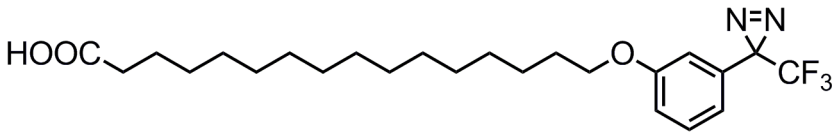

6-3

Methyl 16-(3-(3-(trifluoromethyl)-3H-diazirin-3-yl)phenoxy)hexadecanoate (1.0 eq, 820 mg, 1.7 mmol) was dissolved in 2 mL THF and 4 mL MeOH in a 25 mL round bottom flask. And then 1mL NaOH solution (8.0 M in H_2O) was added into the solution and kept under stirring at 50 ℃ for 3 hours. Aftr cooling the solution in ice bath for 10 mins, diluted HCl solution was added into the mixture dropwise until the pH of the solution reach 3.0. Then the mixture was extracted with EtOAc for three times, and the organic phase was driped with anhydrous $MgSO_4$. 670 mg of the titled compound was obtained as white solid after removing the organic solvent in rotary evaporator with the yield of 73.4%. FD-MS (8 KV): m/z 456.4, calcd.: 456.6 (M+). ^{1}H NMR (300 MHz, CD_2Cl_2): δ ppm 9.90 (b, 1H), 7.23 (t, 1H, J= 8.13 Hz), 6.89 (dd, 1H, J= 8.13 Hz), 6.69 (d, 1H, J= 8.13 Hz), 6.60 (b, 1H), 3.86 (t, 2H, J= 6.85 Hz), 2.26 (t, 2H, J = 7.70 Hz), 1.68 (quin, 2H, J= 7.27 Hz), 1.53 (m, 2H), 1.19 (m, 22H). ^{13}C NMR (75 MHz, CD_2Cl_2): δ ppm 130.40, 118.75, 116.06, 113.13, 68.62, 33.99, 30.03, 29.97, 29.94, 29.83, 29.73, 29.62, 29.49, 29.42, 26.32, 25.07.

4-(Docosyloxy)benzenediazonium tetrafluoroborate (6-4)

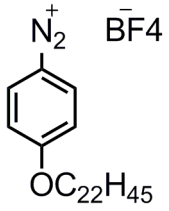

6-4

To a 100 mL flask under Argon gas in ice bath, was added 1 mL (4.0 eq, 8.0 mmol) boron trifluoride diethyl etherate, the solution of 840 mg (2.0 mmol) 4-(docosyloxy)aniline **6-16** in 20 mL anhydrous THF. Then the solution of 700 mg tertbutyl nitrite (3.0 eq, 6 mmol) in 5 mL anhydrous THF was added into reaction

mixture with stirring dropwise. After keeping stirring for 30 minutes under room temperature, the mixture was poured into 100 mL diethyl ether to precipitate the desired product. After filtration and thoroughly washing with diethyl ether, a white solid was obtained (980 mg, 94.0%). FD-MS (8 KV): m/z 401.1, calcd.: 401.3 ([M-N2-BF4]+). ^{1}H NMR (300 MHz, CD_2Cl_2): δ ppm 8.47 (d, 2H, J= 9.36 Hz), 7.27 (d, 2H, J= 9.45 Hz), 4.24 (t, 2H, J= 6.46 Hz), 1.86 (m, 2H), 1.26 (b, 38H), 0.88 (t, 3H, J= 7.03 Hz). ^{13}C NMR (175 MHz, DMSO-d_6): δ ppm 168.71, 136.62, 118.01, 103.44, 70.58, 31.75, 29.48, 29.45, 29.16, 29.11, 28.57, 25.67, 22.55, 14.41.

1,3-Dimethyl-2-(4-(octadecyloxy)phenyl)-2,3-dihydro-1H-benzo[d]imidazole (6-5)

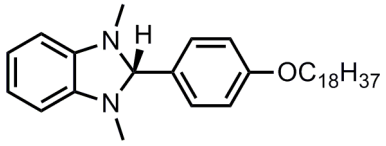

6-5

To a 100 mL flask containg 4-(octadecyloxy)benzaldehyde (1.0 eq, 750 mg, 2.0 mmol) was added 15 mL MeOH and 5 mL THF. And then the solution of N^1,N^2-dimethylbenzene-1,2-diamine (1.05 eq, 280.mg, 2.1 mmol) in 5 mL MeOH was added dropwise into the mixture, followed by the addition of 0.1 mL acetic acid. The mixture was kept under sonication for 2 hrs, and then the white precipitate was filtrated out and repeated washed with MeOH. 920 mg of the title compound was obtained as a white solid (93% crude yield). FD-MS (8 KV): m/z 492.9, calcd.: 492.8 (M+). ^{1}H NMR (3000 MHz, CD_2Cl_2): δ ppm 7.38 (d, 2H, J = 9.33 Hz), 6.85 (d, 2H, J = 9.33 Hz), 6.58 (q, 2H, J = 3.22 Hz), 6.30 (q, 2H, J = 2.98 Hz), 4.70 (s, 1H), 3.90 (t, 2H, J = 6.84 Hz), 2.43 (s, 6H), 1.70 (quin, 2H, J = 7.00 Hz), 1.19 (m, 30H), 0.80 (t, 3H, J = 6.82 Hz). ^{13}C NMR (75 MHz, CD_2Cl_2): δ ppm 130.29, 119.42, 114.59, 105.84, 93.91, 68.48, 33.26, 32.32, 30.08, 30.05, 30.00, 29.98, 29.80, 29.75, 29.67, 26.42, 23.09, 14.27.

Docosan-1-ol (6-6)

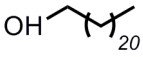

6-6

Tricosan-1-ol (6-6) is commercial available from the TCI-European.

Docosanal (6-7)

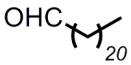

6-7

To the solution of docosan-1-ol (1.0 eq, 6.66 g, 20 mmol) in the mixture of 50 mL DMSO and 100 mL DCM was added N,N-Diisopropylethylamine (7.0 eq, 25 mL, 140 mmol) and folled by the addition of sulfur trioxide pyridine complex (3.5 eq, 11.4 g, 70 mmol). After keeping stirring under room temperature for 30 mins, the mixture was poured onto the ice. The mixture was then extracted with EtOAc, and then dried in the rotary evaporator to yield the crude product. The crude product was purified by silica gel column chromatography with dichloromethane/hexane = 1/4 as eluent to yield 4.32 g of the title compound as a white wax-like solid (68% yield). FD-MS (8 KV): m/z 324.4, calcd.: 324.6 (M+). ^{1}H NMR (300 MHz, $CDCl_3$): δ ppm 9.67 (s, 1H), 2.32 (t, 2H, J = 7.56 Hz), 1.53 (m, 2H), 1.16 (m, 36H), 0.79 (t, 3H, J = 6.89 Hz). ^{13}C NMR (75 MHz, $CDCl_3$): δ 202.90, 43.92, 31.92, 29.69, 29.66, 29.63, 29.58, 29.42, 29.36, 29.17, 22.69, 22.09, 14.10.

Tricos-1-yne (6-8)

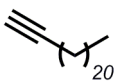

6-8

To a two-necked round-bottom flask containing docosanal (1.0 eq, 2.26 g, 6.96 mmol), and K_2CO_3 (2.0 eq, 1.92 g, 13.9 mmol), was added 30 mL anhydrous MeOH. Then the solution of the (1-diazo-2-oxopropyl)phosphonate (1.1 eq, 1.47 g, 7.66 mmol) in 20 mL anhydrous MeOH was added dropwise into the solution under ice bath. After

stirring under room temperature overnight, 50 mL $NaHCO_3$ solution (5% in H_2O) was added into the mixture to quench the reaction. The reaction mixture was then extracted with diethyl ether (3 × 50 mL), and the combined organic layers were dried in vacuo. The crude product was purified by silica gel column chromatography with hexane as eluent to yield 1.71 g of the title compound as a white wax-like solid (78% yield). FD-MS (8 KV): m/z calcd. for $C_{23}H_{44}$: 320.6 [M+]; found 320.4, ^{1}H NMR (300 MHz, $CDCl_3$): δ ppm 2.08 (t, 2H, J = 7.21 Hz), 1.84 (s, 1H), 1.43 (m, 2H), 1.16 (m, 36H), 0.79 (t, 3H, J = 7.21 Hz). ^{13}C NMR (75 MHz, $CDCl_3$): δ 84.82, 68.00, 31.93, 29.70, 29.66, 29.61, 29.51, 29.36, 29.11, 28.77, 28.51, 22.69, 18.40, 14.11.

1-(Tricos-1-yn-1-yl)-2,3,4,5,6-pentafluorobenzene (6-9)

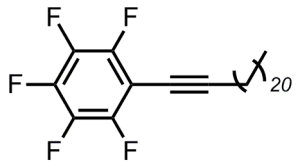

6-9

A two-necked 100-mL round-bottom flask containing tricos-1-yne (1.0 eq, 962 g, 3.0 mmol), perfluoroiodobenzene (1.5 eq, 1.32 g, 4.5 mmol), $Pd(PPh_3)_2Cl_2$ (0.03 eq, 63 mg, 0.09 mmol), and CuI (0.03 eq, 29 mg, 0.09 mmol) was evacuated and refilled with argon gas for three times. Then, 30 mL of anhydrous THF was added into the flask, followed by 10 mL of degassed diisopropylamine. The reaction mixture was stirred under room temperature overnight. After evaporating the solvent, the crude product was purified via silica gel column chromatography with hexane as eluent to obtain 875 mg of the title compound as a white solid (60% yield). FD-MS (8 kV): *m*/*z* calcd. for $C_{29}H_{43}F_5$: 486.6 [M^+]; found: 486.4. ^{1}H NMR (300 MHz, $CDCl_3$): δ ppm 2.39 (t, 2H, J = 7.09 Hz), 1.54 (quin, 2H, J = 8.61 Hz), 1.36 (m, 2H), 1.16 (b, 34H), 0.78 (t, 3H, J = 7.09 Hz). ^{13}C NMR (75 MHz, $CDCl_3$): δ ppm 31.92, 29.69, 29.65, 29.58, 29.42, 29.36, 29.04, 28.74, 28.12, 22.69, 19.76, 14.10.

1,2,3,4,5-Pentafluoro-6-methylbenzene (6-10)

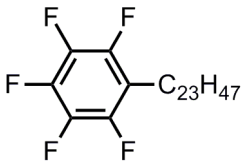

6-10

The solution of 1-(Tricos-1-yn-1-yl)-2,3,4,5,6-pentafluorobenzene (1.0 eq, 865 mg, 1.77 mmol) was dissolved with 50 mL EtOAc in the autoclave tube and degassed for 20 mins by bubbling with Argon gas. Then 100 mg Pd/C was added into the mixture and the autoclave was sealed. After keeping stirring under 15 bar H_2 gas at room temperature, the reaction mixture was passing through a flash column chromatography to remove the ctatalyst to yield 875 mg of the title compound as a white solid (100% yield). FD-MS (8 kV): *m*/*z* calcd. for $C_{29}H_{47}F_5$: 490.6 [M^+]; found: 490.7. ^{1}H NMR (300 MHz, $CDCl_3$): δ ppm 2.58 (t, 2H, J = 6.77 Hz), 1.45 (m, 2H), 1.16 (b, 40H), 0.78 (t, 3H, J = 6.87 Hz). ^{13}C NMR (75 MHz, $CDCl_3$): δ ppm 31.93, 29.69, 29.65, 29.62, 29.58, 29.46, 29.36, 29.27, 29.21, 29.12, 22.69, 22.32, 14.10. ^{19}F NMR (658.9 MHz, $CDCl_3$): δ ppm -163.2, -158.5, -144.7.

3-(3-(Trifluoromethyl)-3H-diazirin-3-yl)phenol (6-11)

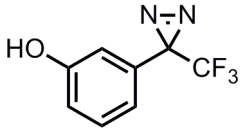

6-11

The diazirine precursor 3-(3-(trifluoromethyl)-3H-diazirin-3-yl)phenol (**6-11**) is synthesized according exactly to the literature.[6] ^{1}H NMR (300 MHz, CD_2Cl_2): δ ppm 7.32 (t, 1H, J= 8.28 Hz), 6.94 (dd, 2H, J= 8.01 Hz), 6.77 (m, 1H), 6.71 (b, 1H).

Methyl 16-(3-(3-(trifluoromethyl)-3H-diazirin-3-yl)phenoxy)hexadecanoate (6-12)

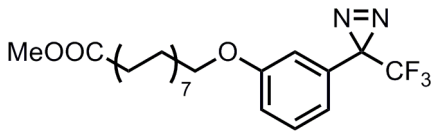

6-12

In the solution of 3-(3-(trifluoromethyl)-3H-diazirin-3-yl)phenol (1.0eq, 2.75 g, 13.6 mmol) in 60 mL Acetone was added methyl 16-bromohexadecanoate (1.1 eq, 5.23 g, 15.0 mmol) and K_2CO_3 (3.0 eq, 5.64 g, 40.8 mmol) in a round-bottom flask. After refluxing with vigorous stirring overnight, the reaction mixture was filtrated and thoroughly washed with dichloromethane. The combined organic solution was then evaporated to give the oil-like crude product. This crude product was purified by silica gel column chromatography by first using Hexane/DCM = 1/1 as eluent to yield the titled compound as a white solid. (820 mg, yield: 13.8 %) FD-MS (8 KV): m/z 470.4, calcd.: 470.6 (M+). ^{1}H NMR (300 MHz, CD_2Cl_2): δ ppm 7.22 (t, 1H, J= 7.91 Hz), 6.86 (dd, 1H, J= 8.74 Hz), 6.80\\68 (d, 1H, J= 7.91 Hz), 6.60 (b, 1H), 3.86 (t, 2H, J= 6.66 Hz), 3.59 (s, 3H), 2.23 (t, 2H, J= 7.62 Hz), 1.70 (m, 2H), 1.20 (m, 24H)

3-(Octadecyloxy)benzaldehyde (6-13)

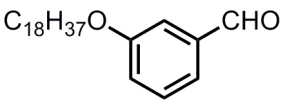

6-13

In the solution of 2.5 g 3-hydroxybenzaldehyde (1.0eq, 20 mmol) in 60 mL Acetone was added 10.0 g 1-Bromooctadecane (1.5 eq, 30mmol) and 8.3 g K_2CO_3 (3.0 eq, 60 mmol). The mixture was heated to 60 ℃ with vigorous stirring overnight. After cooling to the room temperature, the reaction mixture was filtrated and thoroughly washed with dichloromethane. The combined organic solution was then evaporated to give the oil-like crude product. This crude product was purified by silica gel column chromatography by first using Hexane as eluent to wash away the excessive 1-Bromooctadecane, and then using Haxane/DCM (4/1) to give compound **4** as a

white solid. (6.70g, yield: 89 %) FD-MS (8 KV): *m/z* 374.1 (100%), $[M]^+$. HRMS (ESI) *m/z*: Calcd for $C_{25}H_{42}O_2Na$: 397.3083; Found: 397.3073 $[M + Na]^+$. ^1H NMR (300 MHz, CD_2Cl_2, ppm) δ 9.95 (s, 1H), 7.47 – 7.41 (m, 2H), 7.39 – 7.34 (m, 1H), 7.21 – 7.14 (m, 1H), 4.02 (t, J = 6.6 Hz, 2H), 1.91 – 1.69 (m, 2H), 1.52 – 1.14 (m, 30H), 0.88 (t, J = 6.9 Hz, 3H). ^{13}C NMR (75 MHz, CD_2Cl_2, ppm) δ 192.59, 138.47, 130.55, 123.39, 122.13, 113.51, 68.95, 32.49, 30.26, 30.22, 30.16, 30.14, 29.93, 29.70, 26.53, 23.26, 14.45.

2,2,2-Trifluoro-1-(3-(octadecyloxy)phenyl)ethanol (6-14)

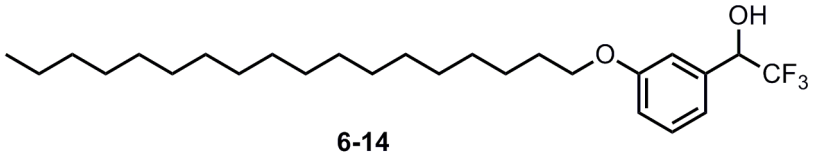

6-14

The synthesis procedure was following the literature[2]. 370mg 3-(octadecyloxy)benzaldehyde **6-13** (1.0eq, 1 mmol) and 0.20 mL $TMSCF_3$ (1.35 eq, 1.35 mmol) was dissolved in the anhydrous DMF (10 mL) in a 50 mL round-bottom flask. To this solution was added 20 mg K_2CO_3 (15% mol, 0.15mmol), and the mixture was stirred vigorously at room temperature overnight. The reaction was quenched with 20 mL solution of HCl (1.0 M) for 1 hour, the mixture then extracted with diethyl ether (3 × 30 mL). Combined organic layers were finally washed with brine solution, dried over anhydrous Na_2SO_4, and then solvent was removed under reduced pressure. This crude product was purified by silica gel column chromatography by using Haxane/DCM (3/1) to give compound **4** as a white solid. (380 mg, yield: 85 %) FD-MS (8 KV): *m/z* 444.3 (100%) $[M]^+$. HRMS (ESI) *m/z*: Calcd for $C_{26}H_{43}O_2F_3Na$: 467.3113; Found: 467.3100 $[M + Na]^+$. ^1H NMR (300 MHz, CD_2Cl_2, ppm) δ 7.32 (t, J = 8.2 Hz, 1H), 7.08 – 6.99 (m, 2H), 6.97 – 6.91 (m, 1H), 5.01 (q, J = 6.8 Hz, 1H), 3.97 (t, J = 6.6 Hz, 2H), 2.40 (br, 1H), 1.90 – 1.67 (m, 2H), 1.58 – 1.15 (m, 30H), 0.89 (t, J = 6.6 Hz, 3H). ^{13}C NMR (75 MHz, CD_2Cl_2, ppm) δ 159.96, 136.15, 130.16, 126.83, 123.10, 119.97, 116.03, 114.14, 73.75, 73.32, 72.90, 72.48, 68.75, 32.53, 30.30, 30.27, 30.21, 30.19, 30.00, 29.97, 29.81, 26.59, 23.29, 14.48.

1-(Docosyloxy)-4-nitrobenzene (6-15)

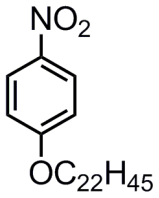

6-15

2.8 g (20.0 mmol) 1-fluoro-4-nitrobenzene, 6.4 g (1.0 eq, 20.0 mmol) docosanol, 8.0 g K_2CO_3, (3.0 eq, 60.0 mmol), and 60 mL anhydrous DMF were added into 100mL flask. The mixture was heated to 100 ℃ with stirring for 24 hours. After cooling to the room temperature, the mixture was poured into water (100 mL) and extracted with dichloromethane (DCM). The organic layer was washed by water and dried over anhydrous MgSO4. The solvent was removed under vacuum and the residue was purified by silica gel column chromatography using Hexane as eluent to give compound 1 as a white solid (3.20 g, yield: 36 %). FD-MS (8 KV): m/z 447.1, calcd.: 447.3 (M+). ^{1}H NMR (300 MHz, $CDCl_3$): δ ppm 8.12 (d, 2H, J= 9.38 Hz), 6.87 (d, 2H, J= 9.25 Hz), 3.97 (t, 2H, J= 6.41 Hz), 1.75 (m, 2H), 1.38 (m, 2H), 1.19 (b, 36H), 0.80 (t, 3H, J= 6.79 Hz). ^{13}C NMR (75 MHz, CD_2Cl_2): δ ppm 164.22, 141.28, 125.87, 114.36, 68.88, 31.92, 29.69, 29.55, 29.34, 28.96, 25.90, 22.68, 14.10.

4-(Docosyloxy)aniline (6-16)

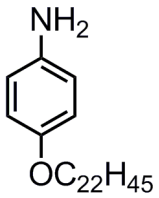

6-16

The solution of 1.45 g compound 1-(docosyloxy)-4-nitrobenzene **6-15** in 30 mL tetrahydrofuran was bubbled with argon gas for 30 minutes before addition of 20 wt% Pd/C (290 mg) in an open test tube held within a Parr bottle. The reaction solution was agitated using a Parr shaker under a hydrogen atmosphere (5 bar) for 12 hours. After removing the catalyst by filtration, the solvent was removed under vacuum to

give a pink solid (1.30g, 96.3%). FD-MS (8 KV): m/z 417.1, calcd.: 417.7 (M+). ^{1}H NMR (300 MHz, CD_2Cl_2): δ ppm 6.69 (d, 2H, J= 9.05 Hz), 6.60 (d, 2H, J= 9.05 Hz), 3.84 (t, 2H, J= 6.86 Hz), 1.70 (m, 2H), 1.26 (b, 38H), 0.87 (t, 3H, J= 7.03 Hz). ^{13}C NMR (175 MHz, CD_2Cl_2): δ ppm 152.13, 140.23, 115.99, 115.47, 68.62, 31.92, 29.68, 29.65, 29.60, 29.46, 29.43, 29.35, 26.05, 22.68, 13.87.

4-(Octadecyloxy)benzaldehyde (6-17)

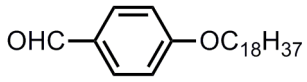

6-17

To a flask containing methyl 4-hydroxybenzaldehyde (1.0 eq, 3.67 g, 30.0 mmol) and 1-bromooctadecane (1.2 eq, 11.0 g, 36.0 mmol) was added K_2CO_3 (3.0 eq, 12.0 g, 90.0 mmol), and 100 mL acetone. The reaction mixture was heated to 70 ℃ with vigorous stirring overnight. After cooling the mixture to room temperature, the inorganic salt was removed by filtration and repeated washing with acetone. After removing the organic solvent in rotary evaporator, the crude product was purified by silica gel column chromatography using Hexane as eluent to yield eluent to yield 9.54 g of the title compound as a white solid (100% yield). FD-MS (8 KV): m/z 358.4, calcd.: 358.6 (M+). ^{1}H NMR (3000 MHz, CD_2Cl_2): δ ppm 9.89 (s, 4H), 7.84 (d, 2H, J = 9.06 Hz), 7.0. (d, 2H, J = 8.91 Hz), 4.08 (t, 2H, J = 6.68 Hz), 1.84 (quin, 2H, J = 7.87 Hz), 1.30 (m, 30H), 0.92 (t, 3H, J = 7.19 Hz). ^{13}C NMR (75 MHz, CD_2Cl_2): δ ppm 190.90, 164.65, 132.13, 130.20, 115.07, 68.90, 32.36, 30.07, 30.03, 29.97, 29.93, 29.74, 29.71, 29.44, 26.30, 23.08, 14.26.

Reference:

[1] I. Horcas, R. Fernandez, J. Gomez-Rodriguez, J. Colchero, J. Gómez-Herrero, A. Baro, A.WSXM: A Software for Scanning Probe Microscopy and a Tool for Nanotechnology Rev. Sci. Instrum. 2007, 78, 013705

[2] L. Arnold, S. R. Puniredd, C. von Malotki, W. Pisula, N. Koshino, H. Higashimura, M. Baumgarten, M. Wagner, K. Müllen, *Journal of Porphyrins and Phthalocyanines*, **2012**, *16*, 05n06,-564.

[3] X. Cheng, A. V. Heyen , W. Mamdouh , H. Ujii , F. De Schryver , S. Höger , and S. De Feyter *Langmuir*, **2007**, *23*, 1281.

[4] J. Luo, Y. Zhou, Z. Q. Niu, Q. F. Zhou, Y. G. Ma, J. Pei; *J. Am. Chem. Soc.*, **2007**, *129*, 11314.

[5] M. Kastler, W. Pisula, D. Wasserfallen, T. Pakula , K. Müllen, *J. Am. Chem. Soc.*, **2005**, *127* , 4286.

[6] E. J. Lawrence, G. G. Wildgoose, L. Aldous, Y. A. Wu, J. H. Warner, R. G. Compton, P. D. McNaughter, *Chem. Mater*. **2011**, *23*, 3740.

9. Acknowledgement

First of all, I would like to thank my PhD advisor, , for his continuous scientific and personal support during my entire Ph.D work. Those discussions and suggestions were definitely an essential part for the success of this work. In the past, I had never met a scientist who was so passionate and serious about science, and his enthusiasm and attitude in the research would definitely be a driving force for me in the future work.

Furthermore, I like to thank who has paved the basis for the success of this work. In the entire Ph.D period, he has supervised my research and guided my entire research career from macrocyclic synthesis to graphene chemistry. Meanwhile, he also helped me a lot in my personal life. I really appreciated his continuous supporting even when I was sick for a lone period.

Additonally, I would like to thank my project leader , who helped me a lot on the work publication and Ph.D thesis writting. His efforts had also played a critical factor in the success of this work.

Moreover, I like to thank my parents, my sister and my wife. They had been supporting me all the time. Without their encouraging, it would be impossible for me to accomplish this works.

I would like to thank my cooperation partners, for the great 2D WAXS measurements and his help on the manuscript submission.

I liked to thank , who supported my work with the mass spectrum measurement and valuable discussion.

Furthermore, I wanted to thank all collaborators from the Max Planck Institute for Polymer Research, in particular for his fantastic NMR measurements and his guidance on the 2D NMR analysis.

And I also liked to thank all members from the group for the magnificent colleagueship, in particular:

My office mates for their help in my life.

My lab mates: for their help in my experiment.

I would also like to thank all the group members who organized parties, barbecues and other social events for this fantastic life.

10. List of Publication

1. **Y. Liu**, "Sulfur-Annulated Hexa-peri-hexabenzocoronene Decorated with Phenylthio Groups at the Periphery" *Angew. Chem. Int. Ed.*, **2015**, *54*, 2927 –2931.

2. **Y. Liu**, "A Shape-Persistent Polyphenylene Spoked Wheel" *J. Am. Chem. Soc*, **2016**, *138*, 15539–15542. (Highlighted by Chemistry World)

3. **Y. Liu**, . "Derivatizing Tribenzothiophene Fused Hexa-*peri*-hexabenzocoronenes with Tunable Optoelectronic Properties" *Chem. Asian J*, **2016**, *15*, 2107-2112.

4. **Y. Liu**, "Electrochemical Functionalization of Graphene at the Nanoscale with Self-assembling Diazonium Salts" *ACS Nano*, **2016**, *10*, 7125-7134.

5. **Y. Liu**, "Periodic potentials in hybrid van der Waals heterostructures formed by supramolecular lattices on graphene." *Nat. Commun. (Accepted)*

11. Curriculum Vitae

Yi Liu

Graduate Chemist

08. Jun, 1987, Hubei, China

Education

2012–2016 **Max-Planck Institute for Polymer Research, Mainz**
Ph.D. in Chemistry: Synthesis and construction of new allotropes of carbons with novel structure. Director: [redacted]

2009–2012 **Zhejiang University, Hangzhou**
Master of Engineering: Application of aggregation-Induced emission phenomenon in molecular recognition and detection of saccharides. Director: [redacted]

2005–2009 **Zhejiang University, Hangzhou**
Bachelor of Engineering: Tetraphenylethene-based fluorescent detection of sugars. [redacted]

Research Experience

2012-2016 *Doctoral Dissertation* **Max-Planck Institute for Polymer Research, Mainz**

1) Synthesis of polyphenylene macrocycles composed of sp^2 carbons
2) Synthesis of cyclic polypheylenes with "figure-eight" structure and possible Möbius topology
3) Engineering the energy level of sulfur-containing polycyclic aromatic hydrocarbons via post-modification
4) Design and synthesis of functional building blocks for bottom-up generation of well-patterned graphene nanoribbones

2009-2012 *Master Dissertation* **Zhejiang University, Hangzhou**

1) Synthesis of boronic acid-containing fluorogens featured with aggregation-induced emission properties for specific detection of D-glucose

2) Oligosaccharides recognition with fluorescent receptors of aggregation-induced emission properties

2009-2010 *Research Assistant* **Hong Kong University of Science & Technology, Hongkong**

Synthesis of tetraphenylene-hexaphenylbenzene adducts

2008-2009 *Bachelor Dissertation* **Zhejiang University, Hangzhou**

Synthesis of tetraphenylene-based sensors functionalized with boronic acids and its optical response to monosaccharides

2008-2009 *Student Research Training Program* **Zhejiang University, Hangzhou**

Investigation of negative differential resistance behavior of copper phthalocyanine composite and its electronic device fabrication.

Research Interest

Rational design and tailored synthesis of functional molecules with novel topology

Application of organic synthesis and supramolecular chemistry in functional material development

Skills

Adept at organic synthesis

Experience at optical detection and molecular recognition for small analytes

Proficient at UV-Vis, fluorescent spectroscopy and recycling GPC purification

Skill at Gaussian 03 for molecular modeling and simulation

Fluent English (oral and writing)